

https://dspace.org/

The effect of physico-chemical properties of multi-walled carbon nanotubes and its toxicity on saccharomyces cerevisiae

Phillips, Chantelle Lee

2012-02-14
http://hdl.handle.net/10539/11312

Downloaded from a DSpace repository. https://dspace.org/

THE EFFECT OF PHYSICO-CHEMICAL PROPERTIES OF MULTI-WALLED CARBON NANOTUBES AND ITS TOXICITY ON *SACCHAROMYCES CEREVISIAE*

Chantelle Lee Phillips

A dissertation submitted to the Faculty of Engineering and the Built Environment, University of the Witwatersrand, Johannesburg, in fulfilment of the requirements for the degree of Master of Science in Engineering

Johannesburg, 2011

DECLARATION

I hereby do solemnly declare that the work presented in this dissertation has been carried out by me and has not been previously submitted to any other University/ Organization for an academic qualification / certificate / diploma or degree.

The work I have presented does not breach any copyright.

Signature: .....

Student's full name: Chantelle Lee Phillips.

------ day of ---------- 2011

Faculty/ School: School of Chemical and Metallurgical Engineering

Dedication

To my parents, Cyril and Lorreta Phillips
who always encourage me to be
the best that I can be- I love you!

Acknowledgements

I would like to express my sincere gratitude to my supervisor Professor S .E. Iyuke, for his unending support and faith in me. Through his inspired guidance I learned so much and gained skills required to become an excellent researcher. It was a priviledge to work with him.

I would also like to thank my co-supervisors, Dr K. Rumbold, Prof V. Pillay and Dr C. Yah, for their encouragement and invaluable advice throughout the course of this study.

Post graduate students in the School of Chemical and Metallurgical Engineering, School of Biology, School of Pharmacy and the Wits University microscopy and analysis unit, thank you for all your assistance throughout my work.

My family and church members for their support and prayers, to friends KT, who's support has been a pillar of strength through the trying times - thank you.

And most of all to my Lord and Savior Jesus Christ the omnipotent and omnipresent heavenly father who's faithfulness is eternal.

Abstract

Carbon nanotubes (CNTs) have remarkable properties that distinguish them from other materials and make them desirable in many applications. Despite being promising tools for biology and medicine little is known about the effects and safety of CNTs on biological objects. The toxicity of CNTs is a prime concern and the effects of multi-walled carbon nanotubes (MWCNTs) in vitro have been studied, delivering conflicting results. This is even further aggravated by the limited data on yeast cells. The aim of this study was to test the effects of the physicochemical properties of CNTs and its toxicity on *Saccharomyces cerevisiae (S.cerevisiae)* in vitro. CNTs were produced by the swirled floating catalytic chemical vapour deposition method (SFCCVD) (Iyuke, 2005) and were purified with nitric acid and sulphuric acid treatments. CNT physicochemical properties such as specific surface area, particle size distribution, were characterized by Brunauer-Emmett-Teller (BET), Transmission Electron Microscopy (TEM), Scanning Electron Microscopy (SEM), Raman spectroscopy and Thermal Gravimetric Analysis (TGA). The toxicity of pristine and oxidised MWCNTs was compared and investigated in the yeast species *S.cerevisiae*, by cell growth analysis, electron microscopic examination and cell viability assessment by means of the standard plating technique. *S.cerevisiae* cells were exposed to concentrations of 2, 3, 6, 10, 20 and 40μg/ml of both oxidised and pristine MWCNTs. Compared to the control *S.cerevisiae* growth curves containing MWCNTs there was no significant change at both high and low doses of MWCNTs. Both pristine and oxidized MWCNTs do not affect the growth rate and viability of *S.cerevisiae* cells, this is adduced from the lack of toxicity in the cells during the observed time period. The cellular uptake of MWCNTs was evaluated by using standard fluorescent probes and confirmed by confocal microscopy images. MWCNT's were covalently functionalised by the 1, 3-dipolar cycloaddition of N-tritylglycine and the interactions between the MWCNTs and the covalent modifiers were characterised by H^1 NMR, TEM and TGA. Confocal observations clearly show that MWCNT-FITC are internalised by all (100%) *S.cerevisiae* yeast cells in less than 2 hrs incubation of 20 μg/ml MWCNTs.

Pheochromocytoma (PC12) cells were also cultured in Royal Park Memorial Institute (RPMI) media containing concentrations of nitric acid oxidised MWCNTs ranging from 50 μg/ml to 200 μg/ml. It was observed that oxidised MWCNTs demonstrated no cytotoxicity towards PC12

neuronal cells. No significant CNT toxic effect was found in both *S.cerevisiae* and PC12 neuronal cell lines.

Table of Contents

Contents

Dedication I
Acknowledgements II
Abstract III
List of Tables IX
List of Figures X
List of abbreviations XIV
Preface 1
CHAPTER 1 2
Introduction and Background 2
1.1 Motivation 3
1.2 Research statement 4
1.3 Research questions 4
1.4 Research aims 4
1.5 Research objectives 5
CHAPTER 2 6
Literature Review 6
2.1 Carbon nanotubes 6
2.1.1 Structure of carbon nanotubes 6
2.1.2 Properties of carbon nanotubes 7
2.1.2.1 Chemical Reactivity 7
2.1.2.2 Electrical Conductivity 8
2.1.2.3 Optical Activity 8
2.1.2.4 Mechanical Strength 9
2.1.2.5 Adsorptive Properties 9
2.1.2.6 Zeta potential 11
2.1.3 Synthesis of Carbon nanotubes 12
2.1.3.1 Laser ablation 12
2.1.3.2 Arc discharge 14
2.1.3.3 Catalytic Chemical vapour deposition (CCVD) 14
2.1.4 Characterisation methods of carbon nanotubes 15
2.1.4.1 Raman Spectroscopy 16

2.1.4.2 Transmission Electron Microscopy (TEM) 17
2.1.4.3 Physisorption/ BET surface area 18
2.1.4.4 Scanning Electron Microscopy (SEM) 18
2.1.4.5 Thermal Gravimetric Analysis (TGA) 18
2.1.4.6 X-ray diffraction 19
2.1.4.7 Nuclear magnetic resonance (NMR) Spectroscopy 19
2.1.5 Purification of carbon nanotubes 20
2.1.6 Functionalisation of CNTs 21
2.1.6.1 Covalent functionalisation of CNTs 22
2.1.6.2 Non- covalent functionalisation of CNTs 22
2.1.7 Applications of CNTs 22
2.2 The Yeast Cell 23
2.2.1 *S. Cerevisiae* cell characteristics 23
2.2.2 Yeast cell cycle 24
2.2.3 Cell growth 25
2.2.4 Measurement of microorganism growth 27
2.2.5 Yeast cell viability 29
2.2.5.1 Cell replication based methods 29
2.2.5.2. Methods based on staining 30
2.3 Cell imaging techniques 31
2.4 The Pheochromocytoma PC12 Cell 31
2.6 Toxicity of carbon nanoparticles 32
CHAPTER 3 35
Materials and Methods 35
3.1 Production of carbon nanotubes 35
3.2 Purification or Oxidation of carbon nanotubes 36
3.3 Characterisation of carbon nanotubes 37
3.3.1 Transmission Electron Microscopy 37
3.3.2 BET analysis 38
3.3.3 Raman Spectroscopy analysis 38
3.3.4 Thermogravimetric Analysis 38
3.3.5 Scanning Electron Microscopy (SEM) 38
3.4 Functionalisation of carbon nanotubes 38
3.4.1 Functionalisation of oxidised MWCNTs with thionyl chloride 39

3.4.2 1, 3 – dipolar cycloaddition reaction of N-Tritylglycine 39
3.4.3 Deprotection reaction (cleavage of trityl protecting group) 40
3.4.4 Attachment Reaction of fluorescent probe on free amino sites 41
3.5 ^{1}H NMR analysis 42
3.6 *Saccharomyces cerevisiae* cell cultivation and preservation 42
3.7 *Saccharomyces cerevisiae* cell growth analysis 42
3.8 Construction of the calibration curve 43
3.9 *S.cerevisiae* cell viability analysis 43
3.9.1 Serial Dilution procedure 44
3.9.2 Viable count procedure 45
3.10 *Saccharomyces cerevisiae* cell imaging 45
3.10.1 Yeast cell sample preparation for scanning electron microscopy 45
3.10.2 Preparation of Yeast cells for confocal microscopy 46
3.11 PC12 cell culture 48
3.12 The CytoTox-Glo Cytotoxicity Assay 49
3.13 Cytotoxicity of carbon nanotubes towards PC-12 neuronal cells 49
3.14 Morphometric analysis of PC12 cells 51
3.15 Statistical analyses 52
CHAPTER 4 53
Results and discussion 53
4.1 Characterisation of carbon nanotubes 53
4.1.1 Transmission electron microscopy 53
4.1.2 BET results 56
4.1.3 Raman spectroscopy analysis 57
4.1.4 TGA analysis 64
4.1.5 Scanning electron microscopy (SEM) results 69
4.1.6 Functionalisation of MWCNTs 71
4.2 *S.cerevisiae* Growth Analysis in the presence of MWCNTs 78
4.3 *S.cerevisiae* Cell Viability 82
4.4 Scanning Electron Microscopy analysis of cell morphology 86
4.5 Confocal microscopy results 88
4.6 Neuronal Cell Cytotoxicity of CNTs 92
4.7 Morphology of PC12 cells 93
CHAPTER 5 94

Conclusion and Recommendations 94
5.1 Conclusion 94
5.2 Recommendations 95
REFERENCES 96
Publications and presentations arising from this dissertation 116
Appendix A1: List of chemical used and reagent preparation 117
Appendix A2: NMR Spectra 122
Appendix A3: Growth Curves data 125
Appendix A4: Cell viability Results 151
Appendix A5: PC12 Cytotoxicity viability result 162
Appendix A6: Additional research micrographs and pictures 165

List of Tables

Table 2.1: Gives the adsorption properties and sites of SWCNTs and MWCNTs (Bhushan, 2004) 11
Table 4.1: BET results of MWCNTs 56
Table: 4.2 Raman spectra results of pristine, 30% HNO_3 treated and 1:3 HNO_3:H_2SO_4 treated . 63
Table 4.3: Gives the % Metal catalyst residue of acid treated and untreated MWCNTs 67
Table 4.4: Thermal stability of salts formed from the 30% HNO_3 and 1:3 HNO_3:H_2SO_4* 68
Table A1.1: List of Chemicals.....117

List of Figures

Figure 2.1: Models of 3 atomically perfect SWCNT structures (Terrones, 2003) 6
Figure 2.2: Illustration of the four different adsorption sites on a SWCNT bundle (Bhushan, 2004) 10
Figure 2.3: A schematic of the electrochemical double layer and zeta potential of a charged particle (Lin et al., 2003)..... 12
Figure 2.4: A schematic of a pulsed laser deposition reactor (Sinnot & Andrews, 2001)..... 13
Figure 2.5: Sketch of an electric arc reactor (Bhushan, 2004)..... 14
Figure 2.6: Schematic of a typical thermal CVD..... 15
Figure 2.7: Raman spectrum showing characteristic features of CNTs: radial breathing mode (RBM), the D band, G band and G' band (Belin & Epron, 2005)..... 17
Figure 2.8: Life cycle of the budding yeast *Saccharomyces cerevisiae* 24
Figure 2.9: A typical cell growth curve 27
Figure 2.10: Optical density measuring technique (Jomdecha & Prateepasen et al., 2006)..... 28
Figure 3.1: Apparatus and SFCCVD Reactor used to produce the MWCNTs (Iyuke, S. S.A. Patent 2101,2005,03438, 2005) 36
Figure 3.2: Schematics of reactions for 1,3-dipolar cycloaddition reaction of trityl protected glycine as a form of MWCNT functionalisation 41
Figure 4.1: Typical TEM micrograph of pristine MWCNTs. (a) illustrating MWCNT with open ends and dark spots indicating metal catalyst at a scale of 0.2 μm. (b) illustrating a MWCNT with metal catalyst at a scale of 0.1 μm..... 53
Figure 4.2: Typical TEM micrograph of MWCNTs after1:3 HNO_3:H_2SO_4 acid treatment..... 54
Figure 4.3: Typical TEM micrograph of 30% HNO_3 oxidised MWCNTs. (a) illustrating a single MWCNT with a smooth surface with a 0.1μm scale bar. (b) illustrating a group of MWCNTs with open ends and smooth surfaces..... 54
Figure 4.4: Raman Spectra of pristine MWCNTs 58
Figure 4.5: Curve fitting results of pristine MWCNTs..... 59
Figure 4.6: Raman spectra of 30% nitric acid oxidised CNTs 60
Figure 4.7: Curve fitting results of 30% nitric acid oxidized CNTs..... 60
Figure 4.8: Raman spectra of 1:3 HNO_3:H_2SO_4 oxidized CNTs..... 61
Figure 4.9: Curve fitting results of 1:3 HNO_3:H_2SO_4 oxidised MWCNTs 62

Figure 4.10: Raman spectra of pristine, 30% HNO_3 treated and 1:3 HNO_3:H_2SO_4 treated MWCNTs..... 63
Figure 4.11: Thermal stability of the pristine MWCNTs. The solid line and dashed lines represent TG and DTG curves for the MWCNT samples, respectively..... 64
Figure 4.12: Thermal stability of the 30% HNO_3 oxidised MWCNTs. The solid line and dashed lines represent TG and DTG curves for the MWCNT sample..... 65
Figure 4.13: Thermal stability of the 1:3 HNO_3:H_2SO_4 oxidised MWCNTs. The solid line and dashed lines represent TG and DTG curves for the MWCNT sample..... 66
Figure 4.14: Thermal stability of pristine, 30% HNO_3 and 1:3 HNO_3:H_2SO_4 oxidised MWCNTs..... 69
Figure 4.15. Typical SEM Micrograph of pristine MWCNTs. (a) Illustrating MWCNTs with a 1µm scale bar (b) Illustrating MWCNTs with a 10 µm scale bar..... 69
Figure 4.16. SEM Micrograph of 30% HNO_3 oxidised MWCNTs with 10µm scale bar 70
Figure 4.17 SEM Micrograph of 1:3 HNO_3:H_2SO_4 oxidised MWCNTs with 10µm scale bar.. 70
Figure 4.18. Typical TEM image of unreacted MWCNT sample from the 1, 3-dipolar cycloaddition reaction process with 0.4µm scale bar. 72
Figure 4.19. Typical TEM image of N-Tritylglycine functionalised MWCNTs. (a) with a 0.5µm scale bar (b) with a 0.33 µm scale bar. 72
Figure 4.20. Typical TEM micrograph of FITC-MWCNT sample. (a) 2.5 µm scale bar (b) with a 1 µm scale bar. 73
Figure 4.21: Thermal stability of the unreacted MWCNTs from the 1,3-dipolar cycloaddition reaction. The solid line and dashed lines represent TG and DTG curves for the MWCNT samples, respectively 74
Figure 4.22: Thermal stability of the N-Tritylglycine functionalised MWCNTs. The solid line and dashed lines represent TG and DTG curves for the MWCNT samples, respectively..... 75
Figure 4.23: ^1H NMR spectrum of N-Tritylglycine functionalized MWCNTs in chloroform.... 76
Figure 4.24: NMR spectra obtained after deprotection reaction of the trityl group after treatment with 4M HCl in dioxane 76
Figure 4.25 Confocal image of FITC functionalised MWCNTs after drying with 25µm scale bar 77

Figure 4.26: Growth curve of *S.cerevisiae* incubated with different concentrations of pristine MWCNTs to the control (incubated with no MWCNTs). 80
Figure 4.27: Growth curve of *S.cerevisiae* incubated with different concentrations of oxidized MWCNTs to the control (incubated with no MWCNTs). 82
Figure 4.28: Graph demonstrating the cell viability of *S.cerevisiae* incubated with different concentrations of pristine (P) and oxidized (O) MWCNTs to the control (incubated with no MWCNTs). Error bars represent standard deviation (SD) of two sets of triplicate data from two different experiments. 84
Figure 4.29: MEA plates showing viable and non-viable plates 85
Figure 4.30: Calibration curve representing the relation between cell counts and absorbance of *S.cerevisiae* culture 86
Figure 4.31 SEM micrographs of *S.cerevisiae* cells incubated without MWCNTs. (a) illustrating a group of *S.cerevisiae* cells (b) illustrating a single budding *S.cerevisiae* cell. .. 87
Figure 4.32 SEM micrographs of *S.cerevisiae* cells incubated with pristine MWCNTs. (a) illustrates group of *S.cerevisiae* cells where a single cell lost its intracellular content (b) illustrates group of *S.cerevisiae* cells with intact cell walls. 87
Figure 4.33. Confocal image of *S.cerevisiae* cells incubated with 20µg/ml MWCNT-FITC for 1and 1/2 hrs. (a) at a scale of 5µm (b) at a scale of 2.5 µm. 89
Figure 4.34. Confocal image of *S.cerevisiae* cells incubated with 20µg/ml FITC only for 1and 1/2 hrs at a scale of 2.5µm. 90
Figure 4.35. Confocal image of red stained membrane *S.cerevisiae* cells (a) at a scale of 10 µm (b) at a scale of 5 µm. 90
Figure 4.36: Growth curve of *S.cerevisiae* incubated with 20 µg/ml pristine, oxidized, FITC-MWCNTs and the control. 91
Figure 4.37: Optical phase contrast microscope photographs of PC12 cells (a) incubated without oxidised MWCNTs (b) incubated with oxidised MWCNTs. 93
Figure A1.1: MEA plate showing the characteristic colonial morphologies of *S.cerevisiae* 119
Figure A2.1: NMR spectra of N-Tritylglycine functionalised CNTs 122
Figure A2.2: NMR spectra of N-Tritylglycine product from Sigma Aldrich 123
Figure A6.1: TEM micrograph of pristine MWCNTs 165
Figure A6.2: TEM micrograph of 1:3 HNO_3:H_2SO_4 MWCNTs 166

Figure A6.3: TEM micrograph of pristine MWCNTs where scale bar corresponds to 0.1 µm 166
Figure A6.4: TEM micrograph of 30% HNO_3 oxidised MWCNTs with 0.33 µm scale bar..... 167
Figure A6.5. TEM image of FITC-MWCNTs with..... 167
Figure A6.6. SEM micrograph of yeast cell on bunch of MWCNTs 167
Figure A6.7: Confocal image of *S.cerevisiae* cells incubated with 20µg/ml MWCNT-FITC for 1and 1/2 hrs at a scale of 2.5 µm..... 168
Figure A6.8: Confocal image of red stained membrane *S.cerevisiae* cells at a scale of 5 µm.. 168
Figure A6.9: Confocal image of red stained membrane *S.cerevisiae* cells at a scale of 5 µm.. 169
Figure A6.10: Typical TEM image of unreacted MWCNT sample from the 1, 3-dipolar cycloaddition reaction process, with 0.5µm scale bar 169
Figure A6.11: Typical TEM image of N-Tritylglycine functionalised MWCNTs, with a 0.4 µm scale bar..... 170

List of abbreviations

a-C – Amorphous Carbon

BET- Brunauer-Emmett-Teller

CCVD – Catalytic Chemical Vapour Deposition

CFU – Colony Forming Units

^{13}C NMR - Carbon Nuclear Magnetic Resonance Spectroscopy

CNTs – Carbon Nanotubes

COOH- Carboxylic acid group

DMF – Dimethylformamide

DTG- Derivitive Weight

FITC – Fluorascine isothonayate

H^1 NMR- Proton Nuclear Magnetic Resonance Spectroscopy

LSCM – Laser Scanning Confocal Microscopy

MWCNTs- Multi-Walled Carbon Nanotubes

MEA – Malt Extract Agar

NGF – Nerve Growth Factor

NMR- Nuclear Magnetic Resonance Spectroscopy

NV – Non-Viable

O.D – Optical Density

PBS – Phosphate Buffer Saline

PC12 cells – Pheochromocytoma cells

PenStrap - Penicillin Streptomycin

RBM – Radial Breathing Mode

RPMI – Royal Park Memorial Institute

S.cerevisiae- Saccaromyces Cerevisiae

SEM- Scanning Electron Microscopy

SFCCVD – Swirled Floating Catalyst Chemical Vapour Deposition

SPC – Standard Plate Count

SPB – Spindle Pole Body

SWCNTs - Single-Walled Carbon Nanotubes

TEM- Transmission Electron Microscopy

TGA- Thermal Gravimetric Analyses

YPD - Yeast extract, Bactopeptone, and Dextrose

WFLM – Wide-Field Light Microscope

XRD – X-ray Diffraction

Preface

Chapter one gives the background and motivation of the research, the research statement, questions, aims and objectives are also included. Chapter two is dedicated to the literature review and discusses the structure, properties, synthesis and various characterisation methods of carbon nanotubes. Different purification and functionalisation methods of carbon nanotubes are outlined including applications of CNTs. A brief overview of the yeast cell line *S.cerevesiae* is given/ discussed and attention is given to toxicity studies of carbon nanomaterials as this forms the basis of the research. Chapter three describes the research methodology and the experimental procedures undertaken in the research. Chapter four dwells on the results and discussion of results associated with the CNT characterisation and toxicity results. Chapter five presents the conclusions based on the research outcomes. Recommendations for future work are given and lastly the list of references and appendices are given.

CHAPTER 1

Introduction and Background

Carbon nanotubes (CNTs) are molecular-scale tubes of graphitic carbon known to possess excellent mechanical, magnetic and electrical properties due to their unique topology and structure. CNTs have attracted intense research efforts over the past decade and have become important nanomaterial for use in a wide variety of scientific fields (Muller, et al., 2006; Zhu, et al., 2006). There has been a notable interest in the use of CNTs for biomedical applications such as therapeutic molecules in drug delivery (Bianco, et al., 2005), in medical imaging (Cherekuri, et al., 2004), and cancer treatment (Shvedova, et al., 2009; Wu, et al., 2010). With an increased production and demand for carbon nanomaterials, interaction between these carbon nanomaterials and the environment is inevitable. Toxicological information on carbon-containing particles is limited and published data on the toxic effects of CNTs are often contradictory (Warheit, et al., 2004; Cheng, et al; 2009). Some studies have indicated that CNTs stimulate the growth of cells (Mitchell, et al., 2004; Zhu, et al., 2006). Others, however, have indicated an increase in cell death and therefore could be considered as potential toxicants (Ghafari, et al., 2008; Cheng, et al., 2009). CNTs are manmade or engineered materials and therefore highlighting the urgency to investigate the interaction of CNTs with the environment (Zhang, et al., 2008). CNTs consist of one up to hundreds of concentric carbon shells (Popov, 2004). They are categorised as either Single-Walled Carbon Nanotubes (SWCNTs) or Multi-Walled Carbon Nanotubes (MWCNTs). A SWCNT is a single graphite layer rolled into a hollow cylinder either zigzag, arm chairly or chirally. A MWCNT comprises of a collection of concentrically arranged SWCNTs of varying diameters ranging between 2 and 100 nm. The length and diameters of MWCNTs differ from those of SWCNTs and hence the differences in their properties. The properties of CNTs are determined by their structural characteristics such as chirality, diameter and length (Paillet, et al., 2005).

Yeast cells are unicellular fungi ranging in size from 5 -10 μm, they are widespread in nature and exists in sea, soil and air. The advantages in using yeast cells of the species *S. cerevisiae* for toxicity investigations of nano-particles are several. They are inexpensive, and a variety of laboratory strains are readily available on the commercial market. Additionally, this species of

yeast cells have a low pathogenicity and are easily maintained in culture, than mammalian cells, requiring simple growth media of yeast extract, bactopeptone, and dextrose (YPD) (Mitchell, et al., 2004). Yeast also share all major metabolic pathways with humans and provide the advantages of a well-studied model organism. *Saccharomyces cerevisiae* is an important biological model organism used to study diverse biological processes. They are simpler and more genetically accessible eukaryotic systems as compared to mammalian cells. In addition these cells can be used as a model system for mammalian cells as they are eukaryotes (Mitchell, et al., 2004; Bai, 2007 Jensen, 2000).

Cell viability assessments are commonly used as cytotoxic indicators. The combined approach of using Electron Microscopy and cell viability assessments has proven to be an excellent tool to assess toxicity of CNTs in human macrophage cells (Cheng, et al., 2009). There is however no clear consensus in literature on the toxicity effects of functionalised or non functionalised CNTs. Studies by Lobo et al., 2008 have shown that CNTs leads to cytotoxicity effects on RPMI 1640 media in mouse fibroblast cells. On the other hand some studies by Mitchell, et al., 2004; Flahaut, et al., 2006 have adduced no toxicity of CNTs on *Saccharomyces cerevisiae* cells cultured in YPD media and human endothelial cells cultured in RPMI media respectively. Compounded to this controversy are reports on CNT that indicate adverse effects such as apoptosis on ciliated protozoa, *Tetrahymena thermophila* and human T lymphocyte cells cultured in RPMI media (Ghafari, et al., 2008; Bottini, et al., 2006).

1.1 Motivation

Many applications for carbon nanotubes (CNTs) have been proposed including as drug and vaccine delivery vehicles, biosensors and novel biomaterials. Before CNTs can be effectively integrated into new and existing biomedical devices, the toxicity of CNTs needs to be thoroughly investigated. Toxicological information on carbon nanotubes is limited and published data on the toxic effects of CNTs are often contradictory. Past toxicity assessments have differentiated between single-walled and multi-walled nanotubes, but only a few have investigated the effects of physicochemical modification (Kang, et al., 2008 ; Jia, et al., 2005; Ding, et al., 2005; Zhu, et al., 2006; Saxena, et al., 2007).

1.2 Research statement

Rapid progress in the development and widespread application of nanomaterials needs to be matched by commensurate toxicological investigations. Articles have been published on the potential health effects of CNTs with more focus on mammalian cells as opposed to fungal cells (Bottini, et al., 2005; Herzog, et al., 2007; Cheng, et al., 2009; Herzog, et al., 2009; Jos, et al., 2009; Wu, et al., 2010). Carbon nanotoxicology studies are still in its infancy and insufficient research has been conducted on direct physicochemical carbon nanotube toxicity effects on yeast. Yeast has wide industrial applications and it is imperative that toxicology studies of carbon nanotubes be conducted on yeast cells as they also share major metabolic pathways with humans.

1.3 Research questions

- Do carbon nanotubes affect the growth of *S. cerevisiae*?
- Can the growth of *S. cerevisiae* be enhanced by carbon nanotube concentration in the medium?
- Do functionalised carbon nanotubes remain in the extracellular space or penetrate into the yeast cell?
- Do unfunctionalised or functionalised carbon nanotubes pose a potential health hazard to *S. cerevisiae*?
- How does yeast cells compare to the Pheochromocytoma PC12 neuronal cells in responding to toxicity of CNTs?

1.4 Research aims

The aims of the research were as follows:

- Examine the physicochemical determinants of carbon nanotubes on *Saccharomyces cerevisiae* cytotoxicity.

- Investigate the uptake of functionalised carbon nanotubes by *S. cerevisiae* (Intracellular tracking of CNTs).
- Compare the toxicity of CNTs on: *S.cerevisiae* and PC12 cells.

1.5 Research objectives

In order to achieve the key aims this research has the following objectives:

1. To synthesise, purify and characterise the physicochemical properties of the CNTs
2. To identify and monitor *S.cerevisiae* cell growth and cell viability changes incubated with varying CNT doses.
3. To assess and compare the effect of physicochemical properties of CNTs on *S.cerevisiae* cell growth and viability.
4. To functionalise CNTs by 1,3-dipolar-cycloaddition reaction and assess cell translocation viability.
5. Cytotoxicity testing of oxidised CNTs towards PC12 neuronal cells.

This work was divided into the following areas:

1. The synthesis and characterisation of CNTs by Swirled Floating Catalyst Chemical Vapour Deposition (SFCCVD) method (Iyuke, 2005).
2. Growth and cytotoxicity studies of *S.cerevisiae* cells incubated with CNT.
3. Functionalisation and intracellular tracking of CNTs.
4. Cytotoxicity testing of CNTs with PC12 cells.

CHAPTER 2

Literature Review

2.1 Carbon nanotubes

2.1.1 Structure of carbon nanotubes

Carbon nanotubes (CNTs) are exceptional tubular structures of nanometre diameter made up of graphite sheets. CNTs can comprise of one up to hundreds of concentric shells of carbons (Popov, 2004). A SWCNT is a single graphite layer rolled into a hollow cylinder either zig-zagly, arm chairly or chirally as shown in Figure 2.1. A MWCNT consists of a collection of concentrically arranged SWCNTs of varying diameters ranging between 2 and 100 nm. The length and diameters of MWCNTs differ from those of SWCNTs and hence the differences in their properties. CNTs possess a large length to diameter ratio of approximately 1000 (Daenen, et al., 2003; O'Connell, 2006; Popov, 2004).

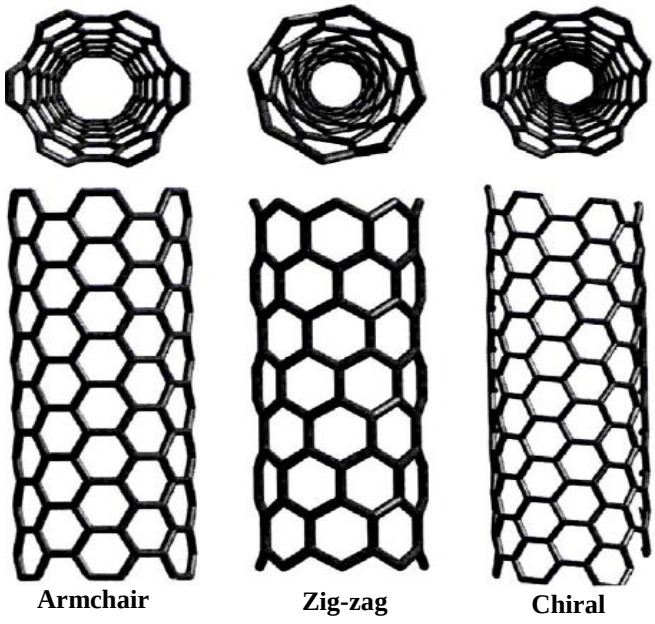


Figure 2.1: Models of 3 atomically perfect SWCNT structures (Terrones, 2003)

MWCNTs were first discovered by Iijima in 1991, who observed that nanotubes consist of several graphitic shells (Popov, 2004; Belin & Epron, 2005).

2.1.2 Properties of carbon nanotubes

Carbon is a unique light atom that can form from one fold up to threefold chemical bond. The planar threefold carbon arrangement forms graphene planes that can adopt a tubular geometry (Bhushan, 2004). CNTs are molecular-scale tubes of graphitic carbon that possess excellent and exciting properties due to their unique topology and structure. Size and shape are factors that strongly influence CNT properties (Wang et al., 2000). The properties of CNTs are determined by their structural characteristics such as chirality, diameter and length (Paillet et al., 2005). The most important properties of the CNTs include high electrical conductivity, zeta potential, tensile strength, high flexibility, elasticity, tremendous mechanical strength, low thermal expansion coefficient and they are highly adsorbent in nature.

2.1.2.1 Chemical Reactivity

Chemical reactivity of a CNT is governed by the local atomic structure and can be changed my CNT mechanical deformation (Park et al., 2003). In comparison to a graphene sheet, the chemical reactivity of carbon nanotubes is considerably increased by the nanotube surface curvature. Chemical reactivity is directly related to the pi–orbital mismatch caused by an increased curvature. The sidewall and end caps of the carbon nanotube structure have different chemical reactivity. Reactivity increases with decreasing nanotube diameter, nanotube end caps are more reactive than the sidewalls (Daenen et al., 2003). Smaller CNTs are more "strained" because they deviate further from the ideal planar structure of graphite, and are thus more reactive (Park et al., 2003).

The graphitic carbon of CNTs makes them extremely resistant to chemical attack. Oxidation studies have shown that, since the end caps are more reactive than the sidewalls, the carbon nanotubes are usually oxidised from their tips, thus, leading to the possibility of opening carbon nanotubes by oxidation methods (Ajayan, 2000). There are points in the structure of CNT which are more reactive that others, such as the more strained curved-end caps and defects due to missing carbon atoms (Park et al., 2003). Purified CNTs are likely to be more reactive as they contain additional defects in the form of carboxylic acid (-COOH) residues (Park et al., 2003). CNT vary significantly in diameter and length and depends heavily on the synthetic procedure

used. Lengths are dependent on the time of synthesis but are typically tens of microns (Park et al., 2003). Cleaned and processed CNTs are normally shorter than pristine CNTs due to the destructive conditions used in the purification process (Park et al., 2003). In studies carried out by Donaldson et al. (1992) on mouse peritoneal cavity, it was established that long fibres had a more pronounced inflammatory effect than short fibres. It is expected that CNTs will cause the same types of pathology that long fibres cause in rats and humans if their lengths are longer than 20 μm.

Compact particles such as CNTs have their harmful effects as a consequence of two factors that act together to contribute to their potential to cause harm: their surface area and reactivity or intrinsic toxicity of that surface (Tran et al., 2000). The smaller the particles are, the more surface area is available per unit mass and any intrinsic toxicity of the CNT surface will thus be emphasised (Duffin et al., 2002). Also the smaller CNTs (i.e decrease in diameter), greater the likelihood of causing harm to the lung. Functionalisation with different groups will result in different toxicity since the particle surface is important in interacting with biological systems (Park et al.,2003).

2.1.2.2 Electrical Conductivity

The electrical properties of CNTs depend on the helical angle of the rolled up graphitic sheet (Wang et al., 2000; Sinott & Andrews, 2001). CNTs with small diameters are metallic or semi-conducting depending on their diameter and chiral angle (Reich et al., 2004; Popov, 2004). Studies have revealed that all armchair tubes are metallic, while chiral and zig–zag carbon nanotubes are either metallic or semiconducting (Ajayan, 2000). In addition a high thermal conductivity, which hold promise to be used in composite materials has been found in these nanomaterials (Sinha & Yeow, 2005).

2.1.2.3 Optical Activity

CNTs show strong structured optical spectra (Reich et al., 2004). Theoretical studies have shown that the optical activity of chiral nanotubes disappears with increasing CNT diameter

(Daenen et al., 2003). Optical spectroscopy gives essential information about the physical properties of a system (Reich et al., 2004).

2.1.2.4 Mechanical Strength

Literature has showed that the mechanical properties of CNTs are determined by their structure. This is attributed to the high anisotropy of graphite (Salvetat et al., 1999). Carbon nanotubes are composed of sp^2–hybridized C–C covalent bonds which are stronger than sp^3 bonds found in diamond because of the greater s character as in sp^2 bonds. The bond strength for an sp^2 C-C covalent bond and sp^3 covalent carbon bond is 602 kJ/mol and 346 kJ/mol respectively (Cottrell, 1958). The bonding structure of CNTs is one of the strongest in nature and provides carbon nanotubes with their unique strength. Carbon nanotubes are one of the most robust and stiffest synthesized structures with a large Young's modulus, high tensile strength, and great length (Ajayan, 2000; Bushan, 2004). Carbon nanotubes have Young's moduli ranging from 1.28 to 1.8terapascal (TPa) (Poole and Owens, 2003). Young's modulus of steel is 0.21TPa, thus the Young's modulus of carbon nanotubes is almost 10 times that of steel. Strength is not the same as stiffness. Young's modulus is a measure of how stiff or flexible a material is and tensile strength is a measure of the amount of stress needed to pull a material apart. The tensile strength of carbon nanotubes is about 45 billion pascals, they are approximately 20 times stronger than steel (Poole and Owens, 2003). Their higher flexibility ensures that they do not break under distortion or upon bending (Dresselhaus et al., 1998; Salvetat et al., 1999). Composition and morphology tuning of polymer or inorganic interfaced nanostructures have shown to enhances the mechanical properties of the material (Verploegen et al., 2007).

2.1.2.5 Adsorptive Properties

SWCNTs and MWCNTs are porous in nature; pores in MWCNTs are divided into inner hollow cavities of small diameters and aggregated pores formed by interaction of isolated MWCNTs (Bhushan, 2004). Studies have shown that SWCNTs are microporous while MWCNTs are mesoporous in nature. The theoretical specific surface area of CNTs ranges over a broad scale

from 1.315 - 50 m^2g^{-1}. In SWCNT bundles, adsorption of gasses can occur inside the tubes (pores), in the interstitial triangular channels between the tubes, in the groove or on the outer surface of the bundle (Figure 2.2). In MWCNTs, adsorption can occur inside the tube, in aggregated pores or on the external walls. Theoretical calculations have determined the existence of a stronger interaction in the molecule adsorption occurring on the surface (Bhushan, 2004).

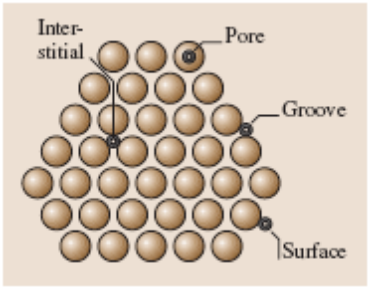


Figure 2.2: Illustration of the four different adsorption sites on a SWCNT bundle (Bhushan, 2004)

When considering adsorption on nanotubes an important problem to solve is the identification of the adsorption sites. Adsorption of gases in a SWCNT bundle can occur inside the tubes (pore), in the interstitial triangular channels between the tubes, on the outer surface of the bundle, or in a groove formed at the contact between adjacent tubes on the outside of the bundle (Bhushan, 2004). Starting from closed-end SWCNTs, simple molecules can adsorb onto the walls of the outer nanotubes of the bundle and preferably on the external grooves. For the more attractive sites, corresponding to the first adsorption stages the adsorption or condensation in the interstitial channel of SWCNT bundles depends on the size of the molecule (or on the SWCNT diameters) and on their interaction energies(Bhushan, 2004). For hydrogen and other small molecules, computational methods have shown that, for open SWNTs, the pore, interstitial, and groove sites are energetically more favourable than the surface site, with respect to the increasing number of CNTs interacting with the adsorbed molecules (Bhushan, 2004). For MWCNTs, adsorption can occur in the aggregated pores, inside the tube or on the external walls and the presence of defects, as incomplete graphene layers, has to be taken into consideration (Bhushan, 2004). Although adsorption between the graphenes (intercalation) has been proposed in the case of hydrogen adsorption in platelet nanofibers, it is unlikely for many molecules due to steric effect and should not prevail for small molecules due to long diffusion path (Bhushan, 2004). Few

studies deal with adsorption sites in MWCNTs, however it has been shown that butane adsorbs more in the case of MWCNTs with smaller outside diameters, which is consistent with another statement that the strain brought to curved graphene surfaces affects sorption (Bhushan, 2004). Most of the butane adsorbs to the external surface of the MWCNTs while only a small fraction of the gas condensed in the pores. Comparative adsorption of krypton or of ethylene on MWCNTs or on graphite has allowed scientists to determine the dependence of the adsorption and wetting properties on the specific morphology of the nanotubes (Bhushan, 2004). Higher condensation pressure and lower heat of adsorption were found on nanotubes with respect to graphite. These differences result mainly from a decrease in the lateral interactions between the adsorbed molecules, related to the curvature of the graphene sheets (Bhushan, 2004). Table 2.1 gives the adsorption properties and sites of SWCNTs and MWCNTs.

Table 2.1: Gives the adsorption properties and sites of SWCNTs and MWCNTs (Bhushan, 2004)

Type of nanotube	Porosity (cm^3g^{-1})	Surface area (m^2/g)	Binding energy of the adsorbate	Adsorption sites	Attractive potential per site (eV)	Surface area per site (m^2/g)
SWNT (bundle)	Microporous V_{micro}: 0.15–0.3	400–900	Low, mainly physisorption 25–75 % > graphite	Surface (A) Groove (B) Pore (C) Interstitial (D)	0.049 0.089 0.062 0.119	483 22 783 45
MWNT	Mesoporous	200–400	Physisorption	Surface Pore Aggregated pores	–	–

2.1.2.6 Zeta potential

Zeta potential has been applied successfully in the field of colloid science to understand and predict the control and stability of colloid systems (Lin et al., 2003). Measuring zeta potential helps in the understanding of coagulation and flocculation processes (Lin et al., 2003). From a theoretical view point, zeta potential is the potential at the boundary of the hydrodynamic shear plane of a charged particle (Daenen et al., 2003). The surface of shear envelopes the particle (Figure 2.3) and the ions associated with the particle are separated from those in the bulk phase.

The material contained within the sheath forms the kinetic unit, which enables the particle to move along with a certain quantity of surrounding liquid and its charge. Zeta potential depends on the particle surface charge, thickness of the electrical double layer and environmental conditions (pH and ion concentration) (Lin et al., 2003). It is therefore, important to always state zeta potential with medium conditions (e.g. pH, conductivity, additives and temperature) (Lin et al., 2003).

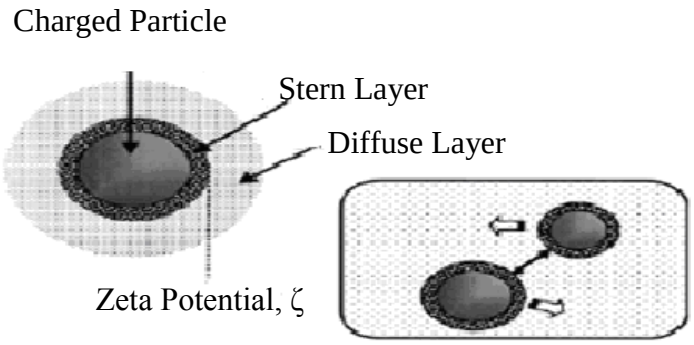


Figure 2.3: A schematic of the electrochemical double layer and zeta potential of a charged particle (Lin et al., 2003).

2.1.3 Synthesis of Carbon nanotubes

Several techniques are used to produce CNTs. Carbon nanotubes are mainly produced by the laser ablation, arc discharge, and catalytic chemical vapour deposition techniques (CCVD) (Sinnott et al., 2001). Laser ablation and electric arc are techniques used in producing CNTs from solid carbon source, while production methods such as CCVD use gaseous carbon source (Bhushan, 2004).

2.1.3.1 Laser ablation

In this method a laser beam is used to vaporise a graphite sheet in the presence of a metal catalyst (Sinnott et al., 2001). Two types of laser devices are generally utilised in this technique namely lasers that operate in a pulsed mode or lasers that operate continuously (Bhushan, 2004).

A graphite sheet containing the catalyst is put in the middle of an inert gas-filled (argon gas) quartz tube placed in an oven maintained at a temperature of 1200˚C (Bhushan, 2004). When the graphite sheet is hit by laser beam, the carbon ablates and jets out. The ablated carbon phase including the catalyst cools and crystallises into nanoparticles which grow into SWCNTs (Sinnott et al., 2001). In the absence of catalysts in the target, the soot product mainly contains MWCNTs. In the presence of catalysts SWCNTs are produced instead of MWCNTs and the SWCNT yield is dependent on the kind of metal catalyst used (Bhushan, 2004). Synthesis based on the vaporisation of a target at a fixed temperature, generally uses a continuous CO_2 laser beam (λ =10.6μm) and power can be varied from 100 - 1600 W (Bhushan, 2004). The synthesis yield is controlled by three parameters namely, the cooling rate of the medium where the active, secondary catalyst particles are formed, the residence time, and the temperature (in the 727 ºC–1827 ºC range) (Bhushan, 2004). In laser ablation technique nickel/yttrium can be used as catalyst. Laser ablation is nearly similar to arc discharge technique because the optimum background gas and catalyst mix is the same as in the arc discharge process (Daenen et al., 2003). The laser ablation technique is one of the three methods currently used to prepare SWCNTs as commercial products (Bhushan, 2004). A schematic of the layout indicating the principle of a laser ablation device is given in Figure 2.4.

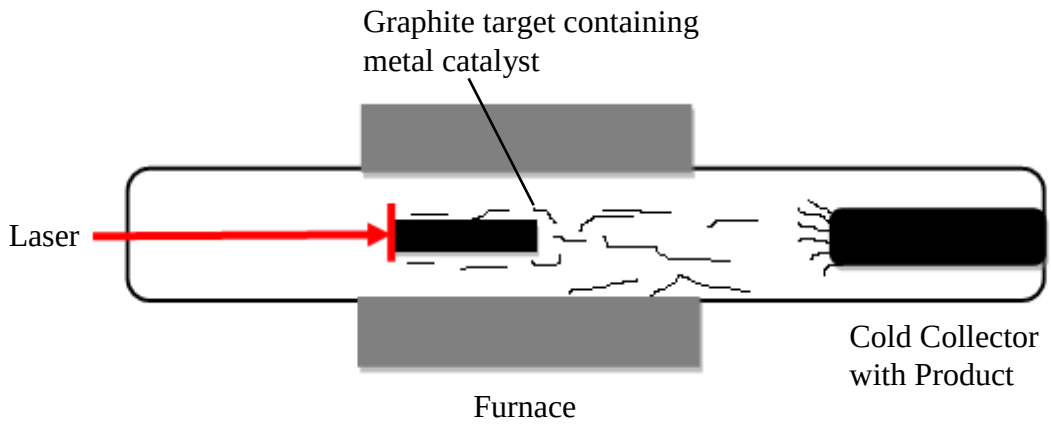


Figure 2.4: A schematic of a pulsed laser deposition reactor (Sinnot & Andrews, 2001)

2.1.3.2 Arc discharge

CNTs are created through arc-vaporisation of two carbon rods placed end to end separated by 1mm, in an enclosure filled with inert gas at a low pressure (Daenen et al., 2003). A high current electric arc is passed through graphite electrodes in the presence of catalytic particles, forming CNTs and soot (Sinnot et al., 2001). The arc discharge method is the most common and easiest way to produce CNTs (Daenen et al., 2003). The arc discharge method however, produces a mixture of compounds which requires separation of nanotubes from soot and catalytic metals (Daenen et al., 2003). The efficiency of nanotubes production depends strongly on the nature of the catalyst as well as experimental conditions (Bhushan, 2004).

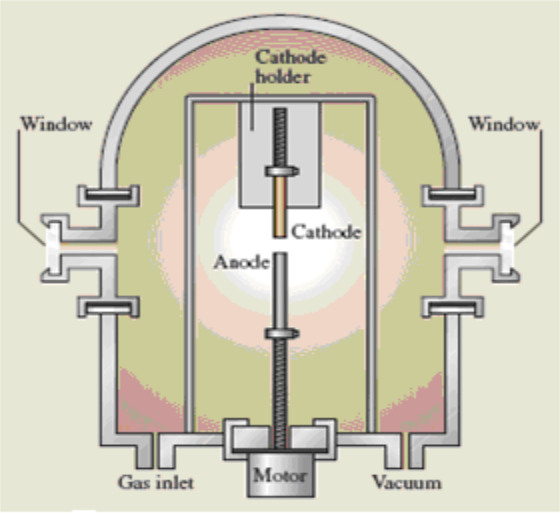


Figure 2.5: Sketch of an electric arc reactor (Bhushan, 2004)

2.1.3.3 Catalytic Chemical vapour deposition (CCVD)

CCVD is the catalytic decomposition of a hydrocarbon or a carbon monoxide feedstock, in the presence of a supported transition metal catalyst (Fe, Co, Ni) (Őncel et al., 2006). The CCVD technique is heterogeneous if a solid substrate is used and homogeneous if the catalytic decomposition takes place in the gas phase (Bhushan, 2004). CCVD synthesis is achieved by placing a carbon source in the gas phase and using an energy source, to transfer energy to a gaseous carbon molecule (Daenen et al., 2003). Generally methane, carbon monoxide, xylene, ferrocene or acetylene, are used as gaseous carbon sources (Daenen et al., 2003). The vapours

are carried into the furnace by an inert (Ar/10% H_2) carrier gas that also controls the partial pressure inside the reactor (Sinnott & Andrews, 2001). The molecule is cracked into reactive atomic carbon by the energy source (Daenen et al., 2003). The carbon then diffuses towards the catalyst coated substrate. The furnace reaction temperatures are typically in the range of 600˚C and 1000˚C (Sinnott & Andrews, 2001). CNTs will be formed on condition that proper parameters are maintained (Daenen et al., 2003). The CCVD method is a "low temperature process" compared to the laser ablation and arc discharge methods, with the formation of carbon nanotubes typically occurring between 600˚C and 1000˚C (Bhushan, 2004). Because of the low temperature operation, the selectivity of the CCVD method is better for the production of MWCNTs (Bhushan, 2004). CNTs produced by CCVD methods are normally much longer than those obtained by arc discharge (Bhushan, 2004). The CCVD method is believed to be the most suitable synthesis process for large scale production, due to its achievable high yield and high purity (Őncel et al., 2006; Iyuke et al., 2007; Mokwena et al., 2007).

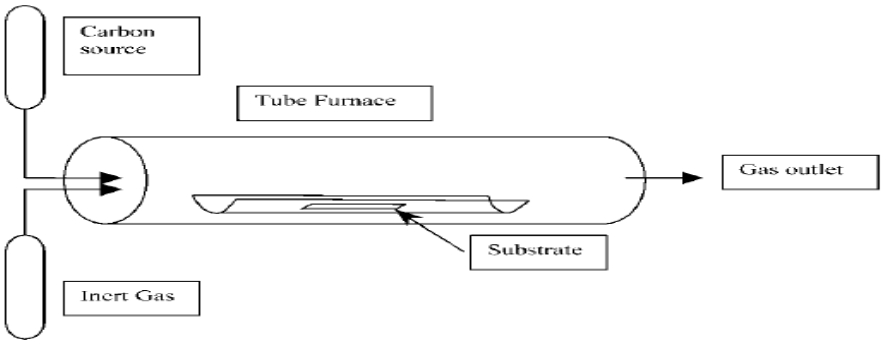


Figure 2.6: Schematic of a typical thermal CVD

2.1.4 Characterisation methods of carbon nanotubes

There are several techniques currently employed in characterising CNTs. These techniques are Raman spectroscopy, Transmission Electron Microscopy (TEM), and the Brunauer-Emmett-Teller (BET).

2.1.4.1 Raman Spectroscopy

Raman spectroscopy is an outstandingly powerful tool useful in studying the vibrational and electronic structures of materials including carbon nanotubes (Costa et al., 2008). Raman is particularly used for the characterisation of carbon nanotubes with respect to their diameters and quality of the sample properties (Costa et al., 2008). Raman spectroscopy can analyse different carbon allotropes including single-wall, double-wall and multi-wall CNTs without sample preparation (Costa et al., 2008). Raman spectroscopy is sensitive to the strengths, lengths and arrangements of chemical bonds in a material. The most significant peaks are at (see Figure 2.7): a) at about 200 cm^{-1} (low frequency peak) known as the radial breathing mode (RBM) vibrations, these peaks are characteristic of SWCNTs, whose frequencies depend on tube diameter; b) A peak found around 1340 cm^{-1}, is known as the residual ill-organised graphite peak. It is termed the D band, due to it being related to scattering from defects present in the CNT; c) a high frequency peak found between 1500 and 1600 cm^{-1} referred to as the G band which corresponds to the C – C stretching tangential mode in graphite; d) a second order mode found between 2450 and 2650 cm^{-1}, called the first overtone of the D mode, and often called the G' mode; e) between 2775 and 2950 cm^{-1} a combination of D and G modes are found. The intensity ratio I_D/I_G is normally used as an indication of the graphitic nature of CNTs (Dressalhaus et al., 2005; Holzinger et al, 2003) (where an I_D/I_G close to 1 is more graphitic and ordered while a I_D/I_G value further from one is more disordered). With Raman a reliable, fast and non-destructive analysis is possible (Belin & Epron, 2005).

Raman spectroscopy is scattering spectroscopy. Scattering involves a momentary distortion of the electrons distributed around a molecular bond. Thus, the molecule is temporarily polarized i.e a momentarily induced dipole that disappears upon relaxation and remission. While
IR spectroscopy is absorption spectroscopy and requires the vibrational mode of the molecule to have a change in the dipole moment or charge distribution associated with it.
IR and Raman spectroscopy are the most common vibrational spectroscopies for assessing molecular motion and fingerprinting species and is based on inelastic scattering of a monochromatic excitation source where the routine energy range is from 200 – 4000 cm^{-1}. Selection rules is dictated by the molecular vibrations which are probed. Symmetrical molecular

vibrations relates to Raman active modes while asymmetric molecular vibrations relates to IR active modes.

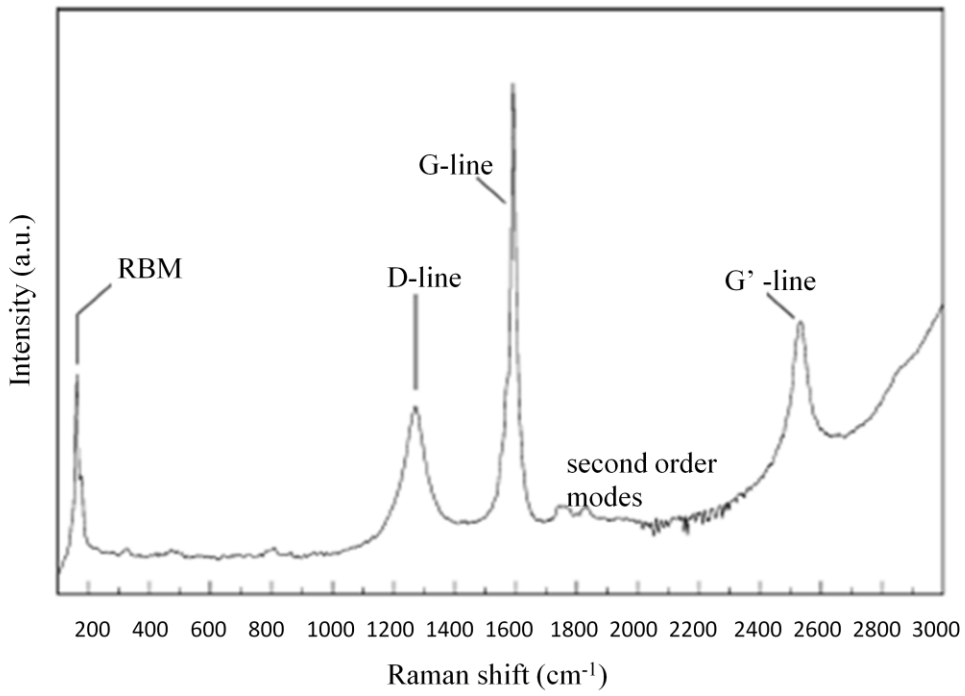


Figure 2.7: Raman spectrum showing characteristic features of CNTs: radial breathing mode (RBM), the D band, G band and G' band (Belin & Epron, 2005)

2.1.4.2 Transmission Electron Microscopy (TEM)

TEM is a powerful imaging tool to analyse CNTs at the atomic scale and provides more detailed geometrical features than SEM images (Bhushan, 2004). TEM is used to characterise the morphology (size, shape, particle arrangement) and physical properties of the CNTs (Musso et al., 2006). TEM assists in determining CNT structural quality as well as the type of contact between the CNT and the support. TEM provides information on parameters such as length, number of walls, diameter, and the nature of the CNT apex. TEM is useful in assessing the quality of CNTs.

2.1.4.3 Physisorption/ BET surface area

A gas sorption measurement (physisorption) is a characterisation technique that analyses porous material non-destructively. Specific surface area, pore volume as well as sample pore size distribution can be established by a gas sorption measurement. Nitrogen adsorption is a reliable method in characterisation of porous solids (Li et al., 2004). Pore size distribution and surface area are important properties of carbon materials (Darmstadt & Ryoo, 2008). Gas sorption (both adsorption and desorption) at the surface of a solid material is the most popular method for determining the surface area as well as the pore size distribution of porous materials (Brunauer et al., 1938; Darmstadt & Ryoo, 2008). The specific surface area of solid materials is generally determined by applying the Brunauer-Emmett-Teller (BET) equation to nitrogen adsorption data between relative pressures of approximately 0.05 and 0.3 (Darmstadt & Ryoo, 2008).

2.1.4.4 Scanning Electron Microscopy (SEM)

Scanning electron microscopy supplies valuable information on sample structural arrangement, spatial distribution, density as well as geometrical features of the sample and can produce images down to length scales of 10nm. Structural features at the 10 nm to 10μm can be analysed (Bhusan, 2004).

2.1.4.5 Thermal Gravimetric Analysis (TGA)

Thermogravimetry analysis (TGA) is the branch of thermal analysis which determines the mass change of a sample as a function of temperature in the scanning mode or as a function of time in the isothermal mode (Hatakeyama & Quinn, 1999). TGA is used to characterise material decomposition and material thermal stability under a variety of conditions and to examine the kinetics of the physicochemical processes occurring in the sample. The mass change characteristics of a material are strongly dependent on the employed experimental conditions (Hatakeyama & Quinn, 1999).

2.1.4.6 X-ray diffraction

X-ray diffraction (XRD) is a non destructive characterisation method used to probe the sample for information on the crystal structure, d-spacing, the residual stress of a unit cell, structural strain as well as sample impurities. CNT diameters and chirality distribution and various layers of MWCNT can be observed by XRD. The XRD profile is not useful in differentiating between microstructural details and graphite structure of CNTs but can assist in determining sample purity (Belin & Epron, 2005).

2.1.4.7 Nuclear magnetic resonance (NMR) Spectroscopy

NMR spectroscopy is a physical method for direct investigation of nuclear energy levels which determine molecular structure, molecular order and molecular mobility (Lui, 2008). NMR is a technique that provides unmatched information on the molecular levels of a solid (Nelson & Brammer, 2009). It is a powerful technique that can provide detailed information on the topology, dynamics and three-dimensional structure of molecules in solution and the solid state. Thus, structural and dynamic information is obtainable (with or without "magic angle" spinning (MAS)) from NMR studies of quadrupolar nuclei (that is, those nuclei with spin $S > \frac{1}{2}$) even in the presence of magnetic dipole-dipole interaction broadening (or simply, dipolar broadening) which is always much smaller than the quadrupolar interaction strength because it is a magnetic vs. an electric interaction effect (Bhushan, 2004). It is a versatile experimental tool that studies the properties of solids and molecules (Zurek & Autshbach, 2009). The value of proton nuclear magnetic resonance (^{1}H NMR) develops from its ability to reveal the different types of protons in a molecule, the relative quantities of those protons as well as details about their chemical environments (Nelson & Brammer, 2010). Carbon Nuclear Magnetic Resonance (^{13}C NMR) can be used to determine the diameter distribution of CNTs in a bulk sample and quantify the degree of fluorination (Zurek & Autshbach, 2009). It is plausible that given sufficient amount of accurate and theoretical data it might be possible to predict shapes and widths of NMR signals for different sample compositions computationally (Zurek & Autshbach, 2009).

2.1.5 Purification of carbon nanotubes

CNTs contain impurities in the form of amorphous carbon (a-C), fullerenes, graphitic carbon, and metal catalyst particles (Cao et al., 2001; Li et al., 2005; Porro et al., 2007, Zhang et al., 2007). There are two major forms of impurities in current CNT preparations namely, the metal catalyst residue and the carbonaceous component, which normally takes the form of amorphous carbon and nanographitic structures (Nelson & Brammer, 2010). Impurities found in CNTs, termed 'nanojunk', can significantly affect the properties and the use of CNTs in numerous applications (Cao et al., 2000, Chen et al., 2002, Porro et al., 2007, Pellicer et al., 2009). Metal catalyst particles remain in the tips of CNTs, synthesised via the catalytic CVD method (Porro et al., 2007). Acute toxic effects associated with CNTs have been attributed to the metal catalyst particles found in CNTs (Ballesteros et al., 2008). Consequently CNTs need to be purified before further applications and studies (Dillon et al., 1999; Zhao et al., 2006). In medical applications, metal particles constitute a toxic threat to cells; it is thus necessary that they are removed to ensure detailed characterisation of bulk properties of CNTs (Ballesteros et al., 2008).

Several CNT purification techniques have been developed. CNT purification techniques include acid treatment, base treatment, oxidation, refluxing, filtration, functionalisation, and centrifuging (Nelson & Brammer, 2009). Variations in parameter conditions, such as acid concentration, time and temperature, as well as combination of treatment techniques, influence the overall quality and efficiency of the employed purification technique.

CNT purification methods are classified into three groups, namely physical, chemical, and a combination of the two (Hou et al., 2008). Chemical purification methods effectively remove amorphous carbon and metal particles but moreover influence the CNT structure due to oxidation (Hou et al., 2008). The physical methods do not involve oxidation and as a result they do not damage the CNT structure. The physical method generally removes graphitic sheets, aggregates and carbon nanospheres; however it is time consuming and it can therefore be considered to be an ineffective and inefficient purification method (Hou et al., 2008).

Wet acid treatment typically, removes the metal catalyst and is often employed as a first step purification procedure (Hurst et al., 2008). Dissolving CNTs in nitric acid is known to be

effective in dissolving metal particles (Chen et al., 2002; Hernadi et al., 1996). Nitric Acid purification is a commonly employed purification technique; various authors have employed this technique (Dillon et al., 1999; Pellicer et al., 2009; Zhoa et al., 2006). 30% HNO_3 purification is known to be a mild and effective purification technique, resulting in no CNT structural damage (Cottoeue et al., 2003; Hernadi et al., 1996). 1:3 parts HNO_3/H_2SO_4 purification treatment is commonly employed, studies of these acid treatment results have been reported by Biro, et al. (2004), Zhang, et al. (2007), Chattopadhyay, et al. (2002) and have been shown to be effective in removing both amorphous carbon and catalyst metals contained in CNTs. Purification of CNTs, removal of carbonaceous impurities and elimination of the catalyst remains a challenge (Colomer et al., 1999; Feng et al., 2008; Hurst et al., 2008) as effective removal of impurities from CNTs without structural damage is nearly impossible (Cao et al., 2001; Porro et al., 2007; Hurst et al., 2008).

2.1.6 Functionalisation of CNTs

Functionalisation of carbon nanotubes is essential for the integration of these materials into different systems for technological, biological and biomedical applications (Pastorin et al., 2006). CNTs can be covalently functionalised with reactive species such as nitrenes, radicals and carbenes which enhances their solubility in a wide range of solvents (Holzinger et al., 2003; Pastorin et al., 2006). By functionalising CNTs their surfaces are chemically modified to enable further conjugation of more complex molecules for optimal performance (Poplawska et al., 2010). Chemically modified CNTs can be easily fixed onto a surface via chemical bonds from the surface to the nanotube (Dettlaff-Weglikowska et al., 2002). Various attempts have been made to explore their applications including carriers for drugs, genes, and proteins, contrast agents for bioimaging and biosensors (Hu et al., 2009). Integration of other functional agents such as drugs, proteins and genes can also be implemented to endow the CNTs with multifunctions and applications. The molecules can be physically adsorbed or chemically immobilised into the porous structures or onto the surfaces of the colloidal particles, making CNTs more compatible with the organisms (Hu et al., 2009).

The most common means of pre-functionalisation is acid oxidation. The oxidation/ purification procedure modifies the surface with carboxylic groups which can be used for further coupling (Poplawska et al., 2010, Xue et al., 2010).

CNTs can be functionalised in two ways either covalently or non-covalantly.

2.1.6.1 Covalent functionalisation of CNTs

Covalent functionalisation of CNTs allows functional groups to be attached to the tube end or side walls, and form sp^3 carbon sites on the tubes (Lui, 2008). End wall covalent functionalisation occurs on the open tube ends. Functionalisation with different amines has been investigated to obtaining soluble CNTs, via covalent bonds.

2.1.6.2 Non- covalent functionalisation of CNTs

Non covalent functionalisation is a widely used approach to exfoliate bundles and prepare individual CNTs. Non-covalent functionalisation includes functionalisation with surfactants, with polycyclic aromatic compounds, with polymers and bimolecules (Lui, 2008).

2.1.7 Applications of CNTs

Since the discovery of CNTs the properties, separation and potential of these fascinating systems have been studied intensely (Zurek & Autschbach, 2009). The versatility of CNTs have resulted in a wide range of proposed applications such as, electron field emitters, artificial muscles, Schottky diodes, molecular transistors, magnetic tips for magnetic scanning probe microscopy and as DNA and protein sensors (Zurek & Autschbach, 2009). CNTs have been shown to possess great potential as superior adsorbents for the removal of organic and inorganic pollutants such as dioxin (Rao et al., 2007). Other applications include ultrastrong fibres for nanostructured

composite materials, hydrogen storage for fuel cells, circuit elements in molecular electronics, and light sources for field emission displays (Nelson & Brammer, 2009).

2.2 The Yeast Cell

2.2.1 *S. Cerevisiae* cell characteristics

Yeast cells are unicellular fungi ranging in size from 5 -10 μm, they can be cylindrical, spherical or oval in shape. Yeasts are important for their ability to ferment carbohydrates within various substances (Lewis & Enevoldsen, 1972). In nature yeast exists on plants and in soil and has been used prehistorically in the making of wines and bread. Today yeasts are used industrially in various fermentation processes, as a vitamin source, as feeds and foodstuffs and are used in the production of numerous steroid hormones and antibiotics. Pure yeast cultures are grown in a medium containing nitrogen sources, sugar, minerals and water. Yeasts are fast growers and usually divide every few hours. Majority of cultivated yeasts belong to the genus *Saccharomyces*. Yeasts normally referred to as brewer's yeasts are strains of *S. cerevisiae* and have been widely used for the production of ethanol. *S. cerevisiae* is the most ideal eukaryotic model organism in biological studies and is commercially significant among the yeasts (Rosa & Péters, 2006). Most yeasts are recognised as safe, they are easy to be modified genetically and undergo easy separation in downstream processing. *S. cerevisiae* is the most studied of the simple eukaryotes and is the first eukaryote to have its genome fully sequenced and its physiology and genetics thoroughly characterised (Rosa & Péters, 2006). The completed yeast genome sequence made it possible for the development of numerous novel tools for analysing all molecular components of the cell and their interactions (Scherens and Goffeau, 2000). Yeast gene genetics is an essential part of individuals working with higher eukaryotes and has become very useful as a reference towards the sequencing of human and other higher eukaryotic genes (Mitchell, et al., 2004). *S. cerevisiae* now serves as a model organism for interpreting and understanding eukaryotic cell function such as human DNA sequences (Bostein et al., 1997). Yeasts have the advantage of fast growth, ease of genetic manipulation, abundance of metabolic activities and safety. These characteristics of yeasts are used in the food, chemical and pharmaceutical industries (Rosa & Péters, 2006).

2.2.2 Yeast cell cycle

If eukaryotic cells are supplied with sufficient nutrients and growth is not inhibited in any way, cells continuously increase in size and undergo cell and nuclear division at intervals characteristic of the species (Carlile & Watkinson, 1996). Yeasts typically grow by a repeated budding process, producing cells of single colonies (Deacon, 2006). As shown for *Saccharomyces cerevisiae* in Figure 2.8, in each sequence of the yeast cycle a young bud emerges from a predictable point on the mother cell, the bud grows apically (Deacon, 2006). Between consecutive cell divisions, events occur in a regular sequence resulting in a cell cycle divisible into four phases, G1, S, G2 and M (Carlile & Watkinson, 1996; Irons, 2008; Deacon, 2006). S (synthesis) and M (mitosis) indicate phases characterised by major nucleus events, and phases G1 and G2 are the intervals between S and M (Carlile & Watkinson, 1996). At its fastest, the cycle takes approximately one and a half hours in *S. cerevisiae*, but the time can vary widely depending on the availability of nutrients (Deacon, 2006). The most important checkpoint in the cycle is the point termed 'start'. At this stage the cell integrates all the information from environmental and intracellular signals and determines whether the cell cycle will continue or enter the stationary phase or undergo sexual reproduction (Deacon, 2006; Carlile & Watkinson, 1996).

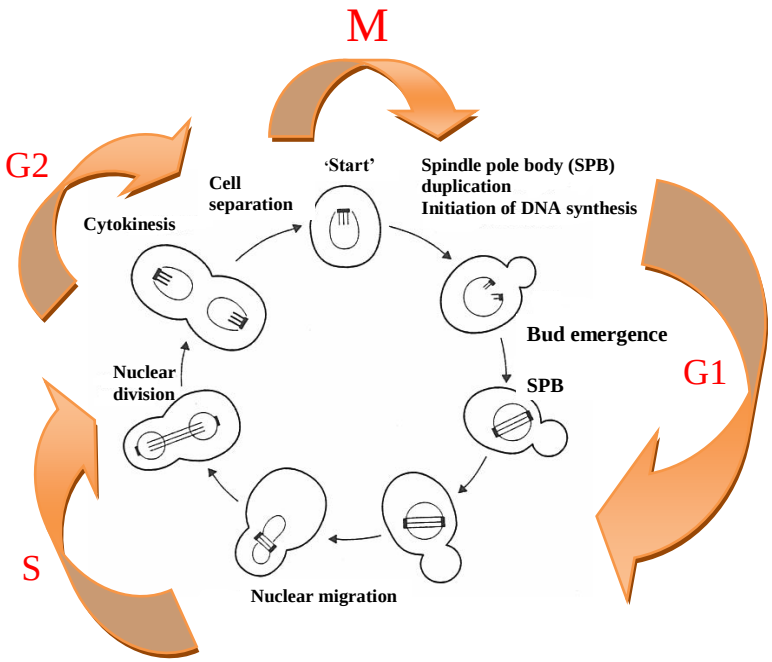


Figure 2.8: Life cycle of the budding yeast *Saccharomyces cerevisiae*

2.2.3 Cell growth

When a liquid nutrient medium is inoculated with a seed culture, the organisms selectively take up nutrients from the medium and convert them into biomass (Shuller & Kargi, 1992). A typical batch curve (Figure 2.9) indicates the phases of a batch curve namely; lag phase, exponential or logarithmic phase, stationary phase, and death phase (Shuller & Kargi, 1992; Carlile & Watkinson, 1996; Alcamo, 2001; Mitchell et al., 2004).

- **Lag phase**

The lag phase commences immediately after inoculation and it is a period where the cells adapt to the new environment (Shuler & Kargi, 1992). Microorganisms reorganise their molecular constituents when they are transferred to a new medium. There is no significant increase in cell numbers with time and therefore little or no reproduction occurs in this phase. Instead, the cells grow in size synthesising enzymes and incorporating various molecules from the medium (Alcamo, 2001; Mitchell et al., 2004). High metal ion composition, a low oxygen supply and accumulation of inhibiting metabolic products may contribute significantly to a longer lag phase prior to growth and later to a lower growth rate (Lewis & Enevoldsen, 1972; Emeis, 1965).

- **Exponential or Logarithmic phase**

After the lag phase the population enters an active stage of growth known as the logarithmic or exponential phase (Alcamo, 2001). At this stage, cells have adjusted to their new environment (Shuller & Kargi, 1992). The mass of each cell increases rapidly and is followed by reproduction (Alcamo, 2001; Shuller & Kargi, 1992). As each generation time passes, the number of cells doubles and the graph rises in a straight line if logarithms of the numbers are taken (Alcamo, 2001). Yeast cell numbers increase by a budding process; where a mother and daughter cell take the place of a single cell (Lewis & Enevoldsen, 1972).

- **Stationary phase**

This phase is characterised by the equilibrium of the growth and death rates. The cells remain metabolically active despite a zero net growth (Shuller & Kargi, 1992).

- **Death phase**

The death phase follows the stationary phase. In this phase the number of dying cells exceeds the number of new cells formed (Alcamo, 2001). Apoptosis is a form of cell "suicide" whereby the cell decides its own fate by activating a genetic programme of cell death. While, necrosis is a passive uncontrolled form of cell death often observed in response to a toxic insult, apoptotic cell death is characterised by classical morphological hallmarks such as cell shrink-age, plasma membrane blebbing and chromatin condensation. This can be contrasted to necrosis which is the form of cell death observed in response to many acute noxious stimuli and is a passive phenomenon associated with an increase in cell volume, swelling of intracellular organelles and membrane blebbing, with the eventual lysis of the cell. The biochemical mechanisms involved in apoptotic cell death are not fully understood. The nuclear changes observed in apoptotic cells are often accompanied by cleavage of the DNA into oligonucleosomal fragments which can be visualized as a DNA "ladder" when separated by conventional gel electrophoresis. This oligonucleosomal laddering of DNA is a phenomenon not usually seen in necrotic cell death and is considered a biochemical hallmark of apoptosis. Biochemical evidence of apoptosis should be accompanied by morphological and ultrastructural studies. Although it is known that neuronal cell death during development occurs by apoptosis, the mechanisms underlying neurotoxin-induced neuronal cell death remain poorly understood (Walkinshaw & Waters, 1994).

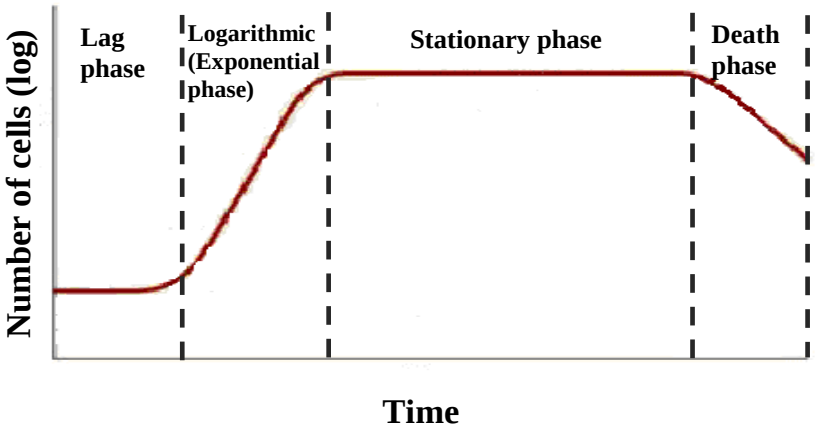


Figure 2.9: A typical cell growth curve

Growth is the most essential response of a cell to their physicochemical environment as a result of replication and changes in cell size (Shuller & Kargi, 1992). Failure in cell growth can result in loss of cell viability and subsequently autolysis may occur (Ryder et al., 1983).

2.2.4 Measurement of microorganism growth

Growth of unicellular organisms such as yeasts and bacteria refers to an increase in the number of individuals or in cell mass. Microorganism growth can be measured in a number of ways. The easiest and most widely used method is to measure the increase in turbidity of the broth culture over a time period using a spectrophotometer, nephlometer or a colorimeter. The higher the number of cells, the higher the turbidity value (light scattering).

A spectrophotometer measures the amount of light transmitted (T) or absorbed (A); a monochromatic beam is transmitted through the liquid culture. Transmittance is defined as the ratio of the transmitted light to the incident light which is measured using a blank sample. The cells suspended in culture solution may preclude the passage of light and thereby affect its transmission. The intensity of transmitted light energy through the culture solution as well as that of the incident light are measured on a photoelectric cell and converted to electrical energy which is recorded on a galvinator as 0% - 100% T at a power rating of 20 Watts. The density of the cell suspension is expressed as absorbance or as optical density (O.D.) rather than %T. O.D.

is directly proportional to the concentration of cells, while % T is inversely proportional to the concentration of suspended cells. In other words, as culture turbidity increases, O.D increases and %T decreases, indicating a growth of cell population in the culture (Cappiccino & Sherman, 1983). It is important to use an absorption that is unique to the cell, it must be free of absorptions from other molecules in the vicinity of the wavelength maximum as this will add experimental errors. The absorption wavelength is determined by doing a wavelength scan on a UV-vis spectromer. The maximum wavelength point is the transmission at which the absorbtion is measured (Cappiccino & Sherman, 1983).

The schematic diagram of the UV-vis spectrophotometer (wavelength of 600 nm for yeast cells) is shown in Figure 2.10. In Figure 2.10 a light source is imaged upon the sample and a fraction of the light is transmitted or reflected from the sample. The light from the sample is imaged upon the entrance slit of the monochromator which separates the wavelengths of light and focuses each of them onto a photodetector. The light-sensitive detector follows the sample chamber and measures the intensity of light transmitted from the cuvettes and passes the information to a meter that records and displays the value to the operator on an LCD screen

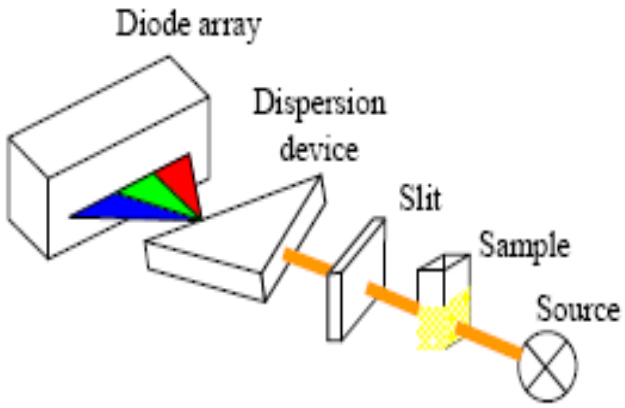


Figure 2.10: Optical density measuring technique (Jomdecha & Prateepasen et al., 2006)

2.2.5 Yeast cell viability

Viability refers to whether a yeast cell population is 'alive' or 'dead'. 'Live' cells are defined as having the ability to grow and proliferate (Heggart et al., 1999). This characteristic is usually evaluated based on the ability of cells to grow and produce macro-colonies on agar plates or micro-colonies on media covered microscope slides (Heggart et al., 1999). There are several methods of viability determination; some commonly used methods are the staining method and the cultivation or cell replication method.

2.2.5.1 Cell replication based methods

Cell replication methods for yeast viability evaluations are based on the ability of cells to reproduce if viable. The two methods which are based on the replicative ability of microbial cells are the standard plate count technique (SPC) and the slide count technique.

2.2.5.1.1 Standard plate count technique

The plate count which involves the growth of yeast cells on nutrient agar plates is one of the most common methods used in research laboratories and in quality control to estimate yeast viability (Heggart et al., 2000). Results of this method are normally expressed as colony forming units (CFU) per millilitre, with the assumption that each colony originated from a single yeast cell. The SPC or viable plate technique is sensitive and has the advantage of only counting living cells and is more cost effective in comparison to other methods. Regrettably it takes a longer time to obtain quantitative results, up to 2-4 days (Imai et al., 1993; Heggart et al., 2000).

2.2.5.1.2 Slide count technique

This method involves the layering of thin film agar on a microscope slide and overlaying a dilute suspension of yeast cells. Cells are then covered with a cover-slip and incubated at room temperature for about 18 hours or less. After incubation, percentage viability is microscopically

determined by counting microcolonies. (Heggart et al., 1999). Both the cell-based replication methods (SPC and slide count techniques) give direct indication of yeast cell proliferation capabilities. The plate count however remains a standard procedure for measuring viability because of its simplicity (Heggart et al., 1999). Yeast and bacterial cells grow best at temperatures 27 – 37˚C carefull attention should be given to operating at temperatures above this range as this may result in cell death. Operating within this temperature limit does not affect cell viability, operating at temperatures below this range decreases cell growth but does not affect cell viability.

2.2.5.2. Methods based on staining

Generally viability stains do not depend on the yeast cell's ability to divide but rather rely on the permeability of the cell membrane as well as the activity of the intra-cellular enzymes. The staining methods are often based on the membrane's ability to exclude the penetration of the dye and the dye's ability to penetrate into the cytoplasm of a dead or dying cell (Heggart et al., 2000). Colourisation of yeast cells by vital stains involves the penetration of dye into the cytoplasm where live cells either metabolically convert dye to a colourless form, while dead cells remain coloured or live cells chemically modify the stain producing a colour change (Heggart et al., 2000). Two categories of vital stains exist namely brightfield and fluorescent stains. The staining method is simple and results are obtained instantly, this method however only distinguishes between dead and living cells and accurate determination of differences in the ability of cells to proliferate is difficult, also lightly stained cells are difficult to interpret (Imai et al., 1993; Heggart et al., 1999).

In the staining method methylene blue or fluorescein diacetate are used to stain the cells. The methylene blue stained method correlates poorly with other viability evaluation methods, such as the plate count methods and often overestimates live cell populations when actual viability drops below 90% (Heggart et al., 1999). Obtaining a true representative of yeast's viability status is however restricted by the limits of the method of the employed measurement (Heggart et al., 1999).

2.3 Cell imaging techniques

In the biomedical sciences, confocal microscopy is mainly applied for the imaging of fixed or living tissues that are fluorescently labelled. Confocal microscopy has the advantage over conventional light microscopes by providing an increased resolution and thus eliminating the interference between fluorescence and resolution of structures that are in focus (Paddock, 1999). The resolution attained by laser scanning confocal microscopy (LSCM) (1500 – 2000 X) is slightly greater than that attained by conventional wide-field light microscope (WFLM) (100X) but less than that attained by transmission electron microscopy (TEM) (500 000 X). This bridges the gap between these two microscopic methods (WFLM and TEM) (Paddock, 1999).

Image formation in a confocal microscope differs fundamentally from that in a WFLM. In a WFLM the specimen is bathed in light from a xenon or mercury source and can directly be viewed by the eye. While the illumination in a confocal microscope is achieved by scanning focused beams of light (normally from a laser) across the specimen. The confocal approach has facilitated the imaging of live specimens, improved the images of multi-labelled specimens and enabled the collection of three dimensional specimen data (Paddock, 1999).

The LSCM is built around a conventional light microscope but uses a laser as opposed to a lamp as a light source, sensitive photomultiplier tube detectors and a computer to control the scanning mirrors and to facilitate collection and to display the image. A valuable feature of most LSCMs is the ability to zoom an image using the same objective lens with no loss of resolution (Paddock, 1999). Confocal microscopy is fairly easy to operate and has become an integral part in multi-user imaging facilities.

2.4 The Pheochromocytoma PC12 Cell

Pheochromocytoma (PC12) cells are derived from a spontaneous rat adrenal medullary tumor and were established as a cell line by Greene and Tischler in 1976. Undifferentiated PC12 cells multiply logarithmically and they resemble cells of late embryonic rat adrenal medulla in their ability to synthesise, store, and secrete dopamine and acetylcholine in response to calcium influx during depolarization (Gormand, 2008).

PC12 cells have been widely used to study responses of differentiated neuronal cells because they respond to nerve growth factor (NGF) by undergoing differentiation into a sympathetic-like neuronal phenotype. Differentiated PC12 cells have many of the properties of post-mitotic sympathetic neurons-they stop dividing, grow extensive neurites and become electrically excitable (Walkinshaw & Waters, 1994).

2.6 Toxicity of carbon nanoparticles

In a study done by Ghafari, et al. (2008); they investigated the impact of carbon nanotubes on the ingestion and digestion of bacteria by ciliated protozoa. To fully demonstrate the different modes of impact in cell behaviour change to cell death, the ciliated protozoan *Tetrahymena thermopile* was exposed to a wide range of single-walled carbon nanotube concentrations ranging from 0 - 17.2 μg/ml. Oxidised SWCNTs were used to ensure that the nanotube impacts were studied without the interference of surfactants. The SWCNT lengths were mainly < 500 nm with diameter sizes ranging from 2 to 10 nm. The *Tetrahymena* cultured in Osterhout's containing SWCNTs, were monitored over a 3 day period with a phase contrast video microscopy. At SWCNTs concentrations of < 6.8 μg/ml, no loss of cell viability after 3 days was observed. At a concentration of 11.9 μg/ml, control cultures remained healthy for 72 hrs but thereafter, cell aggregation, matrix accumulation, cell death and diminished cell mobility was observed. It was also found that SWCNTs could enter the ciliated protozoan, and concluded that cell death, aggregate size and loss of mobility increases with increasing SWCNT concentration and that nanomaterial can be considered as potential toxicants.

Mitchell, et al. (2004) investigated the toxicity effects of nanoparticles in *S. cerevisiae*, by using gold and silver colloids. In the study, the effects of 13nm Au colloid and 10nm Ag colloid on the growth of yeast species *S. cerevisiae* were compared to control samples, cultured in a growth media of yeast extract, bactopeptone, and dextrose (YPD). Growth curves as a function of time were generated for various conditions, by using a UV-Vis spectroscopy ($OD_{600\ nm}$). To ensure a maximum number of viable young cells, a yeast cell culturing time of 15 hrs was selected. The analysis of the yeast growth cycle began from the lag phase. It was found that the lag phase for *S. cerevisiae* occurred at the optical density at 600 nm less than or equal to 0.2. Throughout the

study the optical density was maintained between 0.09 and 0.1 $OD_{600\ nm}$ before exposing cells to the metal variables as well as at the beginning of each experimental run. From the experiments it was observed that cell growth was enhanced at low concentrations of Au (< 3.6×10^{-4}M Au), while at high levels of Au (9.1×10^{-4}M -1.5×10^{-3}M), growth decreased below the level of the control. The authors concluded by stating that metals at lower concentrations have no significant effect on the growth of *S. cerevisiae*, but also admit that results are limited by incomplete data for Ag colloids and time constraints which did not allow experiments to be repeated.

Maynard, et al. (2004) suggested that CNT toxic properties are similar to those observed for other fibrous particles such as asbestos due to its low solubility in aqueous media. This has led to an increase in pulmonary toxicity studies of carbon nanotubes on animals. Lam, et al. (2004) also investigated lung toxicity of unpurified single walled carbon nanotubes in mice and concluded that if carbon nanotubes reach the lungs, they could be more toxic than carbon black and quartz. While carbon nanotube toxicity studies on guinea pigs conducted by Huczko, et al. (2001) found no pulmonary changes after 4 weeks and concluded that carbon nanotubes are unlikely to be associated with health risks.

Toxicity studies of CNT properties upon treatment or functionalisation have shown to have an altering effect. Work done by Kang, et al. (2008) compared the toxicity of commercially obtained MWCNTs before and after physicochemical modification (via common purification and functionalisation routes and annealing) on a bacterial system. In their work *Escherichia coli* (*E.coli)* K12 cells were grown in LB medium at 37˚C and were harvested at midexponential growth phase. Conclusive toxicity studies were done which included assays for both cell membrane integrity and cell metabolic activity. Results demonstrated a correlation between bacterial cytotoxicity and MWCNT physicochemical properties. They observed higher toxicity with MWCNTs that were uncapped, short, debundled an dispersed in solution. They concluded that physicochemical modifications of MWCNTs alter their cytotoxicity in bacterial systems and underlined the need for carefull documentation of physical and chemical characteristics when reporting the toxicity of carbon-based nanomaterials. Zhang, et al (2008) showed that acid treated MWCNTs and SWCNTs have an increased effect on cell toxicity in human cervical carcinoma HeLa cells as compared to the untreated CNTs. Bottini, et al (2006) compared the

toxicity of pristine MWCNTs to oxidised MWCNTs on human T lymphocyte cells. To evaluate the effects of MWCNTs on cell viability the Trypan Blue exclusion assay was utilised. They found oxidised MWCNTs to be more toxic than pristine MWCNTs and to induce massive loss cell viability through programmed cell death at dosses of 400 μg/ml. They concluded that there is a high probability for CNTs to be toxic at sufficiently high concentrations and stressed the importance that toxicity studies be undertaken in conjunction with nanomedical applications of CNTs.

Cheng, et al (2009) tested the toxicity of MWCNTs in human macrophage cells using imaging and the standard spectrophotometric assay. Cells were exposed to both purified and unpurified MWCNTs. The study found a decrease in cell viability in cells exposed to unpurified MWCNTs due to necrosis. Cells were exposed to both purified MWCNTs and Fe_2O_3 (the main contaminant in CNTs), they found that toxicity was only yielded by the former. They suggested that MWCNTs may cause mechanically pierce through the plasma membrane and result in oxidative stress and cell death. Herzog, et al (2009) studied the toxicity effect of SWCNTs in human lung epithelium *in vitro*. Toxicity of SWCNTs dispersed in cell culture medium were compared to that of SWCNTs dispersed in dipalmitoylphosphatidylcholine (DPPC). The results of the study revealed that SWCNT samples dispersed in culture medium suppress inflammatory responses of A549 and NHBE cells while SWCNT dispersed in DPPC lead to an increase in particle toxicity.

CHAPTER 3

Materials and Methods

3.1 Production of carbon nanotubes

Materials used for the production and purification of MWCNTs are, ferrocene, sulphuric acid and nitric acid supplied by Merck Chemicals, Gauteng, South Africa. A list of chemicals used in the dissertation is listed in Appendix A1. The method used to produce MWCNTs was reported by Makwena, et al. (2007), Iyuke, et al. (2007) and Abdulkareem, et al. (2007), and is termed Swirled Floating Catalyst Chemical Vapour Deposition (SFCCVD). The apparatus used for the MWCNT production is schematically represented in Figure 3.1. It consists of a vertical silica plug flow reactor that is immersed in a furnace with a temperature regulator. Valves, rotameters and pressure controllers were connected to the equipment. The reactor is connected to a condenser that leads to two delivery cyclones where the product (MWCNTs) are collected. Nitrogen was turned on to purge the system of any impurities, thereafter the reactor and ferroncene heater were switched on while nitrogen was running. At a reactor temperature of 300˚C nitrogen was turned off to prevent it from reacting with oxygen. MWCNTs were prepared by the catalytic decomposition of acetylene in argon gas flow using ferrocene as the catalyst. The production of nanotubes was carried out at a reactor temperature range of (700 – 900) ºC and ferrocene heater at 150˚C with one hour reaction time using acetylene flow of 100 ml/min. After reaction, the system was cooled down to room temperature and the product was characterised and analysed by Transmission Electron Microscopy (TEM), physisorption/ desorption (BET), Raman Microspectroscopy, Surface Electron Microscopy (SEM) and Thermal Gravimetric Analysis (TGA).

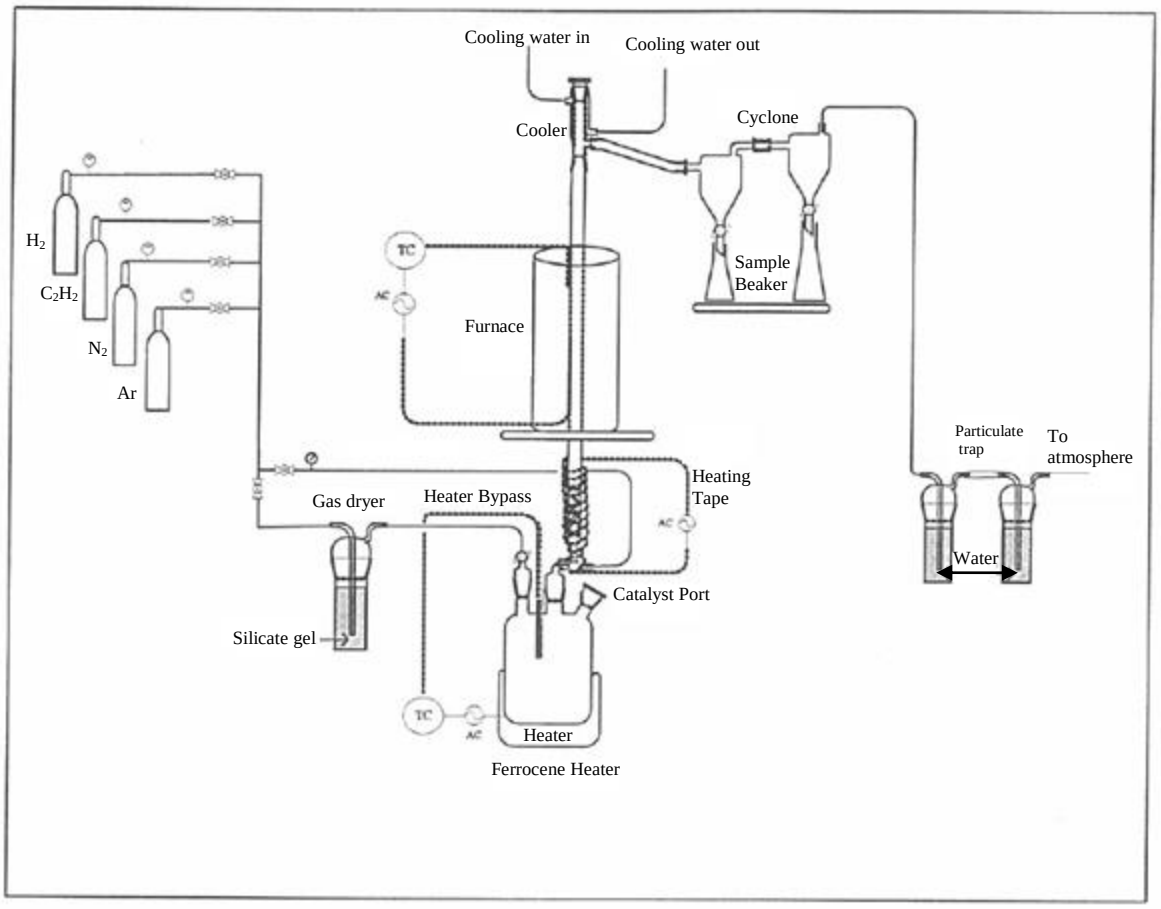


Figure 3.1: Apparatus and SFCCVD Reactor used to produce the MWCNTs (Iyuke, S. S.A. Patent 2101,2005,03438, 2005)

3.2 Purification or Oxidation of carbon nanotubes

MWCNTs produced by CVD method contained impurities such as amorphous carbon, catalyst particles and related graphitic particles. These impurities influence the properties of MWCNTs adversely and require purification before further use. Two different purification or oxidation procedures were followed namely, a mild acid treatment and a concentrated acid treatment.

Mild Acid Treatment

1g of pristine MWCNTs were suspended in 50 ml of a 30% nitric acid mixture in a 250 ml beaker and was stirred (100 rpm) for 2hrs at room temperature. This was done to remove most of the metal catalyst particles and to increase the functional groups on the MWCNT surface. After 2hrs, the suspension was filtered and rinsed with copious amounts of distilled water until the pH of the suspension reached 7.0. The rinsed MWCNTs were collected and finally dried in an oven at 120ºC for 24hrs. After 30% HNO_3 acid treatment the average diameter decreased by 20%.

Concentrated Acid Treatment

1g of pristine MWCNTs were suspended and stirred in 50 ml mixture of sulphuric acid and nitric acid, in a 3:1 (v/v) ratio ($3H_2SO_4$:HNO_3, 98% and 50%, respectively) for 2hrs at room temperature. After 2hrs the resultant MWCNT-suspension was filtered and washed with distilled water until the pH reached 7. The filtrate was finally dried in an oven at 120ºC for 24hrs. After the concentrated acid treatment process, the average MWCNT diameter decreased by 9%.

3.3 Characterisation of carbon nanotubes

3.3.1 Transmission Electron Microscopy

The morphology of oxidised MWCNTs were analysed using a JEOL JEM-100S Transmission Electron Microscope. MWCNT samples were prepared for TEM analysis, by placing approximately 0.5 mg of MWCNTs into ependorf tubes containing 1 ml methanol. Ependorf tubes containing MWCNTs and methanol were sonicated for 10 min to ensure a homogeneous dispersion of MWCNTs is obtained. After sonication, MWCNTs were placed onto a coated copper grid using a pipette and dried in air prior to direct imaging.

3.3.2 BET analysis

Approximately 0.3 g of sample were degassed in N_2 at 150 °C for 4 hours prior to analysis using a Micromeritics Flow Prep 060 sample degas system. The surface area and pore size distributions were then obtained at -196 °C. The pore size distribution with specific surface areas of the samples, were determined via N_2 adsorption or desorption according to the BET method using a Micromeritics Tristar, surface area and porosity analyser. In order to confirm the accuracy of the results, the analysis was repeated at least twice for all samples.

3.3.3 Raman Spectroscopy analysis

The Raman spectra of MWCNTs were recorded on a Bruker Senterra dispersive Raman microscope. MWCNT samples were placed in glass cuvettes and were excited with an argon ion laser at 514.5 nm excitation using a 50× objective lens.

3.3.4 Thermogravimetric Analysis

The thermal stability of MWCNTs was performed at a heating rate of 10ºC/min in air using a Perkin Elmer TGA 4000 Thermogravimetric Analyser with a final set point temperature of 900˚C.

3.3.5 Scanning Electron Microscopy (SEM)

Scanning Electron Microscopy analyses were performed on a JEOL 840 electron microscope operated at 10 kV. Scanning Electron Microscopy was used to investigate the nanoscale structure of the MWCNTs.

3.4 Functionalisation of carbon nanotubes

Pristine MWCNTs were mildly oxidised prior to functionalisation to introduce carboxylic groups (-COOH), and this mild oxidation is referred to as pre-functionalisation of MWCNTs, which is

described in section 3.3. 1g of MWCNTs was treated with 30% nitric acid and the mixture was stirred for 2 hours, before washing with distilled water and drying in the oven. The oxidation procedure modifies the surface with carboxylic groups which are required for further coupling (Poplawska et.al, 2010).

3.4.1 Functionalisation of oxidised MWCNTs with thionyl chloride

500 mg of pre-functionalised MWCNTs (MWCNT-COOH) were dispersed in 5 ml dimethylformamide (DMF) and sonicated for 10 min to obtain a homogeneous suspension. The later was charged with 50 ml Thionyl Chloride ($SOCl_2$) in a 250 ml flask. The mixture was placed in a 70˚C oil bath under reflux for 24 hrs. After 24 hrs, the flask contents were transferred to 50 ml falcon tubes and centrifuged for 15 min at 6000 rpm. The supernatant was discarded and the solid scooped onto petri-dishes. The later was washed with methanol and allowed to dry in a fume cupboard overnight.

3.4.2 1, 3 – dipolar cycloaddition reaction of N-Tritylglycine

The recovered MWCNTs were then functionalised with 1, 3-dipolar cycloaddition; the procedure is as follows (Georgakilas et.al., 2002).

1.42 g Paraformaldehyde was dispersed in 50 ml dimethylformamide (DMF) by sonicating and 1.42g of trityl protected glycine was added to 25 ml of DMF and mixed by shaking slightly. Recovered MWCNTs were dispersed in 25 ml DMF and sonicated for 10 min. Solutions of paraformaldehyde, MWCNT suspension in DMF and trityl protected glycine were mixed together in a 250 ml beaker, and the reaction temperature was raised to 130˚C and the mixture kept for 96 hrs. After 96 hrs, the resulting solution was cooled to room temperature and transferred to 50 ml falcon tubes. The unfunctionalised MWCNTs were separated from the functionalised material by centrifuging the reaction mixture for 15 min at 6000 rpm. The supernatant was collected and solvent was evaporated using a rotor evaporator until an oily brown residue was obtained. The resulting residue was diluted with an equal volume of

chloroform and distilled H_2O. The solution was mixed by shaking and transferred into a separating funnel. Contents in the separating funnel were washed 3 times with distilled H_2O. The organic material was separated from the non-organic material which was collected in the distilled water used in washing. After washing, anhydrous sodium sulphate was added to the organic phase material collected after separating and then filtered to remove the sodium sulphate. The filtered solution was placed in a rotor evaporator to evaporate the solvent. The functionalised MWCNTs were isolated by precipitation with diethyl ether (75% v/v) and methanol (25% v/v) and the solid was washed several times with diethyl ether.

After the 1, 3-dipolar cycloaddition reaction, functionalised MWCNTs were taken for proton NMR analysis to track the progress of functionalisation. The sample was prepared for NMR analysis by dissolving 10 mg of functionalised MWCNTs in chloroform in NMR tubes.

3.4.3 Deprotection reaction (cleavage of trityl protecting group)

After NMR confirmation of trityl group attachment, free amino groups were made available by the removal of the trityl group (Georgakilas et al., 2002). To cleave the trityl group from functionalised MWCNTs, 33.30 mg MWCNTs was dispersed in 600 µl of a 4 M solution of HCl in dioxane. The solution was placed in a glass vile and shaken for 2 hrs at room temperature at 150 rpm. After 2 hrs the solvent was separated under reduced pressure for 30 minutes. 150 µl of diethyl ether and 50 µl of methanol were then added to the MWCNTs. The resulting solution was magnetically stirred under reduced pressure for a further 30 minutes. After 30 minutes, 200 µl DMF was added to 200 µl of diethyl ether and shaken at 150 rpm for 30 minutes. After drying the solvent off, the sample of dried MWCNTs was taken for ^{1}H NMR analysis to confirm the removal of the trityl protection group at the MWCNT chain-end.

3.4.4 Attachment Reaction of fluorescent probe on free amino sites

A solution of FITC (a fluorescent probe) was prepared by mixing 400 µl of DMF with 3.66 mg of FITC. 200µl of prepared FITC solution was added to amino modified MWCNTs and was further shaken for 4 hrs at 150 rpm.

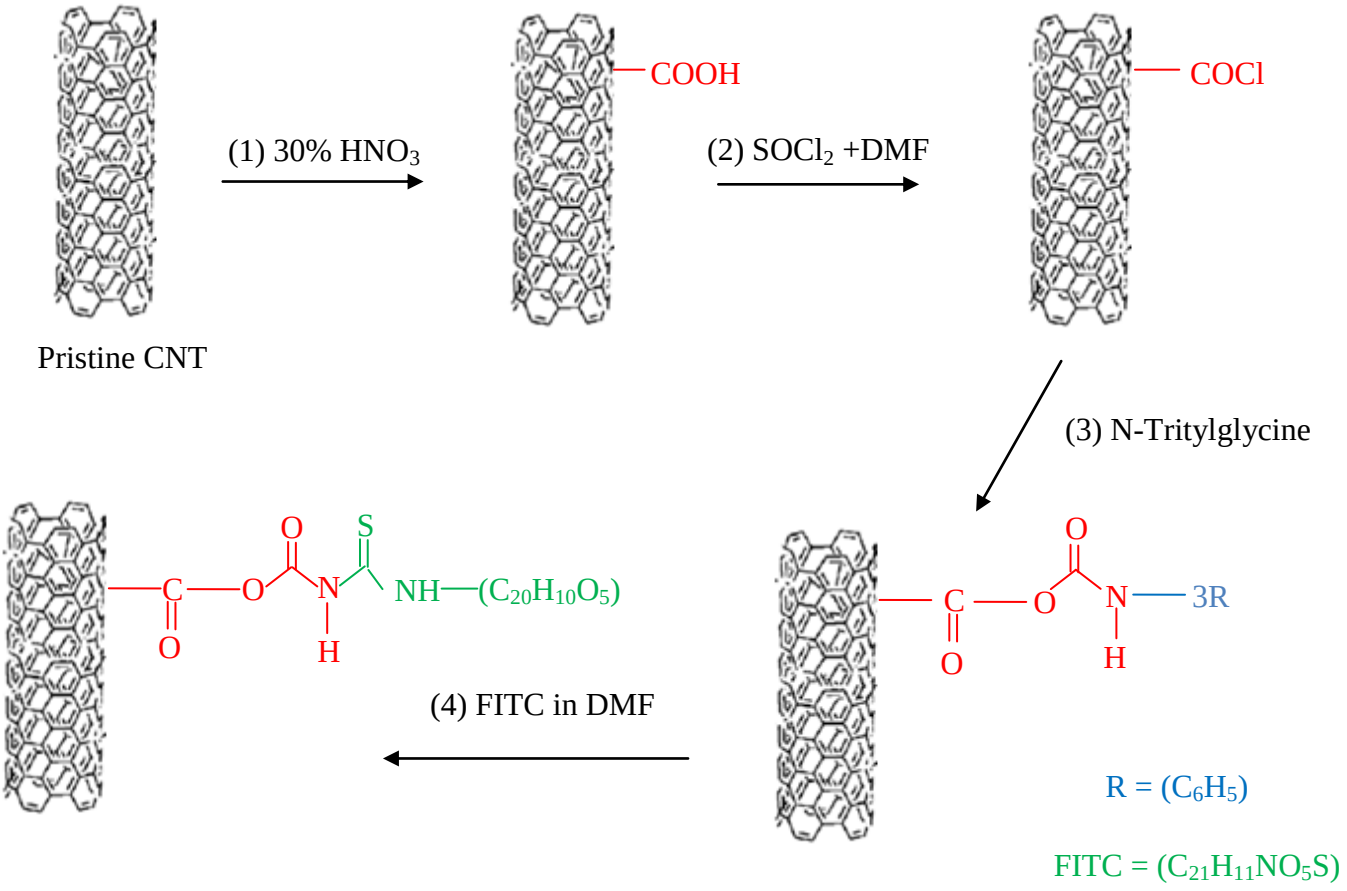


Figure 3.2: Schematics of reactions for 1,3-dipolar cycloaddition reaction of trityl protected glycine as a form of MWCNT functionalisation

3.5 ^{1}H NMR analysis

Samples were prepared for ^{1}H NMR analysis by adding Chloroform-d, 99.8 atom, an NMR solvent, to a small amount of MWCNTs in a 5 mm NMR tube (Wilmad, 503-PS) using a pipette.

^{1}H NMR measurements were acquired on a Bruker Avance 300 (300.13 MHz) spectrometer.

3.6 *Saccharomyces cerevisiae* cell cultivation and preservation

A pure *S.cerevisiae* strain was obtained from the School of Molecular and Cell Biology; University of the Witwatersrand; Johannesburg. A frozen stock of S.cerevisiae was cultivated aerobically at 30ºC and 200 rpm in growth medium containing yeast extract, peptone, and glucose (YPD) in 500 ml Erlenmeyer flasks (100 ml operating volume).

The strain was preserved by streaking onto malt extract agar plates every 3 – 4 weeks to maintain sterilisation and strain viability. This was done by spreading a loop full of overnight culture onto an agar surface plate. The culture was rapidly dragged across the surface of the agar plate. The streaked plates were incubated inverted at 30ºC for 48 hours until discrete colonies developed on the surface of the agar plates and plates were stored at 4ºC.

3.7 *Saccharomyces cerevisiae* cell growth analysis

Yeast growth was monitored by measuring the absorbance of light by the yeast sample using a spectrophotometer.

S.cerevisiae was cultured overnight in 10 ml sterile liquid YPD medium (1% (w/v) yeast extract, 2% (w/v) peptone, 2% (w/v) glucose) inoculated with an individual colony obtained from malt extract agar (MEA) petri-plate. The flask was shaken at 200 rpm in an orbital shaker at 30ºC for 16 - 18 hrs. 1 ml of overnight culture suspension was then added to each of the 500 ml Erlenmeyer flasks containing 100 ml fresh sterile YPD medium and pristine and oxidised CNTs: 2, 3, 6, 10, 20 and 40µg/ml. Yeast cells grown without CNTs were used as the control experiment. Samples of CNTs were accurately weighed using a balance. Flasks containing CNTs and culture were incubated in an orbital shaker at 30˚C at 200 rpm for 30 hrs. Growth was

monitored by measuring the absorbance at 600 nm of cultures grown in YPD medium for 30 hours. Exponential and stationary phase cultures were diluted to $A_{600} < 1$ for determination of the growth curves. Optical density was measured every 2 hrs with an Ultrospec 2000 UV-vis spectrophotometer. 1 ml Aliquots were collected aseptically from the culture flasks and transferred to semimicro methacrylate cuvettes. Percent transmittance or absorbance of light was measured at a wavelength of 600 nm and a path length of 1 cm. Absorbance was determined by comparing the percent transmittance of the sample (yeast suspension) to a control/blank (YPD medium). A UV-vis spectrophotometer at 600 nm wavelength was used to measure cell growth by absorbance. Aliquots were taken every 2 hrs to generate the growth curve. The experiments were done in duplicates and values averaged. An analysis of covariance was conducted and the level of significance was chosen as $P < 0.05$.

3.8 Construction of the calibration curve

A calibration curve of the relation between absorbance and cell amounts was produced by inoculating 100 ml fresh YPD media with 1 ml overnight culture in 500 ml Erlenmeyer flask with shaking at 200 rpm and 30˚C. This was done by measuring the optical density(OD) of a *S.cerevisiae* cell culture every 2 hrs as well as by directly plating every 2 hrs and counting the cells cultured onto MEA plates after 48 hr incubation. This was done for 10 hrs until an OD value of 1 was reached and consequently the relation between OD values and cell counts can be used to calibrate the growth curves of the yeast in the experiments.

3.9 *S.cerevisiae* cell viability analysis

In order to examine the impact of pristine and oxidised MWCNTs on the viability of *S.cerevisiae*, the standard plate counting (SPC)/ colony efficiency procedure was used. Plates containing appropriate growth media were gelled with agar and used for counting viable cells. Cultured samples were diluted in a buffer (bacto-peptone water) solution which neither harms the cells nor supports growth and spread on the agar surface and plates were incubated. Colonies were counted on the agar surface following a 48 hr incubation period and the results were then reported in terms of colony forming units (CFU).

Cell viability analysis was done at all three phases of *S.cerevisiae* cell growth, at 0hrs (lag phase), 6hrs (exponential phase), and 24hrs (stationary phase) respectively. The cells in YPD media without MWCNTs were used as a control. The assessment compared viable cell numbers of cells incubated with MWCNTs (both pristine and oxidised) at concentrations of 3 µg/ml, 20 µg/ml and 40 µg/ml to the control. The procedure applied is described in detail in Figure 3.3. A six-fold dilution was used in this experiment and the original culture sample was diluted to a 10^{-6} dilution after 24 hrs incubation and 10^{-5} for 0 hrs and 6hrs incubation. All plates were inverted and incubated at 30ºC for 48 hrs and colonies (between 30 and 300) were counted using a Coulter Counter.

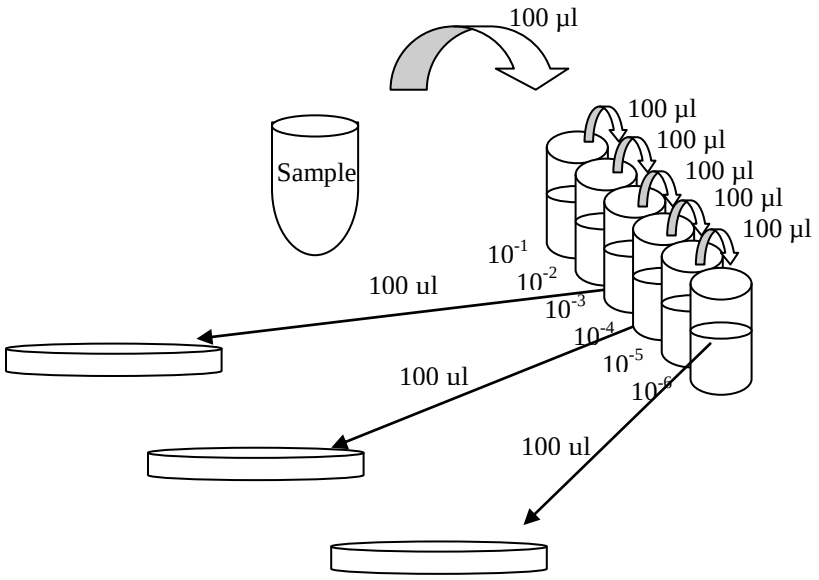


Figure 3.3: Schematic of the serial dilution procedure

3.9.1 Serial Dilution procedure

- Each sample tube was vortexed to ensure a homogenous dispersion, after vortexing 100 µl of the sample was transferred aseptically to an eperndorf tube containing 900 µl of fresh sterile buffered petone water. This resulted in a 10^{-1} dilution of the initial sample.
- The afore mentioned procedure was repeated, transferring 100 µl every time aseptically and vortexing through out until a 10^{-6} dilution was achieved.

- Petri dishes were labelled and 100 µl of each 10^{-4}, 10^{-5} and 10^{-6} dilution cultures were aseptically transferred to the plates; this was done in tri-plicate.
- After cultures were transferred onto the plates, a glass spreader was dipped into a glass petri dish containing ethanol. The glass spreader was passed briefly through the burner flame and the flame was allowed to burn out. The transferred liquid on the MEA plates was uniformly spread over the entire plate using the flamed spreader whilst turning the plate continuously and spreading.
- This was repeated in triplicate for all the samples at different concentrations, every 0 hrs, 6 hrs, and 24 hrs.
- After spreading, plates were incubated at 30˚C and inverted for 48 hrs.

3.9.2 Viable count procedure

- After plates were incubated and inverted for 48 hours, isolated colonies were counted and values were recorded. Plates that had more than colonies 300 and less than 30 were regarded as non-viable and were labelled NV (non-viable). Counts that fall in this region are considered to be statistically invalid or inaccurate.
- Colony counts for each plate was recorded and each colony was a 'colony forming unit' (CFU) and represents what was once a single cell inoculated on the plate.
- The values obtained per plate were averaged and the number of viable cells per ml were determined by the following calculation:

$$\frac{no\ of\ viable\ \ cells}{ml} = \frac{CFU}{volume\ \ plated} \times dillution\ factor$$

3.10 *Saccharomyces cerevisiae* cell imaging

3.10.1 Yeast cell sample preparation for scanning electron microscopy

Yeast cells were cultured onto glass slides suspended in the flasks. Glass slides were removed from flasks containing culture and CNTs and rinsed in falcon tubes containing 30ml sterile

distilled water. After washing, the glass slides were fixed with 3% Gluteraldehyde overnight at room temperature. Slides were then dehydrated in a series of increasing concentrations of ethanol at 10% increments up to 100% for 10 minutes in each concentration. After dehydration, slides were critically point dried, mounted and coated with thin carbon and normal gold palladium and then viewed under a JSM-840 scanning electron microscope.

3.10.2 Preparation of Yeast cells for confocal microscopy

Preparation of mounting solution

Mounting solution was prepared by dissolving 100 mg of polyethyleneimine in 10 ml Phosphate buffer saline solution (PBS). The pH was adjusted to above 8 with 0.5 M Sodium carbonate buffer (pH = 9) and the volume was increased to 100 ml by adding glycerol. The mounting solution was mixed thoroughly and stored at – 20˚C.

Preparation of slides

One glass slide was prepared for each sample; a circle was etched in the centre of each slide using a diamond pen. The slides were rinsed thoroughly with distilled H_2O and wiped with Kimwipe to remove dust and glass chips remaining from etching. The circles on the glass slides were then outlined using a black marker. 30 µL of 1% polyethyleneimine was transferred into each circle. The slides were dried by allowing the slide to sit at room temperature for 5 min. After 5 min, the remainder of the mounting solution was aspirated off and the slides were washed thoroughly with distilled H_2O. Slides were shaken dry and placed in a moist chamber.

Growth and incubation of yeast cells without functionalised CNTs

Yeast cells were grown to an OD_{600} of 0.4 – 0.6 in 10 ml of YPD media. This was done by firstly growing an overnight culture (16 – 18 hrs) to saturation in 3 ml sterile YPD media. 10 ml of fresh YPD media was inoculated with 100 µL of overnight culture and incubated at 30˚C and

shaken at 180 rpm using an orbital shaker. The 10 ml culture reached an OD_{600} of 0.4 – 0.6 in 10 ml of YPD media after 4 hrs of incubation.

Harvesting and fixation of yeast cells without f-CNTs

After 4 hrs incubation the 10 ml culture was removed and 1.4 ml of 37% formaldehyde (warmed to 37˚C in a water bath) was added to the 10 ml culture. The 10 ml culture containing formaldehyde was incubated for 5 min at 37˚C with gentle shaking. The culture was then left on the bench top (at room temperature) for 1 hr. After an hour the cells were centrifuged for 3 min at 3000 rpm and the supernatant was discarded. The yeast cell-pellets were washed three times with phosphate-buffered saline (PBS) (pH 7.2). After washing yeast cells were reconstituted in 500 µL PBS.

Staining of yeast cell membrane incubated without functionalised CNTs

To stain the yeast cell membrane a red fluorescent cell linker kit from Sigma, Missouri, USA was used (PKH26-GL). This cell linker kit is used or applicable for general cell membrane labeling for both *in vitro* and *ex vivo* cell labeling. The PKH26-GL cell linker kit uses patented membrane technology that incorporates a fluorescent dye with long aliphatic tails (PKH26) into lipid regions of the cell membrane (Horan et al., 1989). Contents contained in the kit, maintain cell viability, and maximize dye solubility and staining efficiency.

Dye solution was made up by preparing a 2×10^{-6} molar PKH26 dye solution in polypropylene tubes using Diluent C (supplied with the kit). To the yeast cell slurry, 1 ml of Diluents C was added to the slurry and mixed by pipetting to ensure even dispersion. 1 ml of cells was rapidly added to 1 ml of dye solution and the sample was immediately mixed by pipetting. The sample was incubated at 25˚C for 5 minutes and inverted periodically to assure mixing during the staining period. Cells were centrifuged at 6000 rpm for 10 minutes at 25˚C to remove cells from the staining solution. The supernatant was removed and the cell pellet was transferred to a new tube for further washing (a minimum of 3 washes was done with PBS). 60 µL of cells were transferred onto the prepared slides in the moist chamber by pipetting. Cells on the glass slides

were allowed to settle for 30 min. After 30 min slides were rinsed twice by dipping into coplin jars filled with PBS to remove any cells that did not adhere to the slide. Cells were then examined using fluorescence microscopy. Slides were viewed with a Zeiss confocal laser scanning microscope.

Growth of yeast cells and incubation with functionalised CNTs

Yeast cells were grown to an OD_{600} of 0.4 – 0.6 in 10 ml of YPD media. This was done by growing an overnight culture (16 – 18 hrs) to saturation in 3 ml sterile YPD media. 10 ml of fresh YPD media was inoculated with 100 µL of overnight culture and incubated at 30˚C and shaken at 180 rpm using an orbital shaker, until an OD_{600} of 0.4 – 0.6 was reached. For the examination of the cellular uptake of fluorescently labeled FITC-MWNT conjugates, the 10 ml culture was removed and incubated with 20 µg/ml of FITC labeled MWCNTs at 30˚C with no shaking for 1 and a half hours. A cell suspension mixed with 2 mg FITC without MWCNTs was used as a control.

Harvesting and fixation of yeast cells incubated with f-CNTs

After incubation with CNTs, 1.4 ml of 37% formaldehyde (warmed to 37˚C in a water bath) was added to the 10 ml culture. The 10 ml culture containing formaldehyde was incubated for 5 min at 37˚C with gentle shaking. The culture was then left on the bench top at room temperature for 1 hr. After an hour the cells were centrifuged for 3 min at 3000 rpm and the supernatant was discarded. The pellet was washed three times with PBS (pH, 7.2). After washing yeast cells incubated with f-CNTs were reconstituted in 500 µL PBS and transferred onto glass slides using a pipette and covered with a cover-slip. Cells were then examined using fluorescence microscopy slides and viewed with a Zeiss confocal laser scanning microscope.

3.11 PC12 cell culture

PC12 cells were maintained in RPM1 medium supplemented with 10% v/v donor horse serum, 5% v/v fetal bovine serum and 1% v/v PenStrap (penicillin streptomycin). All cells were cultured

in plastic culture flasks at 37˚C in a humidified incubator in which the CO_2 level is kept constant at 5%.

3.12 The CytoTox-Glo Cytotoxicity Assay

Cell-viability test

.

A CytoTox-Glo assay was used to measure cell viability. All the samples were sterilized for 24 h under UV irradiation and placed in individual wells of 24-well culture plates. PC12 cells were seeded in each well at concentration of 5×10^5 cells/ml. The incubation was performed under a CO_2 (5%) atmosphere and at a temperature of 37 °C for different times. The viability was determined after 0, 2, 4, 22 and 24 hrs. The cells were incubated with a specific concentration of oxidized MWCNTs (0, 50, 100 and 200 µg/ml).

3.13 Cytotoxicity of carbon nanotubes towards PC-12 neuronal cells

To determine the cytotoxicity of CNTs a cytotoxicity assay was done on PC-12 neuronal cells incubated with oxidised MWCNTs. The CytoTox-Glo from Promega, Madison, USA. The CytoTox-Glo Cytotoxicity Assay (Figure 3.4) is described, by the manufacturer, as a single-reagent-addition, luminescent and homogeneous assay that allows for the number of dead cells in cell populations. The CytoTox-Glo Assay is reported to show excellent correlation with other methods of assessing cell viability (CytoTox-Glo™ Cytotoxicity Assay, Promega, USA). The CytoTox-Glo™ Assay is able to measure a distinct protease activity associated with cytotoxicity (CytoTox-Glo™ Cytotoxicity Assay, Promega, USA). The luminogenic peptide substrate (alanyl-alanylphenylalanyl-aminoluciferin; AAF-Glo™ Substrate) measures “dead-cell protease activity”, which has been released from cells that have lost membrane integrity. The AAF-Glo™ Substrate is unable to cross the intact membrane of live cells and thus does not generate any appreciable signal from the live-cell population and the assay selectively detects only dead cells. The CytoTox-Glo™ Assay relies on the properties of a proprietary thermostable luciferase (Ultra-Glo™ Recombinant Luciferase), which generates a stable "glow-type" luminescent signal. The Lysis Reagent (provided with the assay kit) delivers the luminescent signal associated with

the total number of cells in each assay well. Viability is calculated by subtracting the luminescent signal resulting from experimental cell death from total luminescent values. The advantages of the assay are that it is able to measure the relative number of dead cells in culture (CytoTox-Glo™ Cytotoxicity Assay, Promega, USA). The assay measures the relative number of remaining viable cells using a total lysis protocol and it improves data by reducing statistical probability of false positives (or negatives) (CytoTox-Glo™ Cytotoxicity Assay, Promega, USA).

Methodology:

As per manufacturer's instructions:

- 96 well plate containing cells in culture medium were prepared by adding 12 µl of PC12 cell culture to each well in triplicate.
- 12 µl of fresh sterile media containing CNTs were then added to the 96 well plates containing cells.
- Cells were cultured for no more than 24 hrs, as recommended by manufactures' instructions not to expose cells to the test compound (i.e. CNTs) for longer than 24 hrs to ensure that cytotoxicity is not underestimated. Samples taken for testing was done at 2, 4, 22 and 24 hrs respectively.
- After 2 hrs incubation 12, 5 µl of CytoTox-Glo Cytotoxicity Reagent was added to all wells.
- The 96-well plate was then taken to the Victor X3 and mixed by orbital shaking for about 30 seconds and incubated at room temperature for 15 min.
- The luminescence was then taken on the Victor X3 and recorded (representing signal obtained from dead cells).
- 12,5 µl of Lysis Reagent (provided with Assay kit) was then added to each well and taken to the Victor X3 and were mixed again by orbital shaking for 30 seconds and incubation at room temperature for 15 minutes.
- The Luminescence was recorded again on the PerkinElmer Victor X3 (Signal obtained from total cell population)
- This procedure was repeated at 4, 22 and 24 hrs incubation, to obtain the luminescent contribution of viable cells.

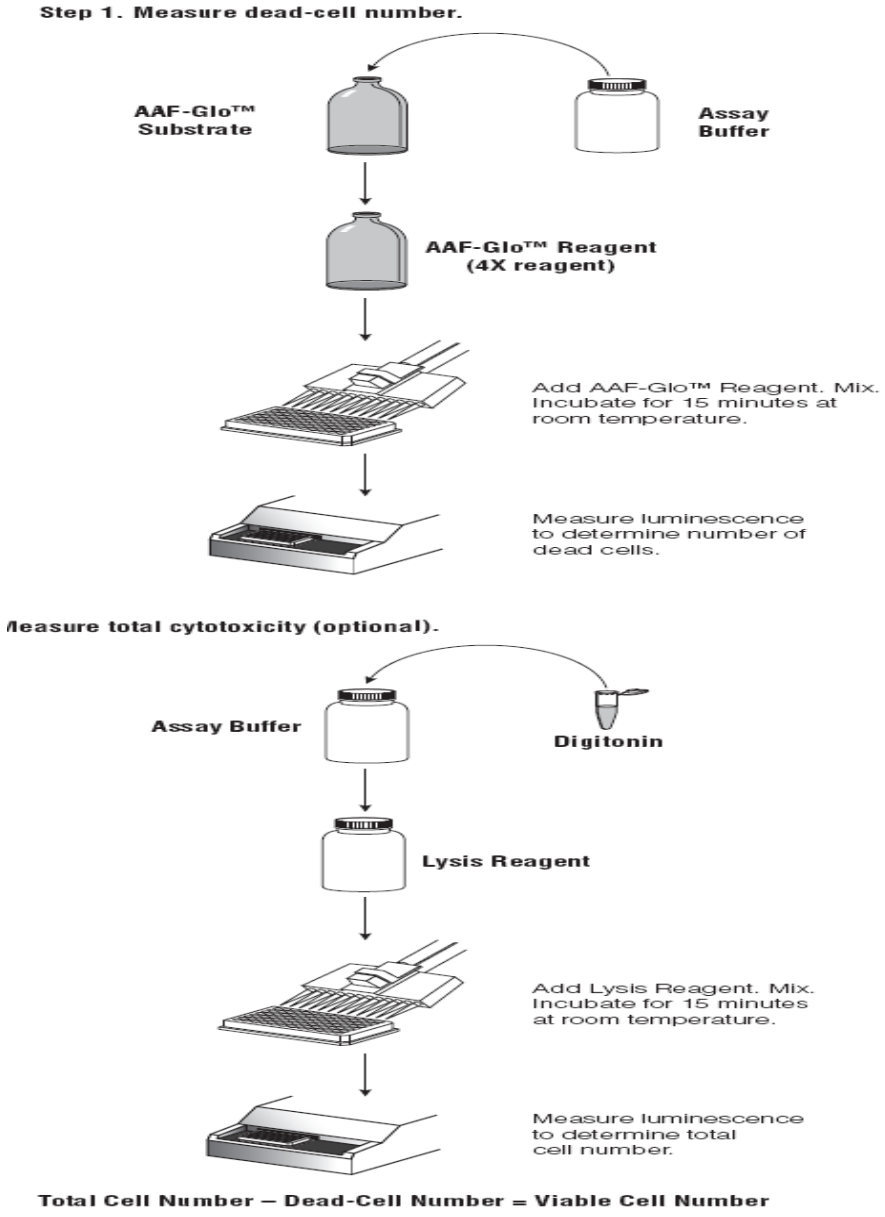


Figure 3.4: Schematic diagram of the CytoTox-Glo™ Cytotoxicity Assay (CytoTox-Glo™ Cytotoxicity Assay, Promega, USA).

3.14 Morphometric analysis of PC12 cells

The morphology of PC12 cells after treatment was analysed by viewing under a bright field microscope. Cells were placed onto a glass slide using a micropipette and covered with a cover slip and viewed.

3.15 Statistical analyses

Statistical analyses were performed using the analysis of variance (One-Way ANOVA) incorporated in the Origin 6.0 Professional software and $P < 0.05$ was considered statistically significant.

CHAPTER 4

Results and discussion

4.1 Characterisation of carbon nanotubes

4.1.1 Transmission electron microscopy

TEM was performed to observe the microstructure and morphology of MWCNTs before and after acid treatment. The average length and diameters of the MWCNTs were characterised by TEM. TEM micrographs of pristine MWCNTs are shown in Figure 4.1, MWCNTs after 1:3 HNO_3:H_2SO_4 acid treatment in Figure 4.2, and MWCNTs after 30% HNO_3 acid treatment from Figure 4.3. The white spots visible in the TEM micrographs are from the supporting TEM grid on which sample is placed for viewing. The support grid consists of a holey carbon coated film which exhibits a high percentage of open area and minimises the total specimen thickness and object distortions arising from film interactions.

0.33 µm

TEM micrographs of pristine MWCNTs produced by SFCCVD

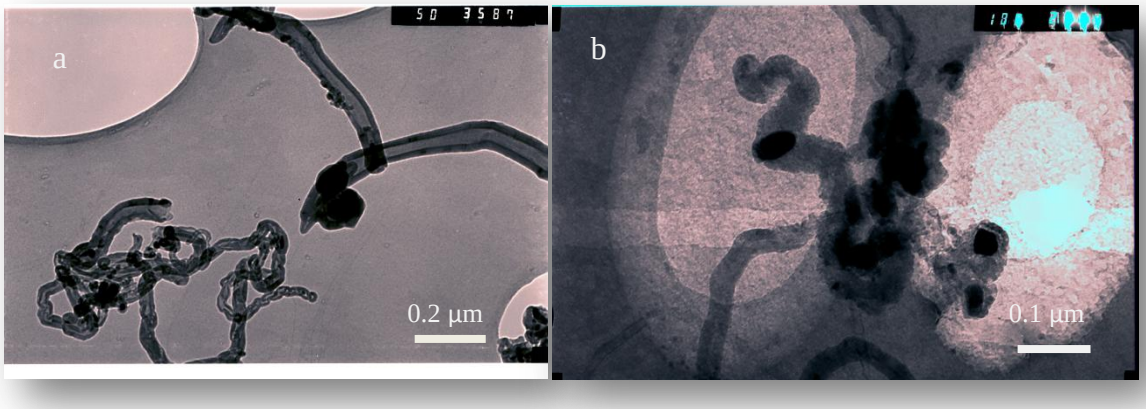


Figure 4.1: Typical TEM micrograph of pristine MWCNTs. (a) illustrating MWCNT with open ends and dark spots indicating metal catalyst at a scale of 0.2 µm. (b) illustrating a MWCNT with metal catalyst at a scale of 0.1 µm.

TEM micrographs of MWCNTs after 1:3 HNO_3:H_2SO_4 acid treatment

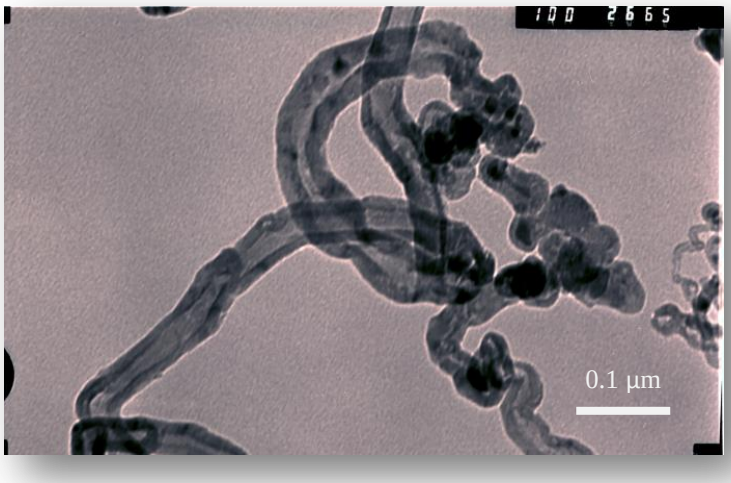


Figure 4.2: Typical TEM micrograph of MWCNTs after1:3 HNO_3:H_2SO_4 acid treatment

TEM micrographs of MWCNTs after 30% HNO_3 acid treatment

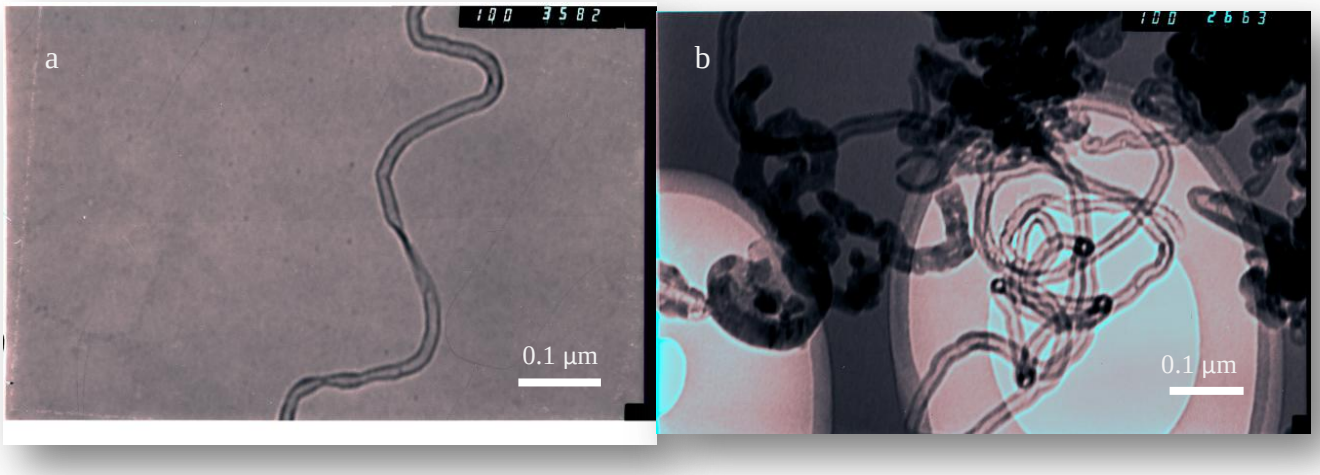


Figure 4.3: Typical TEM micrograph of 30% HNO_3 oxidised MWCNTs. (a) illustrating a single MWCNT with a smooth surface with a 0.1µm scale bar. (b) illustrating a group of MWCNTs with open ends and smooth surfaces

The TEM images of pristine MWCNTs show that the average diameter of MWCNTs is 53nm and length of several micrometers. After 1:3 HNO_3:H_2SO_4 and 30% HNO_3 acid treatments of MWCNTs the average diameter decreased to 48nm and 42 nm, respectively. From the TEM micrographs of pristine MWCNTs, black dots are found on the inside of CNTs, these dots

consist of carbonaceous nanoparticles, amorphous carbon, and catalyst metal particles, as shown in the micrographs in Figure 4.1. From the TEM micrographs, it can be seen that the pristine MWCNTs adopt an entangled morphology which is an indicator of structural defects (Xu et al., 2009). Figure 4.1(a) shows MWCNTs with open ends and this is characteristic of CNTs produced by the CVD method.

Micrographs of MWCNTs after acid treatments show a reduction of black dots found inside MWCNTs. Micrographs of purified MWCNTs are more dispersed with fewer metal particles. This is as a result of the acid treatment process which introduces numerous carboxylic groups on the surface of the MWCNTs, and increases the dispersion of MWCNTs in aqueous media (Zhang et al., 2010). Oxidation processes improve dispersivity and also increase attachment of oxygen containing functional groups on the surface of MWCNTs (Roa et al., 2007). TEM micrographs of purified MWCNTs also show a smooth surface of the MWCNTs containing fewer impurities. No structural defects are observed indicating that the acid treatments (1:3 HNO_3:H_2SO_4 and 30% HNO_3) induced no surface damage. The acid treatment methods were therefore effective in the removal of metal particles and amorphous carbon. The metallic impurities are no longer entrapped inside the individual nanotubes nor along the graphitic walls after treatment. Comparing the TEM micrographs of both acid treatments (Figures 4.2 and 4.3) respectively, the 2hr 30% HNO_3 acid treatment gives a better quality; signifying, relatively, fewer impurities and smoother surface of MWCNTs.

From the TEM results of acid treated MWCNTs, a small amount of metal particles are however still present. It is well known that the method of acid treatment CNTs using strong acids has the disadvantage of cutting the CNTs into short pieces which render them not useful for applications based on CNT length (Georgakilas et al., 2002). From the TEM results it can be seen that the length of CNTs appear to remain the same after acid treatment underscoring the fact that CNTs were not significantly shortened after treatment.

4.1.2 BET results

The BET results in Table 4.1 show the surface area (SA), average pore volume and average pore diameter of the MWCNT samples. The surface area of pristine MWCNTs is 31.6 m^2/g After a 2hr 30% HNO_3 acid treatment the surface area increases to 36.0 m^2/g and after 1:3 HNO_3/H_2SO_4 acid treatment the surface area decreased to 29.5m^2/g. The average pore volume of the pristine MWCNTs was found to be 0.16 cm^3/g. After 30% HNO_3 acid treatment, there was no change in average pore volume as compared to the pristine MWCNTs. However after the 1:3 HNO_3/H_2SO_4 acid treatment the average pore volume of the MWCNTs reduced to 0.10 cm^3/g. The average pore diameter of pristine MWCNTs was 20.6 nm, and after oxidising the MWCNTs both treatments decreased the average pore diameters. The CNTs after 30% HNO_3 acid treatment the average pore diameter of CNTs decreased to 17.3 nm and after 1:3 HNO_3/H_2SO_4 acid treatment the average pore diameter was further reduced to 13.4 nm.

Table 4.1: BET results of MWCNTs

Sample	**SA (m^2/g)**	**Average pore volume (cm^3/g)**	**Average pore diameter (nm)**
Pristine MWCNTs	31.6	0.16	20.6
30% HNO_3 treated MWCNTs	36.0	0.16	17.3
1:3 HNO_3:H_2SO_4	29.5	0.10	13.4

From the results above it can be seen that the effect of 30% Nitric acid treatment introduces an increase in MWCNT surface area and a decrease in average pore diameter. The increase in surface area can be associated to the functional groups introduced onto the surface after nitric acid treatment. During oxidation a weight loss (i.e removal of impurites amorphous carbon and catalyst) occurs and it is probable that the oxidation treatment had roughened the surface and caused the BET surface area to increase due to functional group attachment. The decrease in average pore volume and average pore diameter can be as a result of the stabilisation of open end structures, by the –OH and -COOH groups (Dettlaff-Weglikowska et al., 2002; Kim et al., 2006). From the Table 4.1 it can be seen that after acid treatment there is an increase in surface area with the mild acid purification technique (30% HNO_3), while with the concentrated acid purification technique ($1HNO_3$:$3H_2SO_4$) the surface area decreased. This could be as a result of

the fact that 1:3 HNO_3:H_2SO_4 acid treatment is more aggressive (as seen in TEM micrographs) and causes MWCNT wall structure damage leading to fewer functional group attachment impacting surface area (Tobias et al., 2006), the fewer –COOH functional group attachment can be verified by performing a Kaizer test. A lower average pore volume and average pore diameter was found for the concentrated acid treatment as compared to the pristine and the mild acid treatment technique.

From literature concentrated nitric acid purification technique has been shown to damage tubular structure which further justifies the use of a mild acid purification technique (Tobias et al., 2006). Studies regarding CNT specific surface area and diameter conducted by Bacsa, et al. (2002) indicated that specific surface area decreases with increasing CNT diameter and specific surface area also decreases with an increase in CNT bundles. The larger surface areas can be attributed to the removal of impurities such as amorphous carbon and catalyst particles and the possibly smaller diameters of CNTs after oxidation. To verify this it is recommended that electron diffraction analysis be done on the samples, Energy dispersive X-ray spectroscopy (EDX) can be used to determine the elemental composition of residues from the TGA analysis. Chemical oxidation of CNTs with nitric acid introduces different acidic functional groups, improving their ion-exchange and hydrophilic properties. As a result of improved hydrophilic properties CNTs become more dispersive resulting in a higher specific area being obtained for 30% HNO_3 acid treatment.

4.1.3 Raman spectroscopy analysis

Raman spectroscopy analysis was done to identify changes in the as-prepared and oxidized CNTs and to measure the crystallinity of the sample. A typical Raman spectrum of CNTs consists of two characteristic regions. One in the low frequency range (120 – 300 cm^{-1}) referred to as the radial breathing mode (RBM) which is present in SWCNTs but absent in MWCNTs. In the high frequency modes two characteristic bands are displayed, the D-band (1330 cm^{-1}) and G-band (1585 cm^{-1}), these bands are related to the graphite in-plane vibration with an E_{2g} symmetry intralayer mode and the defect on the nanotubes and amorphous carbon (Feng et al., 2008). The relative intensity of the D-band is thus proportional to the amount of carbon impurities and

defects in the nanotube sample. The width of the D-band can be used as a relative measure of the amount of carbon impurities and a narrow D-band would thus be consistent with a highly pure nanotube. I_D/I_G is normally used to compare the relative measure of the amount of defects present in a nanotube sample (Hurst et al., 2008).

Figure 4.4 gives the Raman spectrum of pristine MWCNTs indicating the characteristic D-band and G-band the absence of the Radial Breathing Mode confirms the MWCNT sample nature.

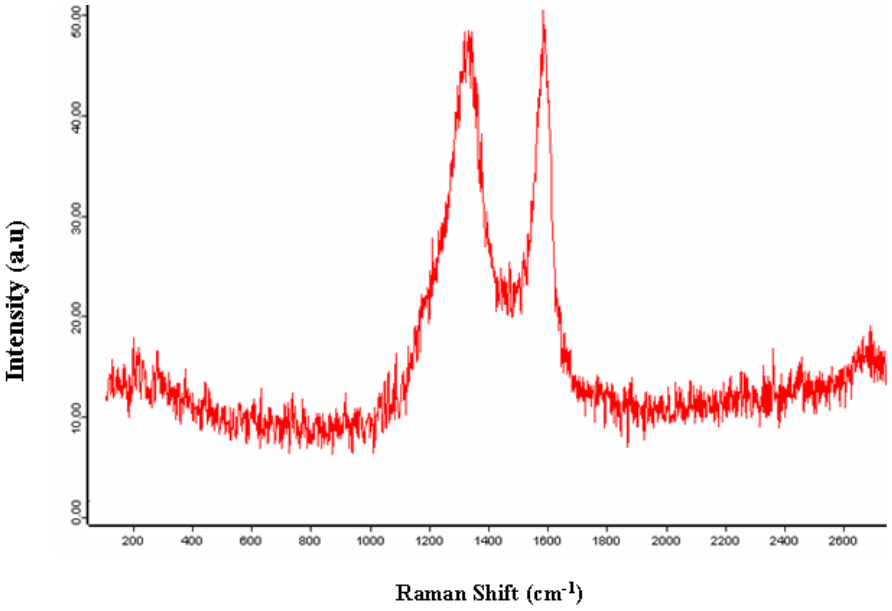


Figure 4.4: Raman Spectra of pristine MWCNTs

As shown in Figure 4.4 the Raman spectrum of pristine MWCNTs exhibits a G band at about1590 cm^{-1} and a slightly lower intensity D band at about 1330 cm^{-1} which is assigned to defects in the nanotube lattice. Figure 4.4 no peaks are present in the low frequency Radial Breathing Mode revealing that the sample is MWCNTs. Curve fitting of pristine MWCNTs Raman spectra was done on the software program OPUS. Curve fitting was done to determine the D band and G band position, D and G band intensities as well as band width as shown in Figure 4.5.

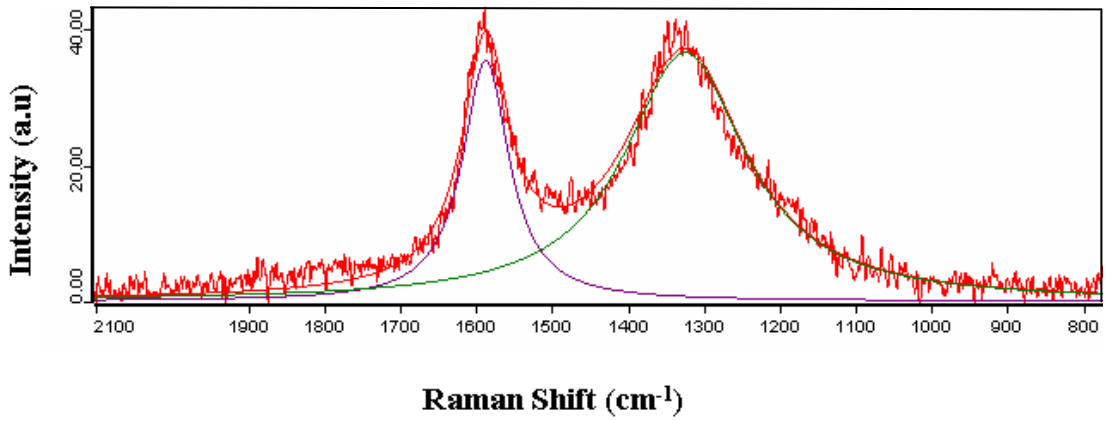


Figure 4.5: Curve fitting results of pristine MWCNTs

Curve fitting was using OPUS software and the raman data was fitted with a Lorentzian function with an error =1.91% . The band intensities for the D band and G band were found to be 36.83 a.u and 35.70 a.u respectively. The relative intensity of the D-band is proportional to the amount of carbon impurities and defects in the nanotube sample. I_D/I_G of pristine MWCNTs was found to be 1.032. The D band width 194.19 cm^{-1} and G band width 74.96 cm^{-1}.

Raman Spectroscopy of acid treated/ oxidized/ purified 30% HNO_3 CNTs

Figure 4.6 gives the Raman spectrum of 30% HNO_3 oxidised MWCNTs. The Raman spectrum exhibits a G band at about 1590 cm^{-1} and a slightly lower intensity D band at about 1330 cm^{-1} which is assigned to defects in the nanotube lattice. Curve fitting of the Raman spectra was done on the software program OPUS. Curve fitting was done to determine the D and G band positions, D and G band intensities as well as the D and G band widths as presented in Figure 4.7.

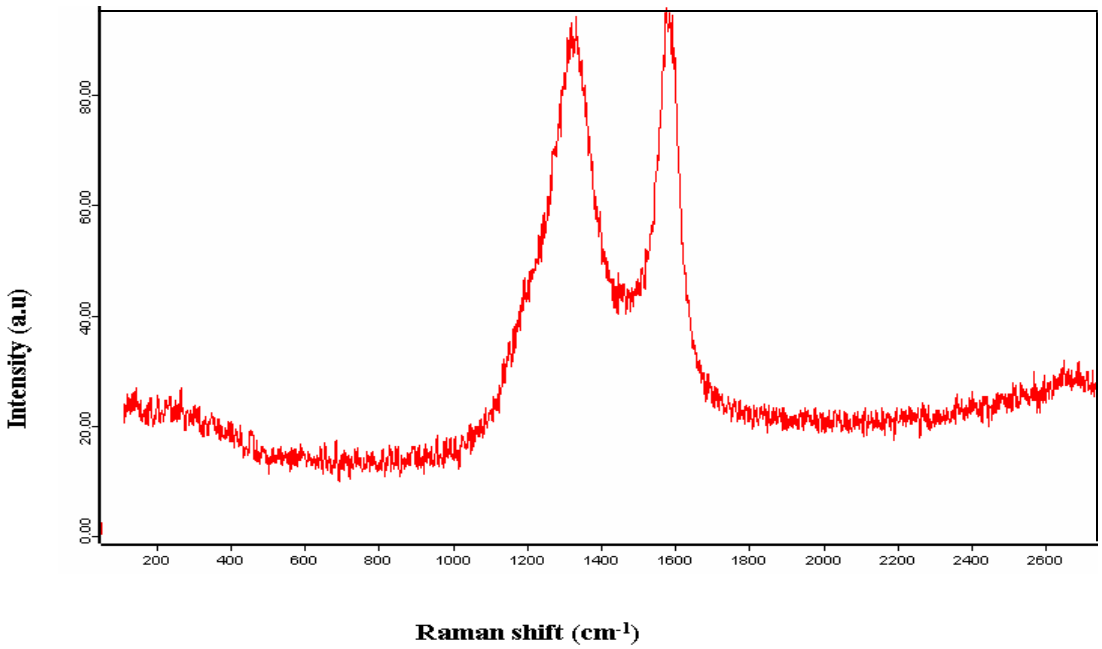


Figure 4.6: Raman spectra of 30% nitric acid oxidised CNTs

The result of the curve fitting of 30% nitric acid oxidised CNTs is shown in Figure 4.7.

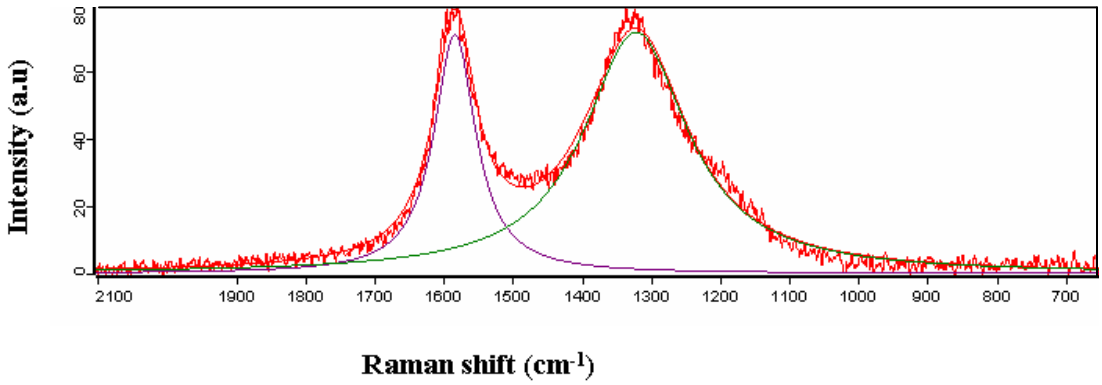


Figure 4.7: Curve fitting results of 30% nitric acid oxidized CNTs

After curve fitting (Figure 4.7) the position of the D band is at 1321.44 cm^{-1} and the G band at 1583.88 cm^{-1}. The band intensities for the D band and G band were found to be 72.00 a.u and 71.27 a.u respectively. The relative intensity of the D-band is proportional to the amount of carbon impurities and defects in the nanotube sample. The I_D/I_G of 30% nitric acid oxidised MWCNTs was found to be 1.01. The D band width 182.61 cm^{-1} and G band width 73.69 cm^{-1}.

Raman Spectra of 1:3 HNO_3:H_2SO_4

Figure 4.8 gives the Raman spectrum of 1:3 HNO_3:H_2SO_4 oxidised MWCNTs. The Raman spectrum exhibits a G band at about 1590 cm^{-1} and a slightly lower intensity D band at about 1330 cm^{-1} which is assigned to defects in the nanotube lattice. Curve fitting of the Raman spectra was done on the software program OPUS. In all three spectra a Lorentzian function was used to extract the data from the curves. Curve fitting was done to determine the D and G band positions, D and G band intensities as well as the D and G band widths as presented in Figure 4.9.

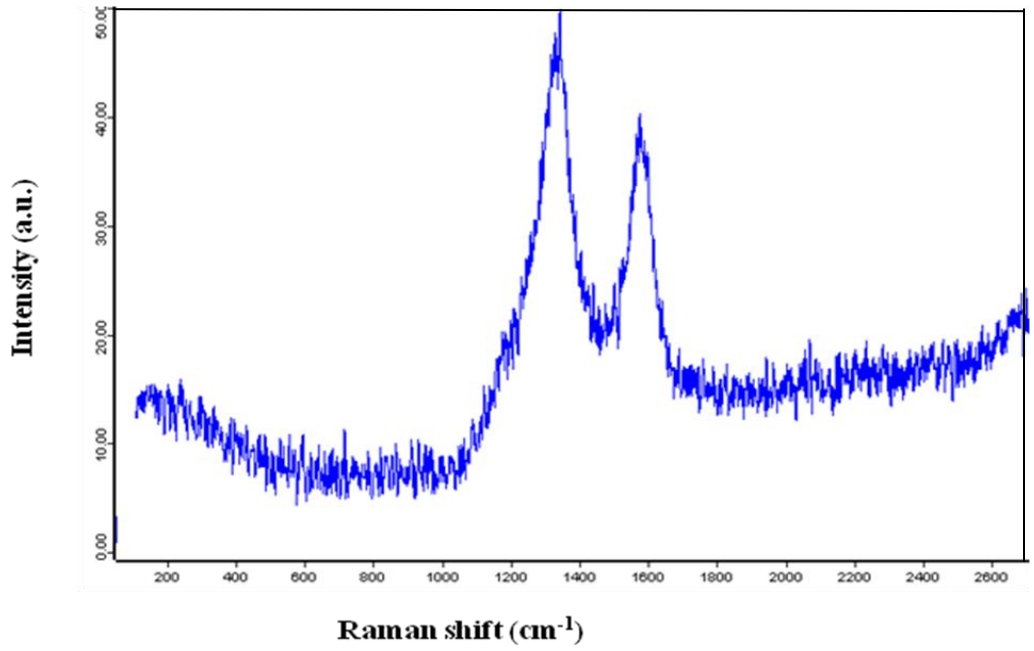


Figure 4.8: Raman spectra of 1:3 HNO_3:H_2SO_4 oxidized CNTs

The results of the curve fitting of 1:3 HNO_3:H_2SO_4 oxidized CNTs is shown in Figure 4.9.

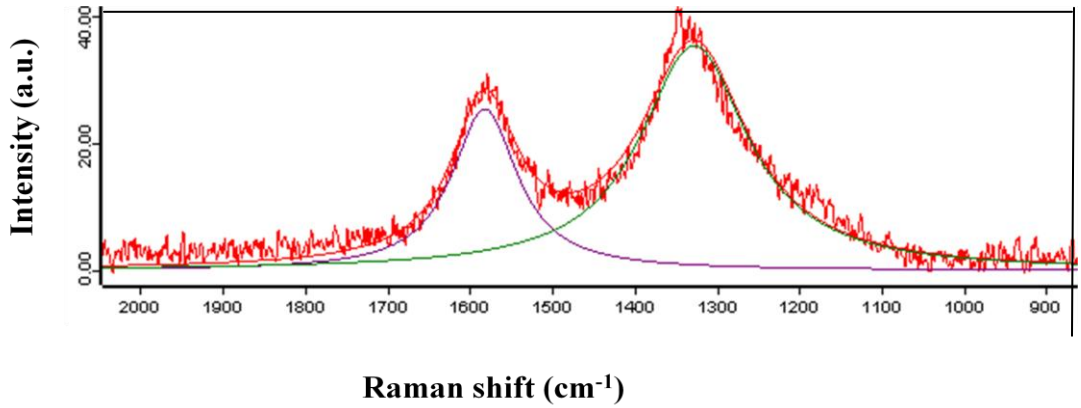


Figure 4.9: Curve fitting results of 1:3 HNO_3:H_2SO_4 oxidised MWCNTs

Curve fitting was using OPUS software and the raman data was fitted with a Lorentzian function with an error = 2.31%. Curve fitting shows the position of the D band is at 1327.34 cm^{-1} and the G band at 1582.00 cm^{-1}. The band intensities for the D band and G band were found to be 35.57 a.u and 25.51 a.u respectively. The relative intensity of the D-band is proportional to the amount of carbon impurities and defects in the nanotube sample. The I_D/I_G of 1:3 HNO_3:H_2SO_4 oxidised MWCNTs was found to be 1.39. The D band width 159.28 cm^{-1} and G band width 97.27 cm^{-1}.

All three spectra

Raman spectra of pristine, 30% HNO_3 oxidized MWCNTs and 1:3 HNO_3:H_2SO_4 oxidised MWCNTs taken at 514.5 nm are shown in Figure 4.10. The spectra of all three MWCNTs show the characteristic D band, corresponding to disordered carbon (around 1350 cm^{-1}) and G band, the split tangential mode between (1500 – 1600 cm^{-1}). The Raman spectra of 1:3 HNO_3:H_2SO_4 shows a higher I_D/I_G ratio as compared to the pristine MWCNT I_D/I_G ratio. The I_D/I_G ratio exhibits the degree of disorder and the amount of defects present in a nanotube sample (Hurst et al., 2008). This 35 % increase in I_D/I_G ratio indicates that structural defects were introduced to the MWCNT sample by the 1:3 HNO_3:H_2SO_4 oxidation procedure. The I_D/I_G ratio of the 30% HNO_3 oxidized MWCNT sample decreased by 2 % in comparison to the pristine MWCNT sample. The decrease in I_D/I_G ratio obtained for the 30% HNO_3 acid treated MWCNTs indicates a decrease in carbonaceous and metalic impurities as observed by TEM analysis, the tubular structure of the MWCNTs are preserved and fewer defects are present in the sample. The width of the D-band can be used as a relative measure of the amount of carbon and metallic impurities

and a narrow D-band would thus be consistent with a highly pure nanotube. The D-band width of 30% HNO_3 oxidised MWCNT sample decreased to 182.61 cm^{-1} from the pristine MWCNT sample with a D-band width of 194.19 cm^{-1}. The lower D-band width indicates a decrease in the amount of carbonaceous and metallic impurities present in the sample and results in a purer MWCNT sample.

From the obtained Raman spectra no peaks are present in the low frequency modes, revealing the absence of SWCNTs. These results indicate that the CNTs that underwent the concentrated acid treatment induced more structural defects on the CNTs than the mild acid treated.

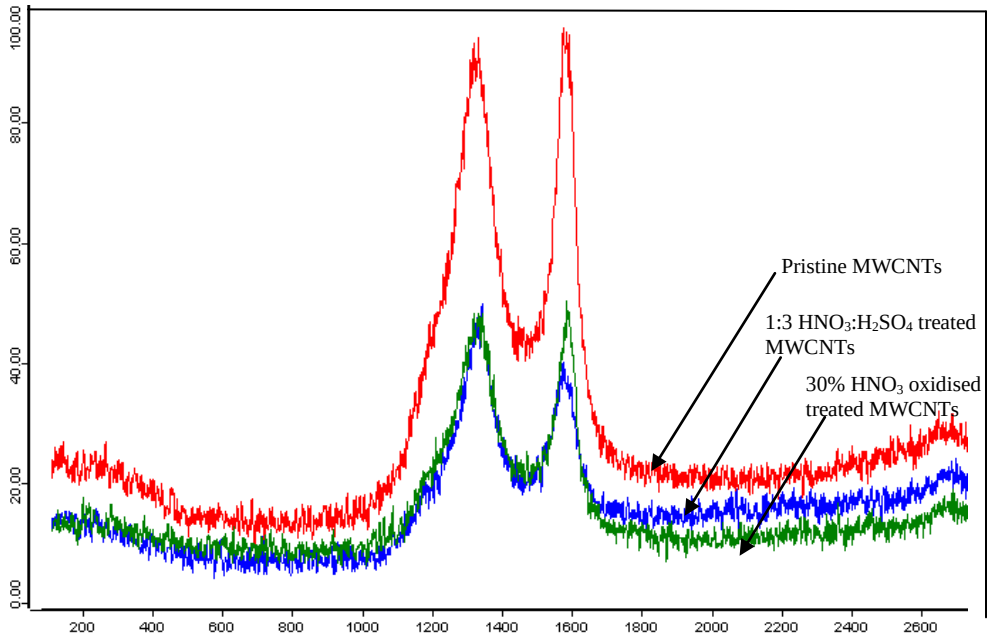


Figure 4.10: Raman spectra of pristine, 30% HNO_3 treated and 1:3 HNO_3:H_2SO_4 treated MWCNTs

Table: 4.2 Raman spectra results of pristine, 30% HNO_3 treated and 1:3 HNO_3:H_2SO_4 treated

Sample	Band position	Band position	Band intensity	Band intensity	Intensity ratio	Band width	Band width
	D1	**G**	**D1**	**G**	**ID/IG**	**D1**	**G**
Pristine MWCNTs	1324	1587	37	36	1.03	194	75
30% HNO_3 acid treated MWCNTs	1321	1584	72	71	1.01	182	74
1:3 HNO_3:H_2SO_4 acid treated MWCNTs	1327	1582	36	26	1.39	159	97

4.1.4 TGA analysis

TGA analysis was employed to determine the chemical stability of MWCNTs and to estimate the amount of residual catalyst present in the sample before and after oxidation/purification. Thermal treatment has been reported as being an important method in controlling the morphology and structure of MWCNTs in purification processes (Choi & Lee, 2009).

TGA analysis of as-prepared/ produced MWCNTs

Figure 4.11 shows the TGA results giving sample mass loss versus temperature in ˚C as well as the derivative weight curve (DTG).

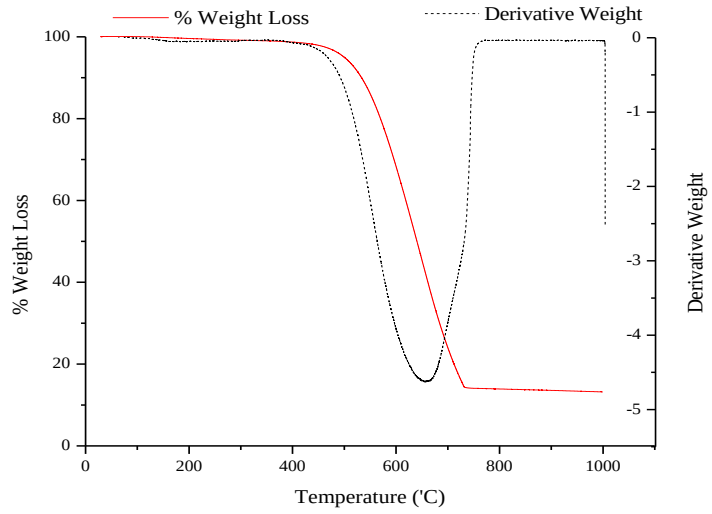


Figure 4.11: Thermal stability of the pristine MWCNTs. The solid line and dashed lines represent TG and DTG curves for the MWCNT samples, respectively

Figure 4.11 shows the TGA graph for the pristine MWCNTs. From this Figure, it is found that the initial burning temperature occurred between (300-350) ˚C and this occurred mainly due to the presence of amorphous carbon in the MWCNTs mixture (Raffa et al., 2008). Combustion of MWCNTs occurs at about 670˚C. It was noted that approximately 13.20 % of the sample remained behind after performing TGA up to 900˚C; the residue is attributed to catalyst weight (Raffa et al., 2008). It is recommended that an XRD analysis be conducted on the residue to verify the catalyst composition.

TGA analysis of 30% nitric acid purified MWCNTs

Figure 4.12 shows the TGA results giving sample mass loss versus temperature in ˚C as well as the derivative weight curve (DTG).

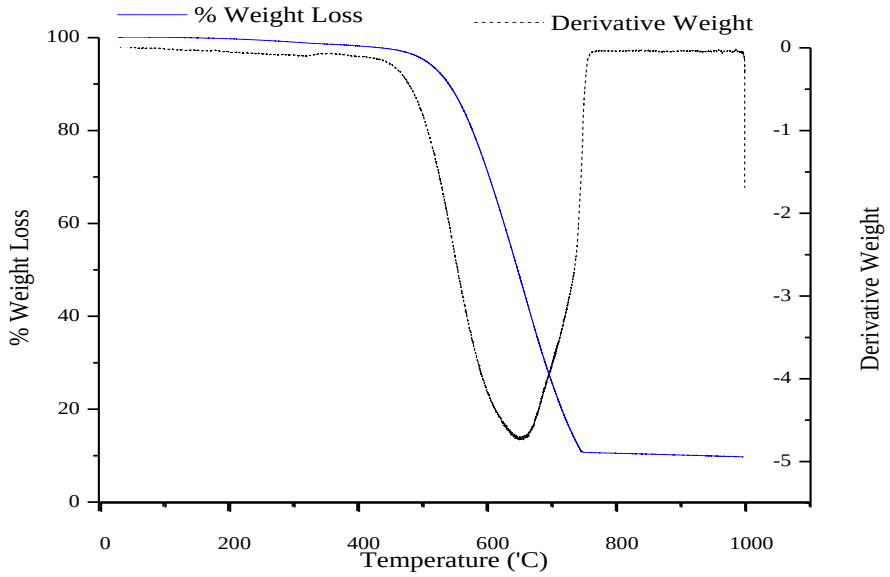


Figure 4.12: Thermal stability of the 30% HNO_3 oxidised MWCNTs. The solid line and dashed lines represent TG and DTG curves for the MWCNT sample

Figure 4.12 shows the TGA graph for the 30% HNO_3 oxidised MWCNTs. From this Figure, it is found that the initial burning temperature was between (300-350) ˚C and this occurred mainly due to the presence of amorphous carbon in the MWCNTs mixture (Raffa et al., 2008). Combustion of MWCNTs occurs at about 670˚C. It was noted that approximately 9.7 % of the sample remained behind after performing TGA up to 900˚C; the residue is attributed to catalyst weight It is recommended that an XRD analysis be conducted on the residue to verify the catalyst composition. A study done by Raffa, et al. (2008) showed that combustion of MWCNTs occurs at about 660˚C and combustion of amorphous carbon occurs at 300-350 ˚C (Raffa et al., 2008), the results obtained here agree well with these findings.

TGA analysis of 1:3 HNO_3:H_2SO_4 purified MWCNTs

Figure 4.13 displays the TGA results giving sample mass loss versus temperature in ˚C as well as the derivative weight curve (DTG).

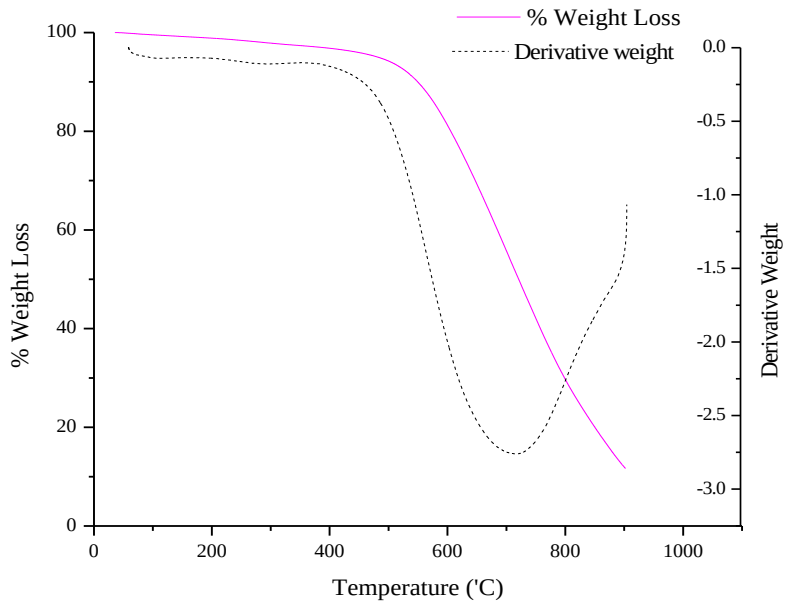


Figure 4.13: Thermal stability of the 1:3 HNO_3:H_2SO_4 oxidised MWCNTs. The solid line and dashed lines represent TG and DTG curves for the MWCNT sample

Figure 4.13 above shows the mass loss of the 1:3 HNO_3:H_2SO_4 oxidised MWCNT sample versus temperature. From the DTG curve 1:3 HNO_3:H_2SO_4 oxidised MWCNTs decompose or burn out at approximately 670˚C, with a final residue of 11.67 % attributed to catalyst weight.
Combustion of MWCNTs occurs at about 700˚C and combustion of amorphous carbon occurs between (300-350) ˚C (Raffa et al., 2008).

TGA Profiles of all 3 together:

The TGA curves of pristine MWCNTs, 30% HNO_3 acid treated MWCNTs and 1:3 HNO_3:H_2SO_4 acid treated MWCNTs were recorded and are shown in Figure 4.14. From the TGA results the data obtained for pristine MWCNTs decomposed the fastest and also reported the highest value

of metal catalyst of 13.20%. After 30% HNO_3 oxidation, the amount of catalyst present in the sample reduced to 9.70% indicating that catalysts impurities were removed by the acid treatment. MWCNTs oxidised by 1:3 HNO_3:H_2SO_4 reported a catalyst percentage (or residual amount of impurities in the sample) of 11.67%, this value is higher than the 30% HNO_3 oxidised MWCNT sample. This higher residue value formed by the 1:3 HNO_3:H_2SO_4 can be explained by the formation of salts due to the different treatments and is explained below.

Table 4.3: Gives the % Metal catalyst residue of acid treated and untreated MWCNTs

MWCNT samples untreated and treated	**% Metal catalyst residue**
Pristine MWCNTs	13.20
30% HNO_3 Treated MWCNTs	9.70
1:3 HNO_3:H_2SO_4 Treated MWCNTs	11.67

A. Metal catalyst salts formed as a result of 30% HNO_3 acid treatment of MWCNTs sample:

Chemical equations (neglecting $H_{2(g)}$ released);

(i) $Ni_{(s)} + HNO_{3\,(aq)} = Ni(NO_3)_2.6H_2O$ (reactivity passivated)

(ii) $Co_{(s)} + HNO_{3\,(aq)} = Co(NO_3)_2.6H_2O$

(iii) $Fe_{(s)} + HNO_{3(aq)} = Fe(NO_3)_2.6H_2O$ (reactivity passivated)

B. Metal catalyst salts formed as a result of 1:3 HNO_3:H_2SO_4 acid treatment of MWCNTs sample:

Chemical equations (neglecting evolution of $H_{2(g)}$);

(i) $Ni_{(s)} + \{HNO_3:H_2SO_4\}_{(aq)} = Ni(NO_3)_2.6H_2O + NiSO_4.7H_2O$

(ii) $Co_{(s)} + \{HNO_3:H_2SO_4\}_{(aq)} = Co(NO_3)_2.6H_2O + CoSO_4.7H_2O$

(iii) $Fe_{(s)} + \{HNO_3:H_2SO_4\}_{(aq)} = Fe(NO_3)_2.6H_2O + Fe_2(SO_4)_3$

Thermal stability of the salts formed in the aforementioned two cases:

Table 4.4: Thermal stability of salts formed from the 30% HNO_3 and 1:3 HNO_3:H_2SO_4*

Metal catalyst salt	Decomposition temperature ,°C
$Ni(NO_3)_2.6H_2O$	56.7
$Co(NO_3)_2.6H_2O$	<100
$Fe(NO_3)_2.6H_2O$	35
$NiSO_4.6H_2O$	53.3
$CoSO_4.7H_2O$	96.8
$Fe_2(SO_4)_3$	480

*Melting or decomposition temperatures from Table 4.4 are from Physical Properties of the Elements and Inorganic Compounds, Perry's Chemical Engineers' Handbook, 7ed.

The treated samples of MWCNTs were dried at 120°C for 24 hrs after acid treatment. At this temperature, the sulfated salts {$Fe_2(SO_4)_3$; $CoSO_4.7H_2O$; $NiSO_4.6H_2O$} formed would be more stable than the nitrated salts{ $Ni(NO_3)_2.6H_2O$; $Co(NO_3)_2.6H_2O$; $Fe(NO_3)_2.6H_2O$} according to the decomposition temperatures in Table2 above. 1:3 HNO_3:H_2SO_4 treatment process could have produced more catalyst salts than 30% HNO_3 treatment process. This could have resulted into 11.67% catalyst residue for the stronger 1:3 HNO_3:H_2SO_4 acid compared to 9.70% catalyst residue for the weaker 30% HNO_3 acid.

Thus the 30% HNO_3 treatment removed more metal catalysts than the 1:3 HNO_3:H_2SO_4. The thermal stability of CNTs is dependent on the side wall ''defects'' and the amount of metallic impurities. Hence, high quality CNTs have fewer "defects'' (caused by residues within the carbon nanotube and the graphitic walls).

From the TGA results, 30% HNO_3 oxidised acid treatment produced the purest sample of MWCNTs with 9.7% of catalyst impurity and the 1:3 HNO_3:H_2SO_4 oxidised acid treatment had 11.67 % catalyst impurity. The pristine MWCNTs had the highest level of catalyst impurities of 13.2%.

Based on these BET, TEM and TGA results, MWCNTs employed for further experimentation were treated by 30% HNO_3 acid treatment as opposed to 1:3 HNO_3:H_2SO_4 acid treatment. The 30% HNO_3 treated MWCNTs will be referred to further in this dissertation as oxidised MWCNTS.

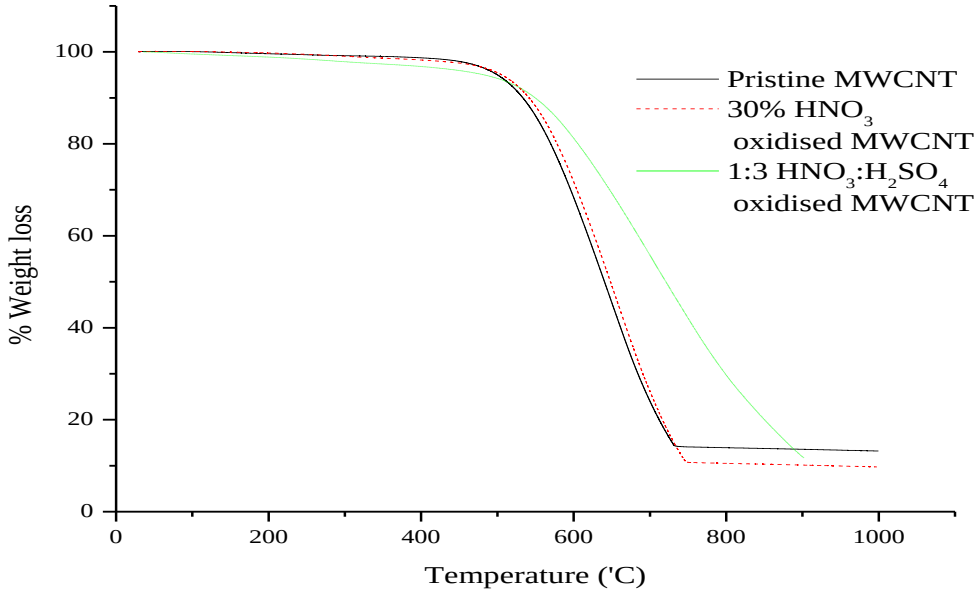


Figure 4.14: Thermal stability of pristine, 30% HNO_3 and 1:3 HNO_3:H_2SO_4 oxidised MWCNTs

4.1.5 Scanning electron microscopy (SEM) results

Surface morphology and crystal structure of MWCNTs were characterized by SEM. SEM images of pristine and oxidized MWCNTS are shown in Figure 4.15- 4.17. As shown in these Figures the MWCNTs show an entangled morphology.

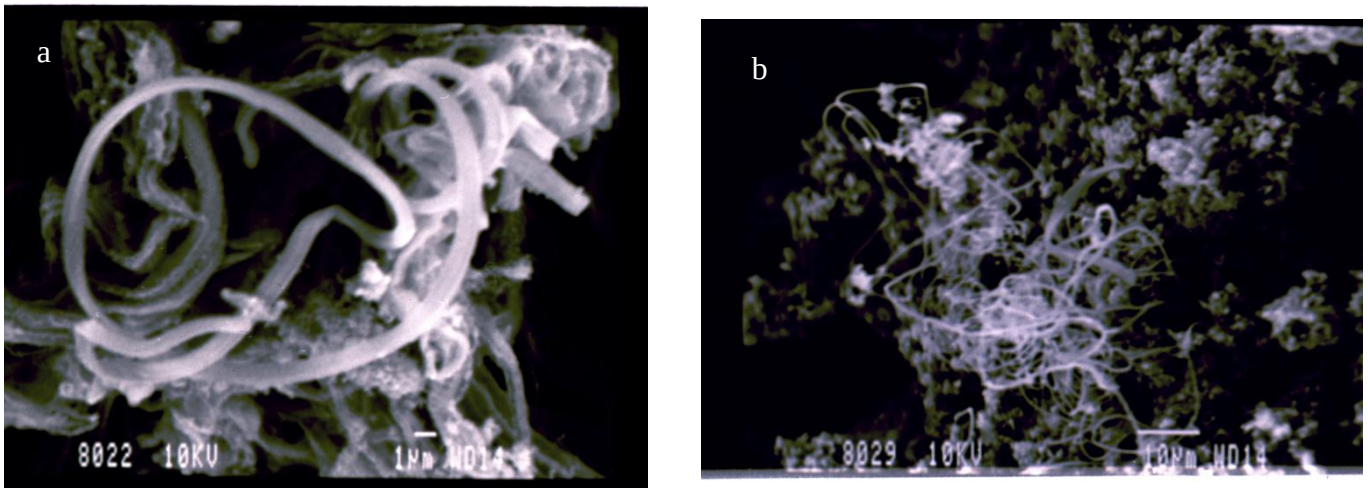


Figure 4.15. Typical SEM Micrograph of pristine MWCNTs. (a) Illustrating MWCNTs with a 1µm scale bar (b) Illustrating MWCNTs with a 10 µm scale bar

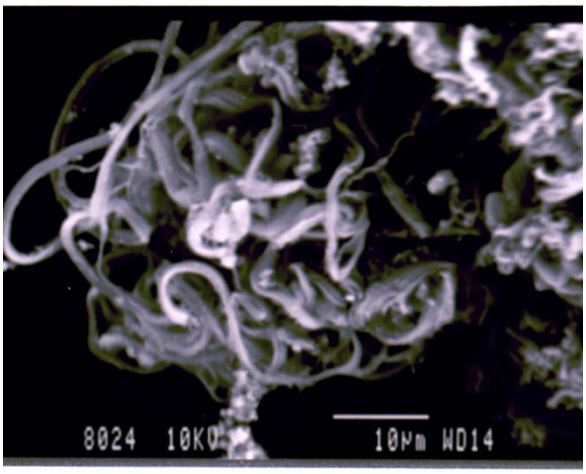


Figure 4.16. SEM Micrograph of 30% HNO_3 oxidised MWCNTs with 10µm scale bar

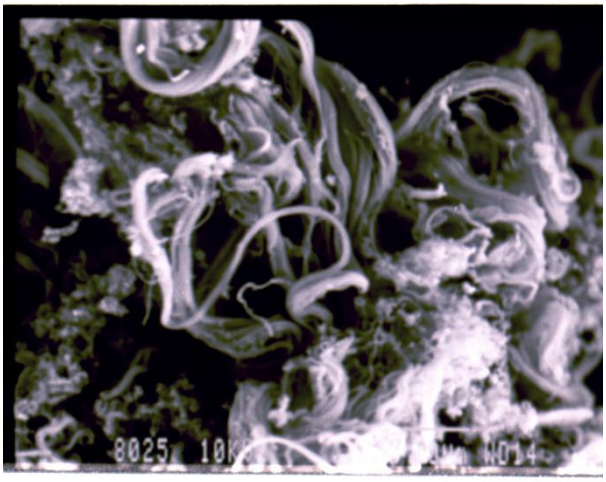


Figure 4.17 SEM Micrograph of 1:3 HNO_3:H_2SO_4 oxidised MWCNTs with 10µm scale bar

Figures 4.15 (a) and (b) show the scanning electron images of pristine MWCNTs while Figures 4.16 and 4.17 indicate images of oxidised MWCNTs respectively. From the micrographs it can be observed that MWCNTs of varying thickness are clustered and bundled together portraying smooth surfaces. No significant differences is obvious between the pristine and oxidised MWCNTs, the diameter distribution was in the range of (0.5-1) µm. The strong entangled morphology that is evident in the micrographs of oxidised MWCNTs are as a result of an increase in the interactive van der Waals force between the MWCNT bundles after catalyst impurity removal from the nanotube surface (Choi & Lee, 2009).

4.1.6 Functionalisation of MWCNTs

Purification of CNTs is essential in preparation of functionalised nanotubes (Dettlaff-Weglikowska et al., 2002). Raw, as-prepared MWCNTs were thus purified prior to chemical modification. It is well reported in literature that the MWCNTs purification method leads to structural changes and affects the MWCNTs functionality and properties (Kim et al., 2006). Purification by acid washing generates open end terminals in the structure which are stabilized by -COOH and -OH groups left bonded on nanotubes at the end or on the sidewall defect sites (Kim et.al, 2006). Carboxylic acid groups -COOH (MWCNT-COOH) attached to the nanotubes after purification can be converted to acidic chloride, MWCNT-COCl, by treating the oxidized MWCNTs with thionylchloride $SOCl_2$. Chloride-functions are then able to react with amine groups (Dettlaff-Weglikowska et al., 2002).

The amount of CNTs recovered after functionalisation with thionyl chloride was 0.43g resulting in a recovery of 85%.

Characterisation of functionalised CNTs

Carboxylic groups were introduced onto the surfaces of MWCNTs by employing acid treatment. FITC is covalently attached to the oxidized MWNT via a 1,3-dipolar cycloaddition reaction of trityl protected glycine (Georgakilas et al., 2002). The progress of functionalisation was tracked by TEM, H^1 NMR spectroscopy, TGA and confocal microscopy.

TEM analysis of functionalised MWCNTs

Transmission electron microscopy (TEM) was used to investigate the structures of the un-functionalised product from the 1,3-dipolar cycloaddition reaction, N-Tritylglycine functionalised MWCNTs and fluorascineisothonayate functionalised MWCNTs and the results are shown in Figure 4.18 - 4.20. Figure 4.18 shows the unfunctionalised MWCNT product from the 1,3-dipolar cycloaddition of N-Tritylglycine. From the TEM images, a considerable reduction in amorphous carbons and catalytic residues, as compared to pristine MWCNTs, can be seen. The unfunctionalised MWCNTs reveal no surface destruction and have an average

diameter ranging from 80-100nm. Figures 4.19 (a) – (b) and Figure 4.20 (a)-(b), show the micrographs of N-Tritylglycine functionalised MWCNTs and FITC functionalized MWCNTs respectively.

Unreacted 1, 3-dipolar cycloaddition MWCNTs

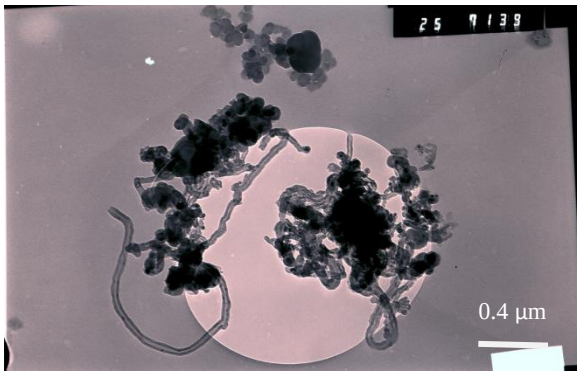


Figure 4.18. Typical TEM image of unreacted MWCNT sample from the 1, 3-dipolar cycloaddition reaction process with 0.4µm scale bar.

N-Tritylglycine protected MWCNTs

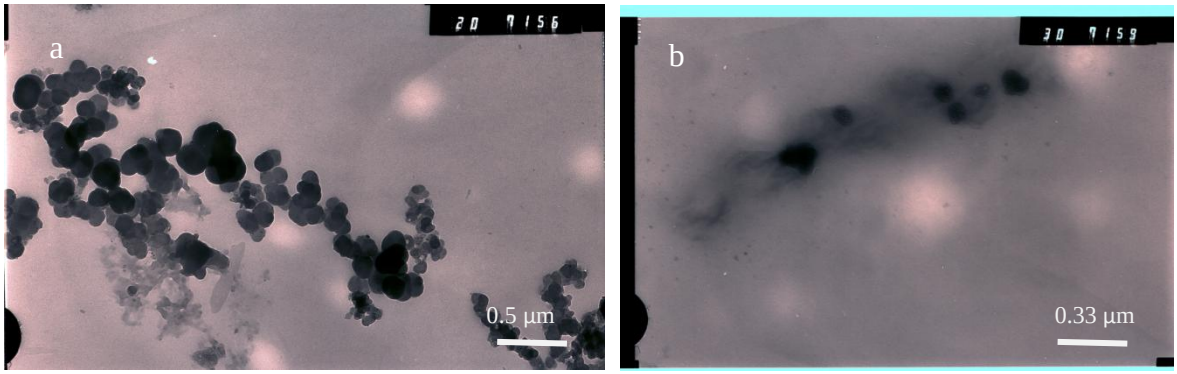


Figure 4.19. Typical TEM image of N-Tritylglycine functionalised MWCNTs. (a) with a 0.5µm scale bar (b) with a 0.33 µm scale bar.

Fluorescein isothiocyanate (FITC) functionalised MWCNTs

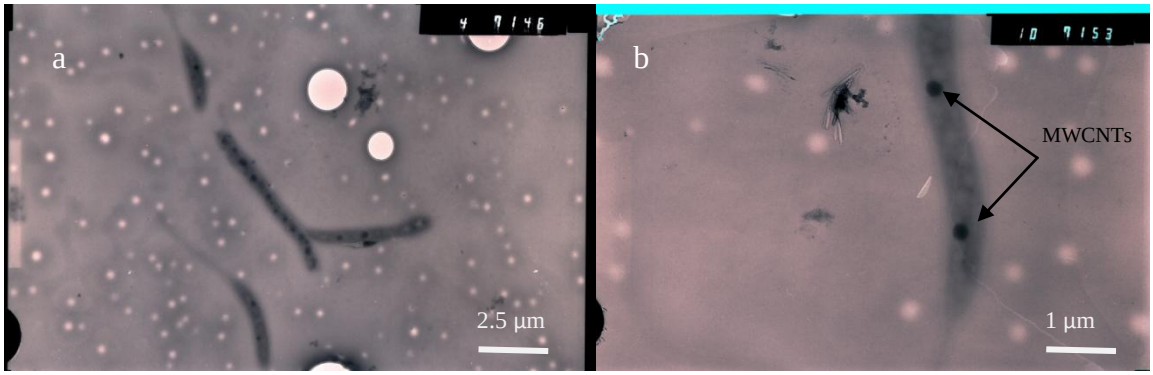


Figure 4.20. Typical TEM micrograph of FITC-MWCNT sample. (a) 2.5 µm scale bar (b) with a 1 µm scale bar.

Based on the TEM images above, a considerable purification of the material can be observed after the 1, 3-dipolar cycloaddition functionalisation process. No impurities including metal particles and amorphous carbon material was observed. The TEM images shown in Figures 4.19 and 4.20 reveal different morphologies as compared to the tubular structure of the unfunctionalised MWCNT materials. The N-Tritylglycine and FITC functionalized MWCNTs seemed to form bundles and aggregates of MWCNTs, glomerate and intercalate in the organic solvents used in the functionalisation process which might have resulted in a different morphology shown in the micrographs displayed in Figures 4.20 (a) and (b).

TGA analysis of functionalised MWCNTs

The thermal properties of the non-functionalised MWCNTs and functionalized MWCNTs (from the 1,3-dipolar cycloaddition reaction) were investigated by TGA and the results are shown in Figures 4.21 and Figure 4.22 respectively. The non-functionalised MWCNTs exhibit very good thermal stability and showed a weight loss at 500˚C of less than 8 and 90% at 800˚C. Two distinct weight loss stages are observed at about 300˚C and 700˚C for the Trityl protected-functionalized MWCNTs. The TGA scan for functionalised MWCNTs show a significant weight loss of 83% at about 300˚C. The first weight loss stage below 300˚C is likely attributed

to the decomposition of covalently bonded moieties on the MWCNT surface resulting from the 1,3-dipolar cycloaddition reaction of N-tritylglycine (or can be attributed to the decomposition of N-tritylglycine). The latter weight loss stage is observed at about 680˚C and is attributed to the combustion of MWCNTs. The TGA graph for the functionalised MWCNT displays a weight loss of 99.5% at 800˚C, indicative of a highly pure sample. The residual amount of impurities in the functionalized sample was 0.5% in comparison to the non-functionalised MWCNTs with a residual amount of impurities in the sample of 10.5%. The decreases of catalyst particles and increase in purity with the MWCNT samples were observed by TEM analysis. The TEM micrographs confirmed the decrease in impurities of both functionalized and non-functionalised product samples after functionalisation by the 1, 3-dipolar cycloaddition reaction.

Figure 4.21 and 4.22 displays the corresponding TGA weight-loss curves of the functionalized and unfunctionalised MWCNT samples, respectively.

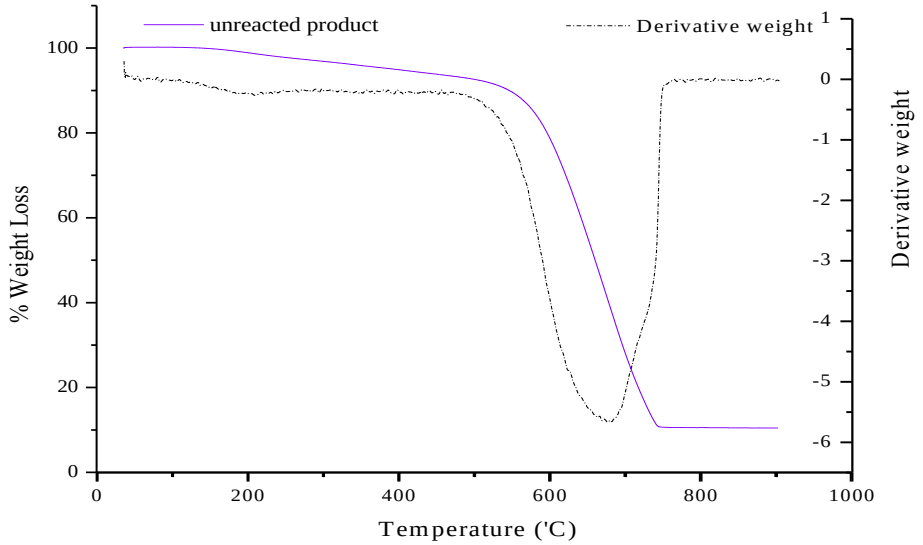


Figure 4.21: Thermal stability of the unreacted MWCNTs from the 1,3-dipolar cycloaddition reaction. The solid line and dashed lines represent TG and DTG curves for the MWCNT samples, respectively

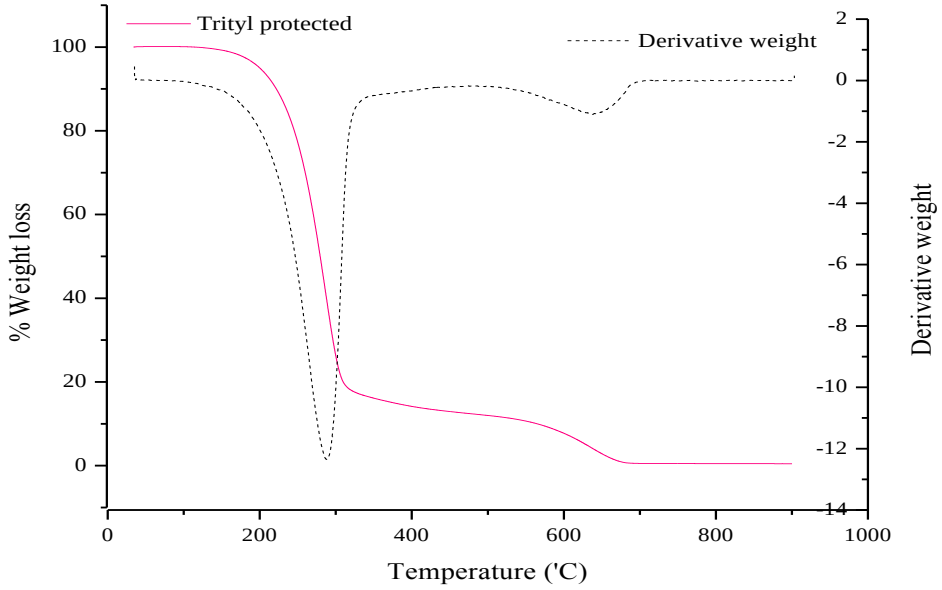


Figure 4.22: Thermal stability of the N-Tritylglycine functionalised MWCNTs. The solid line and dashed lines represent TG and DTG curves for the MWCNT samples, respectively

Nuclear magnetic spectroscopy (NMR) analysis

The ^{1}H NMR spectrum of N-tritylglycine functionalised MWCNTs shows the presence of the trityl chain at about 7.4 ppm as a broad peak, confirming the attachment of the trityl group.

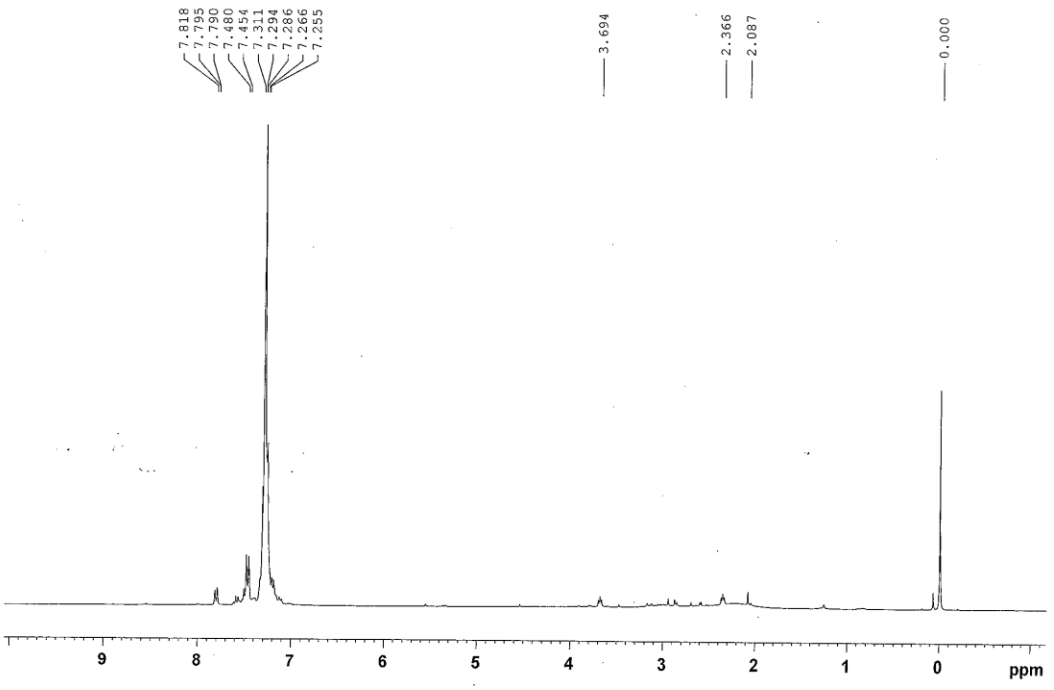


Figure 4.23: ^{1}H NMR spectrum of N-Tritylglycine functionalized MWCNTs in chloroform

Deprotection spectrum

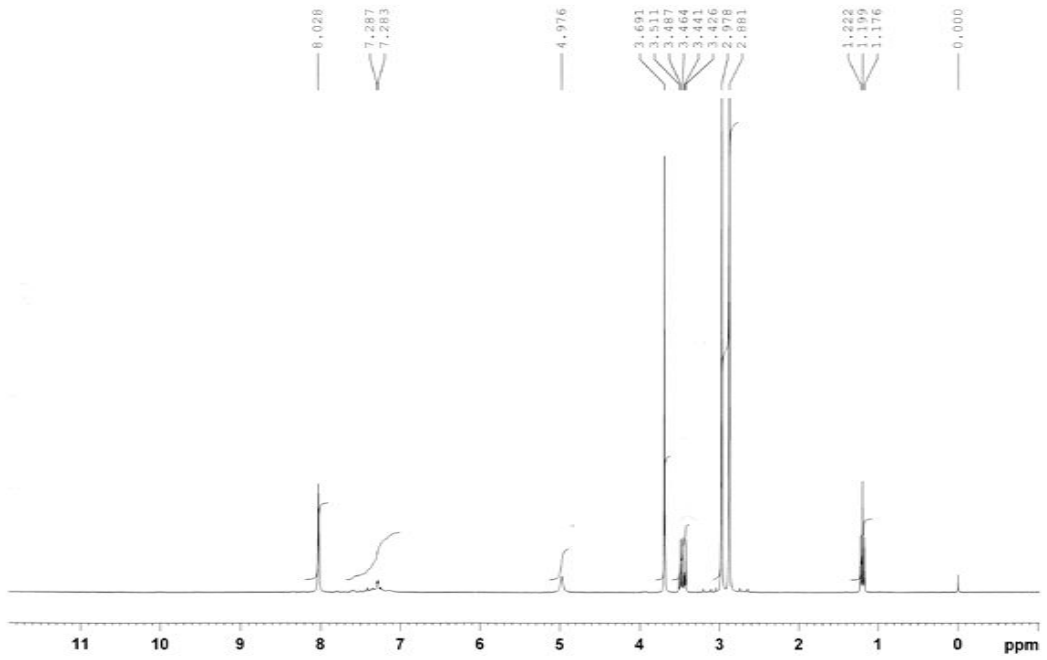


Figure 4.24: NMR spectra obtained after deprotection reaction of the trityl group after treatment with 4M HCl in dioxane

Comparison of the H^1 NMR spectra of the protected and deprotected CNTs (Figures 4.23 and 4.24) clearly shows the presence or attachment of the trityl group as a broad peak at 7.4 ppm and the signal consequently disappeared after treatment with 4M HCl in dioxane (Figure 4.24).

Confocal microscopy of FITC-MWCNTs

Confocal microscopy is a powerfull tool for visualization of fluorescent probes, the results of conjugation of the trityl protecting group and functionalisation with fluorescein isothiocyanate (FITC) to the CNTs were confirmed and characterized by confocal microscopy, as shown in Figure 4.25.

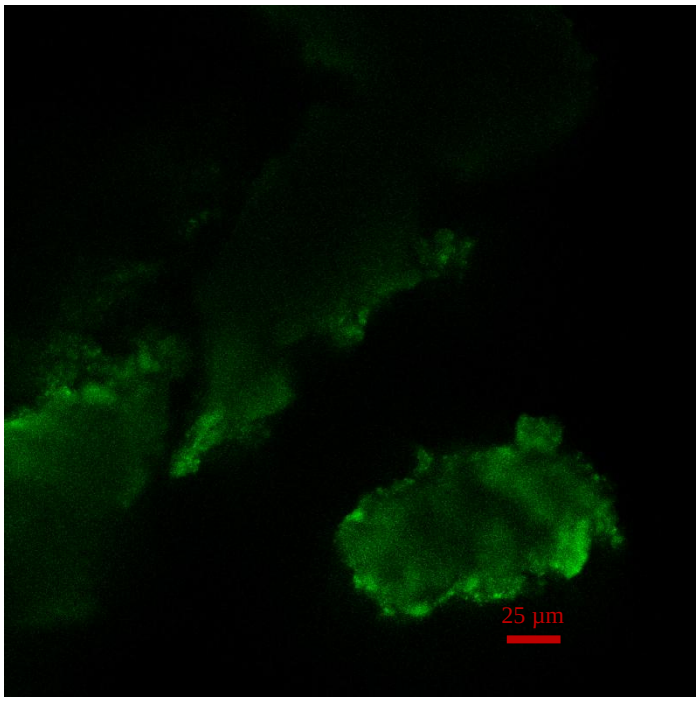


Figure 4.25 Confocal image of FITC functionalised MWCNTs after drying with 25µm scale bar

More pronounced evidence of the functionalisation of MWCNTs was observed by confocal microscopy. Amazing fluorescence was uniformly observed in the fluorescent image of dry MWNT-FITC sample. The fluorescent structures observed with fluorescent microscopy reveals the successful conjugation of FITC to the CNTs.

Characterization of the functionalized MWCNT product with TEM, TGA, ^{1}H NMR and confocal microscopy indicated successful functionalisation of FITC to the MWCNTs.

4.2 *S.cerevisiae* Growth Analysis in the presence of MWCNTs

A critical question amid reports concerning the adherence and uptake of CNTs by cultured cells is whether they are toxic. To test the toxicity of CNTs we assessed the growth of the yeast species *S.cerevisiae* cells which were continuously exposed to dispersion of pristine and oxidised MWCNTs. Figure 4.26 compares the growth curves of *S.cerevisiae* incubated with increasing concentration of MWCNTs from 0µg/ml to 40µg/ml of pristine MWCNTs (specifically: 2, 3, 5, 6, 10, 20 & 40µg/ml) to the control (grown in the absence of pristine MWCNTS).

The growth curves of *S.cerevisiae* grown in YPD broth (Figure 4.26) are consistent with that of microorganism growing in liquid media. Yeast of the species *S.cerevisiae* grow rapidly and spectrophotometer readings were taken every 2 hrs. A standard growth curve comprises of a lag phase, an exponential phase and a stationary phase. During the lag phase, organisms attune to their new environment and do not multiply actively. As indicated in Figure 4.26, growth curves enter the stationary phase at 0hr and remain in this phase until an incubation period of 5hrs is reached. In the stationary phase, growth is slow and no changes in growth of cells incubated with pristine MWCNTs at both high and low concentrations as compared to the control were observed. This indicates that during the early stages of microorganism growth and adaption, pristine MWCNTs do not interfere with the microorganism activity and do not negatively impact the cells process to adapt to the environment. The lag phase is then followed by the logarithmic or exponential growth phase. This phase continues up to a point where all nutrients have been exhausted or until toxic metabolite accumulation occurs at which point growth is slowed (Matousek et al, 2003). After 5hrs incubation cells now entered the exponential phase where cells grew rapidly. The exponential growth phase took place from 5 hrs till~13 hrs incubation as shown in Figure 4.26. In this phase growth curves of *S.cerevisiae* cells incubated with pristine MWCNTs, at all concentrations, closely followed the control curve. Moderate sensitivity was shown in the mid logarithmic phase evidenced by a slower growth of *S.cerevisiae* grown in liquid YPD medium in the presence of pristine MWCNTs as compared to the control. Although

growth of cells incubated with pristine MWCNTs was slightly slower in the exponential phase, while the differences were not statistically significant. No significant differences in growth of *S.cerevisiae* cells incubated with pristine MWCNTs at both low and high concentrations are detected. The stationary phase commences at about 13 hrs incubation. Comparing the growth curves of cultures in the stationary phase, for all pristine MWCNT concentration or doses and the control, no changes were detected.

When the growth profile of the control is compared to that of the cells containing pristine MWCNTs, a shorter exponential-phase is exhibited and the resting state more rapidly reached. There is no significant difference in the growth curves of cultures containing pristine MWCNTs and the control at all three stages of growth. Growth curves were very similar at both lower and higher concentrations of pristine MWCNTs.

An analysis of covariance was conducted to determine if the slopes of the growth curves were significantly different. The level of significance was chosen as $P < 0.05$. From the results no statistical differences in yeast growth are observed through all three growth phases.

No growth inhibition of cultures incubated with MWCNTs is observed .The results demonstrate that pristine MWCNTs do not inhibit cell proliferation and that these MWCNTs are not inherently toxic to *S.cerevisiae* yeast cells. Differences between growth curves occur mainly in the late exponential and stationary phases but is found to be statistically insignificant.

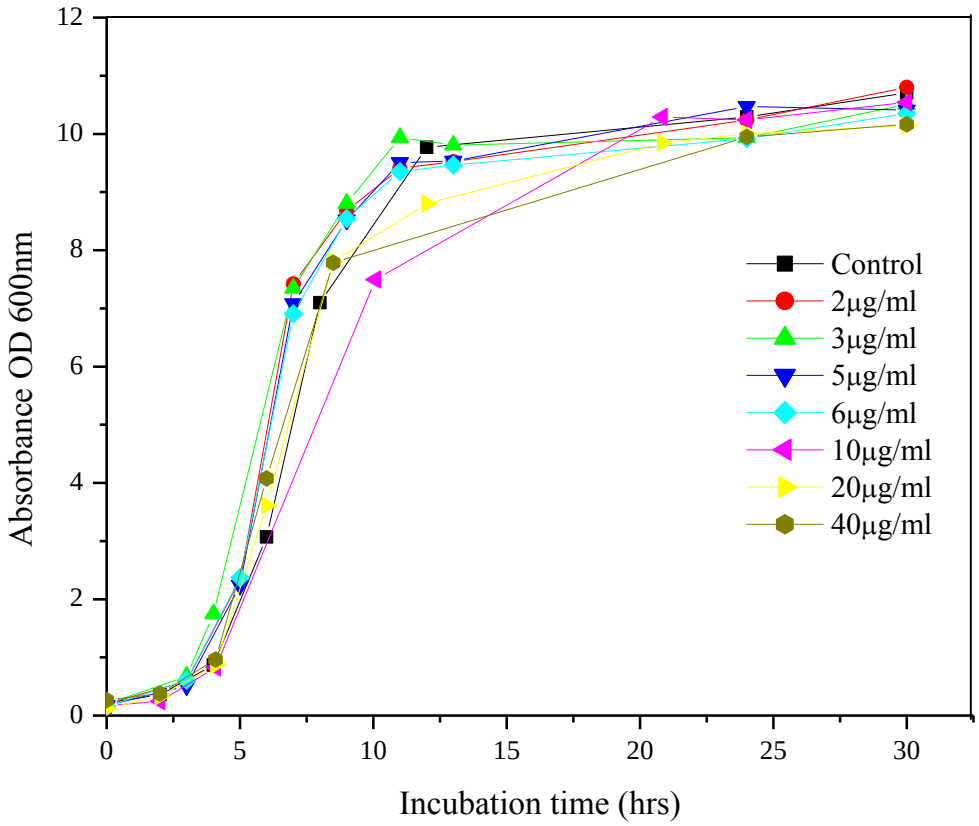


Figure 4.26: Growth curve of *S.cerevisiae* incubated with different concentrations of pristine MWCNTs to the control (incubated with no MWCNTs).

To test the toxicity of oxidised MWCNTs we assessed the growth of *S.cerevisiae* cells which were continuously exposed to dispersion of oxidised CNTs.

The growth curves of *S.cerevisiae* obtained in YPD broth are consistent with that of microorganism growing in liquid media (Figure 4.27). A standard growth curve comprise of a lag phase, during which organisms attune to a new environment and do not multiply actively. In this phase the growth was slow because the cells were adapting to the new surrounding media. Comparing the growth curves of cultures containing different concentrations of oxidised MWCNTs (2-40µg/ml) to the control the curves followed each other closely and no change was detected between cultures containing oxidised MWCNTs and the control. This indicates that during the early stages of microorganism growth and adaption oxidised MWCNTs do not interfere with the microorganism activity and do not negatively impact the cells process to adapt

to the environment. In this phase growth curves of experiments incubated with CNTs followed the control very closely and no differences can be seen. The lag phase is then followed by the logarithmic or exponential growth phase. This phase continues up to a point when all nutrients have been exhausted or until toxic metabolite accumulation occurs at which point time growth is slowed (Matousek et al., 2003). From Figure 4.27, it can be observed that moderate sensitivity is obvious in the mid logarithmic phase. Comparatively, a slower growth rate of *S.cerevisiae* grew in liquid YPD medium in the presence of oxidised MWCNTs at all concentration groups is also observed. Although growth is slightly lower in the exponential phase, in experiments containing oxidised MWCNTs at both low and high concentrations, the differences were not statistically significant. During the stationary phase there is a balance between cell multiplication and death. In the stationary phase cells recovered to a similar growth curves for the cultures containing oxidised MWCNTs as compared to the control.

An analysis of covariance was conducted to determine if the slopes of the oxidized MWCNT growth curves were significantly different from the control. The level of significance is chosen as $P < 0.05$, the results indicate that at the 0.05 level no statistical differences in yeast growth is observed in all three growth phases and the results of the 7 growth curves were not significantly different.

The results demonstrate that both pristine and oxidized MWCNTs did not inhibit cell proliferation and that these MWCNTs are not inherently cytotoxic to *S.cerevisiae* yeast cells.

Measuring the optical density of a yeast suspension (spectrophotometry) is a widely accepted method for evaluating yeast growth. Measuring transmittance with a spectrophotometer is easy and fast, but does not evaluate the viability of organisms in the suspension. It however measures the accumulation of live and dead cells over time with no distinction between the two (Matousek et al., 2003). It was needed to conduct viability assessments in addition to the growth experiments to investigate further the potential lethality of CNTs to *S.cerevisiae*.

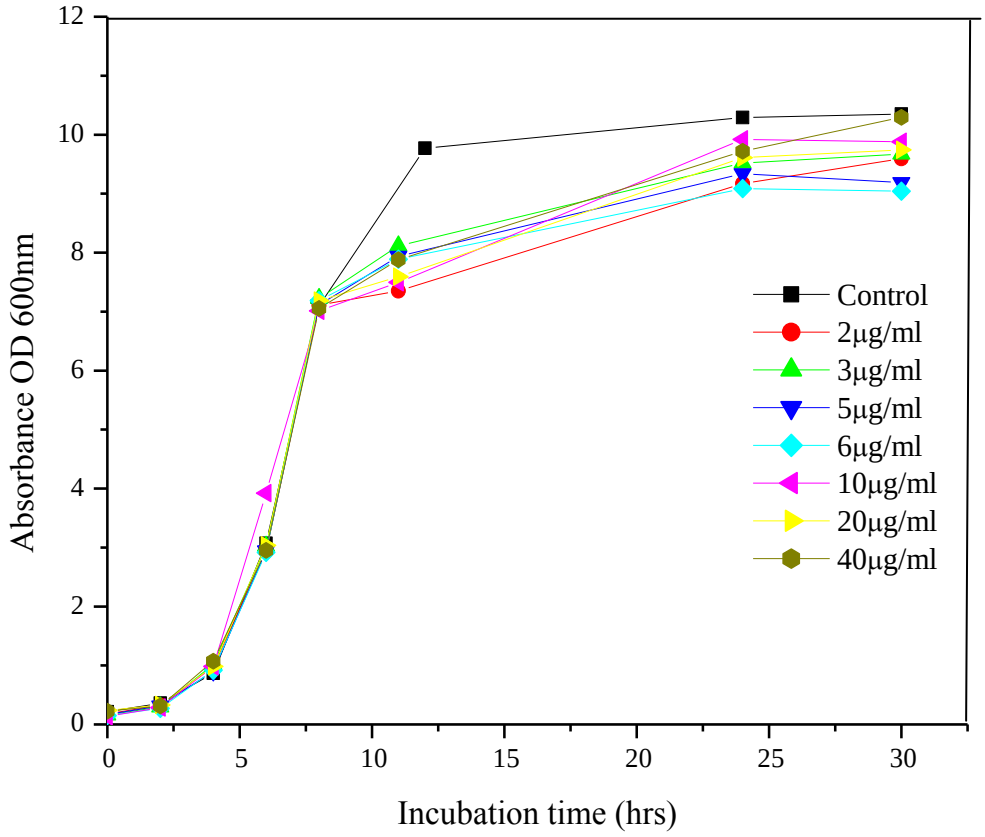


Figure 4.27: Growth curve of *S.cerevisiae* incubated with different concentrations of oxidized MWCNTs to the control (incubated with no MWCNTs).

4.3 *S.cerevisiae* Cell Viability

The influence of both pristine and oxidised MWCNTs on cell viability was assessed by the standard plate counting (SPC) technique. This method is able to distinguish between viable and dead cells as only cells which are viable will grow. At the start of the experiment (0 hr) the cell viability results of the cultures containing different concentrations of pristine and oxidized MWCNTs compared well with the control and no appreciable difference were found with values averaging between 1-2 million CFU/ml. As cells continue to grow and multiply a higher cell count is obtained with time, resulting in a higher viability value. At 5.5 hrs cell viability results indicate a close relationship to the control with slight differences when compared to viability results of cultures incubated with MWCNTs. The 3 µg/ml oxidized MWCNT group compares well with the control group with a viability difference of approximately 2 $\times 10^6$ CFU/ml. The 3

µg/ml oxidized MWCNT group and 40 µg/ml oxidized MWCNT group show very similar viability results, this thus shows that increasing concentration of oxidized MWCNT did not have an effect on cell viability. The 20 µg/ml oxidized MWCNT group compared well with the control with no significant difference evident. All the pristine MWCNT groups at 5.5 hrs shows similar results to the control 5.5 hrs incubation. The 20 µg/ml and 40 µg/ml group are slightly lower than the 3 µg/ml group but all three pristine MWCNT concentration groups, no major reduction was observed as compared to the control. These differences in viability can be as a result of the time involved in performing the serial dilution procedure whilst keeping samples in ice, by placing cells on ice growth is substantially reduced but not stopped thus resulting in the slight differences in viability values as compared to the control.

After 24 hrs incubation the cell viability results of both pristine and oxidized MWCNTs at both low and high concentrations reveal no apparent loss in cell viability of cultures incubated with MWCNTs of concentrations as compared to the control. To determine statistically if the cell viability data differ significantly, the program ORIGIN 6 professional was utilized. The least significant differences ($P < 0.05$) of the mean counts were calculated by One way ANOVA software. The results suggest that both pristine and oxidized MWCNTs have little influence on the cellular proliferation. The cell viability results are well in accordance with the growth experimental results.

Slight differences in cell viability results can be accounted for by the time involved in performing the serial dilution procedure whilst keeping samples on ice; by placing cells on ice growth is reduced but not stopped thus resulting in the slight differences in viability values as compared to the control.

In most cases the difference in viability values is small and no obvious decrease in cell viability was observed at both low and high doses of as-prepared and oxidized MWCNTs, compared with the control.

Neither pristine MWCNTs nor oxidized MWCNTs affected the viability at 30˚C on YPD plates. The reduction of the metal catalyst content of oxidized CNTs did not seem to reduce cell viability and compared closely with cell viability results of the pristine group at both high and low MWCNT concentrations. The experiments were done in triplicates and values averaged. An analysis of covariance was conducted and the level of significance was chosen as $P < 0.05$.

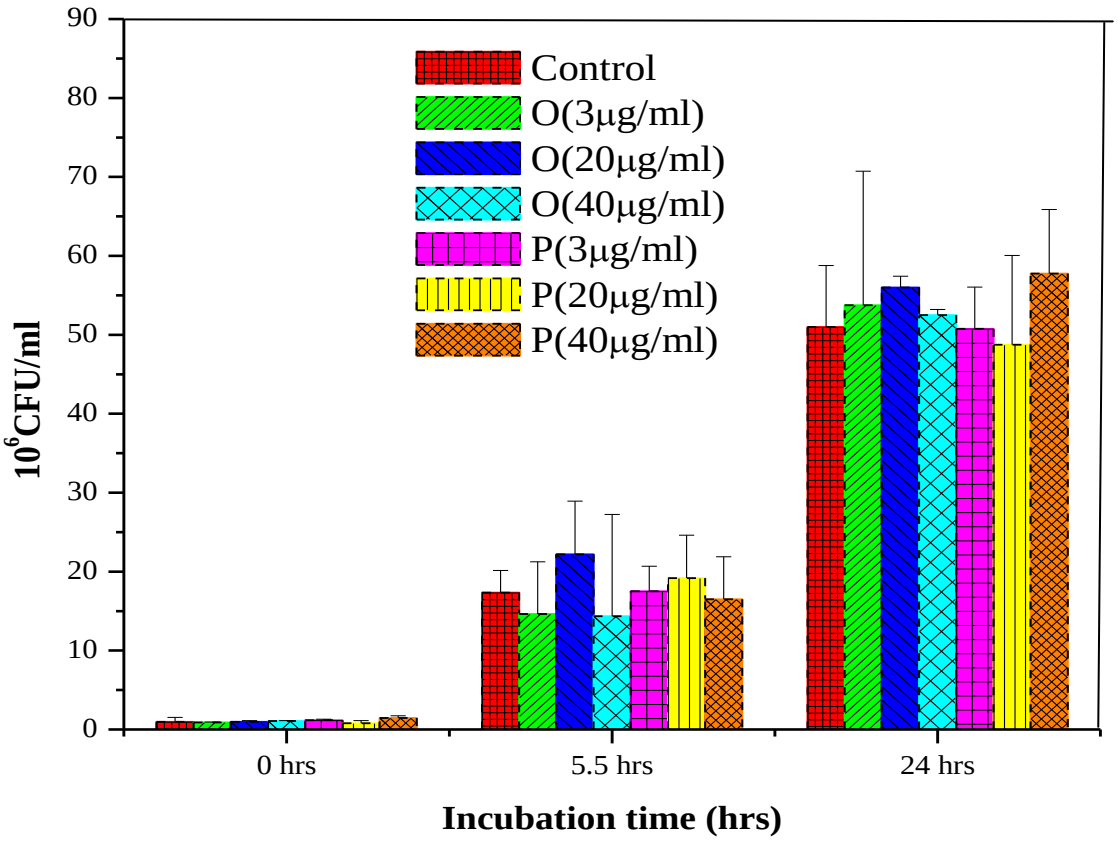


Figure 4.28: Graph demonstrating the cell viability of *S.cerevisiae* incubated with different concentrations of pristine (P) and oxidized (O) MWCNTs to the control (incubated with no MWCNTs). Error bars represent standard deviation (SD) of two sets of triplicate data from two different experiments.

Figure 4.29; show the MEA plate of cell viability analysis, a colony cell count of 30-300 is considered as a viable count. No noticeable changes in cell viability occurred.

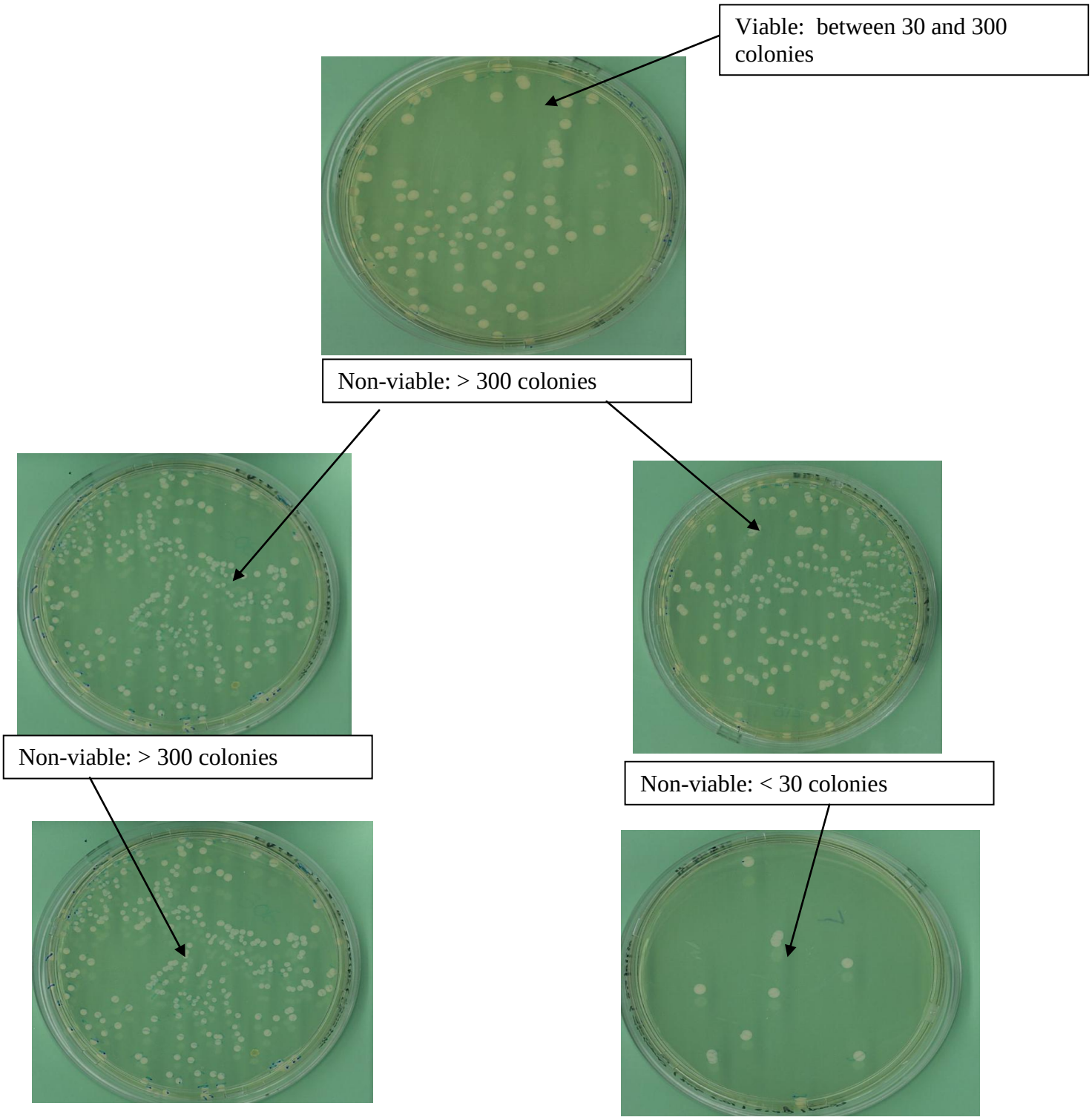


Figure 4.29: MEA plates showing viable and non-viable plates

Calibration/ standard curve results

As discussed in section 3, the calibration obtained is presented in Figure 4.30. From the calibration curve results, a linear relationship exists between the OD values and the number of

yeast cells. The linearity relationship between the OD values measured with a spectrophotometer and the cell number of direct counting cell were acceptably matched, as shown by the correlation coefficient, R^2= 0.970.

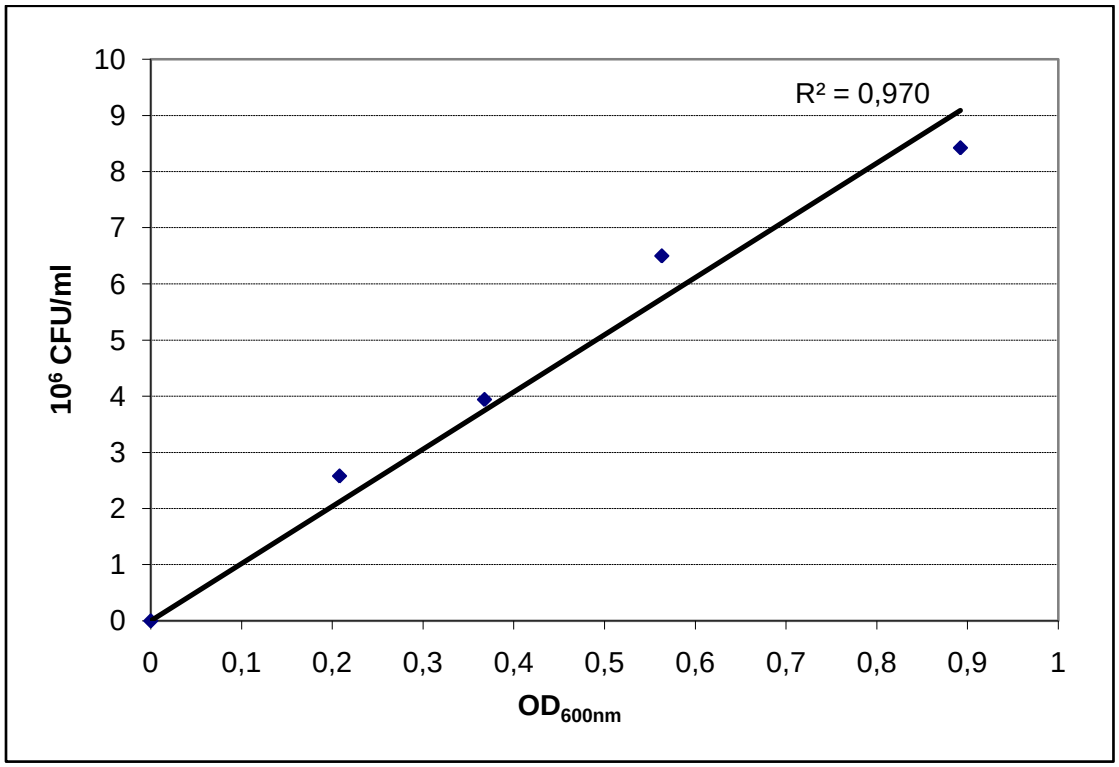


Figure 4.30: Calibration curve representing the relation between cell counts and absorbance of *S.cerevisiae* culture

4.4 Scanning Electron Microscopy analysis of cell morphology

In order to elucidate the effect of CNTs on cell morphology, yeast cell suspensions were incubated with varying concentrations of CNTs and compared to the control which was incubated without CNTs. Yeast cells were incubated with the following concentrations 0, 25, 5 and 100 µg/ml and were incubated for a period of 3 days.

SEM Micrographs of yeast cells without MWCNTS

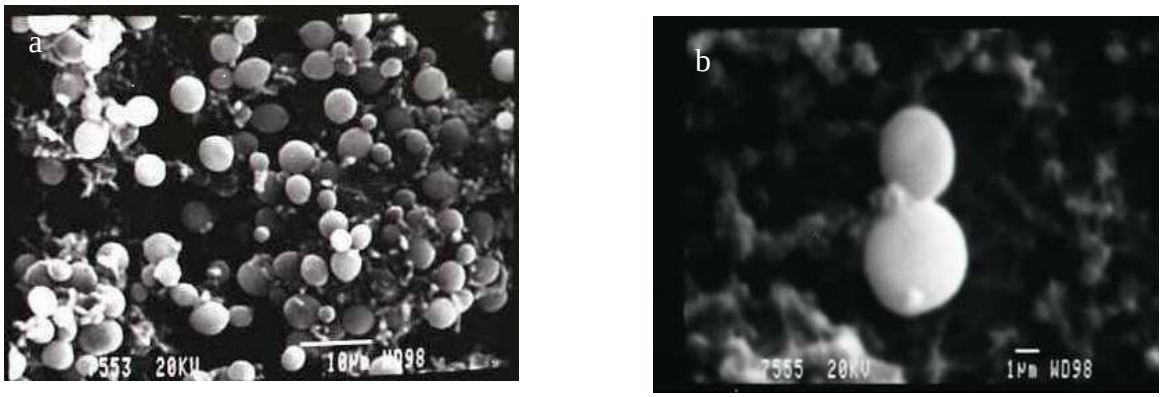


Figure 4.31 SEM micrographs of *S.cerevisiae* cells incubated without MWCNTs. (a) illustrating a group of *S.cerevisiae* cells (b) illustrating a single budding *S.cerevisiae* cell.

SEM Micrographs of yeast cells with MWCNTs

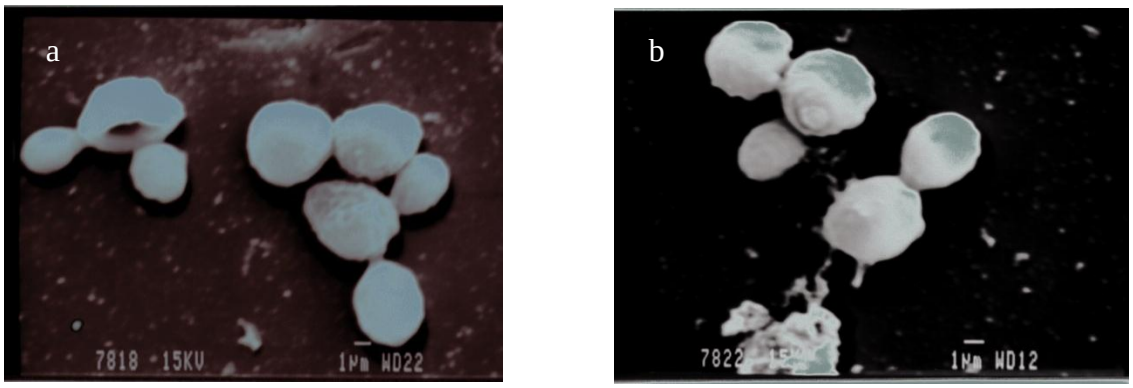


Figure 4.32 SEM micrographs of *S.cerevisiae* cells incubated with pristine MWCNTs. (a) illustrates group of *S.cerevisiae* cells where a single cell lost its intracellular content (b) illustrates group of *S.cerevisiae* cells with intact cell walls.

After 3 days of incubation, *S.cerevisiae* cell suspensions containing no CNTs had the common morphology of yeast cells and showed no morphological damage, for cells incubated with 25 µg/ml, 50 µg/ml of CNTs no cell damage was observed either. However after 3 days incubation of 100 µg/ml concentration of CNTs *S.cerevisiae* cells partly lost its contents, easily detected by a visible cavity in the middle wall became deformed as can be seen in Figure 4.32 (a). Cells lost their intracellular content, resulting in an empty deformed cell wall (typical of an apoptosis cell death). This was only observed in the cells incubated with 100 µg/ml of CNTs and not with the other samples. This suggests that at high concentrations of CNTs they are toxic and seems to

destroy the cell wall as well as the underlying membrane, whilst at lower concentrations they pose no harm or threat. Figure 4:32 depicts the incidence of cellular damage, but clearly this constitutes on 1/8 of the cells in the micrograph and is only a random event.

4.5 Confocal microscopy results

Intracellular trafficking and localisation of MWCNTs

The capacity of the fluorescent-labeled MWCNTs to penetrate into the yeast cells was studied using confocal microscopy. The green luminescence signal exhibited by the tubes allowed the direct imaging of the intracellular localization of CNTs using confocal microscopy. Fluorescence microscopy was used to track the distribution of MWCNT-FITC inside the cells. Confocal observations clearly show that MWCNT-FITC are internalised by *S.cerevisiae* yeast cells. The uptake of the MWCNT-FITC by the *S.cerevisiae* cells was clearly verified by fluorescence microscopy. After incubating *S.cerevisiae* yeast cells with 20 µg/mL of MWCNT-FITC for 1 hr a green fluorescence is observed throughout the cell (Figure 4.33 (a) and (b)). Work done previously on different cell types report fluorescence mainly concentrated on certain compartments of the cell such as the cytoplasm and nuclei (Pantarotto et al., 2004; Lu et al., 2010) or lysosomes. The confocal images clearly show the distribution of MWCNTs everywhere in the cell, this could be as a result of the method used for producing the MWCNTs that are more easily localised. Work done by Kostarelos, et al. (2007) reported that only 60% of S.cerevisiae cells were able to take up CNTs. In this work, however, S.cerevisiae cells took up all MWCNTs. Cells incubated with FITC only (not conjugated to MWCNTs), did not show fluorescence within the cell and was unable to cross the cell membrane barrier without conjugation to MWCNTs (Figure 4.34).

In order to examine *S.cerevisiae* cells incubated without MWCNTs by fluorescence microscopy cells were stained with PKH 26GL Red fluorescent cell linker kit (Sigma-Aldrich; St Louis, MO) and examined under fluorescence microscopy. From Figure 4.35 (a) and (b) the red fluorescence can be observed and the cell membrane of the cells as well as the characteristic budding of yeast cells is also observed.

Endocytosis is known as the general entry mechanism for a range of extracellular materials and it is an energy-dependent process (Pantoroto et al., 2004). The mechanism of internalisation of CNTs into cells is an area that is not well researched or known and investigation into the entry mechanisms of internalized MWCNTs are thus highly recommended.

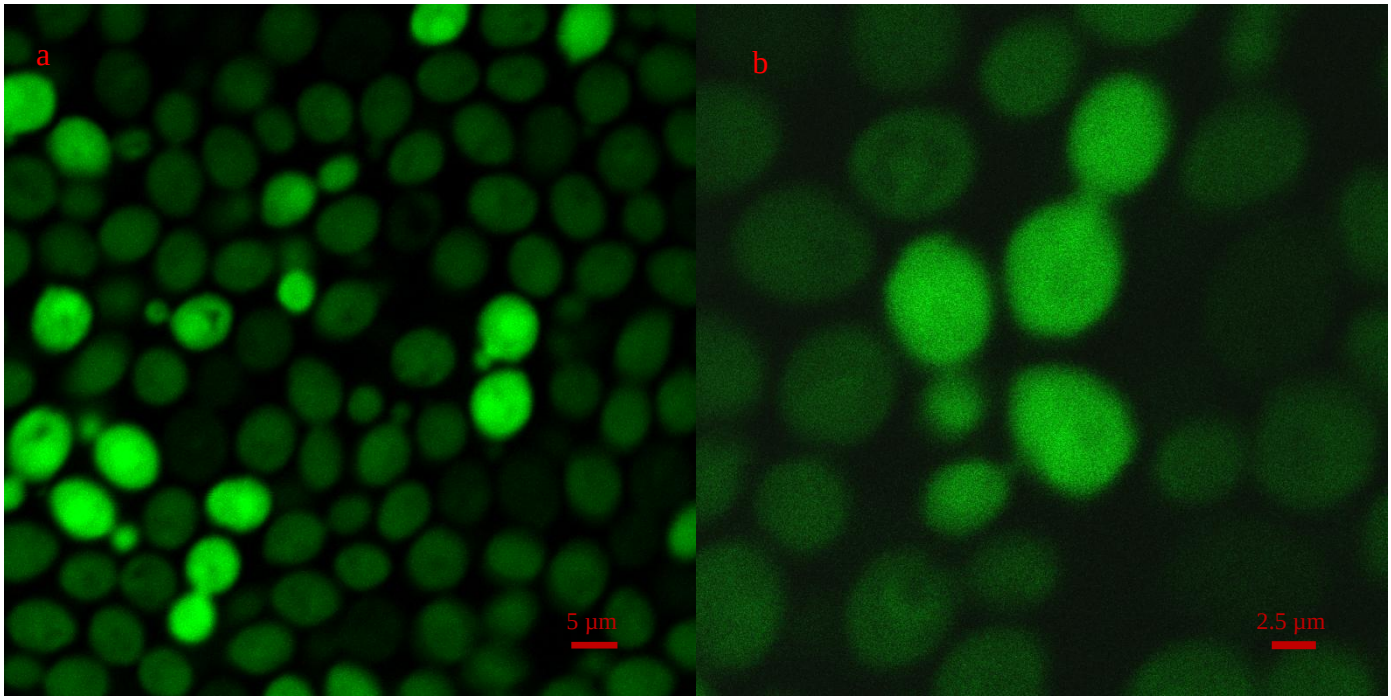


Figure 4.33. Confocal image of *S.cerevisiae* cells incubated with 20µg/ml MWCNT-FITC for 1and 1/2 hrs. (a) at a scale of 5µm (b) at a scale of 2.5 µm.

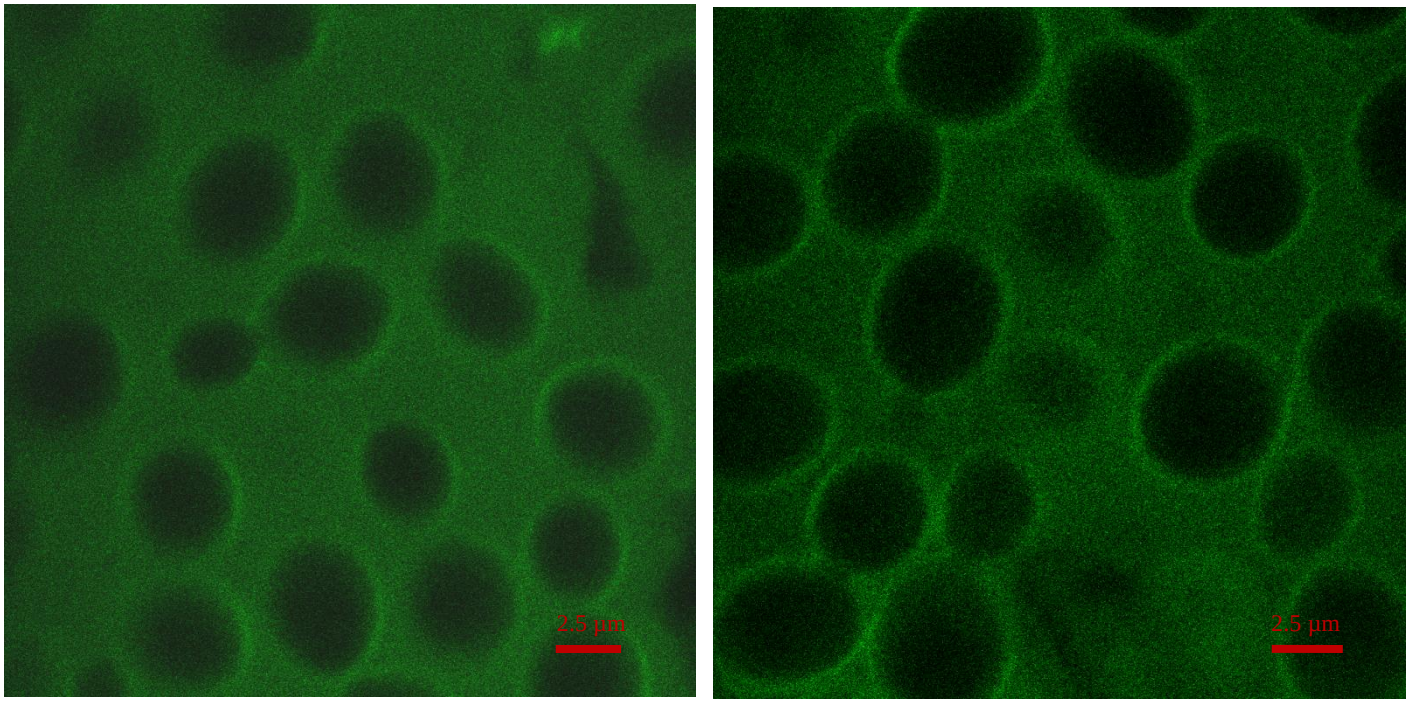


Figure 4.34. Confocal image of *S.cerevisiae* cells incubated with 20µg/ml FITC only for 1and 1/2 hrs at a scale of 2.5µm.

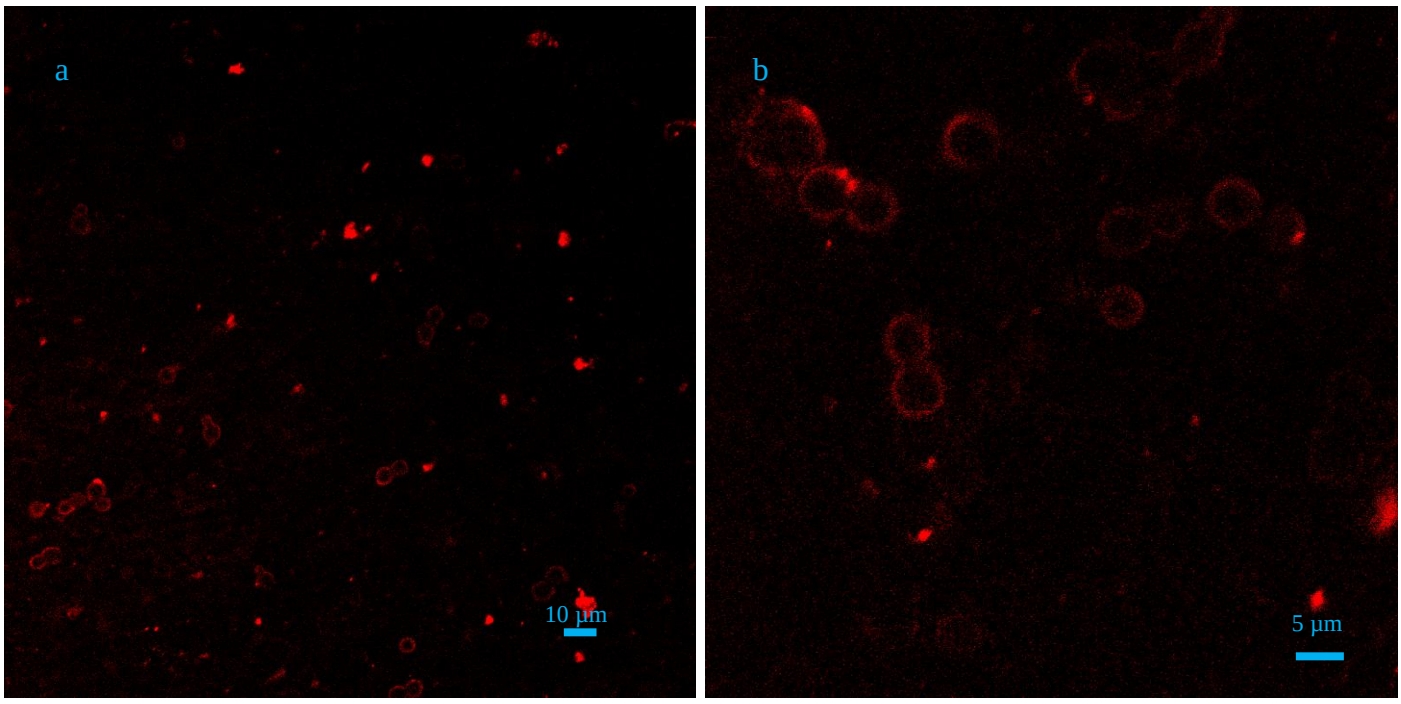


Figure 4.35. Confocal image of red stained membrane *S.cerevisiae* cells (a) at a scale of 10 µm (b) at a scale of 5 µm.

The influence of pristine and 30% nitric acid oxidised MWCNTs and FITC-MWCNTs on cell growth were assessed spectrophotometrically. The growth curves of pristine, oxidised MWCNTs and FITC-MWCNTs compared well with the control with no appreciable difference at a MWCNT incubation of 20µg/ml (Figure 4.36). Interestingly the FITC-MWCNTs taken up by the *S.cerevisiae* cells, as shown by confocal microscopy, showed the same growth pattern similarly to the control, pristine and oxidised MWCNTs.

Analysis of covariance was conducted to determine if the slopes of the oxidised MWCNT growth curves were significantly different from the control. The level of significance was chosen as $P < 0.05$, the results indicate that at the 0.05 level no statistical differences in yeast growth was observed in all three growth phases and that the results of the growth curves were not significantly different.

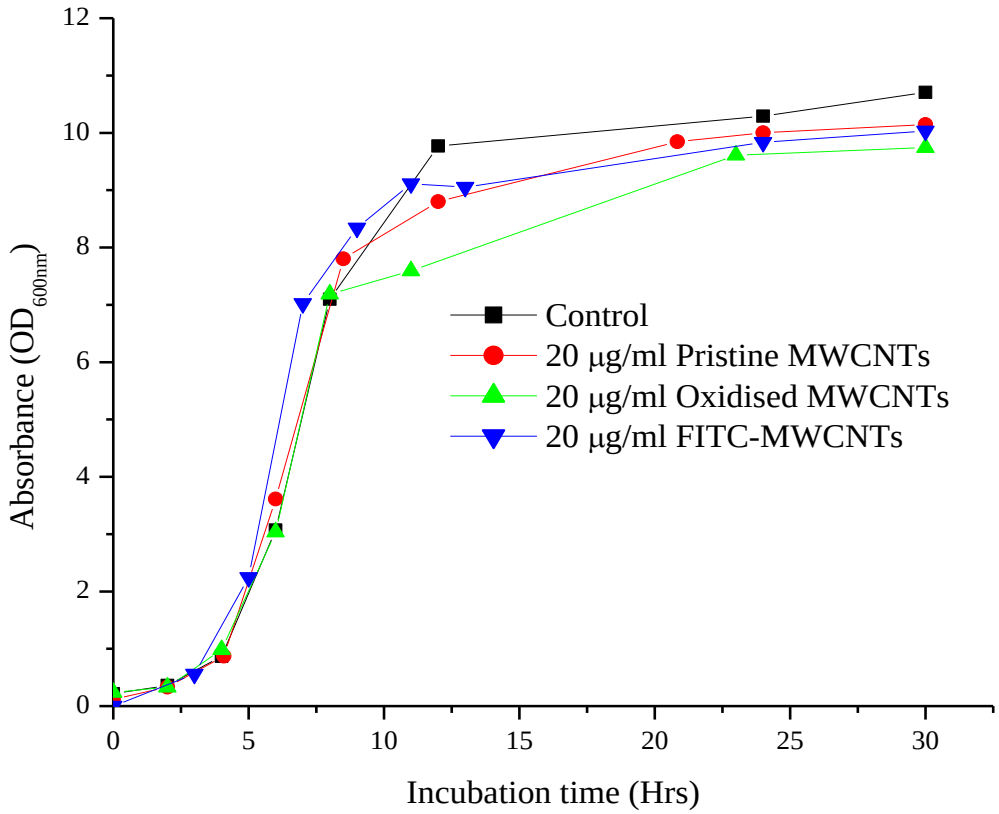


Figure 4.36: Growth curve of *S.cerevisiae* incubated with 20 µg/ml pristine, oxidized, FITC-MWCNTs and the control.

4.6 Neuronal Cell Cytotoxicity of CNTs

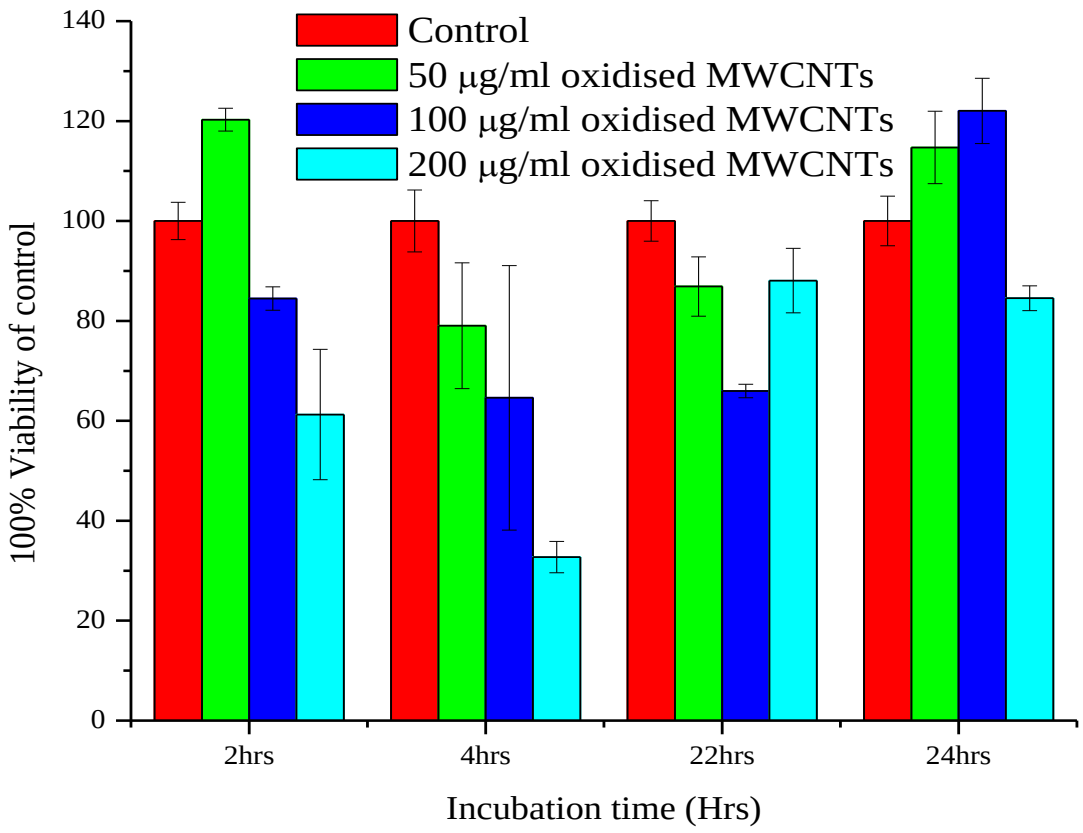


Figure 4.37: Cytotoxic response of Pheochromocytoma PC12 cells to oxidised MWCNTs. Error bars represent standard deviation (SD) of one sets of triplicate data

In this study the CytotoxGlo assay from Promega was utilized to determine the effect of various concentrations of oxidised MWCNTs on the viability of cultured PC12 cells. After 2 hrs incubation of 50 µg/ml oxidized MWCNTs, no loss in cell viability occurs whilst after 4hrs incubation the percentage of viable cells reduces to 79% compared to the control group (incubated with no MWCNTs). The 100 µg/ml and 200 µg/ml oxidised MWCNT concentration groups showed a reduction in the percentage of viable cells immediately after 2 hrs incubation of 84 and 61 percent respectively, as compared to the control group. After 4 hrs incubation, reduction in the percentage of viable cells occurs in all 3 concentration groups (50 µg/ml,100 µg/ml and 200 µg/ml) .It should also be noted that the reduction is concentration dependent . At

22 hrs incubation of the 50 µg/ml and 200 µg/ml oxidised MWCNT concentration groups, the viable cells recover to around 87 % to the control in both groups. This recovery continues and after 24 hrs of incubation all percentage of viable cells recovered and no loss in cell viability was observed in all MWCNT concentrations groups with the exception of the 200 µg/ml MWCNT concentration group which recovered to a viability of 85% as compared to the control. The effect of high concentrations of oxidized MWCNTs on the viability of PC12 cells was found to be suppressive at earlier stages of incubation and this suppressive effect was also concentration dependent at early periods of oxidized MWCNT incubation. However at later periods 22 hrs and 24 hrs the percentage of viable cells at all 3 MWCNT concentration groups had recovered to a level similar to the control and no reduction of viability was observed. The results indicate that at early stages (2 hrs and 4hrs) of incubation of PC12 cells with oxidized MWCNTs a decrease in percentage cell viability may have resulted since at early stages of incubation cells enter a period where they adapt to the new environment. It is postulated that cells incubated with high concentrations of oxidised MWCNTs took a longer time period as compared to the control to adjust to their new environment and thus the reduction in cell viability was observed. However after 24 hrs incubation PC12 cells have reorganised their molecular constituents and no reduction in cell viability is evident. From the above results it can be seen that oxidised MWCNTs caused no cell toxicity after 24 hrs incubation.

4.7 Morphology of PC12 cells

To examine the morphology of PC12 cells, a bright field microscope was used, Figure 4.37 (a)-(b) below gives the typical images of the PC12 cells and does not focus on the effect of MWCNTs of apopstasis.

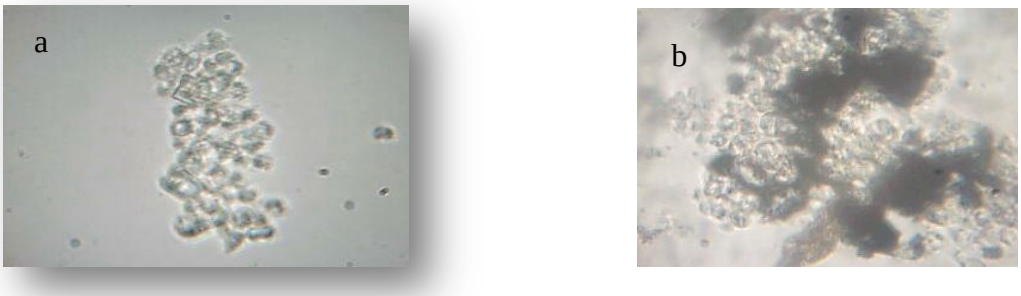


Figure 4.37: Optical phase contrast microscope photographs of PC12 cells (a) incubated without oxidised MWCNTs (b) incubated with oxidised MWCNTs.

CHAPTER 5

Conclusion and Recommendations

5.1 Conclusion

Toxicity effect of as-prepared and oxidized MWCNTs in-vitro was investigated by growth analysis, cell viability analysis, cytotoxicity analysis, and electron microscopic examination on *S.cerevisiae* and Pheochromocytoma PC12 cells. The physicochemical properties of MWCNTs were characterized by TEM, BET, Raman spectroscopy, TGA and SEM analysis. Overall it can be concluded that

- The quality of purified MWCNTs resulting from the 30% HNO_3 acid treatment was higher than that of the pristine MWCNTs as indicated by TEM, BET, TGA, SEM and Raman spectroscopy; whilst the 1:3 HNO_3:H_2SO_4 acid treated MWCNTs induced structural defects.
- The employed acid treatments effectively removed metal catalyst from the MWCNT samples.
- At both high (40 μg/ml) and low (2 μg/ml) concentration of MWCNTs incubation no changes in *S.cerevisiae* growth and cell viability was observed, as compared with the control.
- It has been shown that FITC-functionalised MWCNTs are taken up by *S.cerevisiae* cells in less than 2 hrs incubation and translocated inside all the compartments of *S.cerevisiae* cells. The FITC functionalized MWCNTs did not induce changes in growth of *S.cerevisiae* cells compared to the control.
- FITC without conjugation to MWCNTs are unable to cross the cell membrane barrier.
- The effect of high concentrations of oxidized MWCNTs on the viability of PC12 cells was suppressive at earlier stages of incubation and the suppressive effect was concentration dependent. However at later periods 22 hrs and 24 hrs the percentage of viable cells at all 3 MWCNT doses had recovered to a level similar to the control and no reduction of viability was observed.
- It could be correct to propose that functionalised CNTs (f-CNTs) can transport drugs or other moieties to both yeast and neuronal cells. The common thresholds of drug delivery vary from 1 – 50 μg/ml. Wu, et al (2005) investigated the targeted delivery of Amphotericin B

towards mammalian cells using functionalised MWCNTs, cells were treated with doses of functionalised MWCNTs ranging from 1 – 40 µg/ml. Kam, et al (2005) incubated Hela cells with DNA functionalised CNTs at a dosage of 2.5-5 µg/ml, and Dumortier, et al (2006) incubated primary immune cells with functionalised CNTs at a dosage of 10 µg/ml.

5.2 Recommendations

Higher quality purification of MWCNTs can be achieved by employing a thermal treatment such as vacuum annealing in conjunction with an acid treatment. Further investigations should be done on the entry mechanism of functionalised MWCNTs into cells since this is a field that is not well investigated. Endocytosis-inhibition experiments could be a start.
Interestingly, CNTs can be used as adsorbents in wastewater treatment. *S.cerevisae* has been used for screening of oestrogenic compounds in aqueous samples and quantification of oestrogens in human plasma, bovine plasma and in unextracted activated sludge (Wozei & Hermanowicz, 2006). The combination of functionalised CNTs internalised by *S.cerevisiae* cells could show improved adsorption and hence improved novel applications could be achieved.

Future work should attempt to distinguish the toxicological effects of catalyst impurities separately from carbonaceous impurities that cause defects in CNTs. For complete determination of residue masses, future work should maintain the same final temperature of 1100˚C, an experimental error led to the incompletion of this work.
Figure 4.32 depecits only a random event, it would be recommend that future work be carried out to investigate and establish the threshold of intercellular damage.

In future work the typical powers of the incident light used in the growth experiments should be noted in order to avoid ambiguity introduced into the reproducibility of the experiment as a result of variation associated with fluctuations in the intensity of the light source.

Investigations into the cytoxicity of PC12 cells should be further extended to functionalise MWCNTs with increased doses and time (one week to a month of incubation). The adaption at high concentration dosage of oxidised MWCNTs should be determined. The correlation of molecular reorginisation and cell growth/death should be investigated further.

REFERENCES

Abdulkareem, A.S., Afolabi, A.S., Iyuke, S.E. and Pienaar, H.C., 2007. Synthesis of carbon nanotubes by swirled floating catalyst chemical vapour deposition method. *Journal of Nanoscience and Nanotechnology*, **7**(9), pp. 3233-3238.

Ajayan, P.M., Schadler, L.S., Giannaris, C. and Rubio, A., 2000. Single-Walled Carbon Nanotube Polymer Composites: Strength and Weakness. *Advanced Materials*, **12**(10), pp. 750-753.

Alcamo, I.E., 2001. Fundamentals of Microbiology. Sudbury, Canada: *Jones and Bartlett Publishers*, 6ed, pp. 109-112.

Albuerne, J., Boschetti-de-fierro, A. and Abetz, V., 2010. Modification of multiwall carbon nanotubes by grafting from controlled polymerization of styrene: Effect of the characteristics of the nanotubes. *Journal of Polymer Science Part B: Polymer Physics*, **48**(10), pp. 1035-1046.

Amberg, D.C., 1998. Three-dimensional imaging of the yeast actin cytoskeleton through the budding cell cycle. *Molecular biology of the cell*, **9**(12), pp. 3259-3262.

Andrews, R., Jacques, D., Qian, D. and Rantell, T., 2002. Multiwall carbon nanotubes: synthesis and application. *Accounts of Chemical Research*, **35**(12), pp. 1008-1017.

Araujo, R., Paiva, M., Proenca, M. and Silva, C., 2007. Functionalization of carbon nanofibres by 1,3-dipolar cycloaddition reactions and its effect on composite properties. *Composites Science and Technology*, **67**(5), pp. 806 - 810.

Azarmi, S., Roa, W.H. and Löbenberg, R., 2008. Targeted delivery of nanoparticles for the treatment of lung diseases. *Advanced Drug Delivery Reviews*, **60**(8), pp. 863-875.

Azevedo, R.B., Silva, L.P., Lemos, A.P.C., Bao, S.N., Lacava, Z.G.M., Safarik, I., Safarikova, M. and Morais, P.C., 2003. Morphological study of Saccharomyces cerevisiae cells treated with magnetic fluid. *Magnetics*, **39**(5), pp. 2660-2662.

Bacsa, R.R., Laurent, C.H., Peigney, A., Bacsa, W.S., Vaugien T.H., and Rousset, A., 2002. High specific surface area carbon nanotubes from catalytic chemical vapour deposition process. *Chemical Physical Letter,*. **323** pp. 566-571.

Bai, F., 2007. Process Oscillations in Continuous Ethanol fermentation with *Saccharomyces cerevisae*. Dissertation, University of the Waterloo, Canada, pp. 12-15.

Ballesteros, B., Tobias, G., Shao, L., Pellicer, E., Nogues, J., Mendoza, E. and Green, M.L., 2008. Steam purification for the removal of graphitic shells coating catalytic particles and the shortening of single-walled carbon nanotubes. *Small,* **4**(9), pp. 1501-1506.

Bandow, S., Rao, A.M., Williams, K.A., Thess, A., Smalley, R.E. and Eklund, P.C., 1997. Purification of Single-Wall Carbon Nanotubes by Microfiltration *The Journal of Physical Chemistry B,* **101**(44), pp. 8839 - 8842.

Belin, T. and Epron, F., 2005. Characterization methods of carbon nanotubes: a review. *Materials Science and Engineering B,* **119**(2), pp. 105-118.

Benfell, K.E., Beamish, B.B. and Rodgers, K.A., 1996. Thermogravimetric analytical procedures for characterizing New Zealand and Eastern Australian coals. *Thermochimica Acta,* **286**(1), pp. 67-74.

Bhushan. B., 2004. Springer Handbook of Nanotechnology. *Springer-Verlag, Berlin, Heidelberg,Germany,* pp. 40-63.

Bianco, A., Kostarelos, K. and Prato, M., 2005. Applications of carbon nanotubes in drug delivery. *Current opinion in chemical biology,* **9**(6), pp. 674-679.

Bonard, J., Stora, T., Salvetat, J., Maier, F., Stöckli, T., Duschl, C., Forró, L., De Heer, W.A. and Châtelain, A., 1997. Purification and size-selection of carbon nanotubes. *Advanced Materials,* **9**(10), pp. 827-831.

Bostein, D., Chervitz, S.A. and Michael, C., 1997. Yeast as a model organism. *Science,* **277**(5330), pp. 1259-1260.

Bottini, M., Bruckner, S., Nika, K., Bottini, N., Bellucci, S., Magrini, A., Bergamaschi, A. and Mustelin, T., 2006. Multi-walled carbon nanotubes induce T lymphocyte apoptosis. *Toxicology letters,* **160**(2), pp. 121-126.

Bougrine, A., Naji, A., Ghanbaja, J. and Billaud, D., 1999. Purification and structural characterization of single-walled carbon nanotubes. *Synthetic Metals,* **103**(13), pp. 2480-2481.

Brunauer, S., Emmett, P.H. and Teller, E., 1938. Adsorption of Gases in Multimolecular Layers. *J. Am. Chem. Soc.* **60**(2), pp. 309-319.

Cabral, M.G., Viegas, C.A., Teixeira, M.C. and Sá-Correia, I., 2003. Toxicity of chlorinated phenoxyacetic acid herbicides in the experimental eukaryotic model Saccharomyces cerevisiae: role of pH and of growth phase and size of the yeast cell population. *Chemosphere,* **51**(1), pp. 47-54.

Cappuccino, J.G. and Sherman, N., 1983. Microbiology: A Laboratory Manual. *Menlo Park: Addison-wesley,* pp. 23-77.

Carlile, M.J. and Watkinson, S.C., 1996. The Fungi. London. *Academic Press Limited.* pp. 90-139.

Cao, A., Ci, L., Wu, G., Wei, B., Xu, C., Liang, J. and Wu, D., 2001. An effective way to lower catalyst content in well-aligned carbon nanotube films. *Carbon,* **39**(1), pp. 152-155.

Carey, J.D., 2009. Improving the field emission from carbon nanotubes through chemical functionalisation: a quantifiable approach. *Journal of nanoscience and nanotechnology,* **9**(11), pp. 6538-6541.

Chang, I.P., Hwang, K.C. and Chiang, C.S., 2008. Preparation of fluorescent magnetic nanodiamonds and cellular imaging. *Journal of the American Chemical Society,* **130**(46), pp. 15476-15481.

Chattopadhyay, D., Galeska, I. and Papadimitrakopoulos, F., 2002. Complete elimination of metal catalysts from single wall carbon nanotubes. *Carbon,* **40**(7), pp. 985-988.

Chen, C., Chen, M., Leu, F., Hsu, S., Wang, S., Shi, S. and Chen, C., 2004. Purification of multi-walled carbon nanotubes by microwave digestion method. *Diamond and Related Materials,* **13**(48), pp. 1182-1186.

Chen, H., Xiong, H., Gao, Y. and Li, H., 2010. Covalent functionalization of multiwalled carbon nanotubes with polybutadiene. *Journal of Applied Polymer Science,* **116**(3), pp. 1272-1277.

Chen, J., Chen, S., Zhao, X., Kuznetsova, L.V., Wong, S.S. and Ojima, I., 2008. Functionalized single-walled carbon nanotubes as rationally designed vehicles for tumor-targeted drug delivery. *Journal of the American Chemical Society,* **130**(49), pp. 16778-16785.

Chen, P., Liu, H., Cui, R., Zhang, Z., Pang, D., Xie, Z., Zheng, H., Lu, Z. and Tong, H., 2008. Visualized investigation of yeast transformation induced with Li+ and polyethylene glycol. *Talanta,* **77**(1), pp. 262-268.

Chen, X., Tam, U.C., Czlapinski, J.L., Lee, G.S., Rabuka, D., Zettl, A. and Bertozzi, C.R., 2006. Interfacing carbon nanotubes with living cells. *Journal of the American Chemical Society*, **128**(19), pp. 6292-6293.

Chen, X.H., Chen, C.S., Cheng, F.Q., Zhang, G., Chen, Z.Z., 2002. Non-destructive purification of multi-walled carbon nanotubes produced by catalyzed CVD. *Materials Letters*, **57**, pp. 734-738.

Chen, X., Wu, P., Rousseas, M., Okawa, D., Gartner, Z., Zettl, A. and Bertozzi, C.R., 2009. Boron nitride nanotubes are noncytotoxic and can be functionalized for interaction with proteins and cells. *Journal of the American Chemical Society*, **131**(3), pp. 890-891.

Cheng, C., Müller, K.H., Koziol, K.K.K., Skepper, J.N., Midgley, P.A., Welland, M.E. and Porter, A.E., 2009. Toxicity and imaging of multi-walled carbon nanotubes in human macrophage cells. *Biomaterials*, **30**(25), pp. 4152-4160.

Cherukuri, P., Bachilo, S.M., Litovsky, S.H. and Weisman, R.B., 2004. Near-infrared fluorescence microscopy of single-walled carbon nanotubes in phagocytic cells. *Journal of the American Chemical Society*, **126**(48), pp. 15638-15639.

Chin, S.F., Baughman, R.H., Dalton, A.B., Dieckmann, G.R., Draper, R.K., Mikoryak, C., Musselman, I.H., Poenitzsch, V.Z., Xie, H. and Pantano, P., 2007. Amphiphilic helical peptide enhances the uptake of single-walled carbon nanotubes by living cells. *Experimental biology and medicine (Maywood, N.J.)*, **232**(9), pp. 1236-1244.

Choi, S.K., Lee, S., 2009. Role of thermal treatment on the structural behaviour of the arc SWNTs in the purification system process, *Current Applied Physics*, **9**, pp. 658-662.

Costa, S., Borowiak-Palen E, Kruszyńska M, Bachnatiuk A, Kaleńczuk RJ. 2008. Characterization of Carbon Nanotubes by Raman spectroscopy. *Materials Science-Poland*. **26**(2): 433-441.

Cottrell, T.L., 1958. "The Strengths of Chemical Bonds," 2nd ed., Butterworths, London.

Couteau, E., Hernadi, K., Seo, J.W., Thiên-Nga, L., Mikó, C., Gaál, R. and Forró, L., 2003. CVD synthesis of high-purity multiwalled carbon nanotubes using CaCO3 catalyst support for large-scale production. *Chemical Physics Letters*, **378**(12), pp. 9-17.

Cui, H.F., Vashist, S.K., Al-Rubeaan, K., Luong, J.H. and Sheu, F.S., 2010. Interfacing carbon nanotubes with living mammalian cells and cytotoxicity issues. *Chemical research in toxicology*, **23**(7), pp. 1131-1147.

Daenan, M, De Fouw, R.D., Hamers, B., Janssen, P.G.A., Schouteden, K and Veld, M.A.J., 27 February 2003. The Wondrous World of Carbon Nanotubes 'a review of current carbon nanotube technologies'. *Eindhoven University of Technology*. pp. 1-96.

Dai, H., 2002. Carbon nanotubes: synthesis, integration, and properties. *Accounts of Chemical Research,* **35**(12), pp. 1035-1044.

Dalton A B ET, A., 2004. *Adv. Funct. Mater.*

Darmstadt, H., and Ryoo, R., 2008. Adsorption on Ordered Porous Carbons in Bottani EJ, Tascón JMD. Adsorption by carbons. Amsterdam, London*: Elsevier Ltd*, Chap 18:455-477.

Deacon, J,. 2006. Fungal Biology. Malden, Massachusetts, *Blackwell Publishing,* 4ed, pp. 76-80.

De Nollin, S. and Borgers, M., 1975. Scanning electron microscopy of Candida albicans after in vitro treatment with miconazole. *Antimicrobial Agents and Chemotherapy,* **7**(5), pp. 704-711.

Deng, Z., Dailey, L.A., Soukup, J., Stonehuerner, J., Richards, J.D., Callaghan, K.D., Yang, F. and Ghio, A.J., 2009. Zinc transport by respiratory epithelial cells and interaction with iron homeostasis. *Biometals : an international journal on the role of metal ions in biology, biochemistry, and medicine,* **22**(5), pp. 803-815.

Detriche, S., Zorzini, G., Colomer, J.F., Fonseca, A. and Nagy, J.B., 2008. Application of the Hansen solubility Parameters theory to carbon nanotubes. *Journal of nanoscience and nanotechnology*, **8**(11), pp. 6082-6092.

Dettlaff-Weglikowska, U., Benoit, J.M., Chiu, P., Graupner, R., Lebedlin, S., and Roth, S., 2002. " Chemical functionalization of single walled carbon nanotubes", *Current Applied Physics 2,* pp. 497 -501.

Dillon, A.C., Gennett, T., Jones, K.M., Alleman, J.L., Parilla, P.A. and Heben, M.J., 1999. A Simple and Complete Purification of Single-Walled Carbon Nanotube Materials. *Advanced Materials*, **11**(16), pp. 1354-1358.

Ding, L.H., Stilwell, J., Zhang, T.T., Elboudwarej, O., Jiang H.J., Selegue, J.P., Cooke, P.A., Gray, J.W., and Chen, F.Q.F., 2005. Molecular characterization of the cytotoxic mechanism of multiwall carbon nanotubes and nano-onions on human skin fibroblast. *Nano Letters,* **5**, pp. 2448-2464.

Donkor, A.D., Su, Z., Mandal, H.S., Jin, X. and Tang, X.S., 2010; 2009. Carbon nanotubes inhibit the hemolytic activity of the pore-forming toxin pyolysin *Nano Research,* **2**(7), pp. 517 - 525.

Dresselhaus, M.S., Dresselhaus, G., Saito, R. and Jorio, A., 2005. Raman spectroscopy of carbon nanotubes. *Physics Reports,* **409**(2), pp. 47-99.

Dresselhaus, S.R., 1998. *Physical Properties of Carbon Nanotubes.(Imperial College)*

Dumortier, H., Lacotte, S., Pastorin, G., Marega, R., Wu, W., Bonifazi, D., Briand, J.P., Prato, M., Muller, S. and Bianco, A., 2006. Functionalized carbon nanotubes are non-cytotoxic and preserve the functionality of primary immune cells. *Nano letters,* **6**(7), pp. 1522-1528.

Duque, J.G., Cognet, L., Parra-Vasquez, A.N., Nicholas, N., Schmidt, H.K. and Pasquali, M., 2008. Stable luminescence from individual carbon nanotubes in acidic, basic, and biological environments. *Journal of the American Chemical Society,* **130**(8), pp. 2626-2633.

Emeis, C.C., 1966. Performance and stability of culture yeast. *MBAA Technical Quartlerly,* **3**(4), pp. 265-267.

Esteves, I.A.A.C., Cruz, F.J.A.L., Müller, E.A., Agnihotri, S. and Mota, J.P.B., 2009. Determination of the surface area and porosity of carbon nanotube bundles from a Langmuirian analysis of sub- and supercritical adsorption data. *Carbon,* **47**(4), pp. 948-956.

Feng, Y., Zhang, H., Hou, Y., McNicholas, T.P., Yuan, D., Yang, S., Ding, L., Feng, W., and Liu, J., 2008. Room temperature purification of few-walled carbon nanotubes with high yield. *ACS Nano,* **2**(8), pp. 1634-1638.

Feazell, R.P., Nakayama-Ratchford, N., Dai, H. and Lippard, S.J., 2007. Soluble single-walled carbon nanotubes as longboat delivery systems for platinum(IV) anticancer drug design. *Journal of the American Chemical Society,* **129**(27), pp. 8438-8439.

Firme III, C.P. and Bandaru, P.R., 2010. Toxicity issues in the application of carbon nanotubes to biological systems. *Nanomedicine: Nanotechnology, Biology and Medicine,* **6**(2), pp. 245-256.

Flahaut, E., Durrieu, M.C., Remy-Zolghadri, M., Bareille, R. and Baquey, C., 2006. Investigation of the cytotoxicity of CCVD carbon nanotubes towards human umbilical vein endothelial cells. *Carbon,* **44**(6), pp. 1093-1099.

García, A., Herrero, M.A., Frein, S., Deschenaux, R., Muñoz, R., Bustero, I., Toma, F. and Prato, M., 2008. Synthesis of dendrimer-carbon nanotube conjugates. *Physica Status Solidi (A) Applications and Materials,* **205**(6), pp. 1402-1407.

Garcia, J., Gomes, H.T., Serp, P., Kalck, P., Figueiredo, J.L. and Faria, J.L., 2006. Carbon nanotube supported ruthenium catalysts for the treatment of high strength wastewater with aniline using wet air oxidation. *Carbon,* **44**(12), pp. 2384-2391.

Georgakilas, V., Bourlinos, A., Gournis, D., Tsoufis, T., Trapalis, C., Mateo-Alonso, A. and Prato, M., 2008. Multipurpose organically modified carbon nanotubes: From functionalization to nanotube composites. *Journal of the American Chemical Society,* **130**(27), pp. 8733-8740.

Georgakilas, V., Kordatos, K., Prato, M., Guldi, D.M., Holzinger, M. and Hirsch, A., 2002. Organic functionalization of carbon nanotubes. *Journal of the American Chemical Society,* **124**(5), pp. 760-761.

Georgakilas, V., Tagmatarchis, N., Pantarotto, D., Bianco, A., Briand, J.P. and Prato, M., 2002. Amino acid functionalisation of water soluble carbon nanotubes. *Chemical communications (Cambridge, England),* **(24)**(24), pp. 3050-3051.

Georgakilas, V., Voulgaris, D., Vazquez, E., Prato, M., Guldi, D.M., Kukovecz, A. and Kuzmany, H., 2002. Purification of HiPCO carbon nanotubes via organic functionalization. *Journal of the American Chemical Society,* **124**(48), pp. 14318-14319.

Ghafari, P., St-Denis, C.H., Power, M.E., Jin, X., Tsou, V., Mandal, H.S., Bols, N.C. and Tang, X.S., 2008. Impact of carbon nanotubes on the ingestion and digestion of bacteria by ciliated protozoa. *Nature nanotechnology*, **3**(6), pp. 347-351.

Godoy, J.P.M., Azevedo, R.B., Silva, L.P., Lacava, Z.G.M., Báo, S.N., Silva, O., Pelegrini, F., Gansau, C., Buske, N., Safarik, I., Safarikova, M. and Morais, P.C., 2004. Magnetic resonance investigation of magnetic-labeled baker's yeast cells. *Journal of Magnetism and Magnetic Materials*, **272-276**(Part 3), pp. 2400-2401.

Gormand, A. 2008. The Crosstalk between the ERK and the cAMP Signalling Pathways in PC12 Cells. *Thesis, University of Glassgow,* pp. 30-40.

Grobert, N., 2007. Carbon nanotubes- becoming clean. *Materials Today,* **10**, pp. 28-35.

Hallock, M.F., Greenley, P., Diberardinis, L. and Kallin, D., 2009. Potential risks of nanomaterials and how to safely handle materials of uncertain toxicity. *Journal of Chemical Health and Safety,* **16**(1), pp. 16-23.

Hatakeyama, T., and Quinn, F.X., 1999. Thermal Analysis Fundamentals and Applications to Polymer Science, 2nd edition, *John Wiley & Sons, West Sussex, England,* pp. 1-10.

Heggart HM, Margaritis A, Pilkington H, Stewart RJ, Oowbanick TM, Russell I. 1999. Factors affecting yeast viability and vitality characteristics: A Review, *MBAA Technical Quarterly*, **36**(4): 383-406.

Heggart, H., Margaritis, A., Stewart, R.J., Pikington, H., Sobczak, J., Russell, I., 2000. Measurement of brewing yeast viability and vitality: A review of methods. *MBAA Technical Quarterly,* **37**(4), pp. 409-430.

Herzog, E., Byrne, H.J., Casey, A., Davoren, M., Lenz, A., Maier, K.L., Duschl, A. and Oostingh, G.J., 2009. SWCNT suppress inflammatory mediator responses in human lung epithelium in vitro. *Toxicology and applied pharmacology,* **234**(3), pp. 378-390.

Herzog, E., Casey, A., Lyng, F.M., Chambers, G., Byrne, H.J., and Davoren, M., 2007. A new approach to the testing of carbon-based nanomaterials – The clonogenic assay. *Toxicology Letters,* **174**. Pp. 49-60.

Hernadi, K., Fonseca, A., Nagy, JB., Bernaerts, D., Riga, J., Lucas, A., 1996. Catalytic synthesis and purification of carbon nanotubes. *Synthetic metals*, **77**, pp 31-34.

Holzinger, M., Abraham, J., Whelan, P., Graupner, R., Ley, L., Hennrich, F., Kappes, M. and Hirsch, A., 2003. Functionalization of single-walled carbon nanotubes with (R-)oxycarbonyl nitrenes, *Journal of the American Chemical Society,* **125**(28), pp. 8566-8580.

Horan, P.K., and Slezak, S.E., 1989. Stable cell membrane labelling. *Nature*, **34**, pp. 167-167-168.

Horváth, Z.E., Kertész, K., Pethő, L., Koós, A.A., Tapasztó, L., Vértesy, Z., Osváth, Z., Darabont, A., Nemes-Incze, P., Sárközi, Z. and Biró, L.P., 2006. Inexpensive, upscalable nanotube growth methods. *Current Applied Physics,* **6**(2), pp. 135-140.

Hou, P.X., Bai, S., Yang, Q.H., Liu, C. and Cheng, H.M., 2002. Multi-step purification of carbon nanotubes. *Carbon,* **40**(1), pp. 81-85.

Hou, P., Liu, C. and Cheng, H., 2008. Purification of carbon nanotubes. *Carbon,* **46**(15), pp. 2003-2025.

Hu, H., Zhao, B., Itkis, M.E. and Haddon, R.C., 2003. Nitric Acid Purification of Single-Walled Carbon Nanotubes *The Journal of Physical Chemistry B,* **107**(50), pp. 13838 - 13842.

Hu, J., Chen, C., Zhu, X. and Wang, X., 2009. Removal of chromium from aqueous solution by using oxidized multiwalled carbon nanotubes. *Journal of hazardous materials,* **162**(2-3), pp. 1542-1550.

Hu, P., Tanii, T., Zhang, G., Hosaka, T. and Ohdomari, I., 2007. Ultrasensitive detection of biomolecules using functionalized multi-walled carbon nanotubes. *Sensors and Actuators B: Chemical*, **124**(1), pp. 161-166.

Huczko, A., Lange, H., Calko, E., Grubek-Jaworska, H., and Droszcz, P., 2001. Physiological testing of carbon nanotubes: Are they asbestos-like?, *Pol. Fullerene Sci. Technol.* **9**(2), pp. 251–254 (abstract).

Hurst, K.E., Dillon, A.C., Yang, S., and Lehman, J.H., 2008. Purification of Single Wall Carbon Nanotubes As a Function of UV Wavelength, Atmosphere, and Tepmerature, *The Journal of Physical Chemistry C*, **112**(42), pp. 16296-16300.

Igarashi, H., Murakami, H., Murakami, Y., Maruyama, S. and Nakashima, N., 2004. Purification and characterization of zeolite-supported single-walled carbon nanotubes catalytically synthesized from ethanol. *Chemical Physics Letters,* **392**, pp. 529-532.

Iijima, S., Ajayan, P.M. and Ichihashi, T., 1992. Growth model for carbon nanotubes. *Physical Review Letters,* **69**(21), pp. 3100-3103.

Imai, T., Nakajima, I., and Ohno, T., 1993. Development of a new method for evaluation of yeast vitality by measuring intracellular pH, *MBAA Technical Quarterly,* **30**, pp. 109-113.

Irons, D.J., 2009. Logical analysis of the budding yeast cell cycle. *Journal of theoretical biology,* **257**(4), pp. 543-559.

Iyuke, S.E., Swirled Fluidised Bed Chemical Vapour Deposition Reactor. 2005. *SA Patent Apllication, No 2101,2005,03438.*

Iyuke, S.E., Abdulkareem, S.A., Afolabi, S.A. and Pienaar, C.H.V., 2007. Catalytic production of carbon nanotubes in a swirled fluid chemical vapour deposition reactor. *International Journal of Chemical Reactor Engineering*, **5**.

Iyuke, S.E. and Danna, A.B.M., 2005. Morphological study of carbon nanotubes synthesised by FCCVD. *Microporous and Mesoporous Materials,* **84**(1-3), pp. 338-342.

Jennison, M.W., 1937. The Relations Between Plate Counts and Direct Microscopic Counts of Escherichia coli During the Logarithmic Growth Period. *Journal of Bacteriology,* **33**(5), pp. 461-477.

Jia, G., Wang, H.F., Yan, L., Wang, X., Pei, R., Yan, T., Zhao, Y.L., and Guo, X.B., 2005. Cytotoxicity of carbon nanomaterials: Single-wall nanotube, multi-wall nanotube, and fullerene. *Environmental Science and Technology,* **39**, pp. 1378-1383.

Jiang, H., Zhao, Y., Yang, H. and Akins, D.L., 2009. Synthesis and electrochemical properties of single-walled carbon nanotube–gold nanoparticle composites. *Materials Chemistry and Physics*, **114**, pp. 879-883.

Jomdecha, C., and Prateepasen, A., 2006. The research of low-ultrasonic energy affects to yeast growth in fermentation process, *12th A-PCNDT- Asia-Pacific Conference on NDT, 5th-10th Nov 2006, Auckland, New Zealand.*

Jos, A., Pichardo, S., Puerto, M., Sánchez, E., Grilo, A. and Cameán, A.M., 2009. Cytotoxicity of carboxylic acid functionalized single wall carbon nanotubes on the human intestinal cell line Caco-2. *Toxicology in Vitro*, **23**(8), pp. 1491-1496.

Kam, N.W. and Dai, H., 2005. Carbon nanotubes as intracellular protein transporters: generality and biological functionality. *Journal of the American Chemical Society*, **127**(16), pp. 6021-6026.

Kam, N.S.W., O'Connell, M., Wisdom, J.A., Dai, H., 2005. Carbon nanotubes as multifunctional biological transporters and near-infrared agents for selective cancer cell destruction. *Proceedings of the National Academy of Sciences of the United States of America*, **102**(33), pp. 11600-11605.

Kang, S., Mauter, M.S. and Elimelech, M., 2008. Physicochemical determinants of multiwalled carbon nanotube bacterial cytotoxicity. *Environmental science & technology*, **42**(19), pp. 7528-7534.

Kim, Y., Cho, J., Ansari, S.G., Kim, H., Dar, M.A., Seo, H., Kim, G., Lee, D., Khang, G. and Shin, H., 2006. Immobilization of avidin on the functionalized carbon nanotubes. *Synthetic Metals*, **156**(14-15), pp. 938-943.

Ko, F., Lee, C., Ko, C. and Chu, T., 2005. Purification of multi-walled carbon nanotubes through microwave heating of nitric acid in a closed vessel. *Carbon*, **43**(4), pp. 727-733.

Kostarelos, K., Lacerda, L., Pastorin, G., Wu, W., Wieckowski, S., Luangsivilay, J., Godefroy, S., Pantarotto, D., Briand, J.P., Muller, S., Prato, M. and Bianco, A., 2007. Cellular uptake of functionalized carbon nanotubes is independent of functional group and cell type. *Nature nanotechnology*, **2**(2), pp. 108-113.

Lam, C.W., James, J.T., McCluskey, R., Arepalli, S. and Hunter, R.L., 2006. A review of carbon nanotube toxicity and assessment of potential occupational and environmental health risks. *Critical reviews in toxicology*, **36**(3), pp. 189-217.

Lam, C.W., James, J.T., McCluskey, R. and Hunter, R.L., 2004. Pulmonary toxicity of single-wall carbon nanotubes in mice 7 and 90 days after intratracheal instillation. *Toxicological sciences : an official journal of the Society of Toxicology,* **77**(1), pp. 126-134.

Lamouroux, E., Serp, P. and Kalck, P., 2007. Catalytic Routes Towards Single Wall Carbon Nanotubes *Catalysis Reviews,* **49**(3), pp. 341-405.

Lewis, M.J., and Enevoldsen, B., 1972. Yeast growth and beer flavour. *MBAA Techincal Quarterl,*. **10**(1), pp. 20-28.

Li, Q., Mahendra, S., Lyon, D.Y., Brunet, L., Liga, M.V., Li, D. and Alvarez, P.J.J., 2008. Antimicrobial nanomaterials for water disinfection and microbial control: Potential applications and implications. *Water research,* **42**(18), pp. 4591-4602.

Li, Y., Di, Z., Ding, J., Wu, D., Luan, Z. and Zhu, Y., 2005. Adsorption thermodynamic, kinetic and desorption studies of Pb2+ on carbon nanotubes. *Water research,* **39**(4), pp. 605-609.

Lin, D.Q., Brixius, P.J., Hubbuch, J.J., Thommes, J. and Kula, M.R., 2003. Biomass/adsorbent electrostatic interactions in expanded bed adsorption: a zeta potential study. *Biotechnology and bioengineering,* **83**(2), pp. 149-157.

Lin, S. and Juang, R., 2009. Adsorption of phenol and its derivatives from water using synthetic resins and low-cost natural adsorbents: A review. *Journal of environmental management,* **90**(3), pp. 1336-1349.

Lobo, A.O., Antunes, E.F., Machado, A.H.A., Pacheco-Soares, C., Trava-Airoldi, V.J. and Corat, E.J., 2008. Cell viability and adhesion on as grown multi-wall carbon nanotube films. *Materials Science and Engineering: C,* **28**(2), pp. 264-269.

Lucente-Schultz, R.M., Moore, V.C., Leonard, A.D., Price, B.K., Kosynkin, D.V., Lu, M., Partha, R., Conyers, J.L. and Tour, J.M., 2009. Antioxidant single-walled carbon nanotubes. *Journal of the American Chemical Society*, **131**(11), pp. 3934-3941.

Lui, R., 2008, The Functionalisation of Carbon nanotubes, Dissertation, University of New South Wales, Sydney, Australia, pp. 6-12.

Liu, Z., Chen, K., Davis, C., Sherlock, S., Cao, Q., Chen, X., Dai, H., 2008. Drug Delivery with Carbon Nanotubes for *In vivo* Cancer Treatment. *American Association for Cancer Research,* **68**(16), pp. 6653-6660.

Luongo, L.A. and Zhang, X., 2010. Toxicity of carbon nanotubes to the activated sludge process. *Journal of hazardous materials,* **178**, pp. 356-362.

Ma, L., Wen, J., Lu, W., Caiyin, Q. and Liang, Y., 2008. Efficient immobilization of lactate dehydrogenase in biocomposites of double-walled carbon nanotube-doped alginate gel. *Enzyme and microbial technology,* **42**(3), pp. 235-241.

Ma, P., Mo, S., Tang, B. and Kim, J., 2010. Dispersion, interfacial interaction and re-agglomeration of functionalized carbon nanotubes in epoxy composites. *Carbon,* **48**(6), pp. 1824-1834.

Mackenzie, K., Dunens, O. and Harris, A.T., 2009. A review of carbon nanotube purification by microwave assisted acid digestion. *Separation and Purification Technology,* **66**(2), pp. 209-222.

Martins, M.A.M., Cardoso, M.H., Queiroz, M.J., Ramalho, M.T. and Campus, A.M.O., 1999. Biodegradation of azo dyes by the yeast Candida zeylanoides in batch aerated cultures. *Chemosphere,* **38**(11), pp. 2455-2460.

Matousek, J.L., Campbell, K.L., Kakoma, I., Solter, P.F. and Schaeffer, D.J., 2003. Evaluation of the effect of pH on in vitro growth of Malassezia pachydermatis. *Canadian journal of veterinary research = Revue canadienne de recherche veterinaire,* **67**(1), pp. 56-59.

Maynard, A.D., Baron, P.A., Foley, M., Shvedova, A.A., Kisin, E.R. and Castranova, V., 2004. Exposure to carbon nanotube material: aerosol release during the handling of unrefined single-walled carbon nanotube material. *Journal of toxicology and environmental health.Part A,* **67**(1), pp. 87-107.

Maynard, A.D., 2006. Nanotechnology: assessing the risks. *Nano Today,* **1**(2), pp. 22-33.

Meng, H., Xia, T., George, S. and Nel, A.E., 2009. A Predictive Toxicological Paradigm for the Safety Assessment of Nanomaterials *ACS Nano,* **3**(7), pp. 1620-1627.

Mitchell, D.N., Godwin, H.A., Claudio, E., 2004. Nonoparticle Toxicity in Saccharomyces cerevisiae: A Comparitive Study Using Au Colloid, Ag Colloid, and $HAuCl_4 \cdot 3H_2O$ in Solution, *Nanoscape,* **1**, pp. 59-69.

Mokwena, P., Marshall, A., Afolabi, A.S., Abdulkareem, A.S. and Iyuke, S.E., 2007. Thermodynamic stability of graphitic diamond films produced using CCVD apparatus. *SIAMM - Journal of The South African Institute of Mining and Metallurgy,* **107**(4), pp. 211-214.

Muller, J., Huaux, F., Moreau, N., Misson, P., Heilier, J.F., Delos, M., Arras, M., Fonseca, A., Nagy, J.B. and Lison, D., 2005. Respiratory toxicity of multi-wall carbon nanotubes. *Toxicology and applied pharmacology,* **207**(3), pp. 221-231.

Muller, J., Huaux, F. and Lison, D., 2006. Respiratory toxicity of carbon nanotubes: How worried should we be? *Carbon,* **44**(6), pp. 1048-1056.

Musso, S., Porro, S., Rovere, M., Chiodoni, A. and Tagliaferro, A., 2007. Physical and mechanical properties of thick self-standing layers of multiwall carbon nanotubes. *Diamond and Related Materials,* **16**(4-7), pp. 1174-1178.

Nelson, D.J., and Brammer, C.N., 2009. Pristine single-walled carbon nanotube purity evaluation by using ^{1}H NMR spectroscopy, *Analytical and Bioanalytical Chemistry,* **396**, pp. 1079-1086.

O'Connell, M.J., 2006. Carbon nanotubes: properties and applications, Boca Raton, Florida, *CRC/Taylor & Francis* pp. 1-30.

Öncel, Ç. and Yürüm, Y., 2006. Carbon Nanotube Synthesis via the Catalytic CVD Method: A Review on the Effect of Reaction Parameters *Fullerenes, Nanotubes, and Carbon Nanostructures,* **14**(1), pp. 17-37.

Paddock, S.W., 1999. Methods in Molecular Biology Series: Confocal Microscopy Methods and Protocols, Humana Press Inc, Totowa, New Jersey, pp. 1-20.

Paillet, M., Jourdain, V., Poncharal, P., Sauvajol, J., Zahab, A., Meyer, J.C., Roth, S., Cordente, N., Amiens, C. and Chaudret, B., 2005. Growth and physical properties of individual single-walled carbon nanotubes. *Diamond and Related Materials,* **14**(9), pp. 1426-1431.

Panessa-Warren, B.J., Maye, M.M., Warren, J.B. and Crosson, K.M., 2009. Single walled carbon nanotube reactivity and cytotoxicity following extended aqueous exposure. *Environmental Pollution,* **157**(4), pp. 1140-1151.

Pantarotto, D., Briand, J.P., Prato, M. and Bianco, A., 2004. Translocation of bioactive peptides across cell membranes by carbon nanotubes. *The Royal Society of Chemistry,* **(1)**, pp. 16-17.

Pantarotto, D., Partidos, C.D., Graff, R., Hoebeke, J., Briand, J.P., Prato, M. and Bianco, A., 2003. Synthesis, structural characterization, and immunological properties of carbon nanotubes functionalized with peptides. *Journal of the American Chemical Society,* **125**(20), pp. 6160-6164.

Pastorin, G., Wu, W., Wieckowski, S., Briand, J.P., Kostarelos, K., Prato, M. and Bianco, A., 2006. Double functionalisation of carbon nanotubes for multimodal drug delivery. *Chem. Commun.* **21**(11), pp. 1182-1184.

Pellicer, E, González-Guerrero, A., Nogués, J., Lechuga, LM., Mendoza E., 2009. Assessment of catalyst particle removal in multi-wall carbon nanotubes by highly sensitive magnetic measurements. *Carbon*, **47**, pp. 758-763.

Petford-Long, A.K., Kohn, A., Bromwich, T., Jackson, V., Castaño, F. and Singh, L.J., 2006. Application of TEM to the development of information storage materials. *Thin Solid Films,* **505**, pp. 10-15.

Pillay, K., Cukrowska, E.M. and Coville, N.J., 2009. Multi-walled carbon nanotubes as adsorbents for the removal of parts per billion levels of hexavalent chromium from aqueous solution. *Journal of hazardous materials,* **166**(2-3), pp. 1067-1075.

Popławska, M., Żukowska, G.Z., Cudziło, S. and Bystrzejewski, M., 2010. Chemical functionalization of carbon-encapsulated magnetic nanoparticles by 1,3-dipolar cycloaddition of nitrile oxide. *Carbon*, **48**(4), pp. 1312-1320.

Popov, V.N., 2004. Carbon nanotubes: properties and application. *Materials Science and Engineering: R: Reports*, **43**(3), pp. 61-102.

Porro, S., Musso, S., Vinante, M., Vanzetti, L., Anderle, M., Trotta, F. and Tagliaferro, A., 2007. Purification of carbon nanotubes grown by thermal CVD. *Physica E: Low-dimensional Systems and Nanostructures*, **37**(1-2), pp. 58-61.

Prato, M., Kostarelos, K., and Bianco, A., 2007. Functionalized carbon nanotubes in drug design and discover. *Accounts of Chemical Research*,**41**(1), pp.60-68.

Radford, D.R., Challacombe, S.J. and Walter, J.D., 1994. A scanning electronmicroscopy investigation of the structure of colonies of different morphologies produced by phenotypic switching of Candida albicans. *Journal of medical microbiology*, **40**(6), pp. 416-423.

Raffa, V., Ciofani, G., Nitodas, S., Karachalios, T., D'alessandro, D., Masini, M. and Cuschieri, A., 2008. Can the properties of carbon nanotubes influence their internalization by living cells? *Carbon*, **46**(12), pp. 1600-1610.

Rao, G.P., Lu, C. and Su, F., 2007. Sorption of divalent metal ions from aqueous solution by carbon nanotubes: A review. *Separation and Purification Technology*, **58**(1), pp. 224-231.

Reich, R., Thomsen, C., Maultzsch, J., 2004. Carbon Nanotubes Basic Concepts and Physical Properties, Weinheim, Cambridge, *Wiley-VCH*, pp. 3-50.

Reyhani, A., Mortazavi, S.Z., Nozad Golikand, A., Moshfegh, A.Z. and Mirershadi, S., 2008. The effect of various acids treatment on the purification and electrochemical hydrogen storage of multi-walled carbon nanotubes. *Journal of Power Sources,* **183**(2), pp. 539-543.

Rosa, C., and Peter, G., 2006. The Yeast Handbook, Biodiversity and Ecophysiology of Yeasts, Springer-Verlag, Berlin, Heidelberg, pp. 1-11.

Ryder, D.S., Woods, D.R., Murray, J.P., Masschelein, C.A., 1983. Some Practical Implications of Yeast Growth and Yeast Performance, *MBAA Technical Quarterly,* **20**(1), pp. 9-21.

Saito, T.L., Ohtani, M., Sawai, H., Sano, F., Saka, A., Watanabe, D., Yukawe, M., Ohya, Y. and Morishita, S., 2004. SCMD: *Saccharomyces cerevisiae* Morphological Database, *Nucleic acid research*, **32**, pp. 319-322.

Salvetat, J.P., Bonard, J.M., Thomson, N.H., Kulik, A.J., Forŕo, L., Benoit, W., and Zuppiroli, L.,1999. Mechanical properties of carbon nanotubes, *Applied Physics A Materials Science & Processing,* **69**(3), pp. 255-260.

Sampedro-Tejedor, P., Maroto-Valiente, A., Nevskaia, D.M., Múñoz, V., Rodríguez-Ramos, I. and Guerrero-Ruíz, A., 2007. The effect of growth temperature and iron precursor on the synthesis of high purity carbon nanotubes. *Diamond and Related Materials,* **16**(3), pp. 542-549.

Saxena, R.K.A.W., Mcgee, J.K., Daniels, M.J., Boykin, E., and Gilmour, I., 2007. Enhanced in vitro and in vivo toxicity of polydispersed acid-functionalised single-wall carbon nanotubes. *Nanotoxicology,* **1**, pp. 291-300.

Scherens, B. and Goffeau, A., 2000. The uses of genome-wide yeast mutant collection. *Genome Biology*, **5**(7). pp. 229.

Shi kam, N.W., Jessop, T.C., Wender, P.A. and Dai, H., 2004. Nanotube molecular transporters: internalization of carbon nanotube-protein conjugates into Mammalian cells. *Journal of the American Chemical Society,* **126**(22), pp. 6850-6851.

Shi, Z., Lian, Y., Liao, F., Zhou, X., Gu, Z., Zhang, Y. and Iijima, S., 1999. Purification of single-wall carbon nanotubes. *Solid State Communications,* **112**(1), pp. 35-37.

Shvedova, A.A., Kisin, E.R., Porter, D., Schulte, P., Kagan, V.E., Fadeel, B. and Castranova, V., 2009. Mechanisms of pulmonary toxicity and medical applications of carbon nanotubes: Two faces of Janus? *Pharmacology & therapeutics,* **121**(2), pp. 192-204.

Shuler, M.L., Kargi, F., 1992. Bioprocess engineering: basic concepts, Engelwood Cliffs, New Jersey, *Prentice Hall*, pp. 148-159.

Sinha, N., and Yeow, J.T.W., 2005. Carbon Nanotubes for Biomedical Applications. IEEE Trans. Nanobiosci, **4**(2), pp. 180-195.

Sinnott, S.B., Andrews, R., 2001. Carbon Nanotubes: Synthesis, Properties, and Applications, *Critical Reviews in Solid State and Materials Science,*. **26**(3), pp. 145-249.

Smart, S.K., Cassady, A.I., Lu, G.Q. and Martin, D.J., 2006. The biocompatibility of carbon nanotubes. *Carbon,* **44**(6), pp. 1034-1047.

Srivastava, D.E.A., 1998. *Ann. New York Acad. Sci.*

Stern, S.T. and McNeil, S.E., 2008. Nanotechnology safety concerns revisited. *Toxicological sciences : an official journal of the Society of Toxicology,* **101**(1), pp. 4-21.

Strong, K.L., Anderson, D.P., Lafdi, K. and Kuhn, J.N., 2003. Purification process for single-wall carbon nanotubes. *Carbon,* **41**(8), pp. 1477-1488.

Sudibya, H.G., Ma, J., Dong, X., NG, S., Li, L.J., Liu, X.W. and Chen, P., 2009. Interfacing glycosylated carbon-nanotube-network devices with living cells to detect dynamic secretion of biomolecules. *Angewandte Chemie (International ed.in English),* **48**(15), pp. 2723-2726.

Suzuki, S., Watanabe, Y. and Heun, S., 2006. Photoelectron spectroscopy and microscopy of carbon nanotubes. *Current Opinion in Solid State and Materials Science,* **10**(2), pp. 53-59.

Tagmatarchis, N. and Prato, M., 2005. Carbon-based materials: From fullerene nanostructures to functionalized carbon nanotubes. *Pure and Applied Chemistry,* **77**(10), pp. 1675-1684.

Terrones, M., 2003. *Annu. Rev. Mater. Res.*

Thambirajah, J.J., Zulkali, M.D. and Hashim, M.A., 1995. Microbiological and biochemical changes during the composting of oil palm empty-fruit-bunches. Effect of nitrogen supplementation on the substrate. *Bioresource technology,* **52**(2), pp. 133-144.

Tian, X., He, W., Cui, J., Zhang, X., Zhou, W., Yan, S., Sun, X., Han, X., Han, S. and Yue, Y., 2010. Mesoporous zirconium phosphate from yeast biotemplate. *Journal of colloid and interface science,* **343**(1), pp. 344-349.

Tkacz, J.S., Cybulska, E.B. and Lampen, J.O., 1971. Specific staining of wall mannan in yeast cells with fluorescein-conjugated concanavalin A. *Journal of Bacteriology*, **105**(1), pp. 1-5.

Tobias, G., Shao, L., Salzmann, C.G., Huh, Y., and Green, M.L., 2006. Purification and Opening of Carbon Nanotubes Using Steam. *The Journal of Physical Chemistry B.* 110 (45): 22318-22322.

Vaccarini, L., Goze, C., Aznar, R., Micholet, V., Journet, C. and Dernier, P., 1999. Purification procedure of carbon nanotubes. *Synthetic Metals*, **103**, pp. 2492-2493.

Walkinshaw, G. and Waters, C.M., 1994. Nuerotixin-induced cell death in neuronal PC12 cells is mediated by induction of apoptosis. *Nueroscience*, **63**(4), pp. 975-987.

Wang, Z.L., Poncharal, P. and De Heer, W.A., 2000. Measuring physical and mechanical properties of individual carbon nanotubes by in situ TEM. *Journal of Physics and Chemistry of Solids*, **61**(7), pp. 1025-1030.

Warheit, D.B., 2006. What is currently known about the health risks related to carbon nanotube exposures? *Carbon*, **44**(6), pp. 1064-1069.

Warheit, D.B., Brock, W.J., Lee, K.P., Webb, T.R. and Reed, K.L., 2005. Comparative pulmonary toxicity inhalation and instillation studies with different TiO2 particle formulations: impact of surface treatments on particle toxicity. *Toxicological sciences : an official journal of the Society of Toxicology*, **88**(2), pp. 514-524.

Warheit, D.B., Laurence, B.R., Reed, K.L., Roach, D.H., Reynolds, G.A. and Webb, T.R., 2004. Comparative pulmonary toxicity assessment of single-wall carbon nanotubes in rats. *Toxicological sciences : an official journal of the Society of Toxicology*, **77**(1), pp. 117-125.

Wick, P., Manser, P., Limbach, L.K., Dettlaff-Weglikowska, U., Krumeich, F., Roth, S., Stark, W.J. and Bruinink, A., 2007. The degree and kind of agglomeration affect carbon nanotube cytotoxicity. *Toxicology letters*, **168**(2), pp. 121-131.

Wozei, E., Hermanowicz, S.W., 2006. Developing a yeast-based assay protocol to monitor total oestrogenic activity induced by 17β-oestradiol in activated sludge supernatants from batch experiments, *Water SA*, **32**(3), pp. 345-354.

Wu, W., Li, R., Bian, X., Zhu, Z., Ding, D., Li, X., Jia, Z., Jiang, X. and Hu, Y., 2009. Covalently combining carbon nanotubes with anticancer agent: preparation and antitumor activity. *ACS nano*, **3**(9), pp. 2740-2750.

Wu, W., Wieckowski, S., Pastorin, G., Benincasa, M., Klumpp, C., Briand, J., Gennaro, R., Prato, M. and Bianco, A., 2005. Targeted Delivery of Amphotericin B to Cells byUsing Functionalized Carbon Nanotubes. *Angew. Chem. Int. Ed.***44**, pp. 6358 – 6362.

Wu, X.Z., Chang, W.Q., Cheng, A.X., Sun, L.M. and Lou, H.X., 2010. Plagiochin E, an antifungal active macrocyclic bis(bibenzyl), induced apoptosis in Candida albicans through a metacaspase-dependent apoptotic pathway. *Biochimica et biophysica acta,* **1800**(4), pp. 439-447.

Xiao, H., Zou, H., Pan, C., Jiang, X., Le, X.C. and Yang, L., 2006. Quantitative determination of oxidized carbon nanotube probes in yeast by capillary electrophoresis with laser-induced fluorescence detection. *Analytica Chimica Acta,* **580**(2), pp. 194-199.

Xu, P., Han, X.J., Liu, X.R., Zhang, B., Wang, C. and Wang, X.H., 2009. A study of the magnetic and electromagnetic properties of γ-Fe2O3–multiwalled carbon nanotubes (MWCNT) and Fe/Fe3C–MWCNT composites. *Materials Chemistry and Physics,* **114**(2-3), pp. 556-560.

Xue, C., Zhou, R., Shi, M., Wu, G., Zhang, X., Wang, M. and Chen, H., 2010. Electrochemistry of glucose oxidase immobilized on carbon nanotubes noncovalently functionalized by multihydroxyl and multicarboxyl groups. *Journal of Electroanalytical Chemistry,* **642**(1), pp. 92-97.

Yinghuai, Z., Peng, A.T., Carpenter, K., Maguire, J.A., Hosmane, N.S. and Takagaki, M., 2005. Substituted carborane-appended water-soluble single-wall carbon nanotubes: new approach to boron neutron capture therapy drug delivery. *Journal of the American Chemical Society,* **127**(27), pp. 9875-9880.

Yount, B.A., Lin-Cereghino, J., Lin-Cereghino, G.P. and Fox, M.M., 2006. Preparation of the Yeast Pichia pastoris for Transmission Electron Microscopy. *Microscopy today,* **14**(5), pp. 36-37.

Yu, Z., Hongkun, H. and Chao, G., 2008. Clickable macroinitiator strategy to build amphophilic polymer brushes on carbon nanotubes. *Macromolecules,* **41**(24), pp. 9581-9594.

Yumura, M., Ohshima, S., Uchida, K., Tasaka, Y., Kuriki, Y., Ikazaki, F., Saito, Y. and Uemura, S., 1999. Synthesis and purification of multi-walled carbon nanotubes for field emitter applications. *Diamond and Related Materials,* **8**(2-5), pp. 785-791.

Verploegen, E., Dworken, B.T., Faught, M., Kamperman, M., Zhang, Y., Wiesner, U., 2007. Tuning Mechanical Properties of Block Copolymer/Aluminosilicate Hybrid Materials. *Macromol. Rapid Commun 2.,* **28**, pp. 572 -578.

Zamaleeva, A.I., Sharipova, I.R., Porfireva, A.V., Evtugyn, G.A. and Fakhrullin, R.F., 2010. Polyelectrolyte-mediated assembly of multiwalled carbon nanotubes on living yeast cells. *Langmuir : the ACS journal of surfaces and colloids,* **26**(4), pp. 2671-2679.

Zhang, D., Yan, T., Pan, C., Shi, L. and Zhang, J., 2009. Carbon nanotube-assisted synthesis and high catalytic activity of CeO2 hollow nanobeads. *Materials Chemistry and Physics,* **113**, pp. 527-530.

Zhang, J., Tackaberry, T., Ritzel, M.W., Raborn, T., Barron, G., Baldwin, S.A., Young, J.D. and Cass, C.E., 2006. Cysteine-accessibility analysis of transmembrane domains 11-13 of human concentrative nucleoside transporter 3. *The Biochemical journal,* **394**(Pt 2), pp. 389-398.

Zhang, M., Yudasaka, M. and Iijima, S., 2001. Single-wall carbon nanotubes: a high yield of tubes through laser ablation of a crude-tube target. *Chemical Physics Letters,* **336**(3-4), pp. 196-200.

Zhang, T., Xu, M., He, L., Xi, K., Gu, M. and Jiang, Z., 2008. Synthesis, characterization and cytotoxicity of phosphoryl choline-grafted water-soluble carbon nanotubes. *Carbon,* **46**(13), pp. 1782-1791.

Zhang, W., Sprafke, J.K., Ma, M., Tsui, E.Y., Sydlik, S.A., Rutledge, G.C. and Swager, T.M., 2009. Modular functionalization of carbon nanotubes and fullerenes. *Journal of the American Chemical Society,* **131**(24), pp. 8446-8454.

Zhang, X., Meng, L., Wang, X., Lu, Q., 2010. Preparation and Cellular Uptake of pH-Dependant Fluorescent Single-Wall Carbon Nanotubes, *Chemistry a Euoropean Journal,***16**, pp. 556-561.

Zhang, X.X., Deng, C.F., Xu, R. and Wang, D.Z., 2007. Oxidation resistance of multi-walled carbon nanotubes purified with sulfuric and nitric acids *Journal of Materials Science,* **42**(19), pp. 8377 - 8380.

Zhang, Y., Ali, S.F., Dervishi, E., Xu, Y., Li, Z., Casciano, D. and Biris, A.S., 2010. Cytotoxicity effects of graphene and single-wall carbon nanotubes in neural phaeochromocytoma-derived pc12 cells. *ACS Nano,* **4**(6), pp. 3181-3186.

Zhang, Y., He, H., Gao, C. and Wu, J., 2009. Covalent layer-by-layer functionalization of multiwalled carbon nanotubes by click chemistry. *Langmuir,* **25**(10), pp. 5814-5824.

Zhao, N., He, C., Li, J., Jiang, Z. and Li, Y., 2006. Study on purification and tip-opening of CNTs fabricated by CVD. *Materials Research Bulletin,* **41**(12), pp. 2204-2209.

Zheng, L., Chi, Y., Dong, Y., Lin, J. and Wang, B., 2009. Electrochemiluminescence of water-soluble carbon nanocrystals released electrochemically from graphite. *Journal of the American Chemical Society,* **131**(13), pp. 4564-4565.

Zhu, Y., Ran, T., Li, Y., Guo, J. and Li, W., 2006. Dependence of the cytotoxicity of multi-walled carbon nanotubes on the culture medium. *Nanotechnology,***17**, pp. 4668-4674.

Zurek E, Autschbach J. 2009. NMR Computations for carbon nanotubes from first principles: Present status and future directions, *International Journal of Quantum Chemistry,* 109: 3343-3367.

Publications and presentations arising from this dissertation

Poster Presentation:

7th International Workshop on Biomedical Applications of Nanotechnology, NanoMed 2010
December 2-3, 2010, Berlin, Germany

Toxicity of multi-walled carbon nanotubes in *Saccharomyces cerevisiae*

Phillips C.L. [a*], Iyuke S.E. [a*], Pillay V [b]., Rumbold K. [c], Yah C. [a]
[a] School of Chemical and Metallurgical Engineering, University of the Witwatersrand, Johannesburg, P/Bag 3, Wits 2050, South Africa

[b]Department of Pharmacy and Pharmacology, University of the Witwatersrand, 7 York Road, Parktown, 2193 Johannesburg, South Africa

[c]School of Molecular & Cell Biology, University of the Witwatersrand, Johannesburg, P/Bag 3, Wits 2050, South Africa
* Corresponding authors. E-mail address: chantychem@yahoo.com; sunny.iyuke@wits.ac.za

ABSTRACT
This study examined physicochemical determinants of multi-walled carbon nanotubes (MWCNTs) *Saccharomyces cerevisiae* cytotoxicity. Many applications for carbon nanotubes (CNTs) have been proposed including drug and vaccine delivery vehicles, biosensors and novel biomaterials. Before CNTs can be effectively integrated into new and existing biomedical devices, the toxicity of CNTs needs to be thoroughly investigated. Past toxicity assessments have differentiated between single-walled and multi-walled nanotubes, but only a few have investigated the effects of physicochemical modification. The omission of physicochemical characterization data also complicates efforts to compare toxicity results between research studies. The MWCNTs used in this study were produced by the swirled catalytic chemical vapour deposition (SCCVD) method and were purified by nitric acid treatment. Aggregate properties of MWCNTs before (pristine) and after nitric acid purification (oxidized) were fully characterized by BET, TEM, SEM, Raman spectroscopy and TGA. The toxicity of pristine and oxidized MWCNTs of *Saccharomyces cerevisiae* was compared by employing cell growth analysis, SEM, and cell viability assessment. *S.cerevisiae c*ells were exposed to doses of 2µg/ml – 40 µg/ml of both oxidized and pristine MWCNTs. Compared to the control, *S.cerevisiae* growth curves of pristine and oxidized MWCNTs showed no significant changes in growth at both high and low doses of MWCNTs. However, the SEM result of 100 µg/ml dose of MWCNTs revealed partial loss of contents of *S.cerevisiae* cells.

Appendix A1: List of chemical used and reagent preparation

The following table gives the list of chemicals used in this dissertation; all chemicals were used as supplied.

Table A1.1: List of Chemicals

Chemicals	**Company/ Source**
Nitric acid (50%)	Merck Chemicals (Pty) Ltd, Wadeville, Gauteng, South Africa
Sulphuric acid	Merck Chemicals (Pty) Ltd, Wadeville, Gauteng, South Africa
Methanol	Merck Chemicals (Pty) Ltd, Wadeville, Gauteng, South Africa
Chloroform-d, 99.8 atom %D	Sigma-Aldrich, St Louis, MO, USA
Thionyl Chloride	Merck, Hohenbrunn, Germany
Diethyl Ether	Merck Chemicals (Pty) Ltd, Wadeville, Gauteng, South Africa
Ethanol	Merck Chemicals (Pty) Ltd, Wadeville, Gauteng, South Africa
Ninhydrin	Merck, Darnstadt, Germany
N-Tritylglycine 98%	Sigma-Aldrich, Steinheim, Germany
Paraformaldehyde	Merck Schuchardt OHG, Honenbrunn, Germany
Sodium Sulphate Anhydrous	Merck Chemicals (Pty) Ltd, Wadeville, Gauteng, South Africa
N-Ethyldi-isopropulamine	Merck Schuchardt, Honenbrunn,Germany

Table A1.1 continued.

Chemical	**Company/Source**
Acetone	Merck Chemical, Wadeville, South Africa
PBS Tablets	Biogen (OXOID),Gauteng, South Africa
Yeast extract powder	Merck Chemicals (Pty) Ltd, Wadeville, Gauteng, South Africa
D-glucose powder	Merck Chemicals (Pty) Ltd, Wadeville, Gauteng, South Africa
Peptone powder	Merck Chemicals (Pty) Ltd, Wadeville, Gauteng, South Africa
Malt extract agar	Merck Chemicals (Pty) Ltd, Wadeville, Gauteng, South Africa
90 mm Petri-dishes	Plastpro Scientific, Edenvale, Gauteng, SA
Red cell linker kit	Sigma-Aldrich, St Louis, MO, USA
Fluorescein isothiocyanate (FITC)	Sigma-Aldrich; St Louis, MO, USA
Cytotoxglo assay	Whitehead Scientific
RPMI media	Sigma-Aldrich; St Louis, MO, USA
Fetal bovine serum	Sigma-Aldrich; St Louis, MO, USA
Horse serum	Sigma-Aldrich; St Louis, MO, USA
Peptone buffered water	Merck Chemicals (Pty) Ltd, Wadeville, Gauteng, South Africa
Polyethyleneimine	Merck Chemicals (Pty) Ltd, Wadeville, Gauteng, South Africa
Glycerol	Merck Chemicals (Pty) Ltd, Wadeville, Gauteng, South Africa
Sodium Carbonate Anhydrous	Merck Chemicals (Pty) Ltd, Wadeville, Gauteng, South Africa

Yeast cell culturing

Malt Extract Agar (MEA) (Merck; USA) was prepared by dissolving 20 g in 1 litre distilled water and then autoclaved at 121ºC for 15 min. After autoclaving the solution was allowed to cool (to 45ºC) for approximately 40 min before being poured into 15mm sterile Petri dishes (Plastpro Scientific,). Petri dishes were sealed with (silicon paper?) to avoid contamination and stored at 4ºC before use.

Buffered peptone water was used as the diluting agent and was prepared by dissolving 4g in 800ml distilled water and autoclaving at 121ºC for 20 min and cooled to room temperature before use.

Yeast Extract, Peptone and D-glucose (YPD) media was prepared by dissolving 2g Yeast extract powder and 4g peptone powder in 150 ml distilled water and autoclaving. 4g D-glucose powder was dissolved in 50 ml distilled water and autoclaved. After autoclaving the 50 ml glucose media was added to the peptone and yeast extract mixture to make up the 200 ml YPD media.

Inoculum preparation

Single colonies from pure cultures grown on Malt extract agar plates of yeast species *S.cerevisiae* were inoculated separately into 10 mL of Yeast-peptone-glucose broth medium (YPD) and then incubated for 16-18 hrs at 200 rpm and 30˚C.

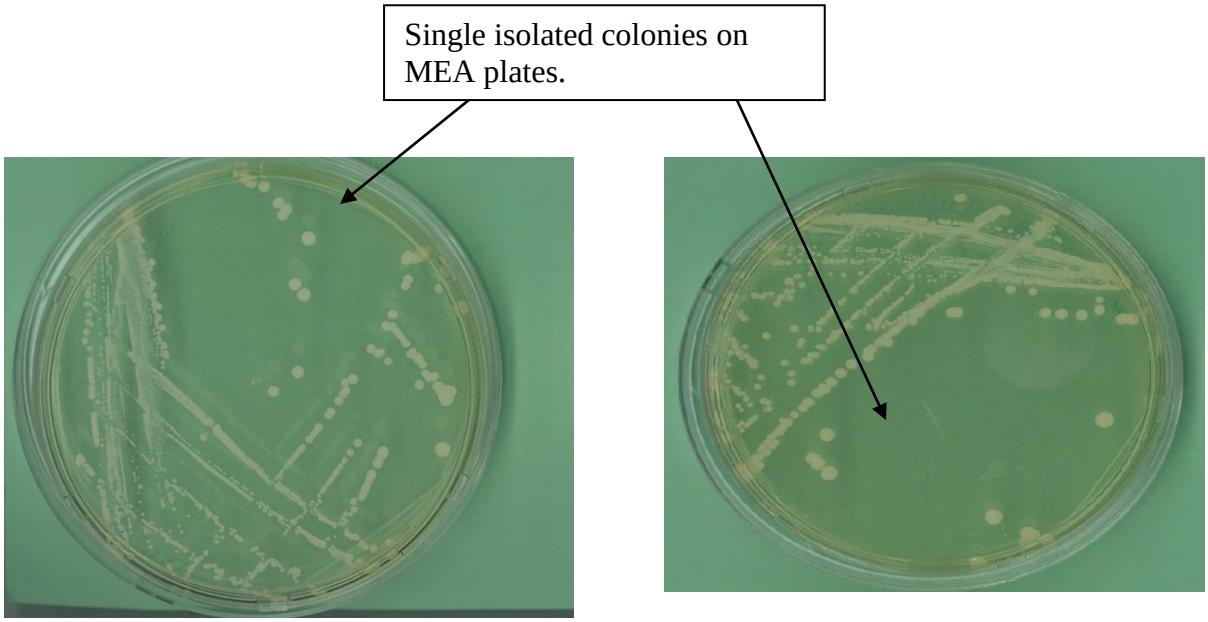


Figure A1.1: MEA plate showing the characteristic colonial morphologies of *S.cerevisiae*

Appendix A2: Standard Curve data

Table A2.1: Standard curve data

Standard Curve data									
Date	**Time**	**Hrs Incubation**	**Dilluti on**	**No of colonies**	**CFU/ ml**	**Dup no.ofcol**	**Dup CFU/ml**	**Ave no of col**	**AVE CFU/ml**
29/07/09	1.00E+03	0	0.001	87	870000	255	2550000	171	1710000
29/07/09	1.00E+04	0	0.0001	29	290000	40	4000000	34.5	3450000
30/07/09	1.00E+03	2	0.001	264	2640000	413	4130000	338.5	3385000
30/07/09	1.00E+04	2	0.0001	----------		45	4500000		
30/07/09	1.00E+03	4	0.001	616	6160000	lawn			
30/07/09	1.00E+04	4	0.0001	73	7300000	74	7400000	73.5	7350000
30/07/09	1.00E+05	4	1.00E-05	11	11000000	8	8000000	9.5	9500000
30/07/09	1.00E+04	6	0.0001	202	20200000	211	21100000	206.5	20650000
30/07/09	1.00E+05	6	1.00E-05	46	46000000	52	52000000	49	49000000
30/07/09	1.00E+06	6	1.00E-06	10	1E+08	2	20000000	6	60000000
30/07/09	1.00E+04	8	0.0001	lawn		lawn			
30/07/09	1.00E+05	8	1.00E-05	129	1.29E+08	118	1.18E+08	123.5	1.24E+08
30/07/09	1.00E+06	8	1.00E-06	4	40000000	4	40000000	4	40000000
30/07/09	1.00E+04	10	0.0001	428	42800000	380	38000000	404	40400000
30/07/09	1.00E+05	10	1.00E-05	109	1.09E+08	84	84000000	96.5	96500000
30/07/09	1.00E+06	10	1.00E-06	17	1.7E+08	9	90000000	13	1.3E+08
30/07/09	1.00E+04	12	0.0001	lawn		lawn			
30/07/09	1.00E+05	12	1.00E-05	150	1.5E+08	177	1.77E+08	163.5	1.64E+08
30/07/09	1.00E+06	12	1.00E-06	37	3.7E+08	10	1E+08	23.5	2.35E+08
30/07/09	1.00E+04	14	0.0001	lawn		lawn			
30/07/09	1.00E+05	14	1.00E-05	112	1.12E+08	104	1.04E+08	108	1.08E+08
30/07/09	1.00E+06	14	1.00E-06	22	2.2E+08	17	1.7E+08	19.5	1.95E+08
30/07/09	1.00E+04	16	0.0001	lawn		lawn			

30/07/09	1.00E+05	16	1.00E-05	136	1.36E+08	118	1.18E+08	127	1.27E+08
30/07/09	1.00E+06	16	1.00E-06	19	1.9E+08	14	1.4E+08	16.5	1.65E+08
30/07/09	1.00E+04	18	0.0001	106*4		92*4			
30/07/09	1.00E+05	18	1.00E-05	190	1.9E+08	138	1.38E+08	164	1.64E+08
30/07/09	1.00E+06	18	1.00E-06	13	1.3E+08	22	2.2E+08	17.5	1.75E+08
30/07/09	1.00E+05	23	1.00E-05	147	1.47E+08	155	1.55E+08	151	1.51E+08
30/07/09	1.00E+06	23	1.00E-06	11	1.1E+08	21	2.1E+08	16	1.6E+08
30/07/09	1.00E+05	24	1.00E-05	246	2.46E+08	203	2.03E+08	224.5	2.25E+08
30/07/09	1.00E+06	24	1.00E-06	30	3E+08	44	4.4E+08	37	3.7E+08
31/07/09	1.00E+05	28	1.00E-05	213	2.13E+08	176	1.76E+08	194.5	1.95E+08
31/07/09	1.00E+06	28	1.00E-06	28	2.8E+08	26	2.6E+08	27	2.7E+08
31/07/09	1.00E+05	42	1.00E-05	261	2.61E+08	167	1.67E+08	214	2.14E+08
31/07/09	1.00E+06	42	1.00E-06	11	1.1E+08	14	1.4E+08	12.5	1.25E+08

Graph Data:

Table A2.2: Standard curve graph data

Hrs Incubation	**AVE CFU/ml**	**CFU/ml**	**Absorbance**
		0	0
0	2580000	2.58	0.208
2	3942500	3.9425	0.3676667
3	6500000	6.5	0.563
4	8425000	8.425	0.892

Appendix A2: NMR Spectra

N-Tritylglycine functionalized CNTs

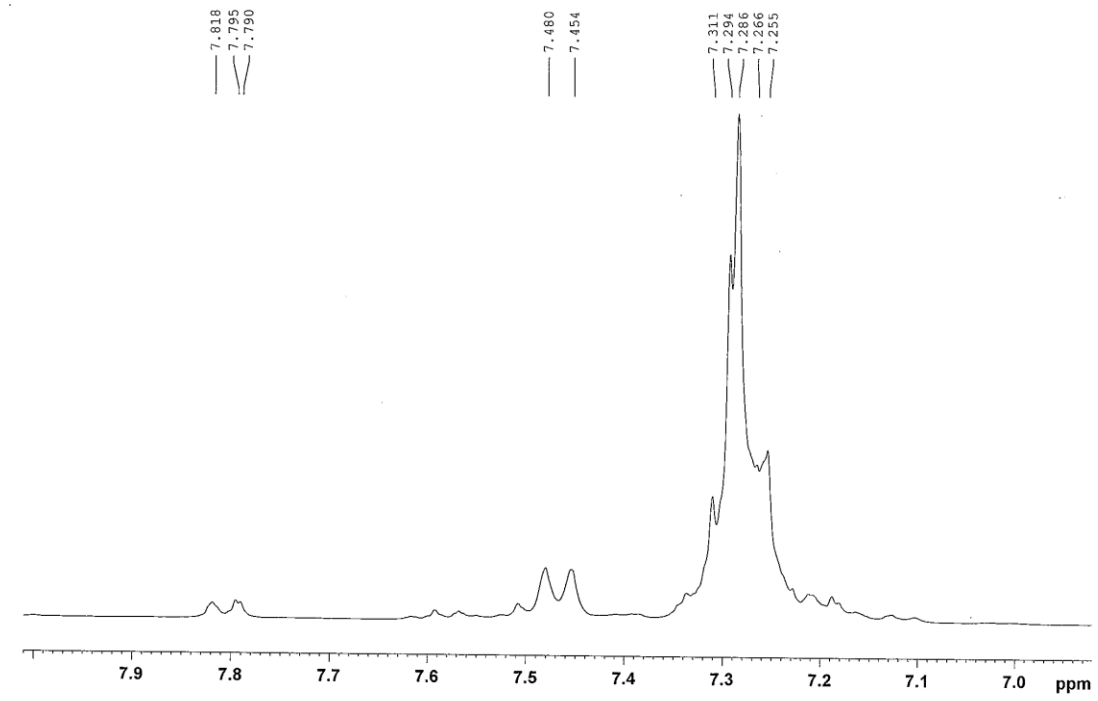


Figure A2.1: NMR spectra of N-Tritylglycine functionalised CNTs

NMR peak of N-tritylglycine

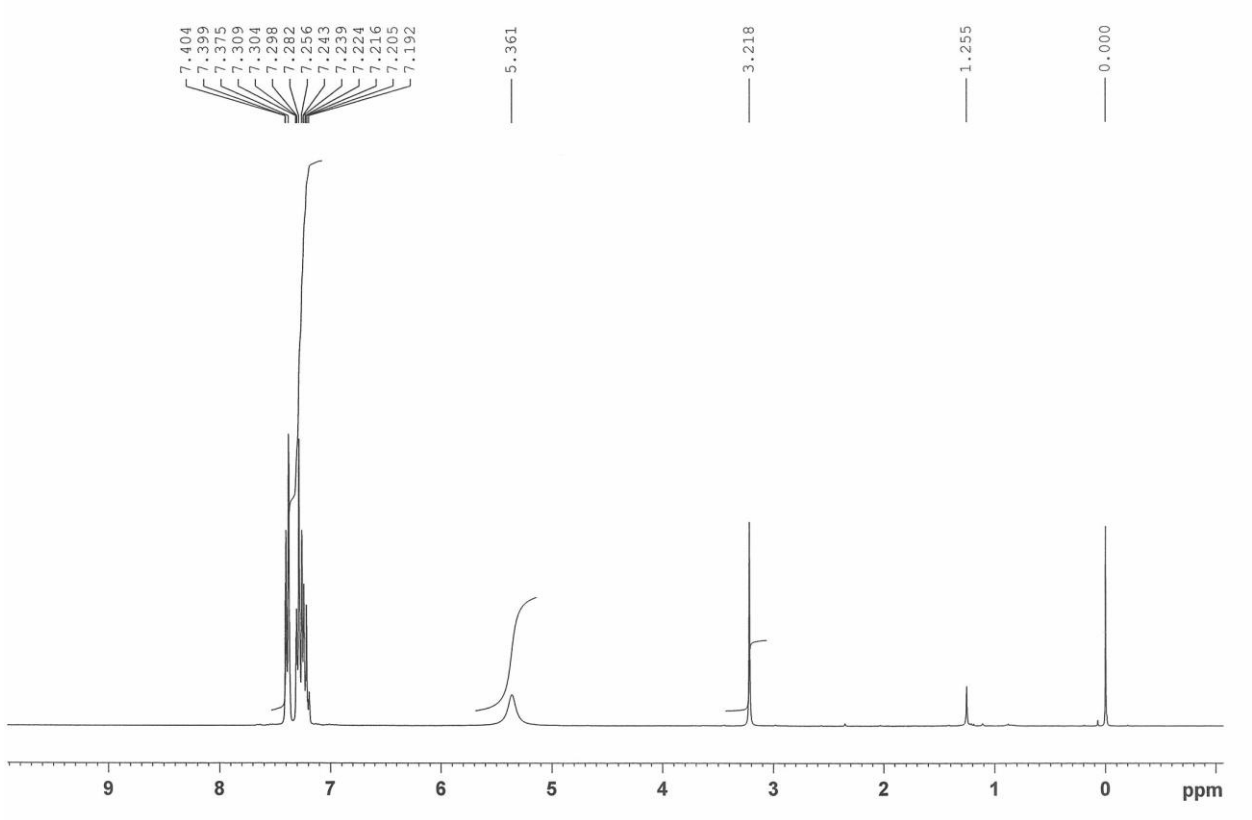


Figure A2.2: NMR spectra of N-Tritylglycine product from Sigma Aldrich

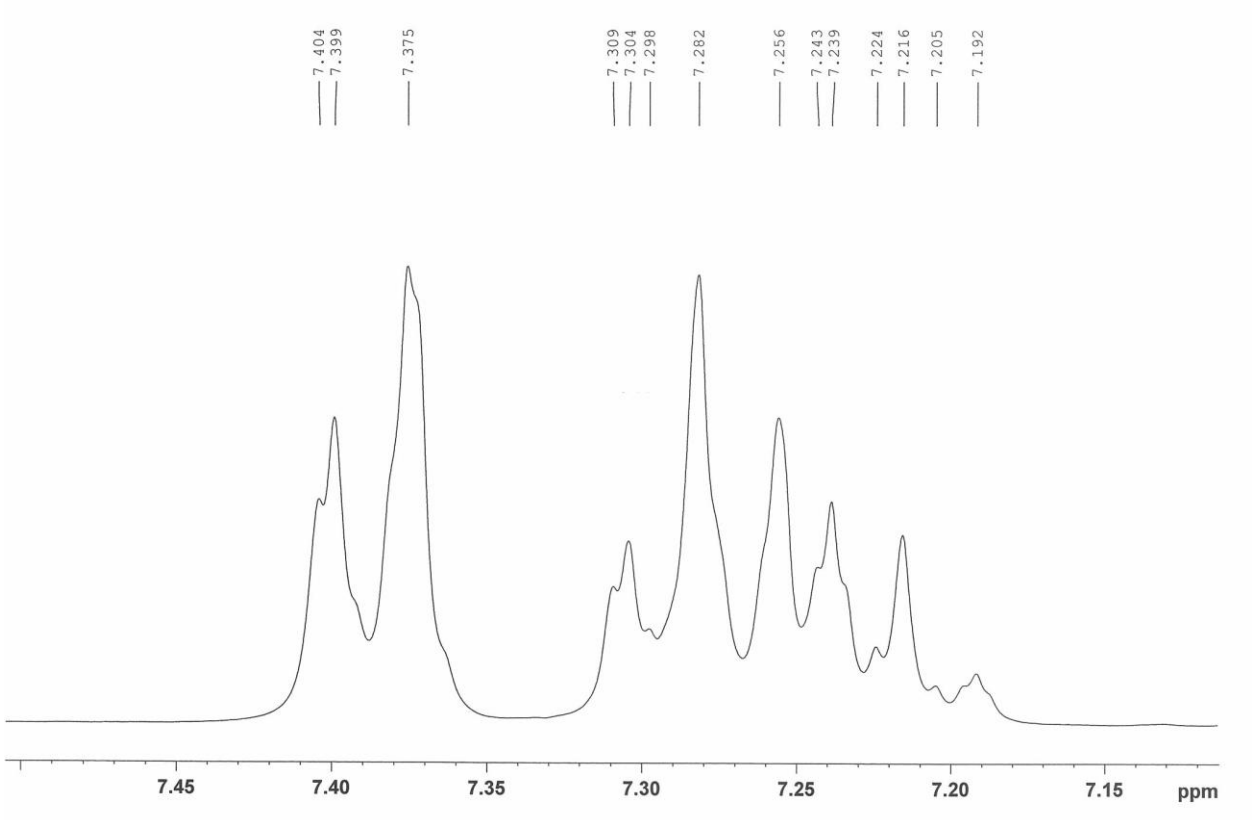
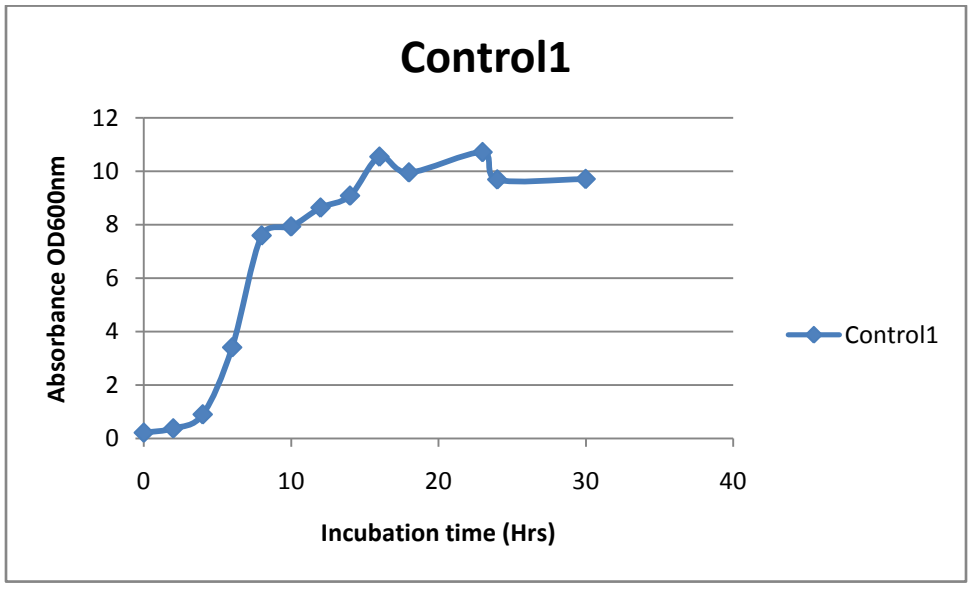


Figure A2.3: NMR spectra of N-Tritylglycine product from Sigma Aldrich

Appendix A3: Growth Curves data

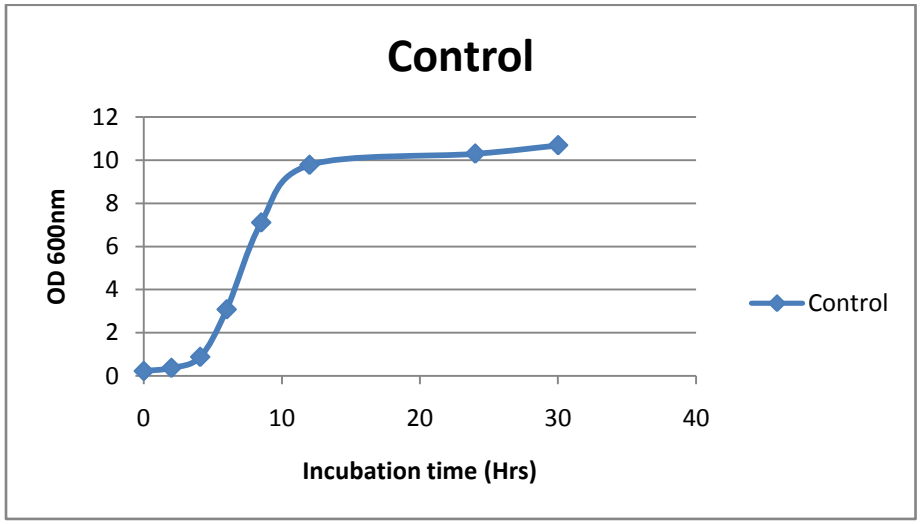
Date commencing Experiment: 27 July 2009
Shaker speed: 200 rpm
Incubator temperature: 30C
Table A : OD600nm measurements of S.cerevisiae during growth in YPD medium.
Control: Vtot= 200ml; Vonc= 2ml; Vbroth= 198ml
Starting OD measurement at 600nm: 0.2

Date	Hrs Incubation	Absorbance 1	Absorbance 2	Absorbance 3	Avrg Absorbance	Dillution	Dill factor	Absorbance
27/07/09	0	0.201	0.211	0.212	0.208	0	1	0.208
27/07/09	2	0.366	0.368	0.369	0.367667	0	1	0.367667
27/07/09	4	0.892	0.891	0.893	0.892	0:00	1	0.892
27/07/09	6	1.133	1.134	1.133	1.133333	1:02	3	3.4
27/07/09	8	0.758	0.759	0.759	0.758667	1:09	10	7.586667
27/07/09	10	0.792	0.793	0.792	0.792333	1:09	10	7.923333
28/07/09	12	0.863	0.863	0.863	0.863	1:09	10	8.63
28/07/09	14	0.908	0.908	0.907	0.907667	1:09	10	9.076667
28/07/09	16	1.054	1.054	1.053	1.053667	1:09	10	10.53667
28/07/09	18	0.995	0.995	0.994	0.994667	1:09	10	9.946667
28/07/09	23	1.07	1.071	1.071	1.070667	1:09	10	10.70667
28/07/09	24	0.968	0.968	0.969	0.968333	1:09	10	9.683333
28/07/09	30	0.883	0.882	0.881	0.882	1:10	11	9.702
29/07/09	44	1.082	1.083	1.082	1.082333	1:10	11	11.90567
29/07/09	46	1.055	1.055	1.056	1.055333	1:10	11	11.60867



Date commencing Experiment: 19 August 2009
Shaker speed: 200 rpm; Incubator temperature: 30C
Sample name: Control
Starting OD measurement at 600nm: 0.215

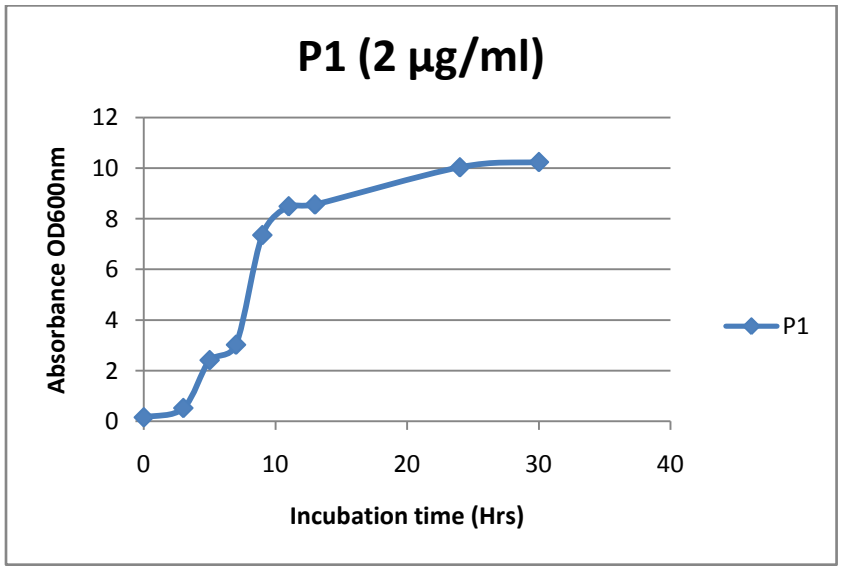
Date	Incubation	Absorbance 1	Absorbance 2	Absorbance 3	Avrg Absorbance	Dillution	Dill factore	Absorbance
19\08\09	0	0.215	0.214	0.214	0.2143333	0	1	0.2143333
19\08\09	2	0.359	0.36	0.361	0.36	0	1	0.36
19\08\09	3.25	0.564	0.562	0.563	0.563	0:00	1	0.563
19\08\09	4.083333	0.869	0.87	0.867	0.8686667	0:00	1	0.8686667
19\08\09	6	0.767	0.768	0.767	0.7673333	1:03	4	3.0693333
19\08\09	8.5	0.709	0.71	0.71	0.7096667	1:09	10	7.0966667
19\08\09	10.083333	0.975	0.975	0.975	0.975	1:07	8	7.8
19\08\09	12	0.978	0.977	0.976	0.977	1:09	10	9.77
20\08\09	20.83333	0.767	0.766	0.765	0.766	1:09	10	7.66
20\08\09	22	0.95	0.951	0.95	0.9503333	1:09	10	9.5033333
20\08\09	24	0.935	0.936	0.936	0.9356667	1:10	11	10.292333
20\08\09	30	1.064	1.07	1.07	1.068	1:09	10	10.68



Pristine CNT growth curves

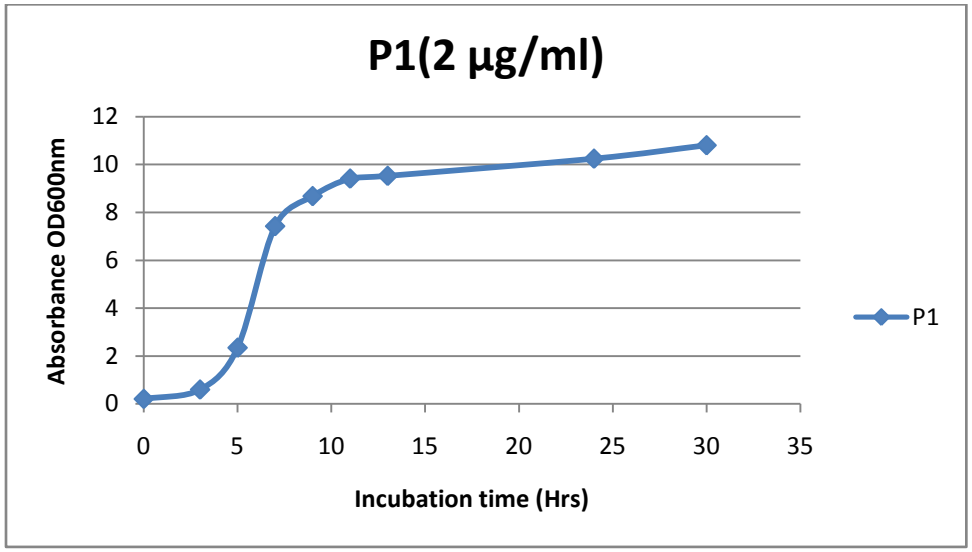
Date commencing Experiment: 19 September 2009
Shaker speed: 200 rpm
Incubator temperature: 30C
Sample P1 Vtot= 200ml; Vonc= 2ml; Vbroth= 198ml; Mcnt=0.40 mg (2 µg/ml)
Starting OD measurement at 600nm: 0.158

Date	Hrs Incubation	Absorbance 1	Absorbance 2	Absorbance 3	Avrg Absorbance	Dillution	Dill factor	Absorbance
19\09\09	0	0.158	0.159	0.16	0.159	0	1	0.159
19\09\09	3	0.526	0.527	0.527	0.526667	0	1	0.526667
19\09\09	5	0.807	0.806	0.804	0.805667	1:02	3	2.417
19\09\09	7	0.708	0.781	0.78	0.756333	1:03	4	3.025333
19\09\09	9	0.736	0.735	0.736	0.735667	1:09	10	7.356667
19\09\09	11	0.846	0.849	0.853	0.849333	1:09	10	8.493333
19\0\09	13	0.856	0.857	0.856	0.856333	1:09	10	8.563333
21\09\09	24	0.903	0.91	0.923	0.912	1:10	11	10.032
21\09\10	30	0.932	0.931	0.93	0.931	1:10	11	10.241



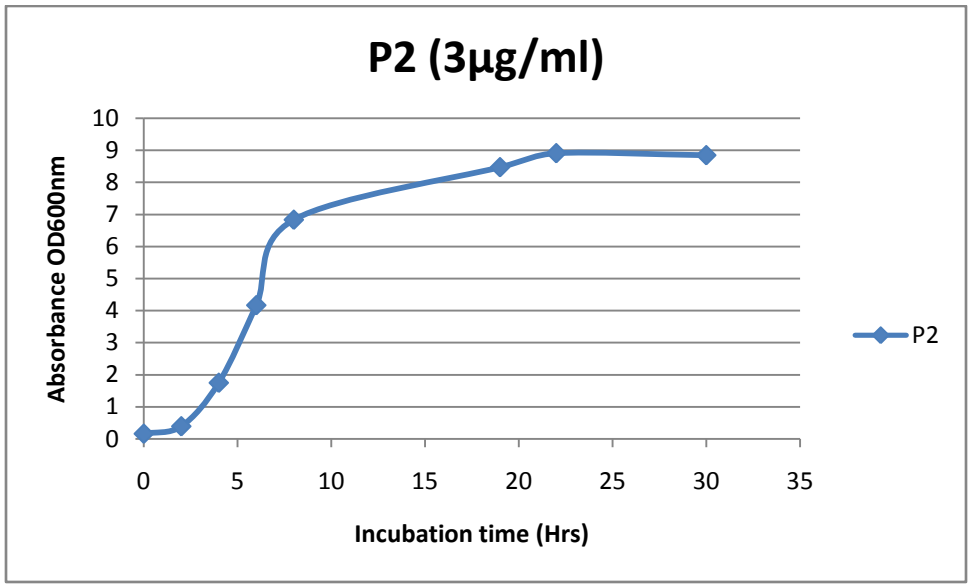
Sample P1 Vtot= 50ml; Vonc= 500 ul; Vbroth= 50 ml; Ccnt= 2 µg/ml
Starting OD measurement at 600nm: 0.201

Date	Hrs Incubation	Absorbance 1	Absorbance 2	Absorbance 3	Avrg Absorbance	Dillution	Dill factor	Absorbance
12\05\10	0	0.201	0.198	0.201	0.2	0	1	0.2
12\05\10	3	0.593	0.591	0.59	0.591333	0	1	0.591333
12\05\10	5	0.585	0.584	0.586	0.585	1:03	4	2.34
13\05\10	7	0.742	0.742	0.742	0.742	1:09	10	7.42
13\05\10	9	0.867	0.868	0.868	0.867667	1:09	10	8.676667
13\05\10	11	0.855	0.856	0.855	0.855333	1:10	11	9.408667
13\05\10	13	0.865	0.866	0.866	0.865667	1:10	11	9.522333
13\05\10	24	0.931	0.93	0.932	0.931	1:10	11	10.241
14\05\10	30	0.981	0.982	0.983	0.982	1:10	11	10.802



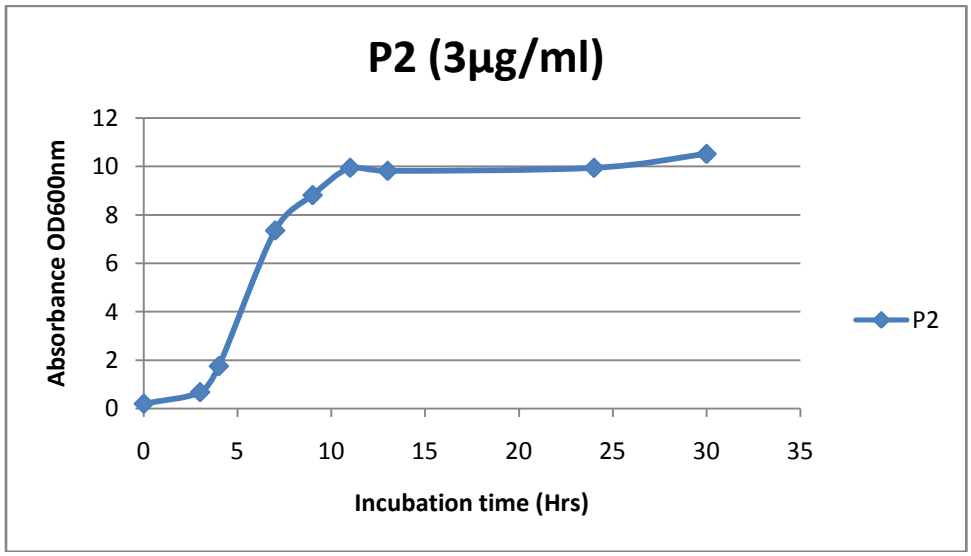
Date commencing Experiment: 1 October 2009
Shaker speed: 180 rpm
Incubator temperature: 30C
Sample P2 Vtot= 100ml; Vonc= 1ml; Vbroth= 100ml; Mcnt=0.3 mg (3 µg/ml)
Starting OD measurement at 600nm: 0.162

Date	Hrs Incubation	Absorbance 1	Absorbance 2	Absorbance 3	Avrg Absorbance	Dillution	Dill factor	Absorbance
1\10\09	0	0.162	0.162	0.161	0.161667	0	1	0.161667
1\10\09	2	0.393	0.394	0.394	0.393667	0	1	0.393667
1\10\09	4	0.584	0.583	0.583	0.583333	1:02	3	1.75
1\10\09	6	0.694	0.695	0.695	0.694667	1:05	6	4.168
1\10\09	8	0.622	0.62	0.622	0.621333	1:10	11	6.834667
1\10\09	19	0.771	0.77	0.77	0.770333	1:10	11	8.473667
1\10\09	22	0.812	0.809	0.809	0.81	1:10	11	8.91
2\10\09	24	0.834	0.833	0.832	0.833	1:10	11	9.163
2\10\09	30	0.804	0.804	0.805	0.804333	1:10	11	8.847667



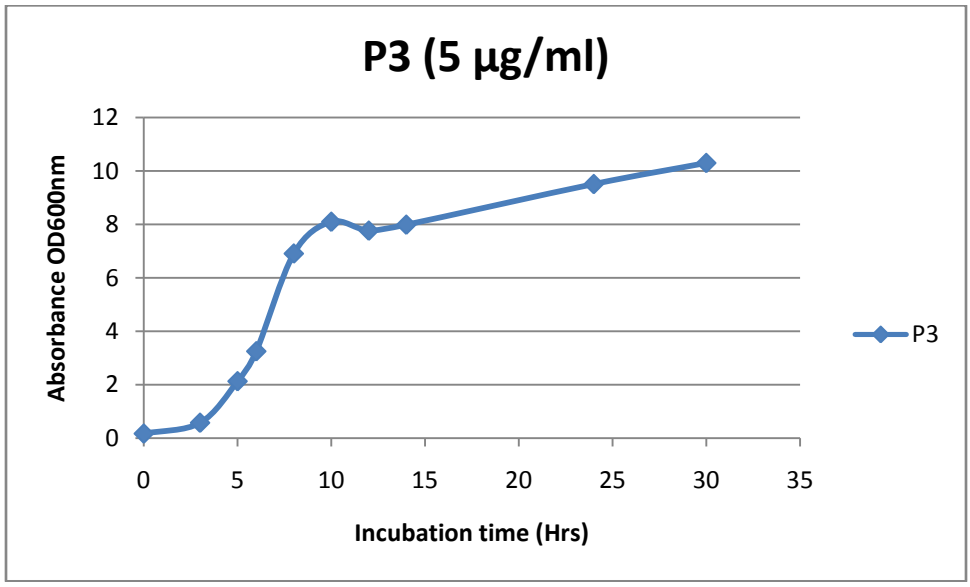
Date commencing Experiment: 12 May 2010
Shaker speed: 200 rpm
Incubator temperature: 30C
Sample P2 Vtot= 50ml; Vonc= 0.5 ml; Vbroth= 50 ml; Ccnt= 3 µg/ml
Starting OD measurement at 600nm: 0.197

Date	Hrs Incubation	Absorbance 1	Absorbance 2	Absorbance 3	Avrg Absorbance	Dilluti on	Dill factor	Absorbance
12\05\10	0	0.197	0.198	0.198	0.19767	0	1	0.19767
12\05\10	3	0.667	0.684	0.671	0.674	0	1	0.674
12\05\10	4	0.584	0.583	0.583	0.58333	1:02	3	1.75
13\05\10	7	0.734	0.735	0.735	0.73467	1:09	10	7.34667
13\05\10	9	0.88	0.881	0.881	0.88067	1:09	10	8.80667
13\05\10	11	0.903	0.903	0.904	0.90333	1:10	11	9.93667
13\05\10	13	0.905	0.904	0.866	0.89167	1:10	11	9.80833
13\05\10	24	0.901	0.905	0.903	0.903	1:10	11	9.933
14\05\10	30	0.955	0.956	0.955	0.95533	1:10	11	10.5087



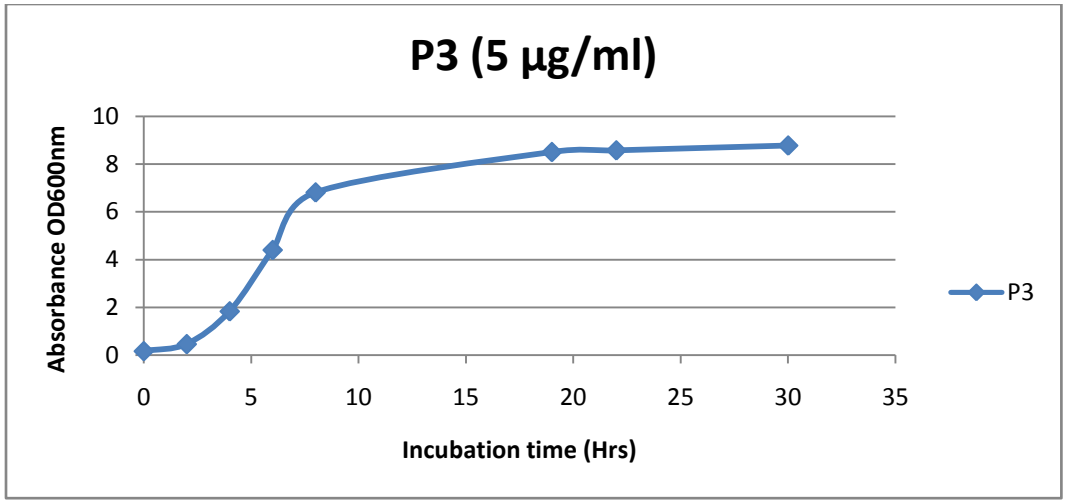
Date commencing Experiment: 19 September 2009
Start time: 9:30 am
Shaker speed: 200 rpm
Incubator temperature: 30C
Sample P3 Vtot= 200ml; Vonc= 2ml; Vbroth= 198ml; Mcnt=1.0 mg
Starting OD measurement at 600nm: 0.170

Date	Hrs Incubation	Absorbance 1	Absorbance 2	Absorbance 3	Avrg Absorbance	Dilluti on	Dill factor	Absorbance
19\09\09	0	0.17	0.169	0.168	0.169	0	1	0.169
19\09\09	3	0.574	0.575	0.574	0.574333	0	1	0.574333
19\09\09	5	0.71	0.708	0.709	0.709	1:02	3	2.127
19\09\09	6	0.812	0.812	0.812	0.812	1:03	4	3.248
19\09\09	8	0.689	0.69	0.692	0.690333	1:09	10	6.903333
19\09\09	10	0.81	0.809	0.809	0.809333	1:09	10	8.093333
19\0\09	12	0.775	0.776	0.777	0.776	1:09	10	7.76
19\09\09	14	0.8	0.798	0.797	0.798333	1:09	10	7.983333
20\09\09	20.833	0.767	0.766	0.765	0.766	1:09	10	7.66
20\09\09	24	0.95	0.951	0.95	0.950333	1:09	10	9.503333
20\09\09	30	0.935	0.936	0.936	0.935667	1:10	11	10.29233



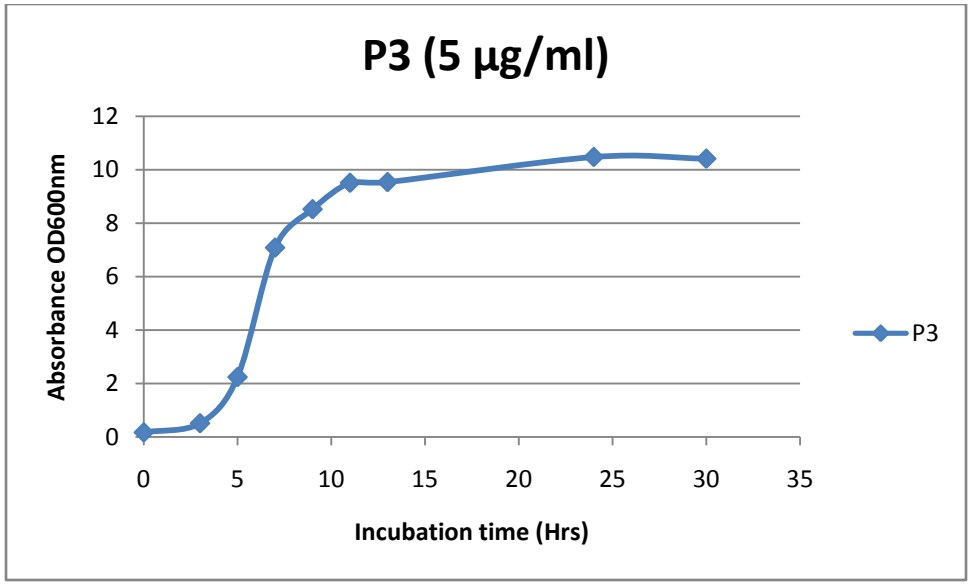
Date commencing Experiment: 1 October 2009
Start time: 9:45 am
Shaker speed: 180 rpm
Incubator temperature: 30C
Sample P3 Vtot= 100ml; Vonc= 1ml; Vbroth= 100ml; Mcnt=0.5 mg
Starting OD measurement at 600nm:

Date	Hrs Incubation	Absorbance 1	Absorbance 2	Absorbance 3	Avrg Absorbance	Dillution	Dill factor	Absorbance
1\10\09	0	0.17	0.169	0.168	0.169	0	1	0.169
1\10\09	2	0.463	0.465	0.464	0.464	0	1	0.464
1\10\09	4	0.611	0.612	0.613	0.612	1:02	3	1.836
1\10\09	6	0.733	0.734	0.734	0.733667	1:05	6	4.402
1\10\09	8	0.619	0.62	0.619	0.619333	1:10	11	6.812667
1\10\09	19	0.77	0.77	0.779	0.773	1:10	11	8.503
1\10\09	22	0.779	0.78	0.779	0.779333	1:10	11	8.572667
2\10\09	24	0.747	0.747	0.746	0.746667	1:10	11	8.213333
2\10\09	30	0.798	0.798	0.797	0.797667	1:10	11	8.774333



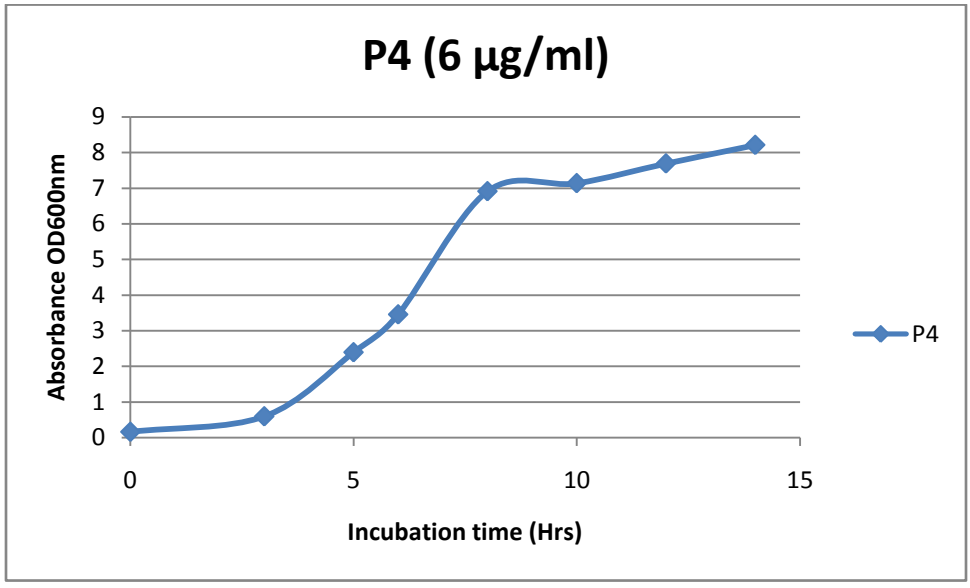
Date commencing Experiment: 12 May 2010
Shaker speed: 200 rpm
Incubator temperature: 30C
Sample P3 Vtot= 50ml; Vonc= 0.5 ml; Vbroth= 50 ml; Ccnt= 5 µg/ml
Starting OD measurement at 600nm: 0.197

Date	Hrs Incubation	Absorbance 1	Absorbance 2	Absorbance 3	Avrg Absorbance	Dillution	Dill factor	Absorbance
12\05\10	0	0.17	0.169	0.168	0.169	0	1	0.169
12\05\10	3	0.511	0.512	0.514	0.512333	0	1	0.512333
12\05\10	5	0.56	0.561	0.559	0.56	1:03	4	2.24
13\05\10	7	0.709	0.708	0.707	0.708	1:09	10	7.08
13\05\10	9	0.851	0.852	0.853	0.852	1:09	10	8.52
13\05\10	11	0.903	0.845	0.845	0.864333	1:10	11	9.507667
13\05\10	13	0.905	0.848	0.847	0.866667	1:10	11	9.533333
13\05\10	24	0.953	0.952	0.951	0.952	1:10	11	10.472
14\05\10	30	0.945	0.946	0.948	0.946333	1:10	11	10.40967



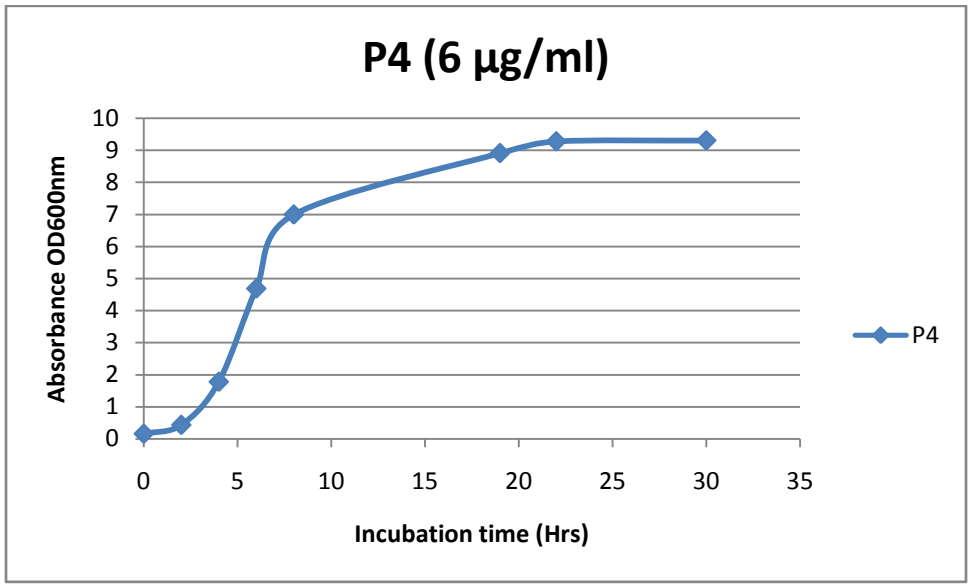
Date commencing Experiment: 19 September 2009
Start time: 9:30 am
Shaker speed: 200 rpm
Incubator temperature: 30C
Sample S1 Vtot= 200ml; Vonc= 2ml; Vbroth= 198ml; Mcnt=1.20 mg
Starting OD measurement at 600nm: 0.156

Date	Hrs Incubation	Absorbance 1	Absorbance 2	Absorbance 3	Avrg Absorbance	Dilluti on	Dill factor	Absorbance
19\09\09	0	0.156	0.157	0.158	0.157	0	1	0.157
19\09\09	2	0.321	0.32	0.319	0.32	0	1	0.32
19\09\09	3	0.592	0.591	0.592	0.5916667	0	1	0.591667
19\09\09	5	0.797	0.796	0.797	0.7966667	1:02	3	2.39
19\09\09	6	0.863	0.863	0.864	0.8633333	1:03	4	3.453333
19\09\09	8	0.691	0.691	0.691	0.691	1:09	10	6.91
19\09\09	10	0.714	0.713	0.714	0.7136667	1:09	10	7.136667
19\0\09	12	0.768	0.769	0.77	0.769	1:09	10	7.69
19\09\09	14	0.819	0.82	821	0.821	1:09	10	8.21



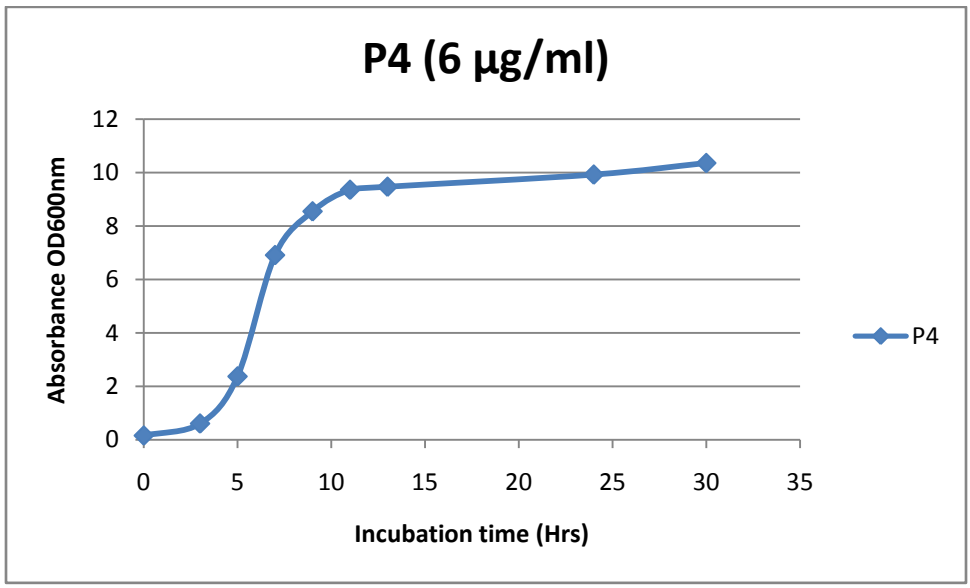
Date: 1 October 2009
Start time: 9:45 am
Shaker speed: 180 rpm
Incubator temperature: 30C
Sample P4 Vtot= 100ml; Vonc= 1ml; Vbroth= 100ml; Mcnt=0.6 mg
Starting OD measurement at 600nm:

Date	Hrs Incubation	Absorbance 1	Absorbance 2	Absorbance 3	Avrg Absorbance	Dilluti on	Dill factor	Absorbance
1\10\09	0	0.156	0.157	0.158	0.157	0	1	0.157
1\10\09	2	0.434	0.431	0.43	0.431667	0	1	0.431667
1\10\09	4	0.591	0.592	0.593	0.592	1:02	3	1.776
1\10\09	6	0.78	0.78	0.782	0.780667	1:05	6	4.684
1\10\09	8	0.638	0.634	0.635	0.635667	1:10	11	6.992333
1\10\09	19	0.81	0.81	0.809	0.809667	1:10	11	8.906333
1\10\09	22	0.843	0.843	0.843	0.843	1:10	11	9.273
2\10\09	24	0.842	0.842	0.842	0.842	1:10	11	9.262
2\10\09	30	0.845	0.846	0.846	0.845667	1:10	11	9.302333



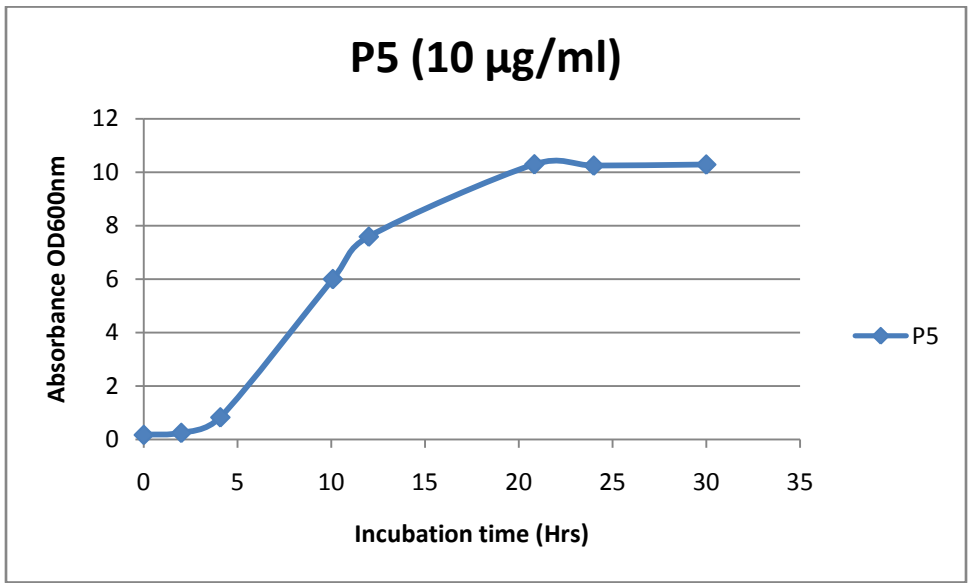
Date commencing Experiment: 12 May 2010
Shaker speed: 200 rpm
Incubator temperature: 30C
Sample P4 Vtot= 50ml; Vonc= 0.5 ml; Vbroth= 50 ml; Ccnt= 6 µg/ml
Starting OD measurement at 600nm: 0.197

Date	Hrs Incubation	Absorbance 1	Absorbance 2	Absorbance 3	Avrg Absorbance	Dilluti on	Dill factor	Absorbance
12\05\10	0	0.156	0.157	0.158	0.157	0	1	0.157
12\05\10	3	0.608	0.607	0.605	0.606667	0	1	0.606667
12\05\10	5	0.594	0.591	0.592	0.592333	1:03	4	2.369333
13\05\10	7	0.69	0.691	0.691	0.690667	1:09	10	6.906667
13\05\10	9	0.855	0.854	0.854	0.854333	1:09	10	8.543333
13\05\10	11	0.85	0.85	0.85	0.85	1:10	11	9.35
13\05\10	13	0.86	0.86	0.861	0.860333	1:10	11	9.463667
13\05\10	24	0.902	0.901	0.902	0.901667	1:10	11	9.918333
14\05\10	30	0.942	0.941	0.94	0.941	1:10	11	10.351



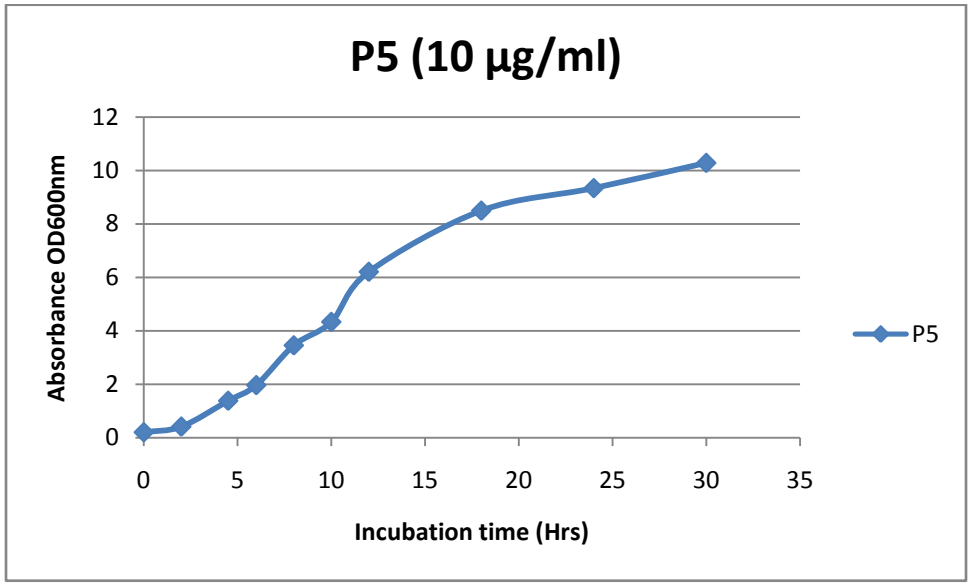
Date commencing Experiment: 19 August 2009
Shaker speed: 200 rpm
Incubator temperature: 30C
Sample P5 Vtot= 200ml; Vonc= 2ml; Vbroth= 198ml; Mcnt=2.00 mg
Starting OD measurement at 600nm: 0.215

Date	Hrs Incubation	Absorbance 1	Absorbance 2	Absorbance 3	Avrg Absorbance	Dilluti on	Dill factor	Absorbance
19\08\09	0	0.169	0.171	0.168	0.169333	0	1	0.169333
19\08\09	2	0.246	0.245	0.245	0.245333	0	1	0.245333
19\08\09	4.083333	0.825	0.828	0.825	0.826	0:00	1	0.826
19\08\09	6	0.911	0.912	0.912	0.911667	1:03	4	3.646667
19\08\09	8.5	0.668	0.67	0.671	0.669667	1:09	10	6.696667
19\08\09	10.08333	0.75	0.75	0.749	0.749667	1:07	8	5.997333
19\08\09	12	0.758	0.759	0.758	0.758333	1:09	10	7.583333
20\08\09	20.83333	1.028	1.029	1.03	1.029	1:09	10	10.29
20\08\09	22	1.085	1.084	1.084	1.084333	1:09	10	10.84333
20\08\09	24	0.931	0.93	0.932	0.931	1:10	11	10.241
20\08\09	30	0.933	0.935	0.936	0.934667	1:10	11	10.28133



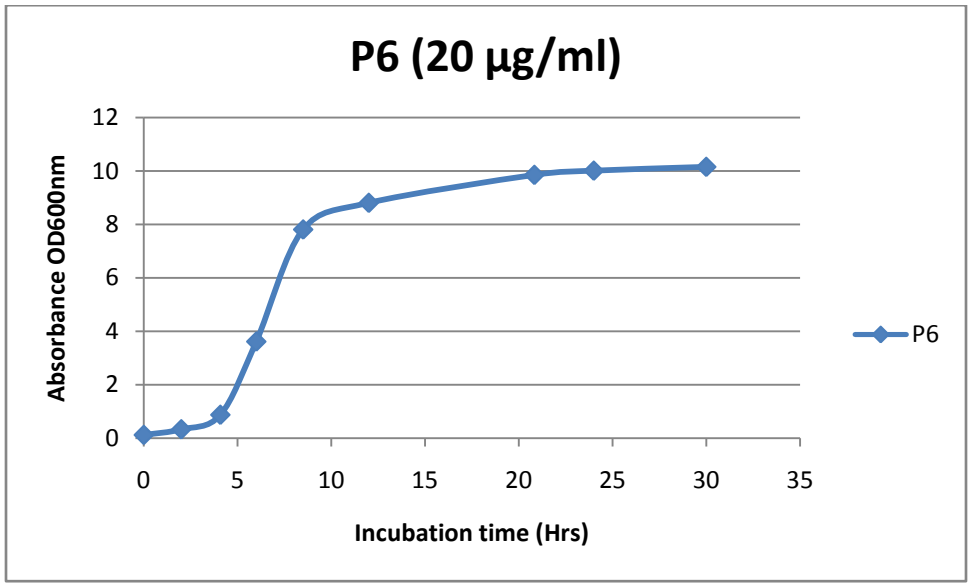
Date commencing Experiment: 15 July 2009
Sample P5 Vtot= 200ml; Vonc= 200ml; Vbroth= 198ml Mcnt=2.00 mg

Date	Hrs Incubation	Absorbance 1	Absorbance 2	Absorbance 3	Avrg Absorbance	Dilluti on	Dill factor	Absorbance
15/07/09	0	0.196	0.197	0.197	0.196667	0	1	0.196667
15/07/09	2	0.41	0.408	0.408	0.408667	0	1	0.408667
15/07/09	4.5	0.686	0.687	0.689	0.687333	1:01	2	1.374667
15/07/09	6	0.979	0.981	0.982	0.980667	1:01	2	1.961333
15/07/09	8	0.687	0.691	0.692	0.69	1:04	5	3.45
15/07/09	10	0.542	0.541	0.54	0.541	1:07	8	4.328
16/07/09	12	0.621	0.62	0.62	0.620333	1:09	10	6.203333
16/07/09	18	0.848	0.849	0.851	0.849333	1:09	10	8.493333
16/07/09	24	0.934	0.933	0.934	0.933667	1:09	10	9.336667
16/07/09	30	0.933	0.935	0.936	0.934667	1:10	11	10.28133



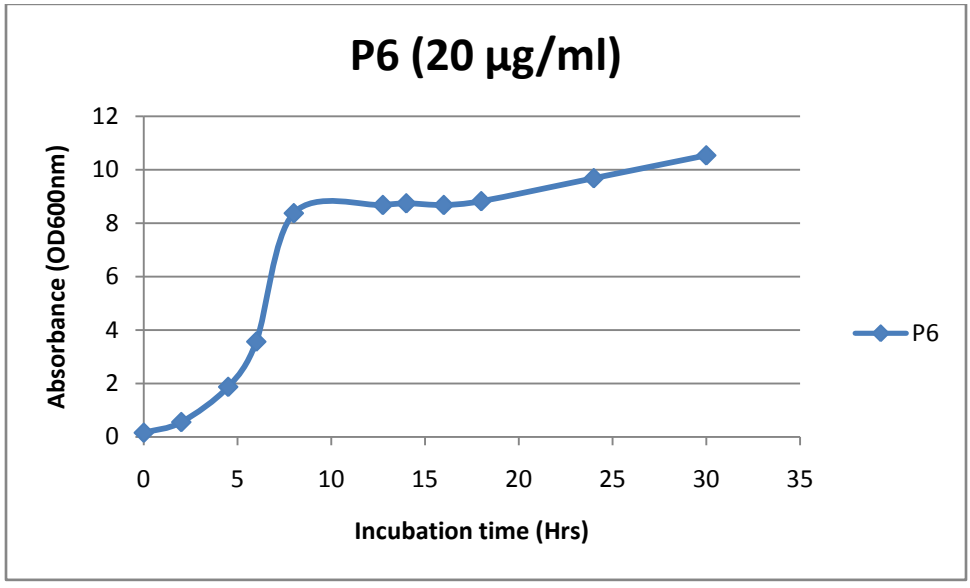
Date commencing Experiment: 19 August 2009
Shaker speed: 200 rpm
Incubator temperature: 30C
Sample P6 Vtot= 200ml; Vonc= 2ml; Vbroth= 198ml; Mcnt=4.00 mg
Starting OD measurement at 600nm: 0.215

Date	Hrs Incubation	Absorbance 1	Absorbance 2	Absorbance 3	Avrg Absorbance	Dilluti on	Dill factor	Absorbance
19\08\09	0	0.119	0.12	0.121	0.12	0	1	0.12
19\08\09	2	0.33	0.33	0.33	0.33	0	1	0.33
19\08\09	4.083333	0.873	0.872	0.872	0.872333	0:00	1	0.872333
19\08\09	6	0.902	0.903	0.904	0.903	1:03	4	3.612
19\08\09	8.5	0.71	0.709	0.709	0.709333	1:10	11	7.802667
19\08\09	10.08333	0.716	0.715	0.714	0.715	1:10	11	7.865
19\08\09	12	0.799	0.8	0.801	0.8	1:10	11	8.8
20\08\09	20.83333	0.895	0.896	0.894	0.895	1:10	11	9.845
20\08\09	24	0.91	0.909	0.909	0.909333	1:10	11	10.00267
20\08\09	30	0.924	0.921	0.922	0.922333	1:10	11	10.14567



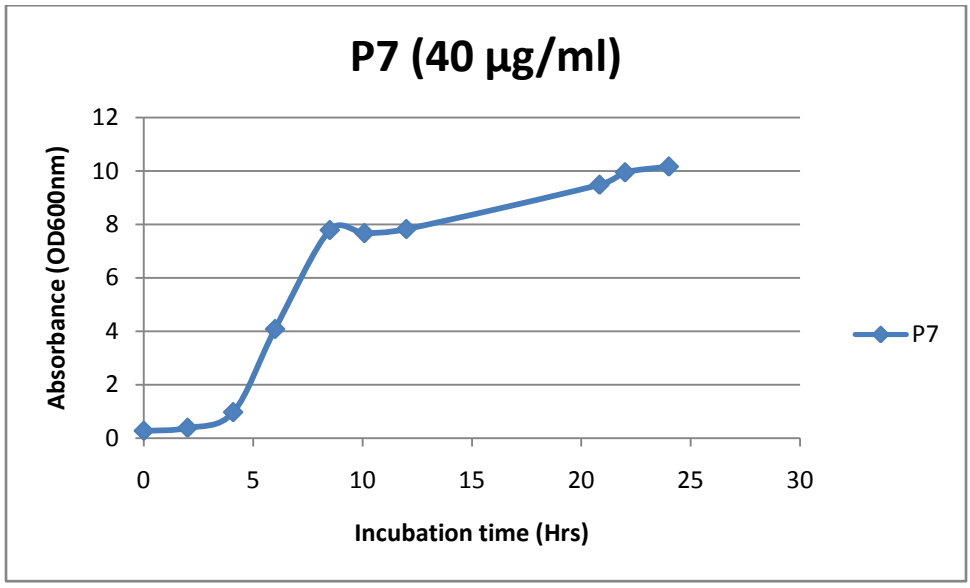
Date commencing Experiment: 6 August 2009
Shaker speed: 200 rpm
Incubator temperature: 30C
Sample P6 Vtot= 200ml; Vonc= 2ml; Vbroth= 198ml; Mcnt=4.00mg
Starting OD measurement at 600nm: 0.165

Date	Hrs Incubation	Absorbance 1	Absorbance 2	Absorbance 3	Avrg Absorbance	Dilluti on	Dill factor	Absorbance
6/8/2009	0	0.157	0.156	0.154	0.155667	0	1	0.155667
6/8/2009	2	0.556	0.554	0.553	0.554333	0:00	1	0.554333
6/8/2009	4.5	0.624	0.625	0.623	0.624	1:02	3	1.872
6/8/2009	6	0.714	0.713	0.712	0.713	1:04	5	3.565
6/8/2009	8	0.838	0.837	0.837	0.837333	1:09	10	8.373333
6/8/2009	12.75	0.867	0.868	0.869	0.868	1:09	10	8.68
7/8/2009	14	0.876	0.874	0.873	0.874333	1:09	10	8.743333
7/8/2009	16	0.867	0.868	0.869	0.868	1:09	10	8.68
7/8/2009	18	0.881	0.882	0.884	0.882333	1:09	10	8.823333
7/8/2009	24	0.968	0.968	0.969	0.968333	1:09	10	9.683333
7/8/2009	30	0.959	0.958	0.957	0.958	1:10	11	10.538



Date commencing Experiment: 19 August 2009
Shaker speed: 200 rpm
Incubator temperature: 30C
Sample P7 Vtot= 200ml; Vonc= 2ml; Vbroth= 198ml; Mcnt=8.01 mg
Starting OD measurement at 600nm: 0.215

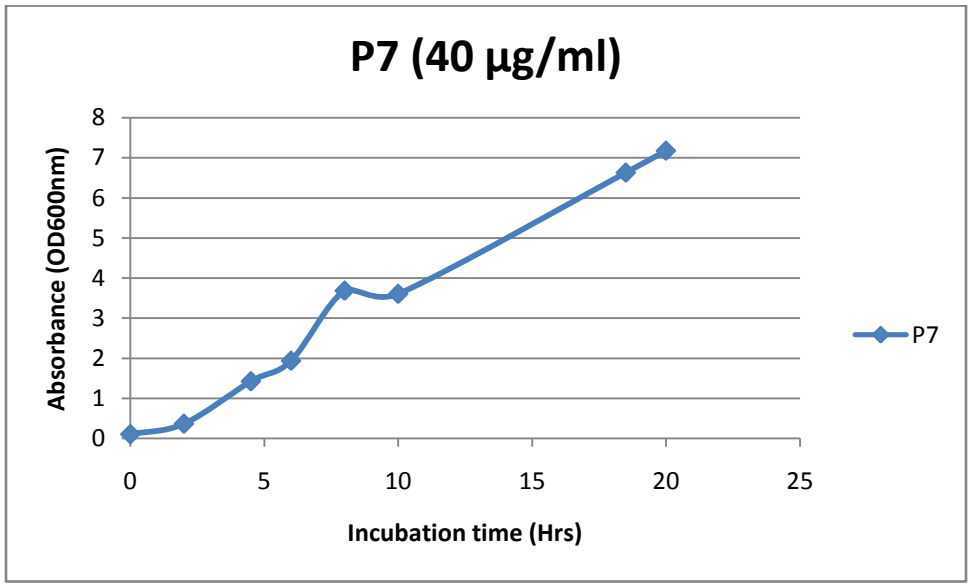
Date	Hrs Incubation	Absorbance 1	Absorbance 2	Absorbance 3	Avrg Absorbance	Dilluti on	Dill factor	Absorbance
19\08\09	0	0.268	0.267	0.266	0.267	0	1	0.267
19\08\09	2	0.379	0.379	0.379	0.379	0	1	0.379
19\08\09	4.083333	0.963	0.964	0.964	0.963667	0:00	1	0.963667
19\08\09	6	1.02	1.019	1.019	1.019333	1:03	4	4.077333
19\08\09	8.5	0.706	0.708	0.709	0.707667	1:10	11	7.784333
19\08\09	10.08333	0.697	0.698	0.697	0.697333	1:10	11	7.670667
19\08\09	12	0.712	0.71	0.711	0.711	1:10	11	7.821
20\08\09	20.83333	0.862	0.861	0.863	0.862	1:10	11	9.482
20\08\09	22	0.905	0.904	0.904	0.904333	1:10	11	9.947667
20\08\09	24	0.923	0.924	0.925	0.924	1:10	11	10.164



Date commencing Experiment: 15 July 2009

Sample P7 Vtot= 200ml; Vonc= 200ml; Vbroth= 198ml Mcnt=8.00 mg

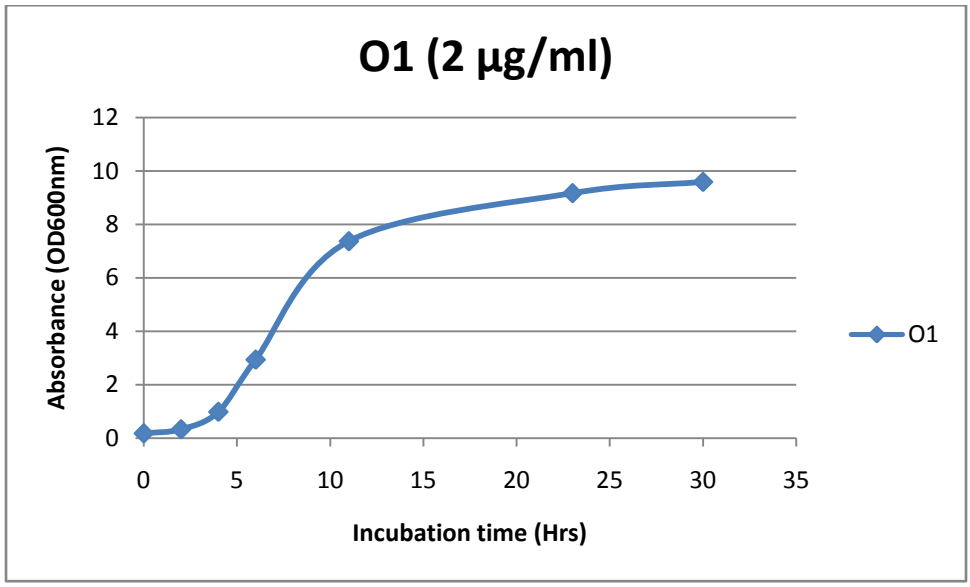
Date	Hrs Incubation	Absorbance 1	Absorbance 2	Absorbance 3	Avrg Absorbance	Dilluti on	Dill factor	Absorbance
15/07/09	0	0.103	0.105	0.104	0.104	0	1	0.104
15/07/09	2	0.363	0.364	0.365	0.364	0	1	0.364
15/07/09	4.5	0.714	0.711	0.71	0.711667	1:01	2	1.423333
15/07/09	6	0.966	0.968	0.969	0.967667	1:01	2	1.935333
15/07/09	8	0.919	0.922	0.922	0.921	1:03	4	3.684
15/07/09	10	0.45	0.451	0.451	0.450667	1:07	8	3.605333
16/07/09	18.5	0.663	0.663	0.663	0.663	1:09	10	6.63
16/07/09	20	0.719	0.718	0.716	0.717667	1:09	10	7.176667



Growth curves of oxidised MWCNTs

Date commencing Experiment: 1 October 2009
Shaker speed: 180 rpm
Incubator temperature: 30C
Sample O1 Vtot= 101ml; Vonc= 1ml; Vbroth= 100ml; Mcnt=0.2 mg
Starting OD measurement at 600nm: 0.176

Date	Hrs Incubation	Absorbance 1	Absorbance 2	Absorbance 3	Avrg Absorbance	Dilluti on	Dill factor	Absorbance
1\10\09	0	0.176	0.177	0.178	0.177	0	1	0.177
1\10\09	2	0.328	0.329	0.328	0.328333	0	1	0.328333
1\10\09	4	0.982	0.984	0.979	0.981667	0	1	0.981667
1\10\09	6	0.98	0.977	0.978	0.978333	1:02	3	2.935
1\10\09	8	0.706	0.705	0.706	0.705667	1:09	10	7.056667
1\10\09	10	0.752	0.749	0.749	0.75	1:09	10	7.5
1\10\09	11	0.737	0.737	0.737	0.737	1:09	10	7.37
2\10\09	23	0.918	0.917	0.916	0.917	1:09	10	9.17
2\10\09	24	0.906	0.904	0.904	0.904667	1:10	11	9.951333
2\10\09	30	0.871	0.872	0.873	0.872	1:10	11	9.592



Date commencing Experiment: 1 October 2009

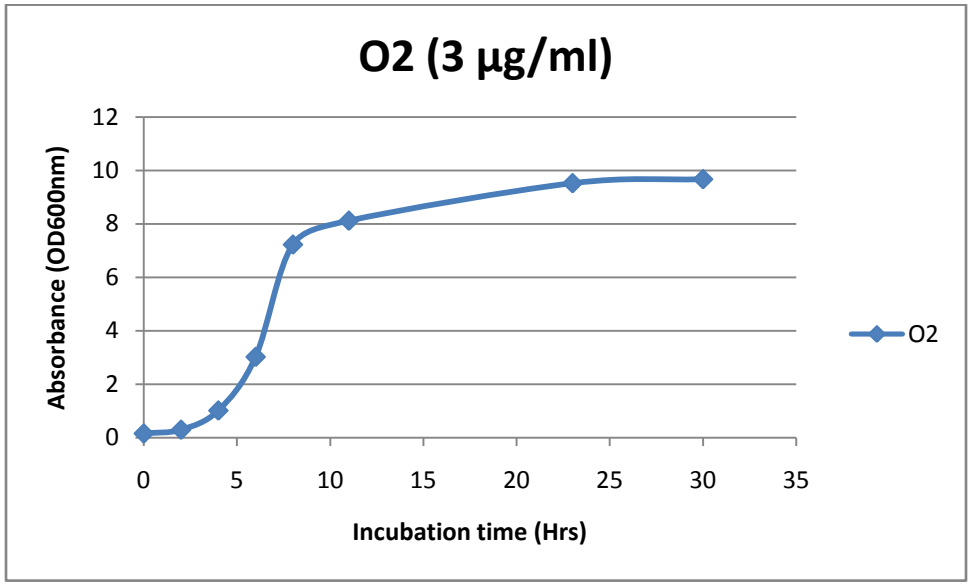
Shaker speed: 180 rpm

Incubator temperature: 30C

Sample O3 Vtot= 101ml; Vonc= 1ml; Vbroth= 100ml; Mcnt=0.3 mg

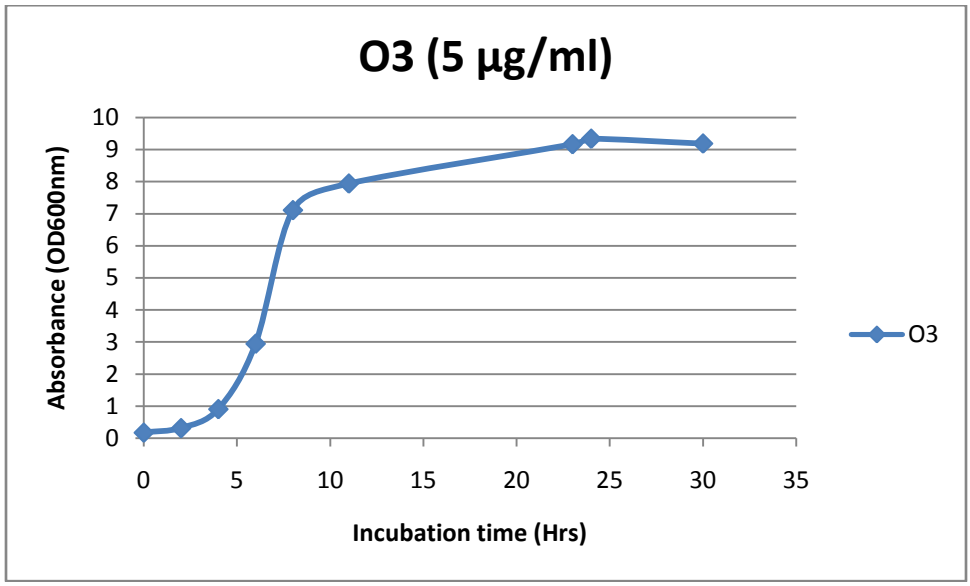
Starting OD measurement at 600nm: 0.158

Date	Hrs Incubation	Absorbance 1	Absorbance 2	Absorbance 3	Avrg Absorbance	Dilluti on	Dill factor	Absorbance
1\10\09	0	0.158	0.159	0.158	0.158333	0	1	0.158333
1\10\09	2	0.297	0.297	0.298	0.297333	0	1	0.297333
1\10\09	4	1.016	1.017	1.016	1.016333	0	1	1.016333
1\10\09	6	1.007	1.008	1.008	1.007667	1:02	3	3.023
1\10\09	8	0.722	0.723	0.722	0.722333	1:09	10	7.223333
1\10\09	10	0.711	0.711	0.711	0.711	1:09	10	7.11
1\10\09	11	0.812	0.812	0.811	0.811667	1:09	10	8.116667
2\10\09	23	0.951	0.952	0.953	0.952	1:09	10	9.52
2\10\09	24	0.967	0.965	0.966	0.966	1:10	11	10.626
2\10\09	30	0.916	0.916	0.916	0.916	1:10	11	10.076



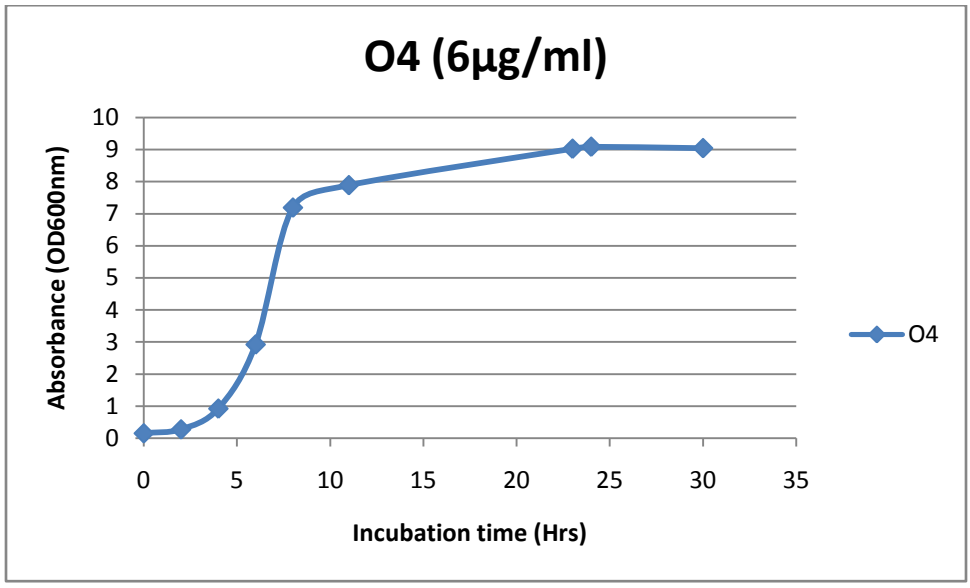
Date commencing Experiment: 1 October 2009
Shaker speed: 180 rpm
Incubator temperature: 30C
Sample O3 Vtot= 101ml; Vonc= 1ml; Vbroth= 100ml; Mcnt=0.5 mg
Starting OD measurement at 600nm: 0.172

Date	Hrs Incubation	Absorbance 1	Absorbance 2	Absorbance 3	Avrg Absorbance	Dilluti on	Dill factor	Absorbance
1\10\09	0	0.172	0.171	0.172	0.171667	0	1	0.171667
1\10\09	2	0.311	0.312	0.313	0.312	0	1	0.312
1\10\09	4	0.903	0.905	0.906	0.904667	0	1	0.904667
1\10\09	6	0.981	0.982	0.981	0.981333	1:02	3	2.944
1\10\09	8	0.71	0.711	0.712	0.711	1:09	10	7.11
1\10\09	10	0.731	0.728	0.726	0.728333	1:09	10	7.283333
1\10\09	11	0.793	0.794	0.795	0.794	1:09	10	7.94
2\10\09	23	0.917	0.916	0.917	0.916667	1:09	10	9.166667
2\10\09	24	0.848	0.849	0.85	0.849	1:10	11	9.339
2\10\09	30	0.841	0.842	0.823	0.835333	1:10	11	9.188667



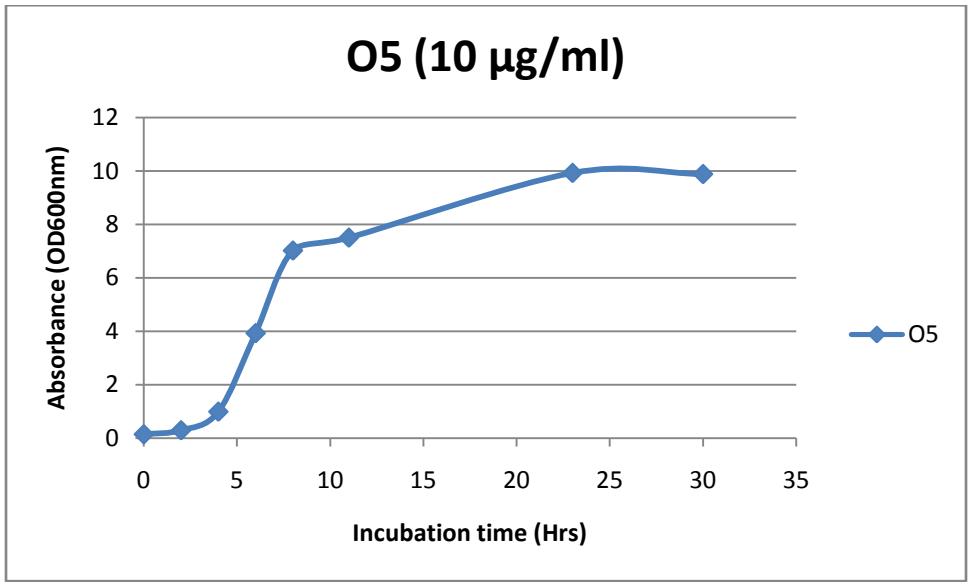
Date commencing Experiment: 1 October 2009
Shaker speed: 180 rpm
Incubator temperature: 30C
Sample O4 Vtot= 101ml; Vonc= 1ml; Vbroth= 100ml; Mcnt=0.6 mg
Starting OD measurement at 600nm: 0.150

Date	Hrs Incubation	Absorbance 1	Absorbance 2	Absorbance 3	Avrg Absorbance	Dilluti on	Dill factor	Absorbance
1\10\09	0	0.149	0.151	0.149	0.149667	0	1	0.149667
1\10\09	2	0.272	0.272	0.272	0.272	0	1	0.272
1\10\09	4	0.919	0.92	0.919	0.919333	0	1	0.919333
1\10\09	6	0.972	0.973	0.974	0.973	1:02	3	2.919
1\10\09	8	0.718	0.719	0.719	0.718667	1:09	10	7.186667
1\10\09	10	0.705	0.704	0.703	0.704	1:09	10	7.04
1\10\09	11	0.789	0.789	0.788	0.788667	1:09	10	7.886667
2\10\09	23	0.902	0.903	0.902	0.902333	1:09	10	9.023333
2\10\09	24	0.825	0.826	0.827	0.826	1:10	11	9.086
2\10\09	30	0.822	0.822	0.822	0.822	1:10	11	9.042



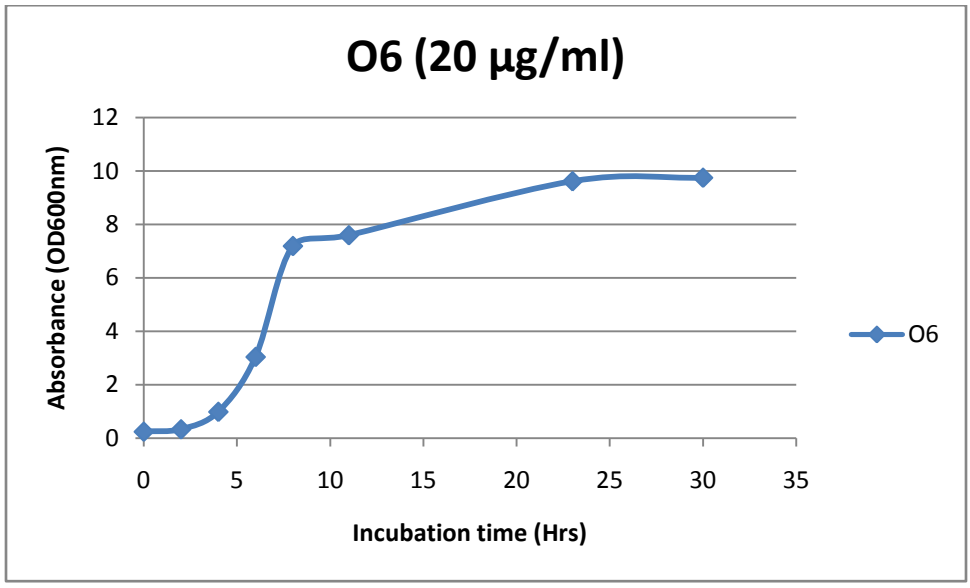
Date commencing Experiment: 1 October 2009
Shaker speed: 180 rpm
Incubator temperature: 30C
Sample O5 Vtot= 101ml; Vonc= 1ml; Vbroth= 100ml; Mcnt=1.0 mg
Starting OD measurement at 600nm: 0.136

Date	Hrs Incubation	Absorbance 1	Absorbance 2	Absorbance 3	Avrg Absorbance	Dilluti on	Dill factor	Absorbance
1\10\09	0	0.136	0.136	0.137	0.136333	0	1	0.136333
1\10\09	2	0.287	0.286	0.287	0.286667	0	1	0.286667
1\10\09	4	0.981	0.983	0.984	0.982667	0	1	0.982667
1\10\09	6	0.981	0.98	0.98	0.980333	1:03	4	3.921333
1\10\09	8	0.703	0.701	0.7	0.701333	1:09	10	7.013333
1\10\09	10	0.722	0.72	0.719	0.720333	1:09	10	7.203333
1\10\09	11	0.748	0.75	0.751	0.749667	1:09	10	7.496667
2\10\09	23	0.992	0.992	0.992	0.992	1:09	10	9.92
2\10\09	24	0.869	0.868	0.868	0.868333	1:10	11	9.551667
2\10\09	30	0.898	0.898	0.898	0.898	1:10	11	9.878



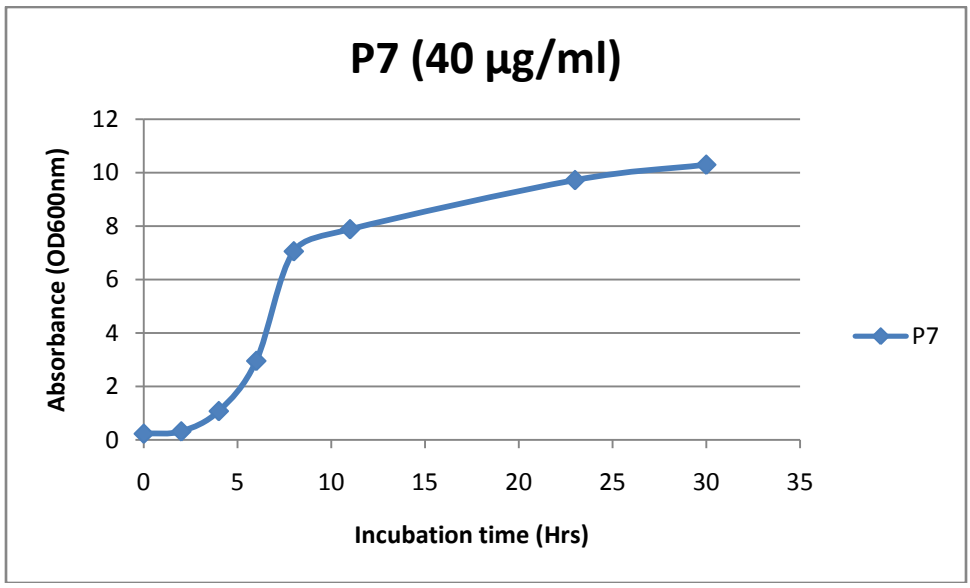
Date commencing Experiment: 1 October 2009
Shaker speed: 180 rpm
Incubator temperature: 30C
Sample O6 Vtot= 101ml; Vonc= 1ml; Vbroth= 100ml; Mcnt=2.0 mg
Starting OD measurement at 600nm: 0.240

Date	Hrs Incubation	Absorbance 1	Absorbance 2	Absorbance 3	Avrg Absorbance	Dilluti on	Dill factor	Absorbance
1\10\09	0	0.24	0.239	0.241	0.24	0	1	0.24
1\10\09	2	0.327	0.331	0.329	0.329	0	1	0.329
1\10\09	4	0.981	0.983	0.984	0.982667	0	1	0.982667
1\10\09	6	1.012	1.012	1.013	1.012333	1:02	3	3.037
1\10\09	8	0.718	0.719	0.719	0.718667	1:09	10	7.186667
1\10\09	10	0.702	0.703	0.704	0.703	1:09	10	7.03
1\10\09	11	0.759	0.759	0.759	0.759	1:09	10	7.59
2\10\09	23	0.961	0.961	0.961	0.961	1:09	10	9.61
2\10\09	24	0.902	0.903	0.902	0.902333	1:10	11	9.925667
2\10\09	30	0.884	0.886	0.887	0.885667	1:10	11	9.742333



Date commencing Experiment: 1 October 2009
Shaker speed: 180 rpm
Incubator temperature: 30C
Sample O7 Vtot= 101ml; Vonc= 1ml; Vbroth= 100ml; Mcnt=4.0 mg
Starting OD measurement at 600nm: 0.225

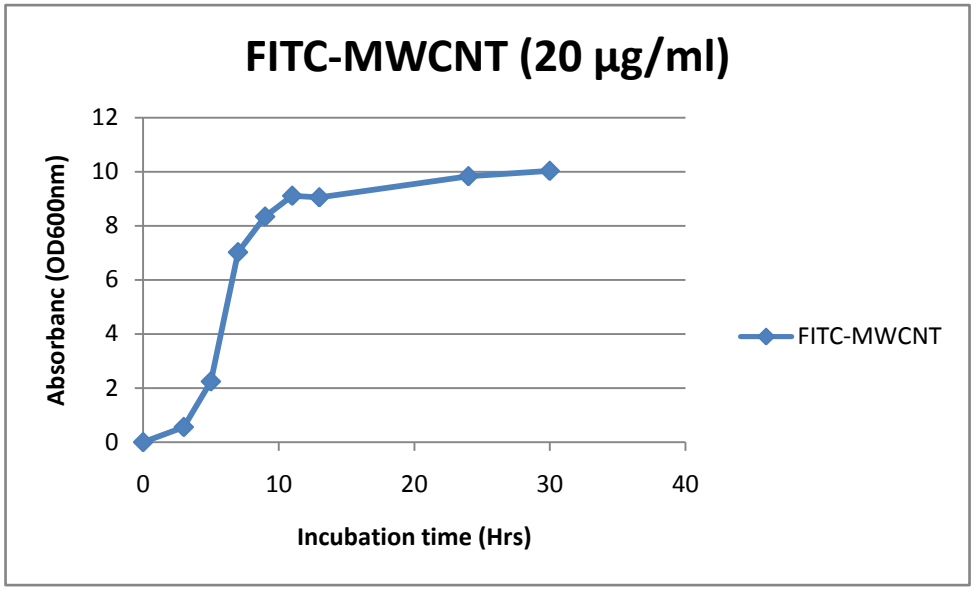
Date	Hrs Incubation	Absorbance 1	Absorbance 2	Absorbance 3	Avrg Absorbance	Dilluti on	Dill factor	Absorbance
1\10\09	0	0.225	0.226	0.226	0.225667	0	1	0.225667
1\10\09	2	0.314	0.311	0.312	0.312333	0	1	0.312333
1\10\09	4	1.073	1.072	1.07	1.071667	0	1	1.071667
1\10\09	6	0.983	0.982	0.986	0.983667	1:02	3	2.951
1\10\09	8	0.707	0.706	0.703	0.705333	1:09	10	7.053333
1\10\09	10	0.701	0.703	0.704	0.702667	1:09	10	7.026667
1\10\09	11	0.789	0.787	0.788	0.788	1:09	10	7.88
2\10\09	23	0.972	0.972	0.972	0.972	1:09	10	9.72
2\10\09	24	0.849	0.851	0.85	0.85	1:10	11	9.35
2\10\09	30	0.937	0.936	0.935	0.936	1:10	11	10.296



Date commencing Experiment: 12 May 2010
Shaker speed: 200 rpm
Incubator temperature: 30C
Sample CNT-FITC Vtot= 50ml; Vonc= 0.5 ml; Vbroth= 50 ml; Ccnt= 20 ug/ml
Starting OD measurement at 600nm: 0.197

Date	Hrs Incubation	Absorbance 1	Absorbance 2	Absorbance 3	Avrg Absorbance	Dilluti on	Dill factor	Absorbance
12\05\10	0					0	1	0
12\05\10	3	0.557	0.559	0.561	0.559	0	1	0.559
12\05\10	5	0.561	0.562	0.56	0.561	1:03	4	2.244
13\05\10	7	0.702	0.702	0.703	0.702333	1:09	10	7.023333
13\05\10	9	0.833	0.836	0.833	0.834	1:09	10	8.34
13\05\10	11	0.828	0.828	0.829	0.828333	1:10	11	9.111667
13\05\10	13	0.823	0.823	0.823	0.823	1:10	11	9.053
13\05\10	24	0.893	0.894	0.895	0.894	1:10	11	9.834
14\05\10	30	0.912	0.913	0.911	0.912	1:10	11	10.032

Hrs Incubation	Absorbance
0	0
3	0.559
5	2.244
7	7.023333
9	8.34
11	9.111667
13	9.053
24	9.834
30	10.032



Appendix A4: Cell viability Results

Colony counter name: Darkfield QUEBEC colony counter (American Optical)

Experimental Start Date: 3 November 2009
Start Time: 11:30 AM
Sample information: Control (0mg CNT)
Sample Name:Control

	PRIMARY			DUPLICATE		Average No.of. col	Ave No of CFU	Ave no of CFU	Ave CFU/ml	Ave 10^6CFU/ml
Date	hrs Incub	Dilluti on	no.of colon	Dilluti on	no of colon					
11/6/2009	0	10^-3	177	10^-3	16	96.5	96500	96500	965000	0.965
11/6/2009	0	10^-4	13	10^-4	6	9.5	95000	Not viable		0
11/6/2009	5.5	10^-4	109	10^-4	150	129.5	1295000	1295000	12950000	12.95
11/6/2009	5.5	10^-5	14	10^-5	31	22.5	2250000	Not viable		0
11/9/2009	24	10^-5	68	10^-5	45	56.5	5650000	5650000	56500000	56.5
11/9/2009	24	10^-6	3	10^-6	12	7.5	7500000	Not viable		
11/9/2009	48	10^-5	73(stressed)	10^-5	92(stressed)					
11/9/2009	48	10^-6	5(stressed)	10^-6	4(stressed)					

Colony counter name: Darkfield QUEBEC colony counter
(American Optical)

Experimental Start Date: 3
November 2009
Start Time:
11:30 AM
Sample information: O(3 µg/ml)
Sample Name: O(3
µg/ml)

	PRIMARY			DUPLICATE		Average	Ave			
							No of CFU	no of CFU	CFU/ml	10^6CFU/ml
Date	hrs Incub	Dillution	no.of colon	Dillution	no of colon	No.of. col				
11/6/2009	0	10^-3	86	10^-3	93	89.5	89500	89500	895000	0.895
11/6/2009	0	10^-4	10	10^-4	4	7	70000	Not viable		0
11/6/2009	5.5	10^-4	133	10^-4	66	99.5	995000	995000	9950000	9.95
11/6/2009	5.5	10^-5	11	10^-5	5	8	800000	Not viable		0
11/9/2009	24	10^-5	57	10^-5	84	70.5	7050000	7050000	70500000	70.50
11/9/2009	24	10^-6	9	10^-6	1	5	5000000	Not viable		
11/9/2009	48	10^-5	200	10^-5	222					
11/9/2009	48	10^-6	203	10^-6	174					

Colony counter name: Darkfield QUEBEC colony counter (American Optical)

Experimental Start Date: 3 November 2009
Start Time:
11:30 AM
Sample information: O(20 µg/ml)
Sample Name: O(20 µg/ml)

	PRIMARY			DUPLICATE		Average	Ave			
Date	hrs Incub	Dillution	no.of colon	Dillution	no of colon	No.of. col	No of CFU	no of CFU	CFU/ml	10^6CFU/ml
11/6/2009	0	10^-3	107	10^-3	86	96.5	96500	96500	965000	0.965
11/6/2009	0	10^-4	7	10^-4	13	10	100000	Not viable		0
11/6/2009	5.5	10^-4	293	10^-4	135	214	2140000	2140000	21400000	21.4
11/6/2009	5.5	10^-5	27	10^-5	17	22	220000	Not viable		0
11/9/2009	24	10^-5	55	10^-5	57	56	5600000	5600000	56000000	56
11/9/2009	24	10^-6	7	10^-6	7	7	700000	Not viable		
11/9/2009	48	10^-5	282	10^-5	278					
11/9/2009	48	10^-6	342	10^-6	270					

Colony counter name: Darkfield QUEBEC colony counter
(American Optical)

Experimental Start Date: 3
November 2009
Start Time: 11:30
AM
Sample information: O(40 µg/ml)
Sample Name: O(40
µg/ml)

	PRIMARY			DUPLICATE		Average	Ave			
							No of CFU	no of CFU	CFU/ml	10^6CFU/ml
Date	hrs Incub	Dilluti on	no.of colon	Dilluti on	no of colon	No.of. col				
11/6/2009	0	10^-3	99	10^-3	115	107	107000	107000	1070000	1.07
11/6/2009	0	10^-4	4	10^-4	20	12	120000	Not viable		0
11/6/2009	5.5	10^-4	86	10^-4	23	54.5	545000	545000	4975000	4.975
11/6/2009	5.5	10^-5	8	10^-5	1	4.5	450000	Not viable		0
11/9/2009	24	10^-5	49	10^-5	57	53	5300000	5300000	53000000	53.00
11/9/2009	24	10^-6	31	10^-6	16	23.5	23500000	Not viable		
11/9/2009	48	10^-5	386	10^-5	268					
11/9/2009	48	10^-6	290	10^-6	302					

Colony counter name: Darkfield QUEBEC colony counter
(American Optical)

Experimental Start Date: 3
November 2009
Start Time: 11:30
AM
Sample information: P(3 µg/ml)
Sample Name: P(3 µg/ml)

	PRIMARY			DUPLICATE		Average	Ave			
							No of CFU	no of CFU	CFU/ml	10^6CFU/ml
Date	hrs Incub	Dilluti on	no.of colon	Dilluti on	no of colon	No.of. col				
11/6/2009	0	10^-3	109	10^-3	126	117.5	117500	117500	1175000	1.175
11/6/2009	0	10^-4	4	10^-4	15	9.5	95000	Not viable		0
11/6/2009	5.5	10^-4	172	10^-4	134	153	1530000	1530000	15300000	15.3
11/6/2009	5.5	10^-5	13	10^-5	21	17	1700000	Not viable		0
11/9/2009	24	10^-5	47	10^-5	notv28	47	4700000	4700000	47000000	47
11/9/2009	24	10^-6	15	10^-6	21	18	18000000	Not viable		
11/9/2009	48	10^-5	207	10^-5	222					
11/9/2009	48	10^-6	73	10^-6	124					

Colony counter name: Darkfield QUEBEC colony counter (American Optical)

Experimental Start Date: 3 November 2009
Start Time:
11:30 AM
Sample information: P(20 µg/ml)
Sample Name: P(20 µg/ml)

	PRIMARY			DUPLICATE		Average	Ave			
Date	hrs Incub	Dillution	no.of colon	Dillution	no of colon	No.of. col	No of CFU	no of CFU	CFU/ml	10^6CFU/ml
11/6/2009	0	10^-3	102	10^-3	55	78.5	78500	78500	785000	0.785
11/6/2009	0	10^-4	5	10^-4	7	6	60000	Not viable		0
11/6/2009	5.5	10^-4	208	10^-4	151	179.5	1795000	1795000	17950000	17.95
11/6/2009	5.5	10^-5	18	10^-5	21	19.5	1950000	Not viable		0
11/9/2009	24	10^-5	68	10^-5	23	45.5	4550000	4550000	45500000	45.5
11/9/2009	24	10^-6	13	10^-6	9	11	11000000	Not viable		
11/9/2009	48	10^-5	263	10^-5	175					
11/9/2009	48	10^-6	225	10^-6	265					

Colony counter name: Darkfield QUEBEC colony counter (American Optical)

Experimental Start Date: 3 November 2009
Start Time: 11:30 AM
Sample information: P(40 µg/ml)
Sample Name: P(40 µg/ml)

	PRIMARY			DUPLICATE		Average No.of. col	Ave			
							No of CFU	no of CFU	CFU/ml	10^6CFU/ml
Date	hrs Incub	Dillution	no.of colon	Dillution	no of colon					
11/6/2009	0	10^-3	166	10^-3	126	146	146000	146000	1460000	1.46
11/6/2009	0	10^-4	19	10^-4	17	18	180000	Not viable		
11/6/2009	5.5	10^-4	101	10^-4	153	127	1270000	1270000	12700000	12.70
11/6/2009	5.5	10^-5	-	10^-5	9		900000	Not viable		
11/9/2009	24	10^-5	56	10^-5	71	63.5	6350000	6350000	6350000	63.5
11/9/2009	24	10^-6	10	10^-6	6	8	8000000	Not viable		
11/9/2009	48	10^-5	-	10^-5	-					
11/9/2009	48	10^-6	-	10^-6	-					

Second Set of Experiments:

Colony counter name: Darkfield QUEBEC colony counter (American Optical)

Experimental Start Date: 26 January 2010
Start Time: 11:30 AM
Sample information: Control(0 µg/ml)
Smple Name: Control(0 µg/ml)

	PRIMARY			DUPLICATE		Average	Ave			
Date	hrs Incub	Dilluti on	no.of colon	Dilluti on	no of colon	No.of. col	No of CFU	no of CFU	CFU/ ml	10^6CFU /ml
26/01/2010	5.5	10^-4	214	10^-3	220	217	2170000	2170000	21700000	21.7
26/01/2010	5.5	10^-5	31	10^-4	28	29.5	not viable			
26/01/2010	24	10^-5	52	10^-4	39	45.5	4550000	4550000	45500000	45.5
26/01/2010	24	10^-6	6	10^-5	1	3.5	not viable			

Colony counter name: Darkfield QUEBEC colony counter (American Optical)

Experimental Start Date: 26 January 2010
Start Time: 11:30 AM
Sample information: P(3 µg/ml)
Smple Name: P(3 µg/ml)

	PRIMARY			DUPLICATE		Average	Ave			
Date	hrs Incub	Dillutio n	no.of colon	Dillution	no of colon	No.of.col	No of CFU	no of CFU	CFU/ml	10^6CFU/ ml
26/01/2010	5.5	10^-4	183	10^-3	212	197.5	1975000	1975000	19750000	19.75
26/01/2010	5.5	10^-5	32	10^-4	9	20.5	not viable			
26/01/2010	24	10^-5	53	10^-4	56	54.5	5450000	5450000	54500000	54.5
26/01/2010	24	10^-6	3	10^-5	7	5	not viable			

Experimental Start Date: 26 January 2010
Start Time: 11:30 AM
Sample information: P (20 µg/ml)
Sample Name: P(20 µg/ml)

	PRIMARY			DUPLICATE		Average No.of. col	Ave No of CFU	Ave no of CFU	Ave CFU/ml	Ave 10^6CFU/ml
Date	hrs Incub	Dilluti on	no.of colon	Dilluti on	no of colon					
26/01/ 2010	5.5	10^-4	205	10^-3	203	204	2040000	2040000	20400000	20.4
26/01/ 2010	5.5	10^-5	20	10^-4	21	20.5	not viable			
26/01/ 2010	24	10^-5	65	10^-4	39	52	5200000	5200000	52000000	52
26/01/ 2010	24	10^-6	4	10^-5	12	8	not viable			

Colony counter name: Darkfield QUEBEC colony counter
(American Optical)

Experimental Start Date: 26 January 2010
Start Time: 11:30 AM
Sample information: P(40 µg/ml)
Smple Name: P(40 µg/ml)

	PRIMARY			DUPLICATE		Average No.of. col	Ave No of CFU	Ave no of CFU	Ave CFU/ml	Ave 10^6CFU/ml
Date	hrs Incub	Dilluti on	no.of colon	Dilluti on	no of colon					
26/01/2010	5.5	10^-4	203	10^-3	195	203	2030000	2030000	20300000	20.3
26/01/2010	5.5	10^-5	31	10^-4	11	29	not viable			
26/01/2010	24	10^-5	65	10^-4	39	52	5200000	5200000	52000000	52
26/01/2010	24	10^-6	4	10^-5	12	8	not viable			

Colony counter name: Darkfield QUEBEC colony counter
(American Optical)

Experimental Start Date: 26 January 2010
Start Time: 11:30 AM
Sample information: O(3 µg/ml)
Smple Name: O(3 µg/ml)

							Ave			
	PRIMARY			DUPLICATE		Average	No of CFU	no of CFU	CFU/ml	10^6CFU/ml
Date	hrs Incub	Dilluti on	no.of colon	Dilluti on	no of colon	No.of. col				
26/01/2010	5.5	10^-4	161	10^-3	225	193	1930000	1930000	19300000	19.3
26/01/2010	5.5	10^-5	16	10^-4	34	25	not viable			
26/01/2010	24	10^-5	13	10^-4	37	37	3700000	3700000	37000000	37
26/01/2010	24	10^-6	4	10^-5	1	2.5	not viable			

Colony counter name: Darkfield QUEBEC colony counter
(American Optical)

Experimental Start Date: 26 January 2010
Start Time: 11:30 AM
Sample information: O(20 µg/ml)
Smple Name: O(20 µg/ml)

							Ave			
	PRIMARY			DUPLICATE		Average	No of CFU	no of CFU	CFU/ml	10^6CFU/ml
Date	hrs Incub	Dilluti on	no.of colon	Dilluti on	no of colon	No.of. col				
26/01/2010	5.5	10^-4	306 not v	10^-3	230	230	2300000	2300000	23000000	23
26/01/2010	5.5	10^-5	32	10^-4	18	25	not viable			
26/01/2010	24	10^-5	more300	10^-4	89	89	8900000	8900000	89000000	89
26/01/2010	24	10^-6	4	10^-5	5	4.5	not viable			

Colony counter name: Darkfield QUEBEC colony counter
(American Optical)

Experimental Start Date: 26 January 2010
Start Time: 11:30 AM
Sample information: O(40 µg/ml)
Smple Name: O(40 µg/ml)

		PRIMARY		DUPLICATE		Average	Ave			
Date	hrs Incub	Dilluti on	no.of colon	Dilluti on	no of colon	No.of. col	No of CFU	no of CFU	CFU/ ml	10^6CFU /ml
26/01/20 10	5.5	10^-4	237	10^-3	313 nv	237	237000	237000	23700 000	23.7
26/01/20 10	5.5	10^-5	20	10^-4	31	29	not viable			
26/01/20 10	24	10^-5	65	10^-4	39	52	520000	520000	52000 000	52
26/01/20 10	24	10^-6	4	10^-5	12	8	not viable			

Average results from 2 sets of duplicate experiments										
	Control	**STDEV**	**P1(0.3 mg)**	**STDEV**	**P2(0.6mg)**	**STDEV**	**P3(1.57)**	**STDEV**	**P4(3.57)**	**STDEV**
hrs Incub	**10^6CFU/ml**		**10^6CFU/ml**		**10^6CFU/ml**		**10^6CFU/ml**		**10^6CFU/ml**	
0	0.965	0.569221	0.895	0.0494975	0.695	0.0120208	0.965	0.1484924	1.07	0.0565685
5.5	17.325	2.8107495	14.625	6.6114484	11.4	5.9043416	22.2	6.7175144	14.3375	12.904699
24	51	7.7781746	53.75	23.688077	82.5	31.819805	56	1.4142136	52.5	0.7071068

Average results from 2 sets of duplicate experiments								
	UP1(0.3)	**STDEV**	**UP2(0.6)**	**STDEV**	**UP3(1.67)**	**STDEV**	**UP4(3.57)**	**STDEV**
hrs Incub	**10^6CFU/ml**		**10^6CFU/ml**		**10^6CFU/ml**		**10^6CFU/ml**	
0	1.175	0.1202082	1.13	0.2969848	0.785	0.3323402	1.46	0.2828427
5.5	17.525	3.1466252	13.65	6.9	19.175	5.4447222	16.5	5.3740115
24	50.75	5.3033009	69	3.25	48.75	11.313708	57.75	8.131728

Appendix A5: PC12 Cytotoxicity viability result

Experiment done in triplicate

Experiment: Neuronal Cell Cytotoxicity Assesment

Date: 4 February 2010

Plate: 2hrs incubation: luminescence reading before lysing

				Avearage luminescence readings before lysing
A	9140	8444	7770	8451.3333
B	6818	5960	7340	6706
C	4334	4716	4638	4562.6667
D	2474	2348	1346	2056

Plate: 4hrs incubation: luminescence reading before lysing

A	3310	3522	3838	3556.6667
B	2690	1784	3256	2576.6667
C	2712	2506	3068	2762
D	1914	2260	884	1686

Plate: 22hrs incubation: luminescence reading before lysing

A	7484	8572	8250	8102
B	6000	5244	5306	5516.6667
C	4360	3334	3394	3696
D	1714	2490	1088	1764

Plate: 24hrs incubation: luminescence reading before lysing

A	7350	8308	8702	8120
B	4106	4060	6184	4783.3333
C	5540	4900	4736	5058.6667
D	928	1500	3670	2032.6667

CALCULATIONS:

No. of Viable cells = average luminescence after lyising - average luminescence before lysing
% Viability = No o viable cells/ average luminescence after lysing
% Viability of control = % Viability / % Viability of control

Plate block key:
A - PC12 cells incubated with no oxidised MWCNTs

B - PC12 cells incubated with 50 µg/ml oxidised MWCNTs
C - PC12 cells incubated with 100 µg/ml oxidised MWCNTs
D - PC12 cells incubated with 200 µg/ml oxidised MWCNTs

Plate: 2hrs incubation: luminescence reading after lysing				**Average luminescence readings after lysing**	**Ave No. of viable cells**	**% Viable**
A	10546	10142	9808	10165.333	1714	16.86122
B	8120	6766	8706	7864	1158	14.72533
C	4884	5228	4970	5027.3333	464.66667	9.242806
D	2694	2494	1910	2366	310	13.10228

Plate: 4hrs incubation: luminescence reading after lysing						
A	8092	8150	7296	7846	4289.3333	54.66904
B	4252	4266	5092	4536.6667	1960	43.20352
C	4394	5304	3112	4270	1508	35.31615
D	2300	2722	1138	2053.3333	367.33333	17.88961

Plate: 22hrs incubation: luminescence reading after lysing						
A	8502	9170	9640	9104	1002	11.00615
B	7116	5636	5548	6100	583.33333	9.562841
C	4720	3636	3600	3985.3333	289.33333	7.259953
D	2062	2646	1152	1953.3333	189.33333	9.6928328

Plate: 24hrsincubation: luminescence reading after lysing						
A	8300	8856	8850	8668.6667	548.66667	6.329308
B	5222	4810	6446	5492.6667	709.33333	12.91418
C	5548	5628	5192	5456	397.33333	7.282502
D	988	1636	3798	2140.6667	108	5.045157

2hrs incubation										
	Row 1			Row 2			Row 3			
	No o viable cells	% Viable	100% Viable of Control	No o viable cells	% Viable	100% Viable of Control	No o viable cells	% Viable	100% Viable of Control	STDEV % Viability
A	1406	13.3321	100	1698	16.7423	100	2038	20.77896	100	3.7278332
B	1302	16.0345	120.270	806	11.9125	71.1523	1366	15.69033	75.51067	2.2869599
C	550	11.2613	84.4675	512	9.79342	58.49521	332	6.680081	32.1483	2.3393253
D	220	8.1663	61.2530	146	5.85405	34.96571	564	29.5288	142.1091	13.052436

4 hrs incubation										
	Row 1			Row 2			Row 3			
	No o viable cells	% Viable	100% Viable of Control	No o viable cells	% Viable	100% Viable of Control	No o viable cells	% Viable	100% Viable of Control	STDEV % Viability
A	4782	59.095403	100	4628	56.785276	100	3458	47.395833	100	6.1964808
B	1562	36.735654	62.163302	2482	58.180966	102.45784	1836	36.056559	76.075378	12.582077
C	1682	38.279472	64.775719	2798	52.75264	92.898447	44	1.4138817	2.9831351	26.470778
D	386	16.782609	28.399178	462	16.972814	29.889463	254	22.319859	47.092451	3.1434646

22 hrs incubation										
	Row 1			Row 2			Row 3			
	No o viable cells	% Viable	100% Viable of Control	No o viable cells	% Viable	100% Viable of Control	No o viable cells	% Viable	100% Viable of Control	STDEV % Viability
A	1018	11.973653	100	598	6.521265	100	1390	14.419087	100	4.0431893
B	1116	15.682968	130.97897	392	6.9552874	106.65549	242	4.3619322	30.251098	5.9310447
C	360	7.6271186	63.699178	302	8.3058306	127.36533	206	5.7222222	39.685052	1.3394223
D	348	16.876819	140.94962	256	9.6749811	148.3605	214	18.576389	128.83193	4.7256404

24hrs incubation										
	Row 1			Row 2			Row 3			
	No o viable cells	% Viable	100% Viable of Control	No o viable cells	% Viable	100% Viable of Control	No o viable cells	% Viable	100% Viable of Control	STDEV % Viability
A	950	11.445783	100	548	6.1878952	100	148	1.6723164	100	4.8914294
B	1116	21.371122	186.71612	750	15.592516	251.98416	262	4.0645361	243.04828	8.8110208
C	8	0.1441961	1.2598186	728	12.935323	209.04238	456	8.7827427	525.18428	6.5253525
D	60	6.0728745	53.057746	136	8.3129584	134.34226	128	3.3701948	201.52854	2.474987

	Average values from triplicate results											
	2hrs incubation			4 hrs incubation			22 hrs incubation			24hrs incubation		
	No o viable cells	% Viable	100% Viable of Control	No o viable cells	% Viable	100% Viable of Control	No o viable cells	% Viable	100% Viable of Control	No o viable cells	% Viable	100% Viable of Control
A	1714	16.8612	100	4289.33	54.669	100	1002	11.006	100	548.6667	6.32931	100
B	1158	14.7253	87.332494	1960	43.204	79.027402	583.333	9.5628	86.88634	709.3333	12.9142	204.0379
C	464.7	9.24281	54.816922	1508	35.317	64.599919	289.333	7.25995	65.96269	397.3333	7.28250	115.06
D	310	13.1023	77.706574	367.333	17.890	32.723473	272.667	13.9590	126.8295	108	5.04516	79.71103

Appendix A6: Additional research micrographs and pictures

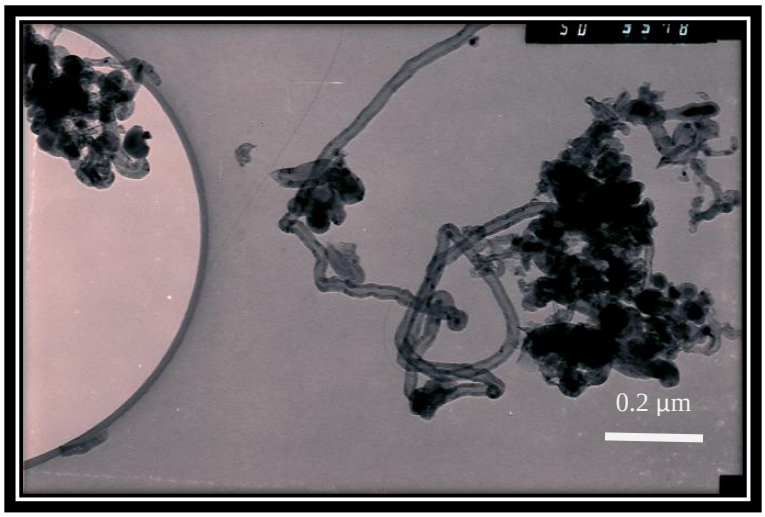


Figure A6.1: TEM micrograph of pristine MWCNTs

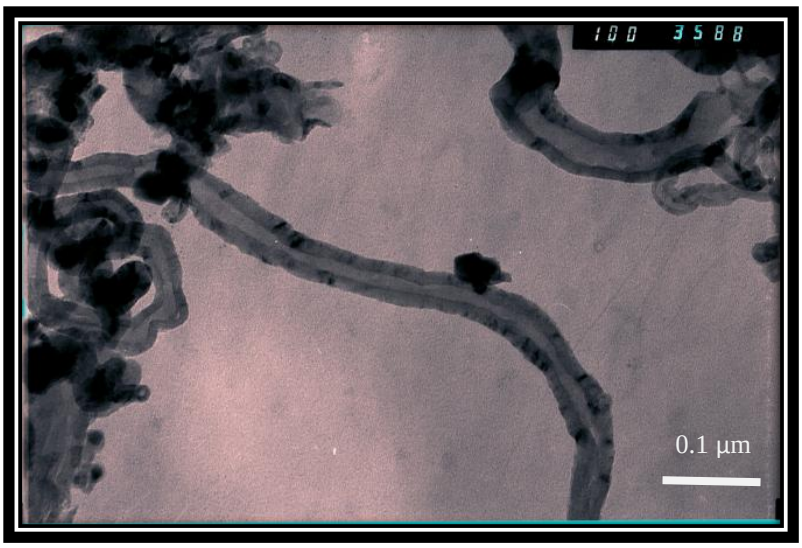


Figure A6.2: TEM micrograph of 1:3 HNO_3:H_2SO_4 MWCNTs

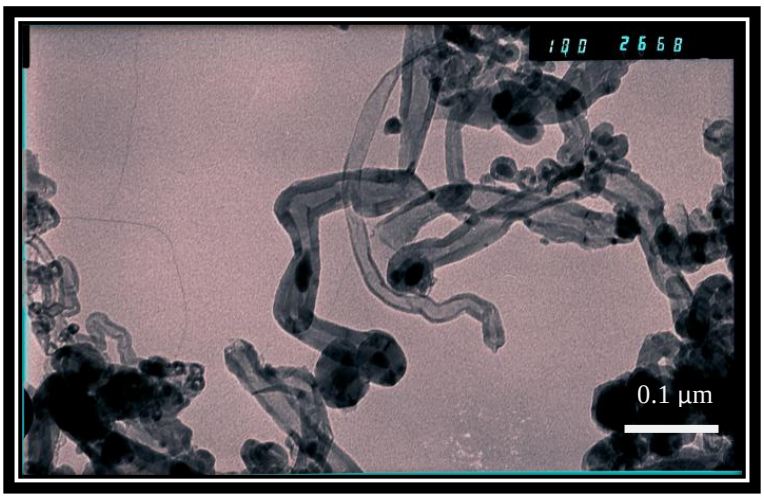


Figure A6.3: TEM micrograph of pristine MWCNTs where scale bar corresponds to 0.1 µm

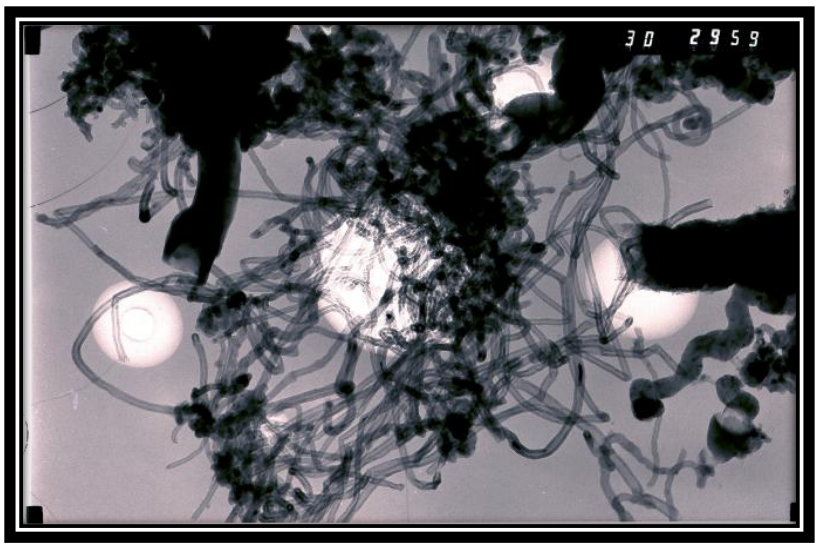


Figure A6.4: TEM micrograph of 30% HNO_3 oxidised MWCNTs with 0.33 µm scale bar

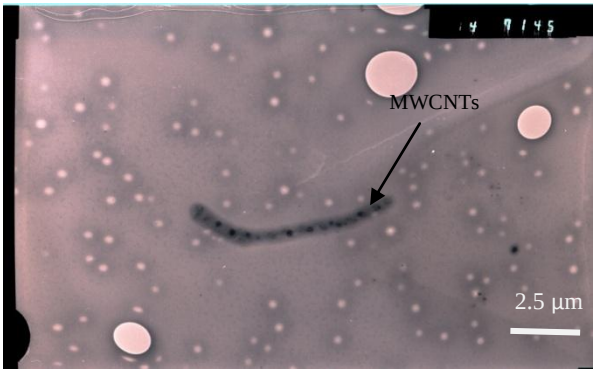


Figure A6.5. TEM image of FITC-MWCNTs with.

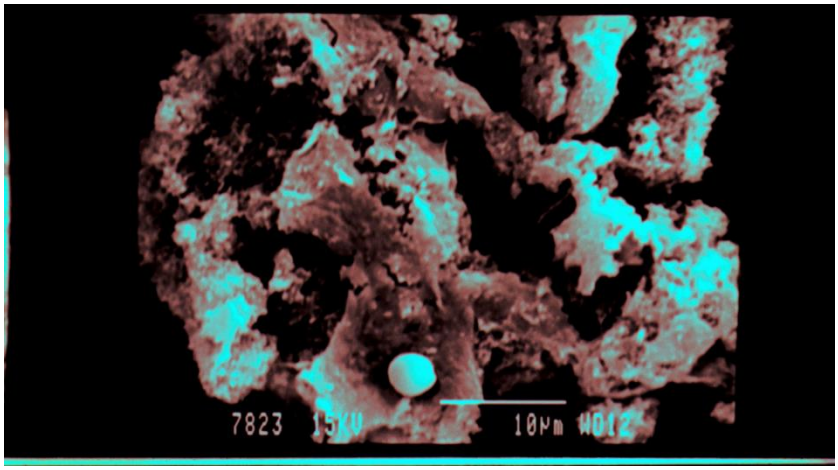


Figure A6.6. SEM micrograph of yeast cell on bunch of MWCNTs

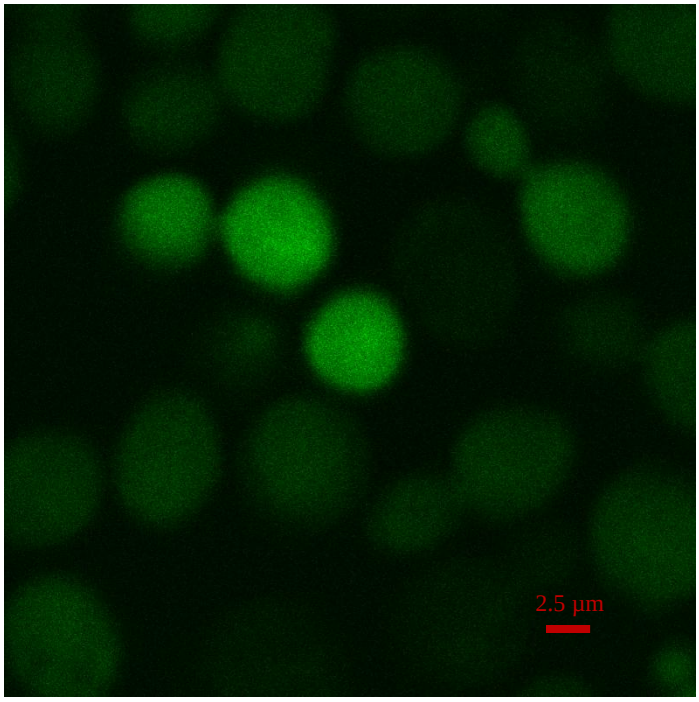


Figure A6.7: Confocal image of *S.cerevisiae* cells incubated with 20µg/ml MWCNT-FITC for 1and 1/2 hrs at a scale of 2.5 µm.

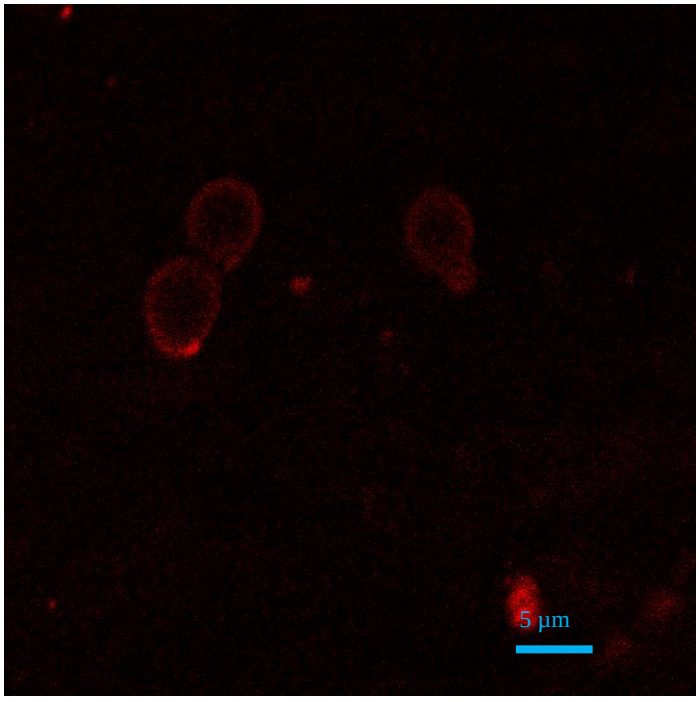


Figure A6.8: Confocal image of red stained membrane *S.cerevisiae* cells at a scale of 5 µm.

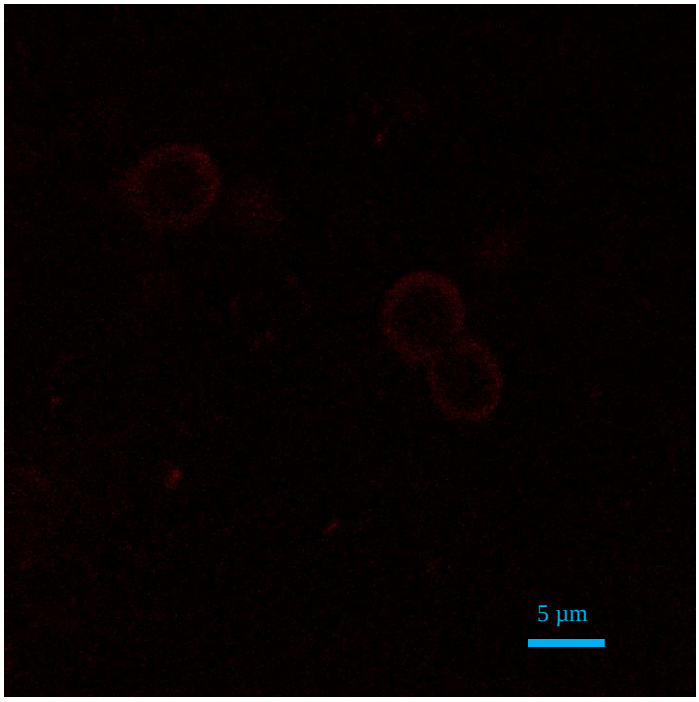


Figure A6.9: Confocal image of red stained membrane *S.cerevisiae* cells at a scale of 5 µm.

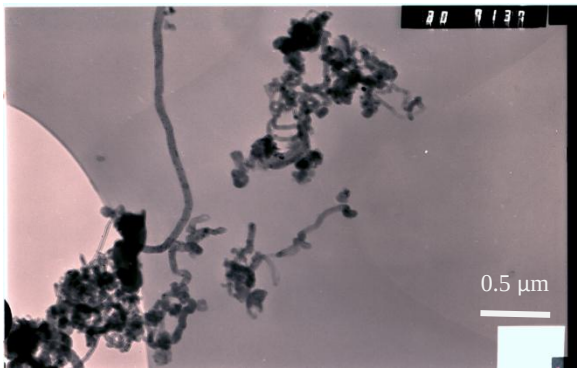


Figure A6.10: Typical TEM image of unreacted MWCNT sample from the 1, 3-dipolar cycloaddition reaction process, with 0.5µm scale bar

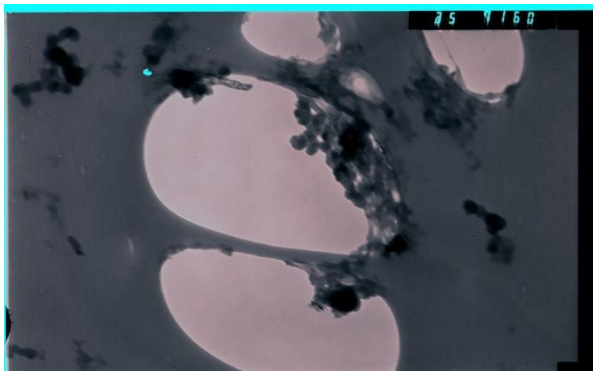


Figure A6.11: Typical TEM image of N-Tritylglycine functionalised MWCNTs, with a 0.4 µm scale bar